QATAR UNIVERSITY

Graduate Studies

College of Engineering

AN INVESTIGATION INTO HYDROPHOBIC MEMBRANE FOULING IN

DESALINATION USING MEMBRANE DISTILLATION TECHNOLOGY

A Thesis in

Environmental Engineering

By

Mashael Abdulla Ahmad M. Al-Obaidli

© 2015 Mashael Abdulla Al-Obaidli

Submitted in Partial Fulfillment

of the Requirements

for the Degree of

Master of Science

April 2015

Committee Page

The thesis of **Mashael Abdulla Al-Obaidli** was reviewed and approved by the following:

We, the committee members listed below accept and approve the Thesis/Dissertation of the student named above. To the best of this committee's knowledge, the Thesis/Dissertation conforms the requirements of Qatar University, and we endorse this Thesis/Dissertation for examination.

Name _____

Signature _____ Date_____

Name _____

Signature _____ Date_____

Name _____

Signature _____ Date_____

Abstract

Demand for freshwater supplies is continuously increasing globally to the extent where some parts of the world became highly water stressed. In particular, the Arabian Gulf states rely heavily on seawater desalination for their freshwater supply which is met using commercial seawater desalination technologies like thermal and reverse osmosis (RO) desalination processes. However, these technologies require considerable power input and actually do have a negative impact on the environment in terms of carbon footprint.

An alternative technology to the conventional desalination processes with potentially lower environmental impacts is the Membrane Distillation (MD) process. Membrane Distillation is a thermally-driven process that utilizes a hydrophobic micro-porous membrane and can utilize low grade heat and solar energy. The driving force of the process is the vapor pressure difference between the sides of the membrane that is induced by the temperature difference between the feed and distillate. However, one of the challenges facing the deployment of MD in large commercial scale desalination of seawater is membrane fouling.

The objective of this study is to investigate and compare the fouling characteristics of three different commercial membranes (PP membrane with pore size of 0.22 μm and 0.45 μm and PTFE membrane with pore size of 0.22 μm) using two feed solutions (seawater from the Arabian Gulf and synthetic 100,000 ppm NaCl solution) using a bench-scale direct contact membrane distillation (DCMD) flat sheet module at hot

iv

water inlet temperature of 75 $^{\circ}$C, cold water inlet temperature of 20 $^{\circ}$C, and hot and cold water flow rate of 1.5 L/min. The study was performed by evaluating the distillate flux performance of the various membranes, measuring their contact angle before and after fouling, testing the quality of the distillate produced and examining the salt rejection, and interpreting membrane surface analysis using Scanning Electron Microscopy (SEM) coupled with Energy Dispersive Spectroscopy (EDS) in order to study the morphology and the composition of the fouling layer.

Initially, the average flux obtained was 50.5 L/m^{2}h, 50.3 L/m^{2}h, and 38.3 L/m^{2}h for PP (0.22 μm) membrane, PP (0.45 μm) membrane, and PTFE (0.22 μm) membrane, respectively. Therefore, PP membrane generated a higher flux than PTFE membrane. In terms of membrane pore size, the results showed that a larger pore size membrane is more prone to fouling and flux decay. In terms of membrane material, PP membrane showed a more rapid flux decline than PTFE membrane. Moreover, the percentage of drop in the average flux was more than 60%, 97%, and 94% for PP membrane of 0.22 μm, PP membrane of 0.45 μm, and PTFE membrane of 0.22 μm, respectively, after almost 19 h, 30 h, and 25 h of operation, respectively.

In terms of feed solution, a lower flux was obtained with the higher salinity feed, the 100,000 ppm NaCl solution. However, the difference was not very large, indicating that initially salinity does not have a great impact on the distillate flux.

The results also showed that fouling/scaling causes the quality of the distillates to deteriorate and that membrane wetting has occurred. A salt rejection of more than

99.9% was achieved initially; however, with continuous operation, a salt rejection as low as 83.5% and 69.9% was achieved when the seawater and the 100,000 ppm NaCl solution were used, respectively. PP membrane of 0.22 μm gave a better salt rejection followed by PTFE membrane of the same size then by PP membrane of 0.45 μm.

The contact angle of a clean PP (0.22 μm) membrane, PP (0.45 μm) membrane, and PTFE (0.22 μm) membrane was found to be 134.8°, 133.2°, and 136.7°, respectively. However, after fouling, the contact angle dropped to 40.5°, 36.1°, and 13.8° for PP (0.22 μm) membrane, PP (0.45 μm) membrane, and PTFE (0.22 μm) membrane, respectively, indicating significant loss of hydrophobicity.

SEM-EDS analysis showed that the salt layer formed on the membranes was not uniform and that the major foulants were $CaCO_3$ and $CaSO_4$. In addition, membrane pore blocking by salts and a cake layer formation (which was a result of the elevated feed temperature that resulted in the formation of temperature polarization) were observed.

The results of the study show that fouling needs to be more investigated in MD process to be practically implemented and considered as competitive to the conventional desalination technologies. An optimum temperature and flow rate should be explored; however, the results of the study urge the need for developing new membranes and improved membrane modules and MD configurations as well as finding optimum procedures for membrane cleaning.

Declaration

Student Declaration

"To the best of my knowledge, the thesis contains no material previously published or written by another person or institution, except where due reference is made in the text of the thesis. The thesis contains no material which has been accepted for the award of any other degree in any university or other institution."

Name _____

Signature _____ Date_____

Supervisor's Declaration

"To the best of my/our knowledge, the thesis conforms the requirements of Qatar University, and we/I endorse this thesis for examination."

Name _____

Signature _____ Date_____

Table of Contents

List of Tables

List of Figures

Acknowledgements

I will be always grateful and indebted to **my family** whose ever present love and caring have been my rock foundation. Many thanks go to my parents, my source of inspiration, for allowing me to follow my ambitions throughout my childhood. I would also wish to thank my brothers and my sisters who were always willing to help. They deserve my deepest thanks for being themselves. My family was always supportive and encouraging especially my mother who was even looking after my children so that I can finish my work. I never would have been able to achieve my goals without you mom!

A special thank you to **my husband** for always standing beside me and for having the patience with me for having taking yet another challenge which reduces the amount of time I can spend with him. He was always there cheering me up and kept encouraging me throughout the course of my research.

My thanks and appreciations also go to **my beloved children**: my 3-year-old son, Ali, and my 6-month-old baby girl, Alreem for always making me smile and specially Ali for understanding on those days when I was writing this Thesis instead of playing with him.

To all the wonderful people in my life, thank you!

Chapter 1: Introduction

Water is the basic component of life on the planet. There is a virtually profound amount of water on earth which is equal to approximately 1.4 billion km^3 (Barlow & Clark, 2002). Of this total, about 97% is saline water represented in oceans. The remaining 3% is fresh water (approximately 35,000,000 km^3). About 2% of the remaining 3%, approximately 24,000,000 km^3, is inaccessible for human use as it remains in the form of glaciers and is frozen in ice caps. Moreover, groundwater, surface water such as lakes and rivers, and plants and the atmosphere hold only 1% (approximately 11,000,000 km^3) of all the fresh water on the earth. However, this water is considered as non-renewable, like fossil fuels, as almost all of it has gradually accumulated over time (Miller, 2003). Figure 1 shows the distribution of water around the world.
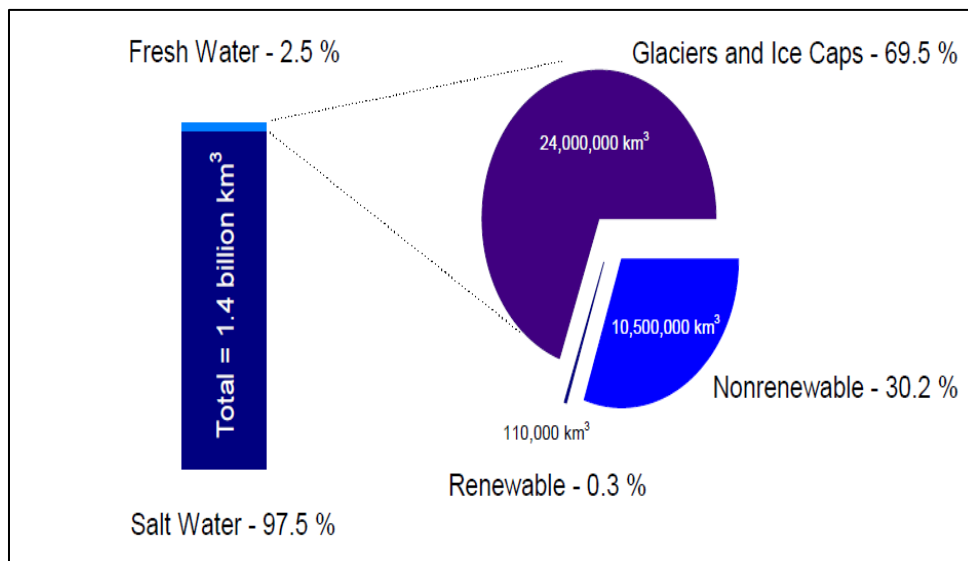
Figure 1: The Distribution of Water around the World (Adapted from: Miller, 2003)

In the last fifty years, the global freshwater demand has doubled almost every 15 years. As the global population is in continuous increase, the freshwater supplies will be under increasing stress. In part, the stress is due to anthropogenic disturbances. This is a result of the fact that a large percentage (approximately 70%) of the global population lives in coastal areas. Therefore, the combined effects of increasing demand on fresh water and the anthropogenic disturbances to the seawater are stressing the need for desalination (Davis, 2006).

Countries around the world are beginning to recognize the future crisis. According to the International Water Management Institute, a non-profit research organization, by 2025, approximately 2.7 billion people, about one-third of the estimated population at that time, will dwell in regions experiencing severe water scarcity (Davis, 2006). Moreover, the increase in freshwater demand is mainly due to the growing global population and the demands of industrialization. At present, water consumption doubles every 20 years, approximately twofold the rate of population growth (Miller, 2003).

Figure 2 shows a prediction of the regions in the world that will be facing water scarcity by 2025. In 2010, the World Health Organization (WHO) has estimated that in the world, one in three people are facing water shortage (Gray et al., 2011).
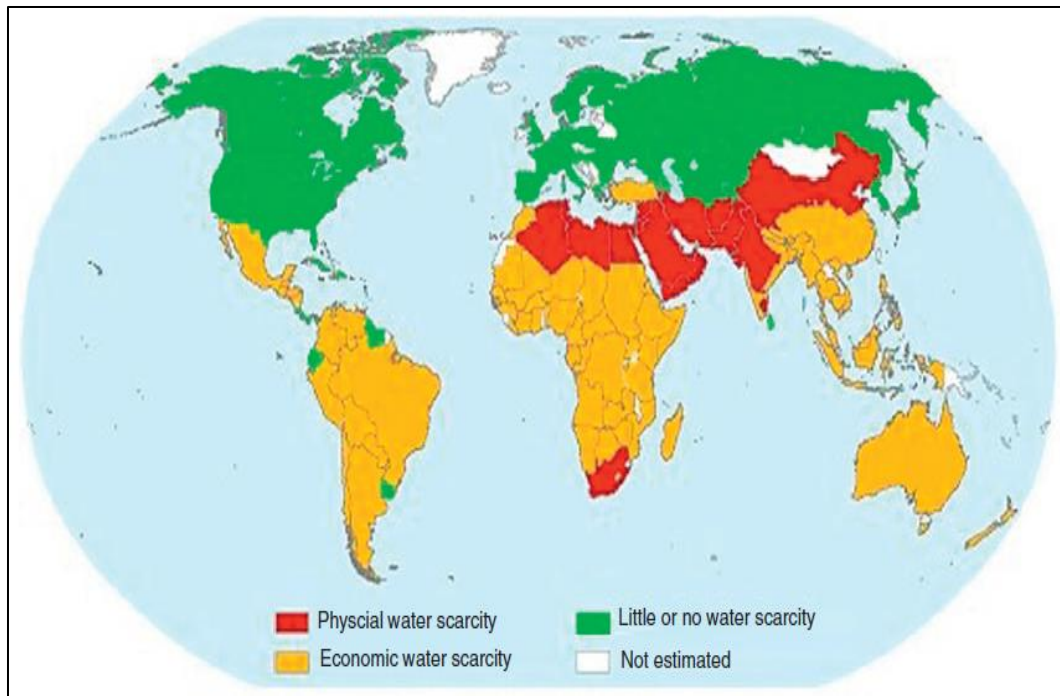
Figure 2: Estimated Water Scarcity in 2025 (Adapted from: Gray et al., 2011)

Despite the worldwide need for freshwater sources, the Middle East countries, along with North Africa's, are considered as the world's most regions with water scarcity (The World Bank, 2012). The Middle East and North Africa region (MENA) is facing significant water management issues with their aquifers being over pumped, their deteriorating water quality, and their limited water supply and irrigation facilities. All of which have great consequences in that they will harm the people's health, the agricultural productivity, and eventually the environment. Moreover, the limited freshwater resources are forcing the MENA countries to search for better opportunities. Accordingly, to prevent the problem from escalating, there are massive water investments in this region. Furthermore, water in MENA already is a vital constraint and if climate change affects weather and precipitation patterns as

anticipated, the region may experience repeated and severe droughts resulting in decreased water availability overall (The World Bank, 2012).

Due to the insufficient water supplies, particularly in the Gulf Cooperation Council (GCC) countries, desalination in the region is greatly needed.

The Desalination Process:

Desalination is a process used to remove dissolved solids, primarily salts and other minerals, from water. Desalination is the key process to produce potable fresh water that is used for drinking, for domestic uses, and for irrigation. The major driving factors behind the desalination process are declining in conventional freshwater resources due to rapid economic and demographic development, prolong drought, climate change, pollution and salinization (Lattemann & Höpner, 2008). However, the process can be used to produce ultrapure water for some industrial processes as well (Elimelech & Phillip, 2011).

The higher the salinity of the source water is and the greater the purity required, the greater the energy input needed for desalination (Saif, 2012). Salinity is the measure of the total dissolved solids (TDS) present in water. It is generally measured in milligrams per liter (mg/L), parts per thousand (ppt) or parts per million (ppm) (Saif, 2012). Table 1 shows the salinity ranges for several water sources.

Table 1: The Salinity Ranges for Several Water Sources (Saif, 2012)

Source Water	Salinity Range (TDS)
Brine water	> 50,000 mg/L (> 50 ppt)
Seawater	15,000–50,000 mg/L (30-50 ppt)
Brackish water	1,500–15,000 mg/L (0.50-30 ppt)
Pure water	< 500 mg/L (< 0.50 ppt)

There are several existing desalination technologies, mostly in small scale applications (Elimelech & Phillip, 2011). However, for large scale seawater desalination, the desalination processes are mostly classified into two groups: thermal and membrane based (Shannon et al., 2008). In thermal processes such as Multi-Stage Flash (MSF) and Multiple-Effect Distillation (MED), the water is evaporated then it is re-condensed (Elimelech & Phillip, 2011). In membrane based processes such Reverse Osmosis (RO), the feed water to the process is forced through a semi-permeable membrane that doesn't allow the passage of various particulates and dissolved ions (DesalData, 2012). These processes are explained in more details in Chapter 2.

Factors Affecting the Choice of a Desalination Technology:

There are several factors that could affect the choice of the technology to be used in a country for desalination. These include: the salinity levels in the source water and its temperature, the amount of water required, and the form and cost of the available energy (Davis, 2006). However, the salinity and temperature of the feed water is considered as the main influencing factor. Table 2 shows the typical salinity and temperature of seawater in the MENA region.

Table 2: The Typical Salinity and Temperature of Seawater in MENA (Fichtner and DLR, 2011)

Water Source	Salinity Range (mg/L)	Temperature (^{o}C)
Mediterranean and Atlantic	38,000 – 41,000	15 – 30
Red Sea and Indian Ocean	41,000 – 43,000	20 – 35
Arabian Gulf Water	45,000 – 47,000	20 – 35

The source water salinity has a great effect on the efficiency and the desalination performances of an RO plant. On the other hand, MED and MSF are not affected as much as RO and are more stable against the salinity of the source water (The World Bank, 2012).

Water security is another factor that affects the choice of desalination process type. For example, compared to RO technologies, thermal desalination processes such as MED operate under a wider range of feed water quality and in the presence of

impurities. Moreover, the requirement for a harmless disposal of brine and other chemicals also dictates the choice of desalination technologies (The World Bank, 2012).

Desalination in the Arabian Gulf Region

Desalination History:

The emphasis on desalination in the Arabian Gulf, particularly in the GCC countries which include Saudi Arabia, the United Arab Emirates (UAE), Oman, Kuwait, Qatar, and Bahrain, began after the Second World War (WWII) with the discovery of oil in the region (Saif, 2012). With the increasing enormous investments in oil exploration in those countries following the oil discovery and with their relatively small population as well as limited manpower, foreign workers were needed. Hence, the GCC countries were impelled to invite a lot of expats to the region which led to the rise of many cities in the Gulf (Winckler, 1997).

During that time, freshwater demands in the GCC countries were met mainly through groundwater that existed in the region. In addition, in the mid-1950s, fresh water could be attained by merely digging down into the soil (Pankratz, 2012). Yet, the increasing drain of groundwater along with its increasing quality deterioration led to the search for new solutions to meet the growing need for fresh water.

At that period of time, thermal desalination technologies were introduced to the Gulf region such as Multiple Effect Boiling (MEB) (Pankratz, 2012) followed by Multi Stage Flash (MSF) after its development in 1958 (Saif, 2012).

Figure 3 shows the cumulative desalination capacity in the GCC countries from 1970. In the 1980s, desalination grabbed a lot of attention in the region. This was due to the 1973 oil price spike which allowed many Gulf countries, especially Saudi Arabia and UAE, to consider and make large investments in their water and energy infrastructures (Saif, 2012).
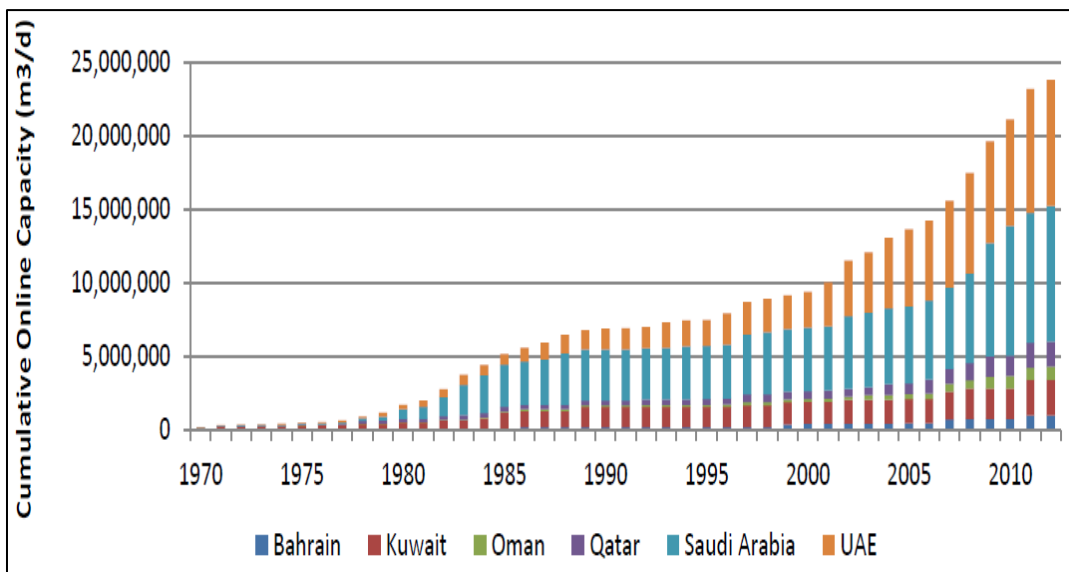
Figure 3: Cumulative Desalination Capacity in the GCC Countries (Adapted from: Saif, 2012)

Desalination Technologies in the Arabian Gulf Countries:

Choosing the suitable desalination technology in the GCC countries depends greatly on the physical characteristics of the region in that some Gulf countries have access to more than one source of feed water (DesalData, 2012). Therefore, the choice is limited for Kuwait, Qatar, and Bahrain as they can only utilize the Arabian Gulf as the source of feed water for desalination. On the other hand, Saudi Arabia, UAE, and Oman have a better advantage in that they have access to other seas such as the Arabian Sea and the Red Sea. The characteristics of those water bodies play a role in determining the suitable desalination technology (Saif, 2012). Nevertheless, the harsh weather conditions of the GCC countries make desalination difficult, despite the fact that 57% of the desalination capacity in the world is taking place in this region (DesalData, 2012). The high salinity and the elevated temperature in the Arabian Gulf participated in influencing the decision making of choosing the most effective desalination technology to be used.

Figure 4 shows the percentage of desalination capacity by technology in the GCC countries and worldwide in 2012. Despite the RO's energy efficiency and dominance in the world, the majority of the world's thermal desalination units are located in the GCC countries (Elimelech & Phillip, 2011). The Gulf Sea's high temperature and salinity, in addition to its high turbidity and the presence of marine organisms have conventionally contributed to high pre-treatment costs for RO. In addition, low grade steam that is generated from gas-fired power plants is widely available and is

considered cheap in the region; hence, the dominance of thermal based desalination technologies in the GCC countries (DesalData, 2012). Nevertheless, recent developments in membrane technology coupled with other technological advances that eliminate the pre-treatment step or decrease it to some extent have increased the interest in using RO or other membrane based technologies in the GCC countries (DesalData, 2012).
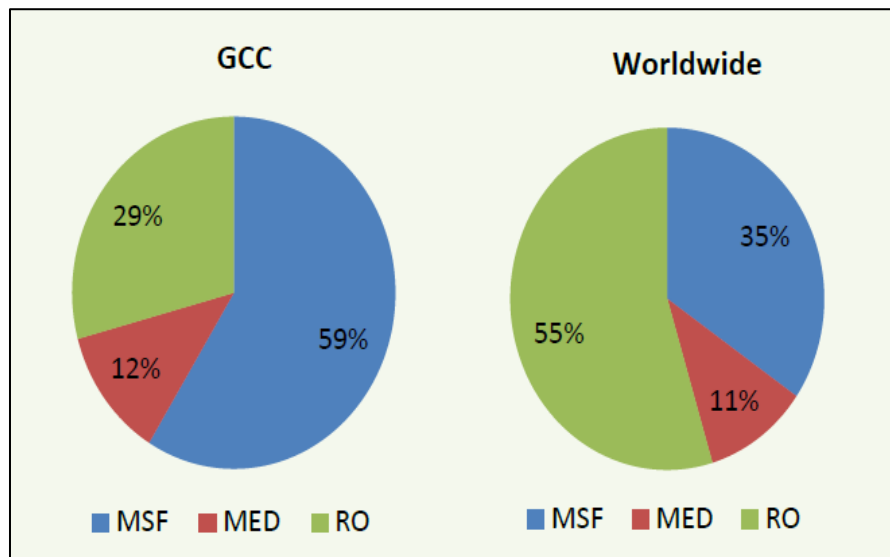
Figure 4: The Percentage of Desalination Capacity by Technology in the GCC Countries and Worldwide in 2012 (Adapted from: Saif, 2012)

Types of Desalination Plants and their Production Capacity:

The Arabian Gulf holds the world's largest desalination plants. Figure 5 shows the installed capacity of the desalination plants in the GCC countries. There are about 199 desalination units in the Gulf countries. Most of the desalination units are joined with

power generation units to save steam transportation and generation costs. In 2012, the total GCC capacity of the desalinated water was about 11 million m^3/day. The GCC countries have the 45% share of the global production of desalinated water. Out of this 45%, Qatar has the production capacity of about 8%. Moreover, most of the desalination units are in the United Arab Emirates and Saudi Arabia (Dawoud & Al Mulla, 2012).
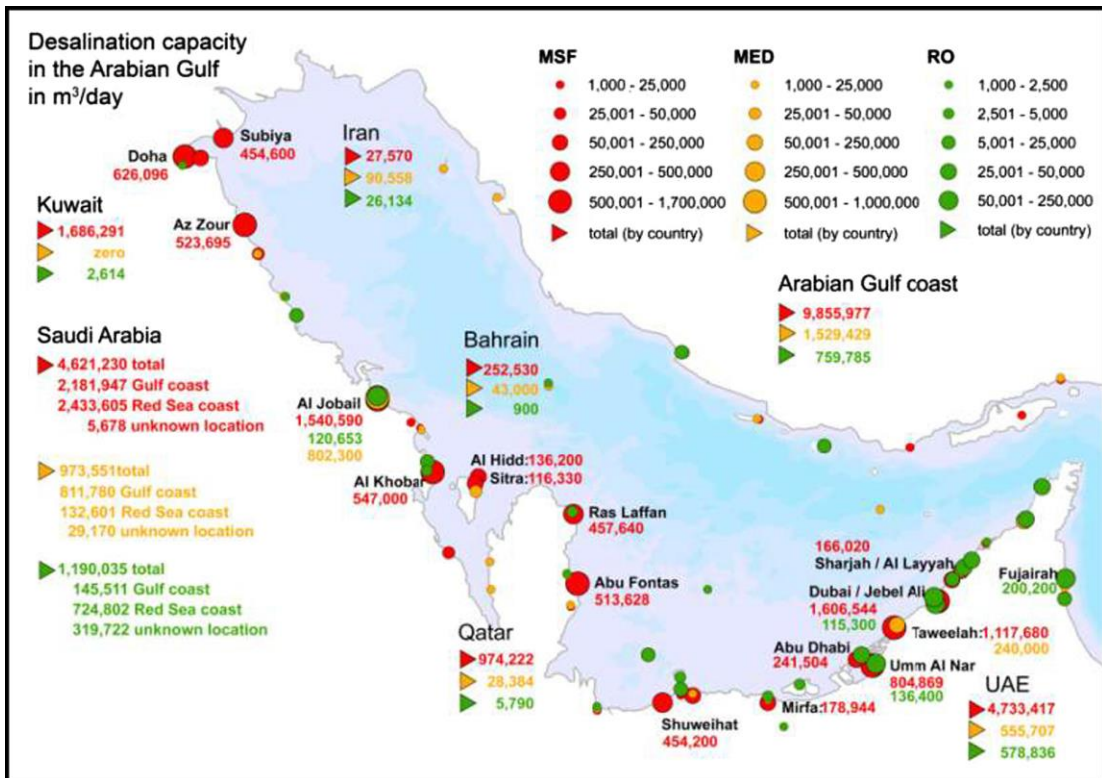
Figure 5: The Installed Capacity of the Desalination Plants in the GCC Countries

(Adapted from: Elhakeem & Elshorbagy, 2013)

Most of the desalination in the region is done using MSF, MED, and RO units. Table 3 shows the desalination technologies used in each of the GCC countries and their

sum in 2010. There were about 129 RO, 53 MSF, 13 MED, 3 combined (MSF+RO), and 1 Vapour Compression (VC) units in the GCC countries. Saudi Arabia has the most RO units in the Gulf region, while UAE has the highest number of MSF units (Dawoud & Al Mulla, 2012).

Table 3: The Number of Desalination Plants Used in the GCC Countries in 2010

(Dawoud & Al Mulla, 2012)

Technology	GCC Country						
	KSA	UAE	Kuwait	Oman	Qatar	Bahrain	Total
MSF	18	20	6	3	5	1	53
RO	76	18	0	31	2	2	129
MED	3	8	0	0	1	1	13
VC	0	0	0	0	0	1	1
ED	0	0	0	0	0	0	0
Combined (MSF+RO)	0	1	0	1	0	1	3
Total	97	47	6	35	8	6	199

Note: very small scale desalination plants are not included in the table

Current and Future Expected Capacity:

The total desalinated water production capacity in the GCC countries in 2010 was about 3000 million m^3/year. However, in 2012, the capacity has increased to 5000

million m^3/year. Due to the growing demand on fresh water, the capacity of desalinated water will continue to increase. Figure 6 depicts the historical and future expected capacity of desalinated water in the GCC countries. It is expected that by 2030, the capacity of desalinated water in the GCC countries will be 9000 million m^3/year (Dawoud & Al Mulla, 2012).
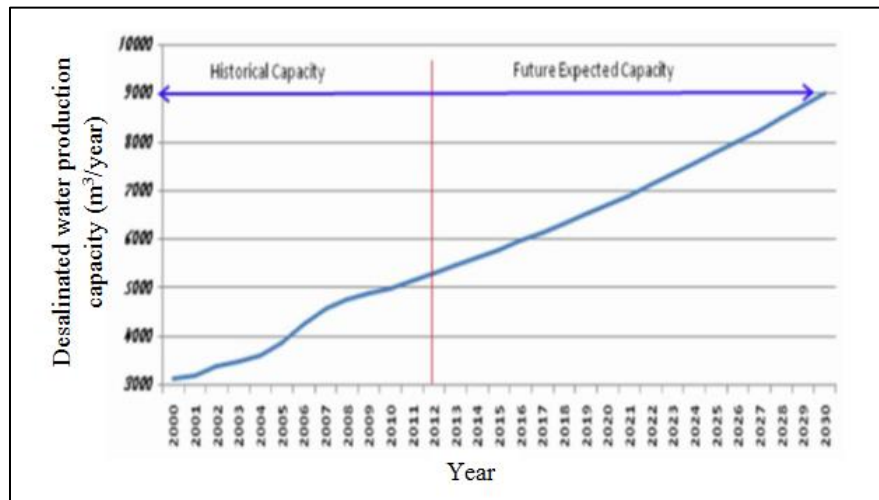
Figure 6: The Historical and Future Expected Capacity of Desalinated Water in the

GCC Countries (Adapted from: Dawoud & Al Mulla, 2012)

Desalination in Qatar:

Qatar's most acute scarcity till date is the availability of fresh water (NDS, 2011). With its low levels of rainfall of 70-90 mm/year (Global Water Intelligence, 2011), one of the lowest in the world, Qatar relies on three sources of water: desalination, groundwater, and recycled water (treated sewage effluent). Nevertheless, Qatar's

freshwater demand for domestic and industrial use is met mainly through desalination (NDS, 2011).

Qatar was among the first countries who adopted desalination as a way of producing fresh water. The first major desalination plant in the country started operation in 1962 (The World Bank, 2012). According to the Minister of State for Energy and Industry, there are a lot of challenges faced by the desalination sector; however, the main ones are its high energy consumption and the carbon emissions associated with the process (NDS, 2011).

Qatar's household consumption of water per capita is one of highest in the world (NDS, 2011). As a result of the growing water demand, Qatar's 30-year master plan for electricity and water had started in 2009. One of the plan's goals is for Kahramaa to increase the desalination capacity by an addition of 1.7 million m³/d between 2016 and 2032 (NDS, 2011; Almalki, 2008; DesalData, 2012). Compared to the existing capacity of 1.2 million m^3/d, this would lead to an increase of approximately 142% (Saifi, 2012).

Qatar has several desalination plants. These plants are located in three cities: Ras Laffan, Ras Abu Fontas, and Ras Girtas. According to National Development Strategy (2011-2016) of Qatar, in future, due to the increasing water demand in the country, Qatar will consider investigating into new technologies that do not consume as much power and that can withstand higher salinity levels than the current processes (NDS, 2011).

The Environmental Impacts of Desalination:

The environmental impact of a process corresponds to the energy it consumes to produce the product. In case of desalination, it is the utilization of energy to produce one cubic meter of desalinated water. Therefore, as the energy consumption increases, the environmental impacts of the process increase. As most of the energy in the world is generated by burning fossil fuel resources, the environmental impacts are directly related to the production of Green House Gases (GHGs). These include carbon dioxide (CO_2), nitrogen oxides (NO_x), and sulphur oxides (SO_x) which trap heat in the atmosphere and cause global warming. Moreover, different types of fossil fuel resources have different environmental impacts. Coal generates the largest amount of greenhouse gas emission and natural gas produces the least (Lattemann & Höpner, 2008).

Another problem with the desalination units is that they pour brine back to the oceans. The brine discharged from the desalination process is characterized by its high salinity and temperature if the process is thermal distillation or its high salinity if the desalination process is reverse osmosis (Elhakeem & Elshorbagy, 2013). This brine is considered dangerous for the marine biodiversity. Moreover, the expelled water may contain some chemicals that are harmful to the marine organisms.

Furthermore, seawater that carries small fish species and plankton is directly pumped from the oceans (Purnama et al., 2005). The process may harm the food chain and

become the reason for the loss of marine biodiversity. The environmental footprint of the desalination process will be further discussed in Chapter 2.

Proposed Solution to the Environmental Impacts of Desalination:

One of the solutions to minimize the harmful effects of desalination is using an alternative technology to the conventional thermal and RO processes. This process is the Membrane Distillation (MD) process. Membrane Distillation is viewed as a very promising technology which is combined with renewable energies and/or waste heat to generate pure water at an equally low cost. There are a lot of advantages of using MD over the widely used RO for desalination purposes. These include: higher quality distillate, effective treatment of high concentration NaCl solutions, utilizing low grade heat, involving long maintenance-free operation periods which reduces the fluctuations in the process, and of lower capital and operational costs. All of which make the MD process the perfect solution to produce fresh water in the Arabian Gulf region, especially in Qatar, by desalting brine solutions.

Membrane Distillation is a process between thermal distillation and reverse osmoses. It utilizes low grade heat and a hydrophobic porous membrane. The MD process involves a brine solution at a high temperature on one side of the membrane and pure water on the other side. The driving force of the process is the vapor pressure difference between the sides of the membrane that is induced by the temperature difference between the feed and distillate.

1.1- Objectives and Scope of Work

Qatar is one of the major desalinating countries in the world. Therefore, highly efficient and cost effective desalination technologies should be investigated to be implemented. The increasing need for fresh water and the available industrial waste heat make MD a highly desired and a more environmentally benign technology to be implemented in the country. Furthermore, for process enhancement, understanding the fouling mechanism and how to prevent it would make the study an ideal case study for MD.

The presented study is done on a single stage DCMD unit using three polymeric hydrophobic membranes and two feed solutions (Qatar coastline seawater and synthetic NaCl solution) to produce good quality distillate with the aim of ultimately reducing the associated environmental impacts of desalination and the carbon footprint of the current conventional desalination technologies.

MD membrane fouling is studied throughout this research. In addition, the quality of the water produced is studied and compared with conventional desalination water in Qatar. Specific objectives of the proposed work include:

- Designing and implementing an experimental program to investigate the extent of fouling of commercial hydrophobic membranes in Direct Contact Membrane Distillation.

- Evaluating the performance of different MD membranes under extreme operating conditions and exploring the flux performance with extended MD operation.

- Examining MD salt rejection after fouling.

- Measuring the contact angle of the membranes to assess their degree of hydrophobicity before and after utilization in the desalination experiments.

- Comparing the fouling characteristics in the three types of membranes used.

- Interpreting membrane surface analysis using Scanning Electron Microscopy (SEM) coupled with Energy Dispersive Spectroscopy (EDS) in order to gain an insight into the fouling mechanisms and to determine the main chemical elements that cause MD fouling.

Chapter 2: Background and Literature Survey

Water is a vital nutrient for human life and a basic commodity for economic sustainability of a region. The last century's rapid industrial and economic growth along with intensive urbanization has exploited the natural freshwater resources and hence intensified the water stress index (Fritzmann et al., 2007). Across the world, it has been strongly recognized that the future of the economic development and sustainability of a country is directly linked with the solutions of local water scarcity issues such as water storage capacity, water quality protection, and advances in supply-enhancing water treatment technologies (National Academy of Sciences, 2004). The scarcity and rapid degradation of freshwater resources has led to an increased demand for alternative freshwater resources and technologies such as desalination.

Desalination is a process used to remove dissolved solids, primarily salts and other minerals, from water. It is the key process to produce potable fresh water. The major driving factors behind the desalination process are declining in conventional freshwater resources due to rapid economic and demographic development, prolong drought, climate change, pollution and salinization (Lattemann et al., 2010). Around the world, about 125 countries are taking the advantage of various desalination processes (Saidur et al., 2011). Desalination of saline water involves a number of technologies. Depending on their water separation mechanisms, they can be classified

broadly into two main categories: thermal desalination and membrane based desalination processes.

2.1- Thermal Desalination

Thermal desalination, also known as distillation desalination, is one of the major technologies to produce fresh water from seawater or brackish ground water as half of the world's desalination plants, mostly concentrated in arid Gulf countries with ample oil and natural gas resources, are based on thermal desalination processes (National Academy of Sciences, 2004). The main objective of thermal desalination of saline seawater in Gulf's fossil fuel rich countries is to produce potable fresh water in order to meet the increasing demand of rapidly expanding urbanization of these areas (Saif, 2012). In addition to produce drinking water, thermal desalination can also be used to produce ultra-pure high quality water for semiconductor and pharmaceutical applications (Elimelech & Phillip, 2011). Through thermal desalination process, 5 to 50 ppm of total dissolved solids (TDS) is separated while a maximum of 50% source water is recovered (Amtaorg, 2007).

For large scale thermal desalination of seawater, there exist the following three main desalination technologies:

1) Multiple Effect Distillation (MED)

2) Multistage Flash Desalination (MSF)

3) Vapor Compression Desalination (VCD)

Being the major desalination technologies, only MED and MSF are briefly discussed below.

2.1.1- Multiple Effect Distillation (MED)

The Multiple Effect Distillation (MED) plants were introduced in the industry in the 1960s. The process is based on a sequence of single effect evaporators where recovery of latent heat of vaporization of first effect (evaporator) (Saidur et al., 2011) is reused as a heat source to produce vapors to the next effect (evaporator) and so on; thus, a good efficiency of heat recovery is obtained in the MED process (El-Dessouky & Ettouney, 2002; Lior, 2005). A typical MED desalination unit is generally comprised of multiple evaporators typically creating 6 to 18 effects, boiler and condenser units as its main components (Lior, 2005). In MED process, steam is produced in the boiler unit and is fed to the tube assembly of the first evaporator unit containing input saline water feed from water pretreatment source, steam feed to the second evaporator and output hot brine feed to the second evaporator as shown in Figure 7.

Various tube configurations most prominently the horizontal tube multiple effect (HTME) and the vertical tube multiple effect (VTME) are used (Lior, 2005). Also, with respect to the saline water feed and the direction of flow of hot steam, the MED process can be configured to feed forward, backward, or parallel feed configurations as mentioned by El-Dessouky and Ettouney (2002).

In MED, salt water is sprayed on top of horizontal tubes to form a thin film. Water vapor flows internally within the tubes (Namboodiri & Rajagopalan, 2014). Moreover, the hot vapors fed from the first evaporator further heats up the hot brine in the second evaporator resulting in steam formation. The steam generated in second evaporator acts as a heat source to the third evaporator and so on. Depending upon the feed configuration, at each stage, there is a temperature difference compared to the previous or next stage; hence, the brine in each stage acts as a condensing medium for vapors fed from the previous stage. The vapors coming from the last evaporator are condensed in a condenser and the still left is rejected into the atmosphere (Saidur et al., 2011).
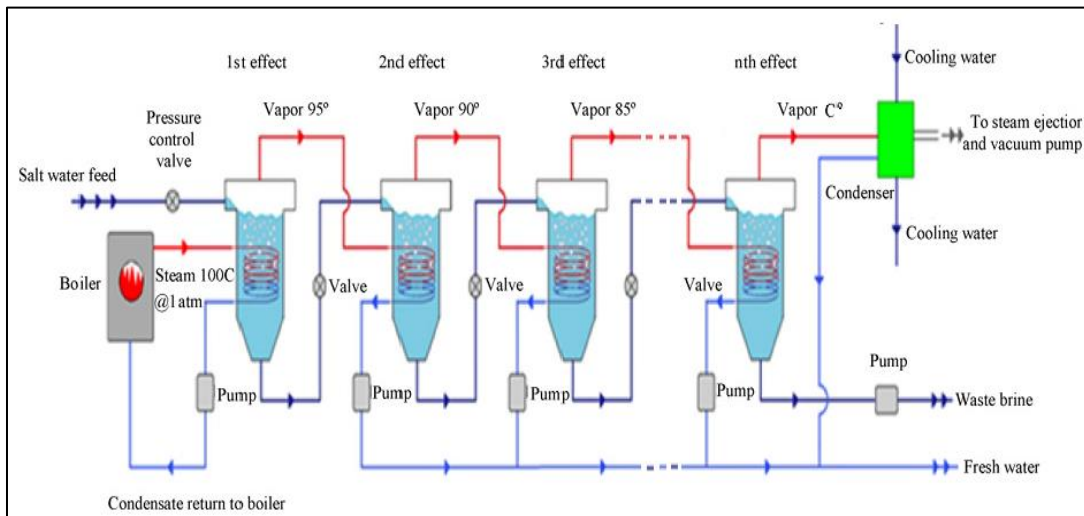
Figure 7: The Process Flow Diagram of a Typical n-Stage MED Desalination Unit

(Adapted from: Saidur et al., 2011)

An important factor in the MED process flow is to maintain a temperature and vapor pressure gradient among the consecutive effects that helps to maintain a good flow of

22

heat between the heating vapor and the saline boiling water at each evaporator stage. To achieve this, each evaporator is equipped with water and vacuum pumps. The water pump maintains the supply of desalinated water at the ambient pressure. Also, the vacuum pump evacuates the space by exhausting the non-condensing gases such as oxygen and nitrogen until the desired pressure range is obtained (Saidur et al., 2011). It also implies that a continuity of both electrical and heat energy is crucial to carry out and maintain a smooth MED process. Additionally, as hot seawater is handled, MED process material selection to handle heated brine is a critical factor in MED system design (Amtaorg, 2007).

2.1.2- Multistage Flash Desalination (MSF)

Multistage Flash desalination (MSF) was introduced in the early 1950s (Cipollina et al., 2009). MSF is the most widely used innovative thermal desalination process where vapor formation is carried out within the liquid bulk instead of the surface of hot tubes within the same vessel (El-Dessouky & Ettouney, 2002; Saidur et al., 2011). Because of the low fossil fuels prices and cogeneration of steam and electricity, major MSF desalination process based water production plants are located in the Middle East (Fritzmann et al., 2007).

The principle operation of MSF desalination process involves the following stages:

1) Water abstraction and pre-treatment sections

2) Flash and heat recovery unit

3) Heating section

23

In water abstraction section, a direct intake of seawater or from the beach wells is taken and fed to the pretreatment section. Compared to direct intake from the sea, the water intake from beach wells gives better quality of water in terms of turbidity, presence of algae, and total dissolved solids (Veza, 2001). At the pretreatment stage, most of the organic and particulate fouling matters such as the natural organic matter (NOMs), sand and clay are removed through coagulation and filtration process. From the pretreatment section, water is pumped through a series of heat recovery units. The construction of heat recovery units is similar to heat exchangers. The brine water flows from a lower heat unit to a higher heat unit. As water flows through preheater tubes of the condenser unit, its temperature increases. The preheated saline water is then fed to brine heater where it is further heated by a low pressure feed of steam. The low pressure steam is generally provided through a steam turbine of a power plant or a cogeneration power with a heat recovery steam generator (El-Nashar, 2001). The extremely hot brine is then allowed to flow through multiple evaporator flash chambers (typically 19–28) having distillate trays to collect the distilled water (Saidur et al., 2011).

A low vapor pressure gradient from a lower temperature to a higher temperature between consecutive stages is maintained through a venting pump installed along with the MSF chambers. The relatively low vapor pressure in each chamber facilitates the seawater to superheat in a few degree raises in temperature. Consequently, it evaporates vigorously resulting in intense bubble generation with supplementary steam turbulence at each stage as it flows from one stage to another consecutive stage

(Lior, 2005). The steam produced is condensed and the distillate is collected through distillate trays. Finally, the aggregate collection of water from all stages is pumped to post treatment section from which it is further distributed in a water distribution network. A typical four stage MSF desalination process is illustrated in Figure 8.
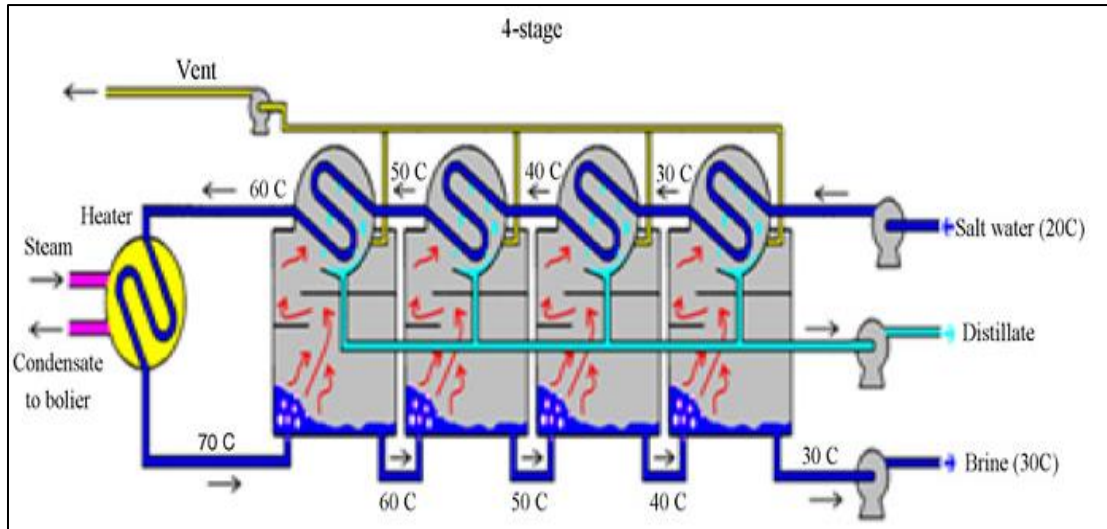
Figure 8: The Process Flow Diagram of a Typical Four Stage MSF Desalination
Process (Adapted from: Saidur et al., 2011)

2.2- Membrane Desalination

The research to separate water through a semipermeable (cellulose acetate (CA)) membrane having desalination properties was started in mid-20th century (Amtaorg, 2007). The major breakthrough in membrane desalination technology was achieved in 1959 when Samuel Yuster along with two of his students, Sidney Loeb and Srinivasa Sourirajan, at the University of California at Los Angeles (UCLA) were able to produce a functional synthetic membrane from cellulose acetate polymer. It was the

first time the reverse osmosis (RO) process has been demonstrated (Fane et al., 2011; El-Dessouky & Ettouney, 2002).

Over the last 60 years, tremendous research and advancement have been made in the membrane desalination technology and RO technology has become the key competitor of the conventional thermal technology based desalination process. The main advantage of membrane desalination over the conventional thermal desalination is that the desalination process takes place below the normal boiling point of the feed solution. Hence, it requires less energy and lower capital costs (National Academy of Sciences, 2004). However, its major disadvantage is the danger of membrane wetting (intrusion of the distillate into the pores of the membrane) and fouling during the process (Banat et al., 1999).

The major membrane based desalination technologies are Reverse Osmosis (RO), Electrodialysis (ED), Microfiltration (MF), Nanofilteration (NF) and Ultrafiltration (UF) (Fane et al., 2011). Except the ED technology, all other major membrane desalination processes are carried out under different trans-membrane pressure ranges as given in Table 4.

Table 4: Trans-membrane Pressure Difference Required for Major Membrane Based

Desalination Technologies (Fane et al., 2011)

Membrane Desalination Technology	Trans-membrane Pressure Difference
RO	~ 5 - 8 MPa
NF	~ 0.5 - 1.5 MPa
MF	~ 50 - 500 kPa
UF	~ 50 - 500 kPa

The major driving factors of the membrane based desalination technologies are the difference of pressure (for RO, NF, MF, and UF) and electrical potential (for ED) on both sides of the hydrophilic membrane (National Academy of Sciences, 2004). The direction of mass flow always takes place from the higher pressure to the lower pressure side (Tomaszewska, 1994).

RO accounts for about 50% of the world's total desalination capacity (Cipollina et al., 2009; Al-Subaie, 2007). Nevertheless, Membrane Distillation (MD) is a very promising alternative membrane based technology for desalination. Therefore, RO and MD are going to be discussed in the next sections.

2.2.1- Reverse Osmosis (RO)

Reverse Osmosis (RO) process is a key emerging technology to produce potable fresh water from seawater for water scare coastal areas (Kumar et al., 2007). It is the most

widely used membrane based desalination process (Fritzmann et al., 2007). In the last couple of decades, it has gained substantial popularity due to the advancement in membrane technology that has developed low pressure high productivity membranes having better salt rejection ratio and improved flux properties (Wilf & Bartels, 2005; Busch & Mickols, 2004; Matsuura, 2001; Amtaorg, 2007).

Reverse Osmosis desalination is a membrane filtration process in which water (solvent) is forced to flow from a higher concentration solution to the lower concentration side through a semipermeable membrane by application of a hydrostatic pressure greater than osmotic pressure (Gullinkala et al., 2010).

In the RO process, highly concentrated saline water is separated from a diluted water by a semipermeable membrane so thin that a stack of five thousand of them would be only one millimeter thick (El-Dessouky & Ettouney, 2002). Normally, equilibrium conditions exist on both sides of the membrane and the magnitude of the pressure that maintains an equilibrium state and totally blocks the flow of solvent is generally known as the osmotic pressure (denoted by π_i). To carry out the RO process, an additional hydrostatic pressure (usually between 50-200 bar) greater than the osmotic pressure is applied to the higher concentration side and the water is forced to cross through the membrane leaving behind highly concentrated saline water (El-Dessouky & Ettouney, 2002). The concept of osmosis, equilibrium condition and RO is depicted in Figure 9.
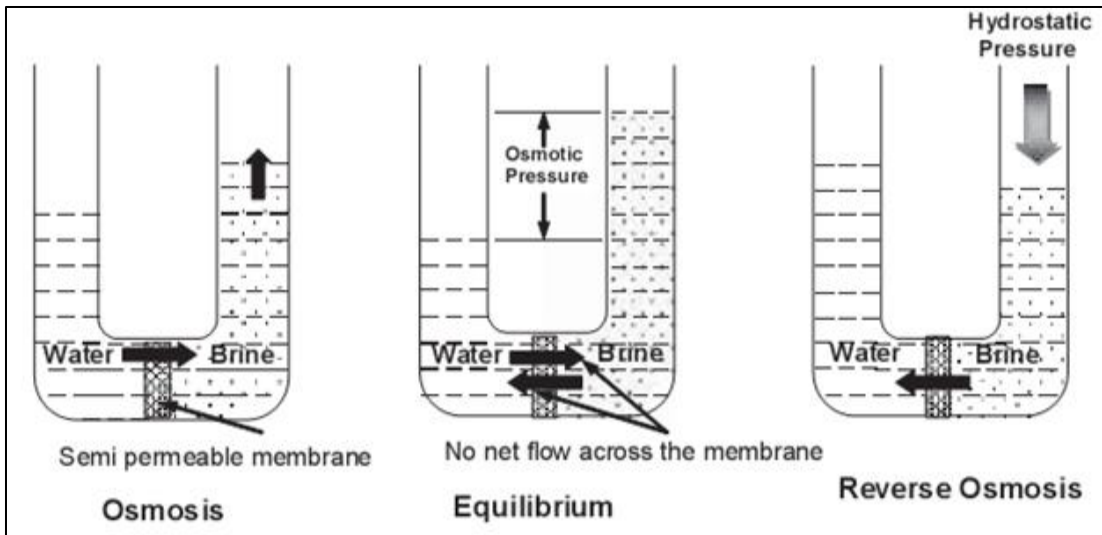
Figure 9: The Concept of Reverse Osmosis (Adapted from: Gullinkala et al., 2010)

As the process goes on, the concentration of solute near the membrane increases due to the accumulation of solute particles on the membrane surface till a point called concentration polarization is reached [this phenomenon will be further discussed in Chapter 3]. The concentration polarization further increases the osmotic pressure of the system and at a certain pressure level, the applied hydrostatic pressure is completely neutralized by the osmotic pressure. Then, no more solvent can be forced to flow from the higher concentration side to the lower concentration side. A further increase in the applied pressure will lead to foul the membrane by precipitating salts and other undissolved materials that will permanently impede the membrane. Hence, through the RO process, compared to input water supply, 10% to 50% product water is obtained (El-Dessouky & Ettouney, 2002; Gullinkala et al., 2010).

The major parameters that define the efficiency and performance of an RO desalination process are osmotic and operating pressure, salt rejection ratio, and

product or permeate recovery (El-Dessouky & Ettouney, 2002). The several stages involved in RO desalination process are shown in Figure 10.
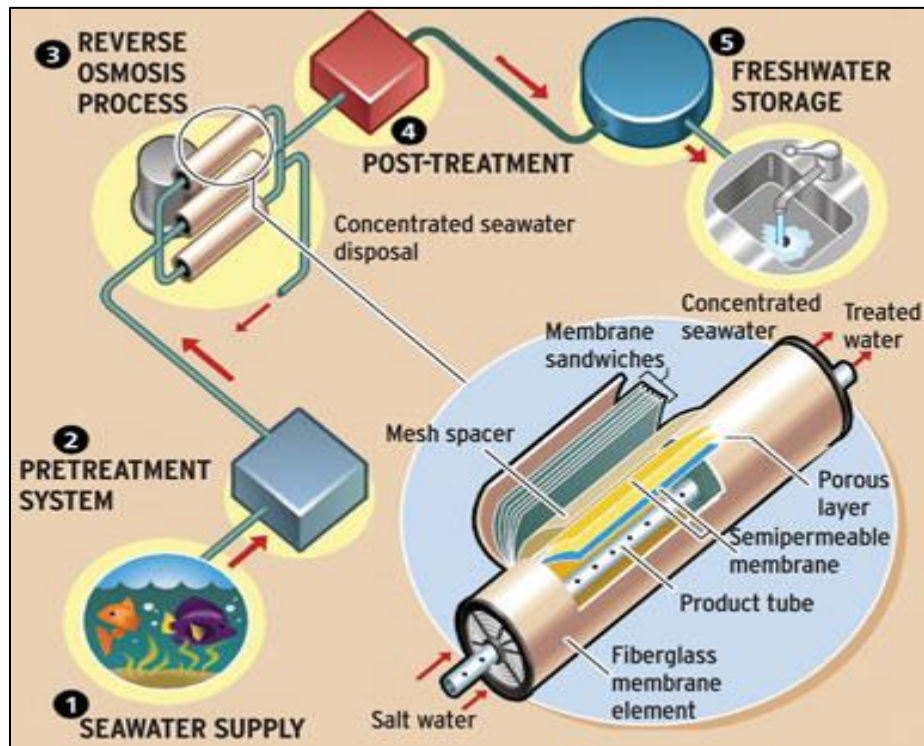
Figure 10: The Several Stages Involved in the RO Desalination Process (Adapted from: Levin, 2004)

2.2.2- Membrane Distillation (MD)

Membrane Distillation (MD) has first appeared in the late 1960s (Bodell, 1963; Weyl, 1967; Mathioulakis et al., 2007; Findley et al., 1969), However, the process has never progressed to be used commercially because of the cost of the membranes and the process at that time (Gray et al., 2011).

MD is a micro-porous hydrophobic membrane based non-isothermal process. In the MD process, fresh water is produced by transporting water vapors from a warm saline water solution through a porous hydrophobic membrane having pore sizes in micrometer ranges. The transportation of water vapors across the membrane is carried out in response to a change in partial pressure due to a thermal gradient. Though the MD technology is still in its research and developmental stage, yet, in contrast to the RO technology, the MD process produces more than 99% salts-free water (Gullinkala et al., 2010).

The efficiency of the MD process is greatly influenced by the MD module design, the hydrophobic membrane, and the thermal management of the MD system. The MD process utilizes various types of configurations to recover the water vapors as they pass through the membrane. Among these configurations, Direct Contact Membrane Distillation (DCMD) and Air Gap Membrane Distillation (AGMD) are the most frequently used desalination configurations. Additionally, Vacuum Membrane Distillation (VMD) and Sweeping Gas Membrane Distillation (SGMD) methods are other alternatives applied for stripping volatile organics or dissolved gases (Gullinkala et al., 2010). Figure 11, 12, 13, and 14 illustrate schematics of the four configurations of the MD process.
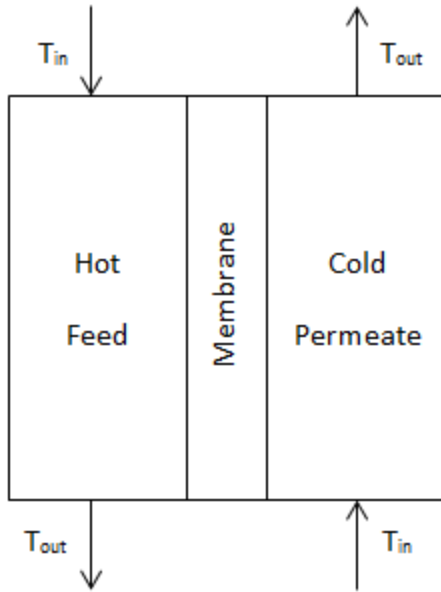
Figure 11: Direct Contact Membrane Distillation (DCMD) Configuration
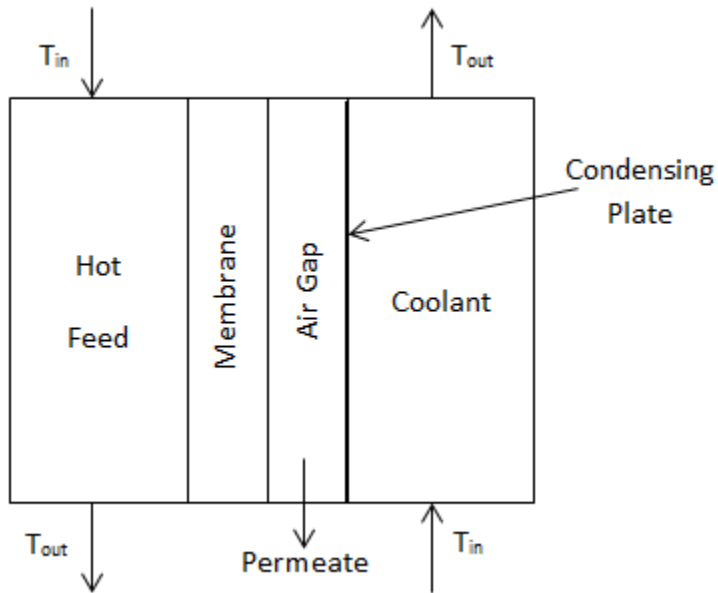
Figure 12: Air Gap Membrane Distillation (AGMD) Configuration
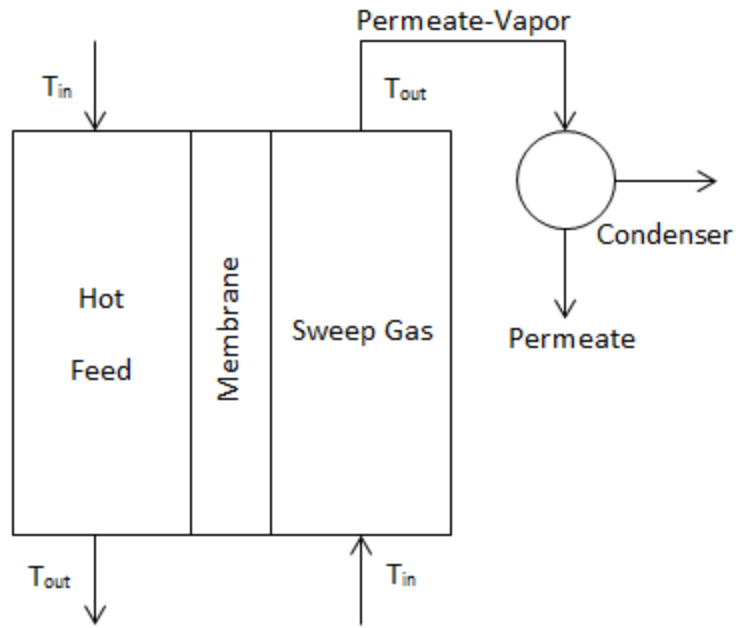
Figure 13: Sweep Gas Membrane Distillation (SGMD) Configuration
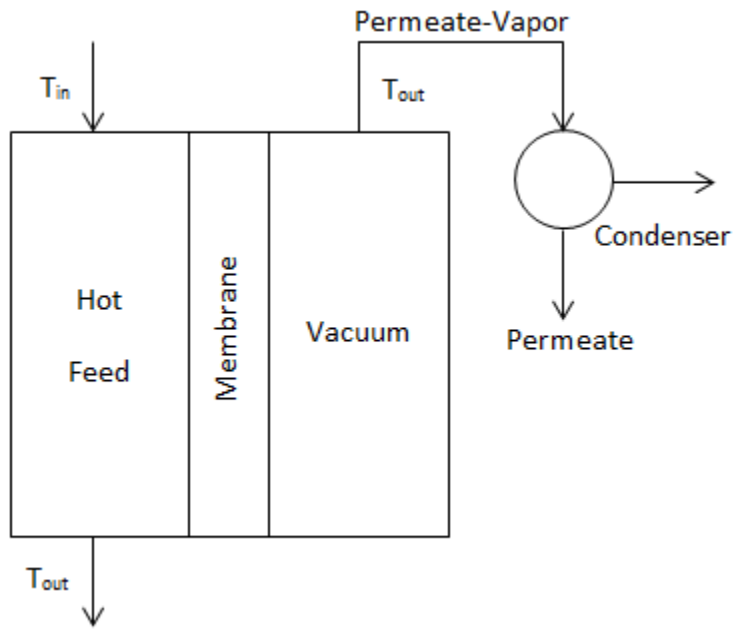
Figure 14: Vacuum Membrane Distillation (VMD) Configuration

2.2.2.1- Direct Contact Membrane Distillation (DCMD)

The membrane used in the DCMD is the only membrane which is directly in contact with the liquid phases (the hot feed and the cold permeate). The temperature of the feed solution is higher than that of the cold solution or the permeate to create a driving force for the vapor transport across the membrane. If the purpose of MD is to desalinate seawater or brine solutions, the permeate is fresh water. Moreover, the membrane in DCMD is the only barrier between both liquids in the process; therefore, the permeate flux in DCMD is relatively high. In addition, the heat loses in DCMD are also relatively high. Furthermore, DCMD is best used for applications where aqueous solutions are needed to be concentrated (Lawson & Lloyd, 1996; Phattaranawik & Jiraratananon, 2001; Lawson & Lloyd, 1997; El-Bourawi et al., 2006; Martinez-Diez & Florido-Diaz, 2001; Martinez-Diez et al., 1999).

2.2.2.2- Air Gap Membrane Distillation (AGMD)

AGMD is a type of MD configurations where there is an air gap interposed between the membrane and the condensation surface to reduce the energy loss by heat conduction in the membrane. Due to the presence of an air gap, resistance to mass transfer in AGMD is higher than the other configurations. Moreover, this configuration has the highest energy efficiency. However, the flux obtained is generally low (Lawson & Lloyd, 1997). Furthermore, AGMD is suitable for all DCMD applications. In addition, it can be employed to separate other volatile substances such as alcohols from an aqueous solution which is not possible in DCMD

as those substances are likely to wet the membrane at the permeate side due to the lower surface tension and/or the smaller contact angle with the membrane. Since there is an air gap in the AGMD configuration, the permeate is not in direct contact with the membrane; hence, there is no danger of membrane wetting at the permeate side (Lawson & Lloyd, 1996; El-Bourawi et al., 2006).

2.2.2.3- Sweep Gas Membrane Distillation (SGMD)

The SGMD configuration is one in which stripping gas is utilized as a carrier for the vapor that is formed and later condensed in an external condenser, which adds to the costs of the process (Rivier et al., 2002). Like AGMD, it can be used for the removal of volatile substances other than water. Compared to AGMD, the resistance to mass transfer is less in SGMD. However, the water vapor can be diluted by the sweep gas which results in higher demands on the condenser capacity. Also, if the flow rate of the sweep gas is relatively small, heat transfer across the membrane will cause the temperature of the sweep gas to increase, which is another disadvantage as it leads to higher vapor pressures at the permeate side; hence, a lower driving force (Lawson & Lloyd, 1996; El-Bourawi et al., 2006; Rivier et al., 2002; Basini et al., 1987; Khayet et al., 2000; Garcia-Payo et al., 2002).

2.2.2.4- Vacuum Membrane Distillation (VMD)

VMD is a configuration in which the permeate side is air or vapor under reduced pressure. This type of configuration is useful when volatiles are being removed from

a liquid. The vapor permeate in the VMD is eliminated continuously from the vacuum chamber to form vapor pressure difference across the membrane. Moreover, an external condenser is needed as for SGMD (Bandini et al., 1992).

2.2.3- Membrane Based Technologies: Challenges

Though membrane based desalination technologies (particularly large scale RO) offer a good alternate, drought-resistant source of potable fresh water, yet, the widespread and intensive application of all such technologies have identified various challenges. According to Saif (2012) and Meerganz von Medeazza (2005), these challenges and their possible impairments linked with the membrane based technologies can be categories based on their association with inputs, with outputs, and with the process related challenges as depicted in Figure 15.
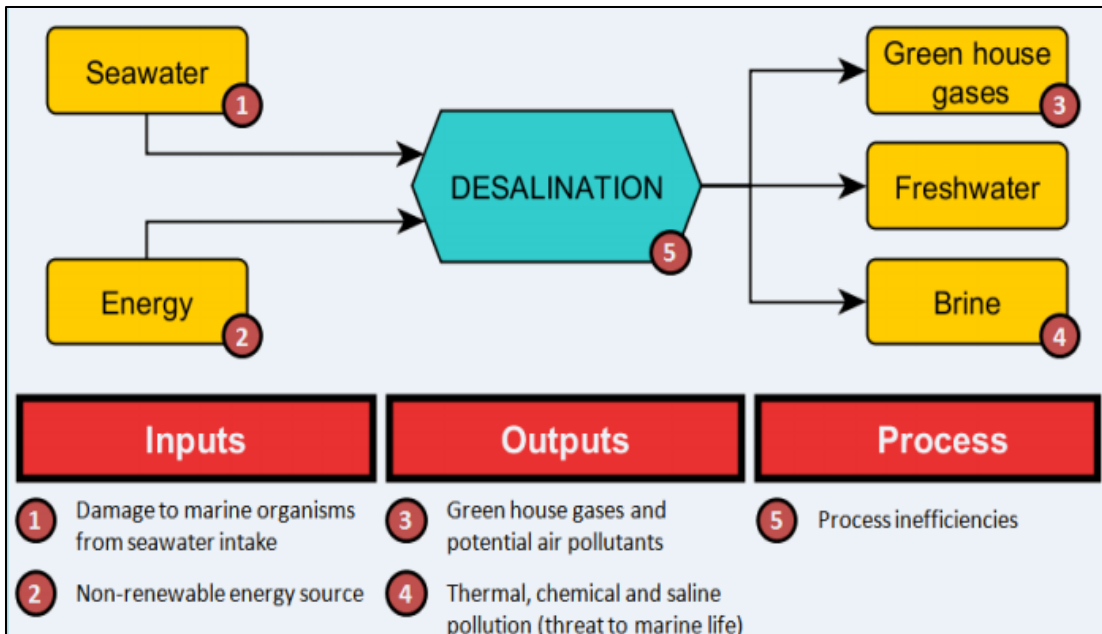
Figure 15: The Challenges Related to Membrane Based Desalination Technologies

(Adapted from: Saif, 2012)

The major concerns associated with the input of membrane based desalination are the environmental impacts such as the impingement and degradation of marine life primarily within the vicinity of seawater intakes. Also, the rapid depletion of non-renewable energy sources such as oil and natural gas and the ever-increasing energy prices are other major present and future challenges for the desalination industry including membrane based technology production units (Bourne, 2008; Saif, 2012; Ghaffour et al., 2013).

The challenges associated with the membrane based desalination processes are mostly related to the efficiency of the desalinating medium (membrane) and its maintenance. Misdan et al., (2012) assert that the major factors that deteriorate the overall

performance of a membrane based desalination unit are membrane fouling problem, boron rejection, and chlorine attack. Intensive research is underway particularly on thin-film composite (TFC) RO membrane to overcome its major issues and hence to improve the throughput of the membrane based desalination units.

Moreover, the major concerns associated with the output of the membrane based desalination technologies are the environmental impacts associated with the discharge and disposal of the highly concentrated hot brine and the variety of chemical agents added to the brine to improve flocculation or prevent foaming during the desalination process. The amount of brine discharged from the desalination plants varies from 15 to 85 percent of the feed flow, depending on the feed water salinity and the desalination technology used. Moreover, the quantity of brine produced by the desalination processes is directly proportional to their recovery rate (the ratio of the product water to the feed water). In general, membrane based technologies have a higher recovery rate than thermal desalination processes which results in a higher salt amount in the concentrate (Younos, 2005). Table 5 shows the types of effluents from the desalination processes.

Table 5: The Types of Effluents from the Desalination Processes (Younos, 2005)

Technology Type	Discharge Flow	Content
RO/ Thermal/MD	Seawater concentrate (Brine)	Salinity and Heat
	Chlorination	Chemical
	Antiscalants	Chemical
RO	Filter backwash	Suspended solids
	De-chlorination	Chemical
	Coagulants	Chemical
	Flocculants	Chemical
Thermal	Corrosion inhibitors	Chemical
	Antifoaming agents	Chemical

The disposal of the hot brine containing chemical additives imparts drastic impacts to the marine environment. Marine desertification of fragile ecosystems such as corals and their safeguard are major challenges that are facing the whole desalination community worldwide (Meerganz von Medeazza, 2005; Bourne, 2008).

In addition to the aforementioned challenges, Bourne (2008) argues that the land use setting and aggregate impacts from the increased numbers of desalination facilities

and the facility ownership (that is potable water production and its distribution issues) are other major concerns that are also presently faced by the desalination community.

2.2.4- Hydrophilic versus hydrophobic Membranes

Hydrophilic and hydrophobic are two distinct characteristics generally attributed to water-activated chemical grouts. The hydrophilic grouts, generally found in concrete and soil, have the ability to absorb water, while the hydrophobic grouts exhibit opposite properties by pushing away the water. Both hydrophilic and hydrophobic membranes are manufactured from synthetic hydrophilic and hydrophobic polymers and are largely used in various water filtering applications including membrane desalination (LaPorte, 2000).

Hydrophilic membranes can be wetted with water and because of their compatibility, they are the preferred filters for aqueous solutions. An important feature of the hydrophilic membranes is their ability to restrict the passage of any gas molecules once they are wetted till the applied pressure surpasses the bubble point and drives out the liquid molecules from the pores of membrane. Also, LaPorte (2000) and Pulat & Akdoan (2002) point out that membrane surface tension, pore size, diffusivity, lubriciousness, biocompatibility, degree of swelling of membrane material, and amphiphilic character are important parameters that determine the diffusion and filtration performance of the hydrophilic membranes.

In contrast to hydrophilic membranes, hydrophobic membranes can only be wetted by low surface tension organic solvents such as alcohol. Since organic solvents do not impede the flow of aqueous solutions in wetted condition, they are not suitable for large scale aqueous filtration processes and are best suited for gas filtration and venting processes.

2.2.5- Membrane Characterization Techniques

Membrane characterization is the evaluation of various structural and morphological properties of a membrane such as membrane pore size, pore distribution, smoothness of membrane surface, surface porosity, layer thickness, free volume, and crystallinity. Membrane characterization is a very essential step to ascertain the suitability of a membrane for a specific separation need. In addition, through membrane characterization, the efficiency and performance of a membrane for a particular application can also be predicted (Chen et al., 2011).

The characterization techniques to determine various morphological characteristics of a porous membrane can be broadly divided into two main categories:

- Characterization techniques that determine the membrane structure related parameters such as pore size, pore distribution pattern, smoothness of membrane surface, surface porosity, and membrane thickness.

- Characterization techniques that determine the characteristics of a membrane such as the actual separation parameters by applying solutes that generally stay inside the membrane.

As the transportation of mass takes place by solution diffusion and then the separation mechanism occurs due to the solubility or the diffusivity gradient, different characterization techniques are used for non-porous membranes. These include permeability methods, differential scanning, calorimetric or differential thermal analysis techniques, X-ray photoelectron spectroscopy (for surface analysis). All of which are used to determine different structural and content related parameters of non-porous membranes (Chen et al., 2011).

Depending on the type of application and the physical characteristic of a membrane, several methods regarding membrane characterization have been developed:

- For membrane pore characterization, thermoporometry, biliquid permporometry, molecular and weight cut-off techniques can be used as investigated by Tam & Tremblay (1991) and Kim et al. (1994). In addition, scanning electron microscopy (SEM), transmission electron microscopy (TEM), X-ray ultramicroscopy (XuM) and atomic force microscopy (AFM) (Hilal et al., 2005; Shirazi et al., 2013) are used.

- For characterization of membrane surface properties, the captive bubble technique, the sessile drop method (Zhang & Hallstrom, 1990; Zhang et al., 1989; Kim et al., 2009), and the atomic force microscopy (AFM) (Hilal et al.,

2005; Shirazi et al., 2013) can be used. In addition, the scanning optical microscopy (SOM) technique can also be used to determine the uniform particle distribution and relatively uniform surface properties of membranes (Hosseini et al., 2012).

2.2.6- Water Quality in Membrane Based Desalination

Water purity is a relative feature of the water and due to the polar nature of water molecules, it is quite difficult to maintain the absolute pure water as stated by Reid (1996). Common water impurities that affect the water quality are turbidity, dissolved salts, metals (including radionuclides), pathogens, organic compounds and microorganisms. The conventional water treatment methods are not proficient to completely remove all these contaminations and even high quality potable water may contain several such impurities and may create harmful effects (Karakulski et al., 2002).

Turbidity is a measure of the relative clarity of a liquid. A solution is turbid due to the presence of macro particles and macro organisms such as mussels, barnacles, algae. Turbidity and fine particulates in the feed water have to be removed prior to desalination in order to have a smooth operation. Moreover, the high TDS in the feed water or the high salinity is a major issue in most desalination technologies. In RO processes, when the feed water salinity increases, the driving force for the mass transport across the membrane is significantly reduced as the operating pressure for RO process depends on the feed salinity (Raluy et al., 2006; Cipollina et al., 2009);

hence, lower flux is generated. Also, this allows leakage of salts through the membrane pores to the permeate side which influences the quality of the distillate. Moreover, the high salt concentration in the feed water results in increased concentration polarization (a boundary layer parallel to the membrane surface), increased scaling, thicker cake layer on the membrane, and reduced performance due to increased osmotic pressure (Cath et al., 2004). On the other hand, in MD processes, high feed salinity leads to the development of a concentration boundry layer (concentration polarization) that is parallel to the temperature bundry layer on the membrane surface. The concentration polarization reduces the feed–membrane interface partial vapor pressure which only slightly reduces the driving force for evaporation (Cath et al., 2004). In addition, high amounts of hardness ions that are soluble in the feed (such as seawater) to a membrane based technology could lead to their precipitation on the membrane which will result in scaling and membrane fouling. Depending on the desalination technology, different types of salt scale could form (Abdel-Jawad, 2011):

- Alkaline soft scale: $CaCO_3$ and $Mg(OH)_2$.
- Non-alkaline hard scale: $CaSO_4$, $CaSO_4.\frac{1}{2}H_2O$, and $CaSO_4.2H_2O$.

To prevent scale formation, certain anti-scalant additives are added to the feed including polyphosphate, polyphosponates, polycarboxylic acid, H_2SO_4 and HCl (Hassan et al., 1998).

The application of various membrane based technologies remarkably improved the potable water quality. The RO process generally softens the water and is capable of removing almost all classes of pathogens along with natural organic materials (NOMs), trace metals, and total dissolved solids (TDSs) (Gagliardo et al., 1998). Very few cases have been reported where few microorganisms particularly viruses can escape through the micro-pores of RO membrane (Reid, 1996).

Moreover, membrane based membrane distillation (MD) process can produce ultra-pure high-quality water for certain industrial applications (Elimelech & Phillip, 2011; Karakulski et al., 2002). In addition, various studies to investigate the water quality enhancement features of membrane based desalination technologies (like RO, MF, NF and UF) show that the quality of potable water has been greatly improved by employing these technologies either alone or in combination with similar or different technologies (Suzuki et al., 1998; Karavoltsos et al., 2008; Kent et al., 2011; Van der Bruggen et al., 1998).

However, in terms of water quality, the only drawback with the membrane based process is the occasion contamination of the pores of RO membrane. In such cases, the membrane itself becomes contaminated with microorganisms and hence adds, rather than removes, live bacteria (Reid, 1996).

2.3- Environmental Footprint of Desalination Process

Though the desalination process is a reliable and an efficient alternative to produce potable water especially in the GCC as in those countries, it accounted for almost half of the world's production capacity in 2012 (Dawoud & Al Mulla, 2012); yet, an increasing trend toward desalination have also raised environmental issues associated with the process. The major environmental concerns associated with desalination process as investigated by Bourne (2008) and Younos (2005) are:

- Ecological impacts linked primarily with seawater intakes.
- Ecological and environmental impacts associated with the discharge of hot brine along with various chemical agents added to the brine (to improve flocculation or to prevent foaming).
- Emission of greenhouse gases (GHG) due to burning of fossil fuels in conjunction with power plant and water desalination process.

The first two issues have already been discussed in Section 2.2.3. However, the emission of greenhouse gases is briefly discussed in the next section.

2.3.1- Green House Gas (GHG) Emissions

As mentioned in Chapter 1, greenhouse gases (GHGs) are gases that trap heat in the earth's atmosphere. As a consequence, they cause global warming. The major greenhouse gases are carbon dioxide (CO_2), methane (CH_4), nitrous oxide (N_2O) and

fluorinated gases such as hydrofluorocarbons (HFCs), perfluorocarbons (PFCs), and sulfur hexafluoride (SF_6). Generally, a natural balance in the quantities of these greenhouse gases exists at the upper atmosphere that maintains the balance of energy transfers between the atmosphere, space, and land. However, the last century's industrial growth, deforestation, and a number of other related factors have intensified the emission of greenhouse gases and ultimately resulted in global and local climate variability and permanent changes (Voutchkov, 2008).

The energy is the prime driving factor while making decisions with regards to any water treatment technology and subsequent water management system (Dolnicar & Schafer, 2006). The large amount of energy requirements for the desalination process, particularly for thermal desalination of water, contributes to the emissions of air pollutants and greenhouse gases. Hence, concerns about their associated environmental impacts have been raised.

Carbon footprint (CF) is referred to the total emission of greenhouse gases measured in million metric tons of carbon dioxide emitted per year ($MMTCO_2e$). The carbon footprint of the desalination process depends on the following two key variables:

1) The amount of electric power required to smoothly run a desalination unit in its full capacity.

2) The second type of source such as hydropower, fossil fuels, wind, solar, etc. used to produce the electricity supplied to the plant.

The total required amount of energy for a desalination process largely depends on the type of desalination technology and the composition of saline water. Thermal technology based desalination generally requires more energy (4 - 6 kWh/m^3 of potable water along with steam) than membrane based desalination units (1 - 6 kWh/m^3 of potable water on average) (Chaudhry, 2012). Moreover, the higher the TDS, the higher the required energy to produce high quality distillate. Therefore, the greater the amount of energy consumed in a desalination process and its subsequent water management, the larger the CF values are. Also, in contrast to conventional non-renewable energy sources, only a nominal amount of GHG emissions takes place from renewable energy sources. In addition, a major portion of the GHG emissions is also associated with cogeneration desalination units (Dolnicar & Schafer, 2006). Generally, compared to stand alone desalination plants, cogeneration plants release higher emissions to the atmosphere due to the massive energy used to produce electricity.

Therefore, several studies (Raluy et al., 2006; Raluy et al., 2004; Bushnak, 1989; Dickie, 2007) have shown that the emissions from desalination plants vary depending on the type of fuel used, the type of desalination technology employed, the boiler efficiency, the feed salinity, and other operational parameters. Table 6 illustrates the airborne emissions from different studies on several desalination plants.

Table 6: The Airborne Emissions from Different Studies on Several Desalination Plants

Gas Emitted	Emission from MSF (kg/m^3)	Emission from MED (kg/m^3)	Emission from RO (kg/m^3)	Reference
CO_2	23.41	18.05	1.2 – 1.78	Raluy et al. (2006)
NO_x	28.3	21.43	4.05 – 2.74	
SO_x	28.1	26.31	11.13 – 9.08	
CO_2	37.0	-	6.0	Raluy et al. (2004)
NO_x	0.06	-	0.009	
SO_x	0.09	-	0.005	
CO_2	10 - 20	3.2 – 17.0	2.8 – 3.6	Bushnak (1989)
CO_2	23.41	18.05	1.78	Dickie (2007)

With the increasing water demand, especially in Qatar, the fossil fuel consumption in desalination plants will continue to increase unless some measures to reduce air emissions are taken. The emission of GHGs from the desalination process can be considerably reduced and offset by adopting a number of strategies. Few of such strategies are as follows:

− Adopting and implementing an energy efficient design and standard operating procedures (SOPs).

- Exploring and utilizing renewable energy sources in the locality of the desalination unit (Cooley & Heberger, 2013) or using waste heat from power plants or petrochemical industries.

- Using carbon dioxide in the desalination production, particularly in RO permeate, in combination with calcium hydroxide or calcium carbonate in order to form soluble calcium bicarbonate which adds hardness and alkalinity and protects from system corrosion.

- Sequestrating CO_2 through vegetation.

- Using warm cooling water in the RO process as desalination of warmer seawater requires less energy to overcome vapor pressure (Voutchkov, 2008).

2.4- Membrane Distillation Desalination: An Emerging Technology

The MD desalination was first known in 1963. Even though, it still has not been implemented at industry level (Pangarkar et al., 2011). Nevertheless, as mentioned earlier, using MD process, more than 99 % salt rejection can be obtained (Gullinkala et al., 2010; Mohammadi, & Safavi, 2009; Gryta, 2010). Also, being the low-grade thermal energy based process with high purity distillate, MD desalination technology is consider as an emerging technology and a better alternative for future water desalination (Meindersma et al., 2006). In addition, one of the major advantages of MD over other conventional processes such as RO or the thermal processes is its

lower operating temperature which directly affects the energy consumption (Escobar & Van der Bruggen, 2011). Furthermore, it is worth mentioning that using a renewable source of energy or waste heat energy from a thermal process or petrochemical processes can make MD a more efficient and an environmentally friendly process. However, compared to the other desalination processes, Martinez-Diez et al., (1999) and Bui et al., (2007) state that the permeate flux is low in MD. Moreover, due to the fact that the membranes can be fouled, as most feed solutions contain sparingly soluble salts (mainly $CaSO_4$ and $CaCO_3$), the flux is expected to become even less. For a process to become commercialized, high flux with extended membrane life is highly required to achieve sustainable operation. Throughout this context, by conducting experiments on a bench scale DCMD unit, the fouling of the MD membrane is evaluated in more details.

2.5- State of the Art in Membrane Distillation

Theoretically in the literature, the MD desalination is considered as the best substitute for desalination process. Compared to other technologies (thermal and membrane based), there are a number of features that makes the MD desalination technology the preferred desalination technology:

- − It is a low-grade thermal energy based technology which is more economical than the other desalination technologies.

- In contrast to the pressure driven RO process, it is a vapor pressure difference based process.

- It is a micro-porous hydrophobic based technology; hence, in contrast to the other membrane based technologies, fouling is not a major problem for MD desalination.

- Though pretreatment has an important positive influence on MD, yet, MD is not sensible to high concentration feed (Pangarkar et al., 2011).

The concept of MD process is not new and it has been known for almost fifty years. However, most of the MD studies were done either on pilot scale or bench scale units. There were lots of advancements regarding the MD technology including the developments of suitable polymeric membranes and the developments of heat and mass transfer models. The historical development and the recent research on MD are presented in this section.

Findley (1967) was the first to use the MD process to separate volatile compounds from water. However, the membranes used were not suitable for the tests. Nevertheless, it was concluded that MD can become a feasible technology if it was of lower cost compared to the conventional technologies, if the life time of the process is extended, and if higher temperatures were used. Furthermore, Findley et al. (1969) have later enhanced the hydrophobicity of the membrane using a material called Teflon. Still, MD was not suitable enough to be commercialized. By the 1980s, MD appeared to be a candidate technique for separation purposes.

Cheng (1981) and Cheng & Wiersma (1982) have examined the separation of fresh water from salt water using a composite membrane structure. The composite membrane consisted of a thin hydrophobic micro-porous layer that was supported by a thin hydrophilic layer which prevented membrane wetting.

Jonsson et al., (1985) were the first to theoritically introduce the heat and mass transport models in Air Gap MD. However, the models didn't take into account the effect of temperature polarization on the heat and mass transport in MD systems.

Drioli & Wu (1985), Drioli et al., (1986), and Drioli et al., (1987) have experimentally studied the fundamental MD parameters such as the permeate flux, temperature, and concentration relationships. The results of their study have shown that Membrane Distillation can be feasible in concentrating saline solutions and producing fresh water. In addition, Calabro et al. (1991) have investigated the applicability of membrane distillation in waste water treatment. Moreover, Calabro et al. (1994) have experimentally studied the suitability of using MD in concentrating orange juice. They have developed a model to fit the experimental results based on Knudsen diffusion. In their model, the concentration polarization effect was neglected.

Sarti et al., (1985), Sarti & Gostoli (1986), Gostoli & Sarti (1987), Gostoli et al. (1987), and Bandini et al., (1991) have produced fresh water from saline water using Membrane Distillation. Different configurations were tested using flat-sheet polytetrafluoroethylene (PTFE) membranes. The effect of the inlet temperature of the

hot and cold streams on the permeate flux was examined. Moreover, different mathematical models were developed that proved to be in good agreement with their experimental data.

Fane et al. (1987), Schofield et al. (1987), and Schofield et al. (1990) have investigated the production of distilled water from aqueous solutions. A heat and mass transfer model of the DCMD process was developed. The significance of the temperature polarization effect in MD was highlighted. Moreover, they have concluded that the presence of solute in the feed (salt water) decreases the permeate flux by reducing the vapor pressure.

Kubota et al. (1988) have used plate-and-frame type MD modules to desalinate seawater. Their experimental results showed that the heat loss was large. They recommended the development of a suitable membrane module with high heat efficiency.

Schneider et al. (1988) have studied the morphology of the MD membrane. The MD membrane pore size, its porosity, and the effect of feed concentration on the permeate flux were investigated. At that period of time, in 1988, MD was still considered as a not competitive process with the large conventional desalination technologies; however, it can be used with the available low-grade waste heat.

Wu et al. (1991) have used polyvinylidene fluoride (PVDF) capillary membrane for treating the wastewater in taurine production. Their results showed that MD is a promising technique in the treatment of industrial wastewater.

De Zaarate et al. (1993) have examined the mass transport in MD using a stirring device to study the effect of stirring rate on MD flux. The experiments were performed using three PTFE membranes and three sodium chloride (NaCl) solutions with different concentration as feed to the process. A model has been developed that showed good agreement with the experimental data.

Phattaranawik & Jiraratananon (2001) and Phattaranawik et al. (2003) have analyzed the role of spacers in improving the heat transfer in a DCMD process. As a result, higher fluxes were achived when spacers were used as well as increased temperature polarization coefficients.

Hsu et al. (2002) have used both synthetic NaCl solution and seawater as feed to a flat sheet DCMD process to investigate the differences in the permeate flux, the quality of distillate produced, and the fouling of the membrane. The hot water inlet temperature was 45 ^{o}C and the cold water inlet temperature was 20 ^{o}C. The feed flow rate was kept at 3.3 L/min and a PTFE membrane of 0.2 μm was used. It was concluded that fouling caused a flux decay. Also, concentration polarization was significant only when NaCl solution was used. However, this was not the case when seawater was used as the percentage of solute in the sweater was relatively low. On the other hand, the investigation showed that temperature polarization had an effect on fouling only when seawater was used as feed. The membrane fouling was obvious when SEM analysis was carried out. Furthermore, to clean the fouled membrane and restore the

decay in flux, ultrasonic cleaning technique was employed. This study showed that this method can extend the life-span of MD membranes successfully.

Cath et al. (2004) have worked on a vacuum enhanced DCMD unit using a feed temperature of 40 °C. The results of their experiments showed that the enhanced configuration offered less temperature polarization effect. This was attributed to the better mixing and better mass transport due to both higher permeability through the membrane and a total pressure gradient across the membrane. The experiments were carried out using NaCl solution and synthetic sea salt solution. It was concluded that a salt rejection of more than 99.9% was achieved in almost all cases.

Gryta et al. (2006) have used a DCMD process to separate saline wastewater that contained NaCl, protein, and effluents produced from the regeneration of ion exchangers. During the process, severe membrane fouling was encountered. It was concluded that fouling was observed due to the heating process of the feed solution and the increasing concentration of solutes. They suggested that in order to remove foulants from the feed, wastewater has to be treated prior to being used in the MD process. Moreover, the morphology of the membrane used and the fouling layer composition were studied. This was done using scanning electron microscopy coupled with energy dispersion spectrometry (SEM-EDS).

Criscuoli et al. (2008) have studied three self-made bench-scale flat modules which are longitudinal-flow, transversal-flow, and cross-flow membrane modules using polypropylene membrane with a pore size of 0.2 μm and pure water as feed to the

systems. For a DCMD and a VMD process, the effect of the operating temperatures and the flow rates of the hot and cold streams on the flux were studied as well as the evaporation efficiency and the energy consumption (DCMD), and the vacuum applied at the permeate side (VMD). The performance of the DCMD and the VMD processes was later compared. Criscuoli et al. (2008)'s results showed that the longitudinal-flow module and the transversal-flow module generated similar fluxes and that the cross-flow module was the most efficient design for generating high fluxes with moderate energy consumptions. Also, according to their study, the performance of the VMD configuration was better than that of the DCMD. The highest flux obtained was 56.2 kg/m^{2}h with the cross-flow module using the VMD process at a feed flow rate of 235 L/h, a feed temperature of 59.2 °C and a permeate pressure of 10 mbar.

Criscuoli et al. (2008) have studied the treatment of water containing different types of dyes using VMD. The effect of the feed temperature, flow rate, and concentration on the permeate flux and on the rejection has been investigated. A complete rejection was obtained using the MD process. Also, it was concluded that flux increases with feed temperature and flow rate. Moreover, to examine the effect of fouling on the VMD performance, experiments with water as feed have been carried out before and after the experiments with dyes. The results showed that the permeate fluxes using water as feed were higher than those obtained with dyes. According to the study, this was attributed to an interaction between the dye solution and the polymeric

membrane material. Nevertheless, the initial fluxes were recovered after prolonged cleaning of the membrane with only water.

Feng et al. (2008) have used PVDF nanofiber membrane to produce drinking water (NaCl concentration <280 ppm) from a 6 wt.% NaCl solution by AGMD process. They were the first to use electro-spun nanofiber membranes in MD. The results showed that the permeate fluxes were equivalent to those obtained by commercial microfiltration membranes (5–28 kg/m^{2}h). They claim that this new approach may enable the MD process to compete with the conventional seawater desalination processes such as thermal distillation and reverse osmosis.

Gryta (2008) has studied the demineralization of tap water (from a lake) using DCMD. Alkaline scaling was formed on the membrane surface and was attributed to the hot feed temperature that caused the decomposition of bicarbonates presented in the feed water. Scanning electron microscopy (SEM) coupled with energy dispersion spectrometry (EDS) was used to analyze the deposits.

Hou et al. (2010) have investigated the removal of fluoride from brackish groundwater by DCMD using a self-prepared hollow fiber PVDF membrane. The results of their experiments showed a high rejection of inorganic salt solutes. The maximum flux obtained was 35.6 kg/m^{2}hr at a hot inlet temperature of 80 °C and a cold inlet temperature of 20 °C. Also, according to their study, the feed concentration does not influence the permeate flux and the fluoride rejection. Moreover, a rapid decline in the module efficiency was faced as the natural groundwater was directly

fed to the process which caused calcium carbonate ($CaCO_3$) to precipitate; hence, clogging the hollow fiber inlets causing membrane surface fouling. This was reduced by acidification of the feed water. Later, the experimental results showed that the efficiency of the membrane module declined gradually when the feed continued to be concentrated. This was attributed to the deposition of CaF_2 on the surface of the PVDF membrane.

Pal & Manna (2010) have studied the removal of arsenic from contaminated groundwater using solar driven DCMD. Flat sheet PTFE and polypropylene (PP) membranes were used in a cross-flow module. The effects of the initial arsenic concentration in the feed, the feed flow rate, and the operating temperature of the streams on the arsenic removal efficiency and flux were examined. The results of the study showed that the most influential factors that have affected the flux were the inlet temperatures of the feed and distillate. Moreover, according to Pal & Manna (2010), the removal efficiency of arsenic was about 100%. They claim that this was achieved without facing membrane wetting even after 120 h of operation.

He et al. (2011) have used nine flat sheet membranes that are commercially available for a DCMD system to examine the effect of membrane difference in terms of type and pore size on the permeate flux and conductivity. They concluded that for the MD process, PTFE membranes are more suitable than PP or PVDF membranes as higher hydrophobicity (due to the contact angle (CA) and liquid entry pressure (LEP) measurements) and higher permeate flux were observed. In addition, the effect of

several operating parameters including the flow mode, the flow rate, the temperature, and the NaCl concentration was examined under the following conditions: hot side inlet temperature of 60 ^{o}C, cold side inlet temperature of 20 ^{o}C, and hot and cold side flow rate of 0.6 L/min for PTFE membrane of pore size 0.22 μm. They concluded that the permeate flux increases with an increase in temperature; however, it decreases with an increase in NaCl concentration. Also, the flux increases with flow rate. Moreover, the counter-current flow mode showed a slightly higher flux than the co-current flow mode.

Hwang et al. (2011) have investigated the effect of module dimensions on the performance of a DCMD process using a PTFE membrane. Membrane characterization was performed and the results of the liquid entry pressure (LEP), the contact angle (CA), the diameter of the pore, the membrane porosity, and the pore size distribution were used to develop a two dimensional (2D) model comprising mass, energy, and momentum balance to predict the permeate flux. In addition, co-current and counter-current flow modes were studied. The results of the study showed that the flux increases linearly with feed temperature and velocity and it seems to reach maximum values asymptotically at high velocity. Also, the flux and the vapor pressure difference decreased with increasing NaCl concentration due to the formation of polarization layers on the membrane used.

Bahmanyar et al. (2012) have simulated the effect of feed inlet temperature, feed flow rate, and feed concentration on the flux in a DCMD process taking into account

the effects of these operating conditions on temperature and concentration polarizations. The simultaneous heat and mass transfer model has been solved numerically using MATLAB. Using the model, the optimum membrane thickness value was found to be from 30 to 60 μm.

Alkhudhiri et al. (2013) have investigated the permeate flux of four different salts including sodium chloride (NaCl), magnesium chloride (MgCl$_2$), sodium carbonate (Na$_2$CO$_3$), and sodium sulphate (Na$_2$SO$_4$) using PTFE membrane in an AGMD process. The influence of membrane pore size as well as the effect of the feed concentration, the feed inlet temperature, the cold water inlet temperature, and the feed flow rate on the permeate flux were studied. The results of the study showed that the flux decreases as the salt concentration and the cold water inlet temperature increase. On the other hand, it increases as the feed inlet temperature and flow rate increase.

Criscuoli et al. (2013) have analyzed the possibility of removing arsenic from water using VMD at low feed temperatures of 20 °C to 40 °C. The higher feed temperature resulted in the highest permeate flux. Moreover, different operating conditions were chosen; however, in all of the carried out experiments, the permeate was arsenic-free. In addition, the study showed that the flux and arsenic rejection was not affected by the concentration of arsenic in the feed and its type.

Zhang et al. (2013) were the first to develop a new model for VMD that measures the gas permeability as a function of membrane length to model the permeate flux. The model prediction was in good agreement with the experimental data.

Adham et al. (2013) have investigated the feasibility of using MD for the desalination of brines from thermal desalination plants. A bench-scale flat-sheet DCMD unit was used under various operating conditions with different MD membranes and three different feed solutions including synthetic NaCl solutions, brine from a thermal desalination plant, and seawater from the Arabian Gulf. The results of the study showed that MD is a feasible and an effective process that can consistently produce high quality distillate (with electrical conductivity of less than 10 μS/cm) from high salinity brines.

Hou et al. (2013) have studied DCMD for simultaneous boron removal and desalination utilizing a flat-sheet self-prepared PVDF membrane with a pore size of 0.22 μm and a contact angle of 82.6 ± 0.7°. Using seawater as the feed to the DCMD process (contaning 4.65 mg/L boron), the salt rejection was over 99.9%. Moreover, when the value of the concentration factor (CF) exceeded 4.0, scale deposits were formed on the membrane surface. This resulted in a drop in the permeate quality and a rapid flux decline. Hou et al. (2013) have recommended the addition of the antiscalant polyacrylic acid to delay the formation of the deposit layer.

Chen et al. (2013) have studied the incorporation of gas bubbling into DCMD to investigate its effects on the performance of MD particularly at high salt

concentrations in the feed. The results of the study showed that gas bubbling improved the flux by 26% when concentrating feed solution from 18% salt concentration to saturation. Also, gas bubbling delayed the occurrence of major decline in flux as a result of crystal deposition. Chen et al. (2013) have validated their results by membrane surface characterization using SEM.

Chapter 3: Direct Contact Membrane Distillation Theory

3.1-Membrane Distillation Configurations

As discussed earlier, there are four types of configurations of Membrane Distillation. These include: Direct Contact Membrane Distillation (DCMD), Air Gap Membrane Distillation (AGMD), Sweeping Gas Membrane Distillation (SGMD), and Vacuum Membrane Distillation (VMD) (Zhang et al., 2010). The difference between these configurations is the nature of the cold side processing of the permeate (Alklaibi & Lior, 2004; Smolders & Franken, 1989). Moreover, which configuration to be employed in MD operations depends on the composition of the permeate, its flux, and its volatility (Lawson & Lloyd, 1997).

The Direct Contact Membrane Distillation (Figure 11) is the only configuration where the membrane is directly in contact with the liquid phases (the hot feed and the cold permeate sides). The evaporation process takes place at feed/membrane interface. The vapor that passes through the pores of the membrane condenses and combines with the cooler solution at the permeate side of the membrane. DCMD is perceived as the simplest form of configuration that has the ability to produce considerable flux (Alkhudhiri et al., 2012). It is typically best suited for applications such as desalination and concentration of aqueous solutions (such as juice

concentrates), in which water is the main permeate component (Lawson & Lloyd, 1997; Martinez-Diez & Florido-Diaz, 2001; Ramaswamy et al., 2013).

As a result of its simple structure and high flux, compared to AGMD and SGMD, laboratory scale DCMD has been broadly studies (Lei et al., 2005). In fact, DCMD is the most popular configuration and more than half of the published references on membrane distillation are based on DCMD (Alklaibi & Lior, 2004; Lawson & Lloyd, 1997; Curcio & Drioli, 2005). However, their major setback in commercial applications is their low energy efficiency. Although DCMD is characterized with having low thermal conductivity, the driving force for mass transfer, which is the vapor pressure difference across the membrane, will also result in a significant conductive heat transfer through the membrane as a consequence of the small membrane thickness. Therefore, only a portion of the supplied heat energy is utilized for production.

Moreover, compared to the other MD configurations, DCMD has the highest heat conduction loss, which leads to having low thermal efficiency (the portion of heat energy that is used for evaporation) (Chernyshov et al., 2005; Meindersma et al., 2006).

Alkhudhiri et al. (2012) have stated that heat loss in DCMD might happen due to trapped air within the membrane, due to conduction, and lastly due to temperature polarization (will be discussed in Section 3.5).

In order to enhance the commercial applicability of the DCMD, Chernyshov et al. (2005) concluded that the membrane and the process parameters must be optimized in order to increase both the flux and the energy efficiency. Moreover, Ramaswamy et al. (2013) also claim that optimization of the membrane structure has the capability of increasing the DCMD flux.

In Air Gap Membrane Distillation (Figure 12), the hot feed solution is in direct contact with the feed side of the membrane only. On the other hand, there is a stagnant air gap that is introduced between the membrane and the condensation surface, in which the water vapor is condensed on (Alkhudhiri et al., 2012). This configuration has the highest energy efficiency. However, the flux obtained is generally low. The Air Gap configuration is the most versatile amongst the MD configurations and can be employed for most membrane distillation applications (Lawson & Lloyd, 1997).

Usually, the air gap in the AGMD is the controlling factor for the heat and mass transfer (García-Payo et al., 2000) due to its larger thermal and mass transfer resistances. Compared to the membrane, the air gap is typically much thicker (2,000-10,000 μm vs. 40-250 μm) and is also characterized with having a lower thermal conductivity (Chouikh et al., 2005; Liu et al., 1998). Hence, compared to DCMD, more energy is used in AGMD to evaporate the feed solution. However, due to the high mass transfer resistance across the air gap, AGMD has a lower flux than DCMD

with the same temperature difference between the hot and cold streams (Liu et al., 1998).

The Sweeping Gas Membrane Distillation (Figure 13) is a configuration in which a stripping gas (inert gas) is utilized as a carrier for the produced vapor. When volatiles are needed to be removed from an aqueous solution, SGMD is used (Rivier et al., 2002; Alkhudhiri et al., 2012). The vapor in SGMD is stripped from the feed by a gas stream and later condensed in an external condenser. Moreover, like AGMD, there is a gas barrier in SGMD that reduces the heat loss, but it is not stationary (Alkhudhiri et al., 2012). Therefore, the rates of mass transfer in SGMD are higher than AGMD as a result of the greater driving force that emanates from the reduced vapor pressure on the membrane permeate side. In addition, compared to AGMD, the heat loss through the membrane is less in SGMD. However, not only an external condenser, but also an air blower or compressed air is required in order to maintain the running of this configuration. As a result, it will lead to an increase in investment and running costs (Khayet et al., 2000).

It is worth mentioning that the SGMD configuration holds a very promise for the future, since it combines a relatively low conductive heat loss with reduced mass transfer resistance. Moreover, SGMD offers much higher permeate fluxes than AGMD, while at the same time maintaining high temperature polarization coefficient and evaporation efficiency. As noted by Ramaswamy et al., (2013), the advantages of SGMD over DCMD include: better selectivity performance, higher evaporation

efficiency, and smaller temperature polarization, even though at a lower permeate flux.

Vacuum Membrane Distillation (Figure 14) is a configuration in which the permeate side is air or vapor under reduced pressure (Bandini et al., 1992). This type of configuration is used when volatiles are being removed from an aqueous solution (Sarti et al., 1993; Alkhudhiri et al., 2012). The vapor permeate in VMD is eliminated continuously from the vacuum chamber to from the driving force which is the vapor pressure difference across the membrane. In theory, of the MD configurations, VMD offers the largest driving force at the same feed temperature. This is because the vapor pressure at the cold side can be reduced to almost zero. In addition, the heat lost by conduction through the membrane is negligible in VMD. However, as for SGMD, an external condenser is needed if the product is liquid (Lawson & Lloyd, 1997; Alkhudhiri et al., 2012) and the risk of membrane wetting is very high when using this configuration (El-Bourawi et al., 2006).

Despite the advantages and disadvantages of each MD configuration, as stated earlier, it is reported in literature that DCMD is the most studied MD configuration. Also, it is best suited for applications where the major feed component is water such as desalination. Therefore, due to its simplicity and ease of operation among others, DCMD was chosen to be employed in this study.

Complete rejection of non-volatiles is one of the major advantages of using DCMD. Moreover, according to Zhang et al. (2010), compared to the other MD

configurations, the permeate flux in a DCMD process is higher. Furthermore, according to the literature, the average flux by DCMD is in the range of 3.6 to 40 L/m^{2}hr, with the value being strongly dependent on the used inlet temperature difference between the hot and cold streams (Lagana et al., 2000).

In addition to the higher flux generated by DCMD, it is stated in literature that the advantages of DCMD in terms of its operational parameters over the other MD configurations are as follows (Wang et al., 2009):

- The feed requires less pre-treatment

- It can be operated at constant pressure

- It is less affected by membrane fouling

3.2- Membrane Module and MD Module Configurations

Commonly in MD processes, there are two types of membrane configurations: Flat sheet and hollow fiber membranes. The flat sheet and hollow fiber membranes can be wetted by water, but are readily wettable by most organic solvents. The organic solvent when brought on one side of the membrane immediately wets the membrane and immobilizes the interface or appears on the other side of the membrane.

Peinemann & Nunes (2010) emphasize that the membrane module and design usually rely on the type of membrane used. The flat sheet membranes are commonly constructed in a panel of configuration. On the other hand, hollow fiber membrane types are constructed into bundles that are installed in housing units or designed to be

unconfined in the fluid. Figure 16 and Figure 17 show a schematic diagram of the flat

sheet membrane and the hollow fiber membrane, respectively.
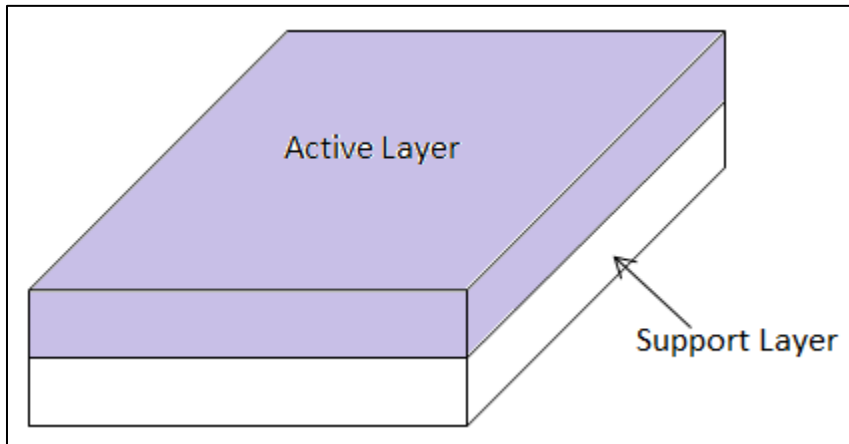
Figure 16: A Schematic Diagram of the Flat Sheet Membrane
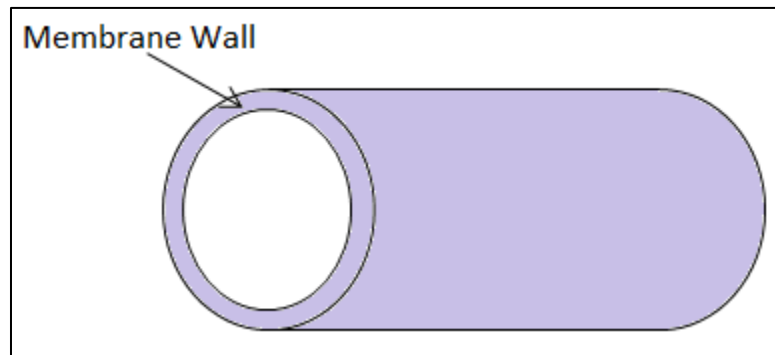
Figure 17: A Schematic Diagram of the Hollow Fiber Membrane

The flat sheet membrane shown in Figure 16 is composed of a thin active layer and a

porous support layer. The support layer provides mechanical strength for the

membrane; hence, allowing the active layer to be manufactured as thin as possible,

which reduces the mass transfer resistance.

The hollow fiber membrane is generally prepared from polyvinylidene fluoride (PVDF), polyvinylidene fluoride-polytetrafluoroethylene (PVDF-PTFE), and polypropylene (PP) composite materials (Teoh & Chung, 2009; Song et al., 2007). On the other hand, the flat sheet membrane is mainly produced from PTFE, PP, and PVDF (Song et al., 2007).

Compared to the flat sheet membranes, the hollow fiber membranes are characterized with having a large specific surface area (Gryta & Tomaszewska et al. 2000), but the core deterrent of the hollow fiber module is its typically low flux (Bonyadi & Chung, 2009). Table 7 shows the typical flux obtained from the flat sheet and the hollow fiber membrane modules.

Table 7: The Typical Flux Obtained from Utilizing the Flat Sheet and the Hollow Fiber Membrane Modules

Membrane Module	Reported Flux (L/m^2h)	References
Flat Sheet	20 - 30 (at $T_{in,hot} = 60$ ^{o}C and $T_{in,cold} = 20$ ^{o}C)	(Alklaibi & Lior, 2004)
Hollow Fiber	1 - 4 (at 40 - 60 °C)	(Bonyadi & Chung, 2007; Bonyadi & Chung, 2009)

However, high-flux hollow fiber membranes with different features suitable for membrane distillation have been developed (Teoh & Chung, 2009; Bonyadi & Chung, 2007; Bonyadi et al., 2009; Zhang et al., 2010) which have a flux of approximately 50-70 L/m^{2}h at 80-90 °C, which is as high as that generated from the flat sheet membranes.

Moreover, there are three main configurations of MD modules. These include: the plate and frame, the hollow fiber, and the spiral wound modules (Lie et al., 2005). However, the spiral wound module is not widely utilized in MD processes as the other two major modules.

In the hollow fiber module, the hollow fiber membranes are bundled and glued together and placed inside the tubular casing module. The feed solution flows through thousands of hollow fibers and the permeate is collected on the outside of the membrane, or vice versa (Alkhudhiri et al., 2012). Figure 18 shows a schematic diagram of the hollow fiber tubular MD module. This configuration has a very high packing density compared to the other modules which can be as high as 3,000 m^2/m^3 (Schneider et al., 1988; Curcio & Drioli, 2005). Moreover, the hollow fiber tubular module has a large active area and a small footprint which make this configuration favorable for commercial applications (Curcio & Drioli, 2005). However, once a hollow fiber is broken, it cannot be replaced. In addition, the hollow fiber membranes are more expensive than the flat sheet membranes.
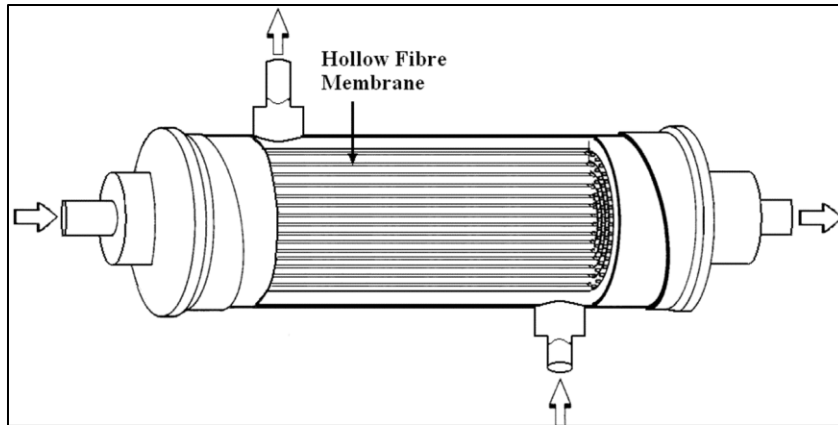
Figure 18: The Hollow Fiber Tubular MD Module (Adapted from: Camacho et al.,

2013)

The plate and frame module is suitable for flat sheet membranes. Figure 19 shows the structure of the plate and frame MD module. It can be used for VMD, AGMD, SGMD, and DCMD. For the plate and frame module, the packing density ranges from 100 to 400 m^2/m^3 (Curcio & Drioli, 2005; Andersson et al., 1985). Even though this configuration has a relatively smaller effective area for the same volume when compared to the hollow fiber module, it is regarded as easy to construct and multiple layers of flat sheet MD membranes can be utilized to enhance the effective area (Curcio & Drioli, 2005). In addition, it is easy to change the configuration's damaged membranes. Therefore, this module is broadly employed in laboratory tests for analyzing the effects of the membrane properties and the MD operation parameters on the flux or the energy efficiency of the process (Curcio & Drioli, 2005; Zhang et al., 2011).
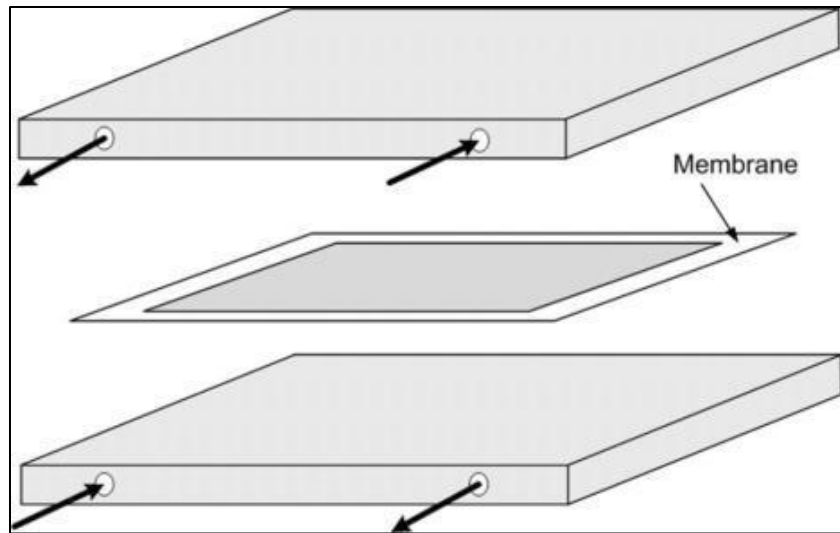
Figure 19: The Plate and Frame MD Module (Adapted from: Camacho et al., 2013)

3.3- Heat and Mass Transfer in DCMD

As stated earlier, the process of DCMD utilizes the difference in vapor pressure that is induced by the difference in temperature as the driving force for the mass transfer across the membrane. Thus, heat and mass transfer in MD are aligned together, and in the same direction from the hot region to the cold region (Qtaishat et al., 2008). Figure 20 demonstrates these processes in DCMD.
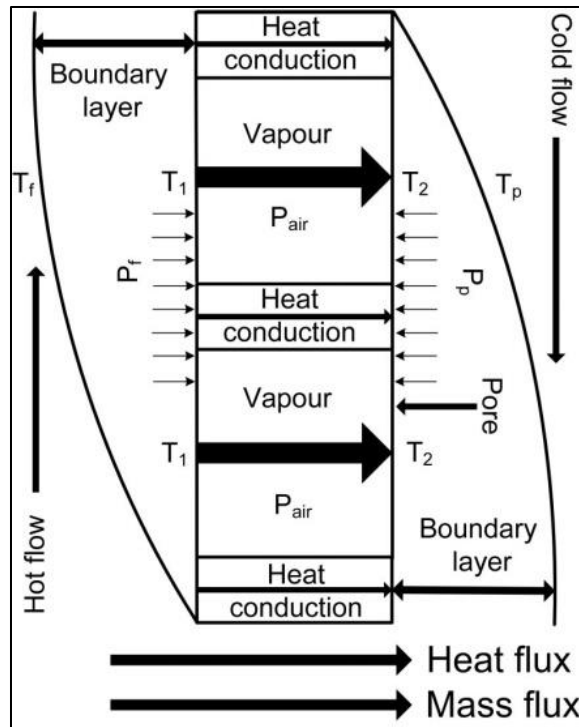
Figure 20: Heat Transfer and Mass Transfer through the Membrane in a DCMD

Process (Adapted from: Camacho et al., 2013)

As shown in Figure 20, the temperature of the feed, T_f, drops across the boundary layer of the feed side to T_1 which is the temperature at the membrane surface. Some water (feed solution) evaporates and is transported through the membrane. Simultaneously, heat is conducted through the membrane to the permeate side. The permeate temperature, T_p, increases across the permeate boundary layer to T_2 at the membrane surface on the cold side as water vapor condenses into the freshwater stream and gains heat from the feed side. Thus, the driving force is the difference in vapor pressure between T_1 and T_2 which is less than the vapor pressure difference between T_f and T_p resulting in a phenomenon called temperature polarization.

3.3.1- Heat Transfer

As stated by Lei et al., (2005), the transfer of heat from the feed side to the permeate side consists of two steps: firstly, the heat transfers from the hot side proceeding towards the cold side across the membrane in the form of sensible heat and latent heat, in order to form the difference in temperature between the bulk flow and the boundary layer; secondly, the heat transfers from the bulk flow of the feed to the boundary layer through heat convection, as a result of the temperature difference arising from the first step.

In the first step, the sensible heat is conducted through the membrane to the cold side, and the latent heat is carried by the water vapor, which is evaporated at the hot stream/membrane pore interface and is condensed at the cold stream/membrane pore interface for DCMD (Martinez-Diez et al., 1999). Therefore, heat transfer in MD can be classified into the following (Alkhudhiri et al., 2012):

1- Convective heat transfer due to mass transfer from the bulk to the liquid/vapor interface through the feed thermal boundary layer, where the heat flux is expressed as follows:

$$Q_f = h_f(T_f - T_1) \qquad (1)$$

where

h_f = the heat transfer coefficient at the feed side (Equation 26).

2- A combination of both conductive heat transfer through the membrane (Q_c), and heat transferred due to water vapor transport (latent heat of vaporization) through the pores of the microporous membrane (Q_v), where the heat flux is expressed as follows:

$$Q_m = Q_C + Q_V \qquad (2)$$

where

$$Q_C = h_m(T_1 - T_2) = \frac{k_m}{\delta}(T_1 - T_2) \qquad (3)$$

and

$$Q_V = J\Delta H_V \qquad (4)$$

where

$h_m =$ the heat transfer coefficient of the membrane.

$k_m =$ the thermal conductivity of the membrane

$\delta =$ the membrane thickness.

$J =$ the mass flux (Equation 21).

$H_v =$ the enthalpy of the vapor (evaluated at the average temperature of the feed and the feed/membrane interface).

3- Convective heat transfer from the vapor/liquid interface through the permeate thermal boundary layer to the permeate side, where the heat flux is expressed as follows:

$$Q_p = h_p(T_2 - T_p) \qquad (5)$$

where

h_p = the heat transfer coefficient at the permeate side.

In Equation 4, H_V is expressed as follows:

$$H_V(T) = 1850.7 + 2.8273T - 1.6 \times 10^{-3}T^2 \qquad (6)$$

where the temperature is in Kelvin and in the range of 273-373 K (Ibrahim & Alsalhy, 2013).

At steady state and by assuming isoenthalpic flow of vapor for Q_v, the heat transfer equations are as follows:

$$Q_f = Q_m = Q_p \qquad (7)$$

Moreover, T_1 and T_2 are expressed as follows:

$$T_1 = T_f - \frac{J}{h_f} H_V \left\{ \frac{T_1 + T_2}{2} \right\} \qquad (8)$$

$$T_2 = T_p - \frac{J}{h_p} H_V \left\{ \frac{T_1 + T_2}{2} \right\} \qquad (9)$$

From Equation 8 and 9, the temperature polarization seems to decrease as convective heat transfer coefficients increase and it increases as the mass flux and temperature increase. To enhance the convective heat transfer coefficient, mesh like spacers can be employed to enhance turbulence and as a result increase the flux.

3.3.2- Mass Transfer

The mass transfer in the membrane distillation process consists of three steps (Camacho et al., 2013; Zhang et al., 2010):

1- The hot feed vaporizes from the liquid/gas interface.

2- The vapor that is derived by the difference in vapor pressure diffuses from the hot interface to the cold interface via the pores of the membrane.

3- The vapor condenses on the distillate side of the membrane.

Hence, the vapor pressure difference and the membrane permeability are the main factors controlling the mass transfer in the MD process (Zhang et al., 2010).

Moreover, the mass transfer in the membrane can be considered as the limiting step for the mass transfer in MD processes if there are good fluid dynamics conditions on the two sides of the membrane (Camacho et al., 2013; Ding et al., 2003). The physical properties of the MD-membrane affect the membrane distillation process. They influence the permeability of the membrane. These properties include the membrane's porosity, tortuosity, and diffusion resistance. Their effects on the membrane permeability are as follows:

1- Since the membrane is not 100% porous, the effective area for mass transfer is less than the membrane's total area.

2- For nearly all practical membranes, the pores of the membrane do not go straight through the membrane and the path for vapor passage is greater than the membrane's thickness.

3- The diffusion resistance is increased by the inside walls of the pores through reducing the vapor molecule momentum (Ding et al., 2003).

The mechanism of mass transport in the membrane pores is controlled by thee major fundamental mechanisms known as Knudsen-diffusion (K), Molecular-diffusion (M), and Poiseuille-flow (P) or a combination between these mechanisms known as the transition mechanism (Kast & Hohenthanner, 2000; Lei et al., 2005). These mechanisms are explained as follows:

1- Knudsen-diffusion: it takes place as a result of the collision of the molecules with the inside walls of the membrane (as the pore size is small) (Ding et al., 2003).

2- Molecular-diffusion: it takes place as a result of the collision of molecules with other molecules (Alkhudhiri et al., 2012).

3- Poiseuille-flow (viscous flow): the vapor molecules act as a continuous fluid driven by the vapor pressure difference (Alkhudhiri et al., 2012).

4- Transition Mechanism: A combination between the three mechanisms (Lei et al., 2005; Kast & Hohenthanner, 2000).

The dominant mass transfer mechanism in the pores is indicated by the Knudsen number (Kn) (Chernyshov et al., 2005; Lei et al., 2005). It is mathematically described as follows:

$$K_n = \frac{l}{d} \tag{10}$$

where

l (or λ)= the mean free path of the molecules.

d = the mean pore size of the membrane.

Kuhn & Forstering (2000) and Albert & Silbey (1997) define the mean free path of the molecules (the water vapor) in the membrane pores as follows:

$$l = \frac{k_B T}{\pi (\frac{\sigma_w + \sigma_a}{2})^2 P_{pore}} \frac{1}{\sqrt{1 + (\frac{M_w}{M_a})}} \tag{11}$$

where

k_B = the Boltzman constant (1.381×10^{-23} J/K) (Cussler, 1997).

σ_w = the collision diameters for water vapor (2.641×10^{-10} m) (Cussler, 1997).

σ_a = the collision diameters for air (3.711×10^{-10} m) (Cussler, 1997).

T = the mean temperature in the pores.

P_{pore} = the mean pressure in the pores.

M_w = the molecular weight of water.

M_a = the molecular weight of air.

In addition, Sperati & DuPont de Nemours (1999) expressed the mean free path of the molecules as follows:

$$\lambda = \frac{k_B T}{\sqrt{2} \pi P_{pore} d_e^2} \tag{12}$$

where

d_e = the membrane pore radius.

At a typical membrane temperature of 60 °C, l is 0.11 μm (Camacho et al., 2013).

Table 8 shows the governing mass transfer mechanism based on the Kn value in a gas

mixture system without a vapor pressure difference across the pores.

Table 8: The Governing Mass Transfer Mechanism in the Membrane Pore based on

the Knudsen Number (Kn) (Ding et al., 2003)

Kn Value	Mass Transfer Mechanism
< 0.01	Molecular diffusion
0.01–1	Knudsen-molecular diffusion transition
> 1	Knudsen diffusion

Since the pore size of the membranes used in the MD processes is in the range of 0.2

to 1.0 μm, then, according to Equation 11, Kn will be in the range of 0.5 to 0.1

(Camacho et al., 2013). Therefore, the dominant mass transfer mechanism in DCMD

is the Knudsen-molecular diffusion transition mechanism.

Even though the mass transfer mechanism is affected by the pore size distribution of

the hydrophobic membrane, Phattaranawik et al. (2003) confirmed that the transition

region will dominate the majority of the membrane area. In addition, according to Lei

et al. (2005), since a total pressure difference doesn't exist in the pores, the

Poiseuille-flow mechanism is not considered and can be ignored.

When $Kn > 1$ (Knudsen diffusion), Khayet et al. (2004) stated that the mass transfer is defined as follows:

$$C_{Kn} = \frac{2\pi}{\varepsilon} \frac{1}{RT} \left(\frac{8RT}{\pi M_w} \right)^{0.5} \frac{r^3}{t\delta} \tag{13}$$

where

ε = the porosity of the membrane.

r = the pore radius.

t = the pore tortuosity.

On the other hand, if $Kn < 0.01$ (Molecular diffusion), Alkhudhiri et al., (2012) stated that the mass transfer is defined as follows:

$$C_D = \frac{\pi}{RT} \frac{PD}{P_{air}} \frac{r^2}{t\delta} \tag{14}$$

where

P = the total pressure inside the pores (equals the partial pressure of air and water vapor).

D = the diffusion coefficient.

P_{air} = the air pressure inside the membrane pore.

In case Kn is in the range of 0.01-1 (transition region), Alkhudhiri et al. (2012) stated that the mass transfer is defined as follows:

$$C_c = \frac{\pi}{RT} \frac{1}{t\delta} \left[\left(\frac{2}{3} \left(\frac{8RT}{\pi M_w} \right)^{0.5} r^3 \right)^{-1} \left(\frac{PD}{P_{air}} r^2 \right)^{-1} \right]^{-1} \tag{15}$$

where PD is the diffusivity of water vapor in the pores. It is described by Phattaranawik et al. (2003) as follows:

$$PD = 1.895 \times 10^{-5} T^{2.072} \tag{16}$$

In addition, there are two other popular mass transfer models for MD. These are the Schofield's model (Schofield et al., 1990) and the dusty-gas model for DCMD (Mason & Malinauskas, 1983; Fernández-Pineda et al., 2002).

The Schofield's model assumes that the total permeability equals the sum of Knudsen permeability and viscous permeability. It describes the vapor diffusion flux as follows:

$$J = \frac{1}{P_{air}} \frac{\varepsilon}{t\delta} \frac{DPM_w}{RT} \Delta P \tag{17}$$

On the other hand, in the dusty-gas model (Mason & Malinauskas, 1983; Mason et al., 1967), the porous membrane is assumed to be an array of dust particles held still in space, and the dust particles in terms of the classical kinetic theory of gases are hypothetically huge molecules in the interactions between gas and surface (Camacho et al., 2013). Moreover, for this model, the Knudsen-viscous transition region is the dominant mass transfer mechanism and a general flux equation is described as follows:

$$J = -\frac{M}{RT} \left[\left(K_0 \bar{v} + \frac{B_0 P_{pore}}{\mu} \right) \frac{P_{T1} - P_{T2}}{b} \right] \tag{18}$$

in which

$$K_0 = \frac{d\varepsilon}{3t} \tag{19}$$

and

$$B_0 = \frac{\varepsilon d^2}{32t} \tag{20}$$

where $\bar{v}$ is the gas' mean molecular speed and b is the membrane thickness.

All of the aforementioned mass transfer models can be simplified as follows (Zhang et al., 2010):

$$J = C_m \Delta P = C_m(P_1 - P_2) \tag{21}$$

where C_m is the membrane mass transfer coefficient, P_1 and P_2 are the vapor pressure at the feed side membrane surface and the permeate side membrane surface, respectively (Alkhudhiri et al., 2012). C_m is proportional to another factor as follows:

$$C_m \propto \frac{d^a \varepsilon}{t\delta} \tag{22}$$

where a is an exponent factor which have a value between 1 and 2, d is the mean pore diameter of the membrane, ε is the membrane porosity in percentage, t is the proportion of the conductive heat, and δ is the membrane thickness (Camacho et al., 2013).

From Equation 22, it can be comprehended that by increasing pore sizes and porosity of the MD membrane, the flux is increased. Also, the flux increases as the tortuosity and thickness of the membrane decrease. However, reducing the thickness of the

membrane also increases the sensible heat loss from the hot side to the cold side, which results in a reduction in flux due to decreased vapor pressure difference (the driving force). The sensible heat loss can be minimized by increasing the membrane porosity which leads to reduced heat transfer coefficient (λ/δ) of the membrane (Camacho et al., 2013).

Many factors affect the thermal (heat transfer) and flux performance (mass transfer) of Membrane Distillation including concentration polarization, temperature polarization, uniform flow distribution, pressure drop, liquid entry pressure, flow turbulence, and inlet feed temperature (Criscuoli et al., 2008). The next sections will discuss these factor in details.

3.4- Concentration Polarization

Concentration polarization is defined by Delaney (1977) and Baker (2012) as the accumulation of solute species at a membrane interface. Strathmann (2009) referred to it as the emergence of concentration gradient at a membrane interface as a result of selective transfer of some species through the membrane due to transmembrane driving forces. Therefore, in MD process, since the membrane is used as a separation medium and as it hydrophobic, there will be a buildup of concentration at the membrane surface compared to the bulk concentration. The retained solutes accumulate at the membrane surface where their concentrations gradually increase at

the interface and decrease at the bulk. This concentration build-up generates a diffusive flow back to the bulk of the feed.

Concentration polarization affects the performance of the separation process. This is because concentration changes in the solution decrease the driving force within the membrane. Martinez-Diez & Florido-Diaz (2001) evaluated the effects of concentration polarization and temperature on the reduction of vapour pressure differences across the membrane. They found that as a result of the high brine temperature and concentration polarization associated with high local fluxes, the highest scaling potential is found at high temperatures. Moreover, Osada & Nakagawa (2010) asserted that concentration polarization leads to increased salt leakage through the membrane as well as increased probability of scale/fouling development. Consequently, the selectivity of separation and the membrane lifetime are deteriorated. In addition, Banat (1994) conducted a study on MD in which he found a slight decrease of 6% in the permeate flux when the concentration of salt in the feed solution increased from 1 to 10 wt% (a 10-fold increase in the feed solution concentration decreased the permeate flux by 6%).

In order to reduce the concentration polarization, the flow rates of the hot and cold streams should be increased as well applying spacers that promote turbulence. This technique results in reduced thickness of the diffusion boundary layer and better turbulent mixing at the membrane surface which is the region in the vicinity of a membrane where the concentrations are different from their value in the bulk

87

solution. However, the most direct technique that is used to promote mixing is through increasing the fluid flow (Li et al., 2011).

3.5- Temperature Polarization

As discussed in Section 3.3.1, the direction of heat transfer in MD is from the feed side (hot solution) to the permeate side which is colder than the feed. As a result, three main heat transfer mechanisms occur simultaneously as follows (Liu et al., 1998):

- From the feed bulk to the feed/membrane interface (through the feed boundary layer).
- From the feed/membrane interface to the membrane/distillate interface (across the membrane).
- From the membrane/distillate interface to the distillate bulk (through the distillate boundary layer).

Figure 21 shows the heat transfer direction across the MD membrane.
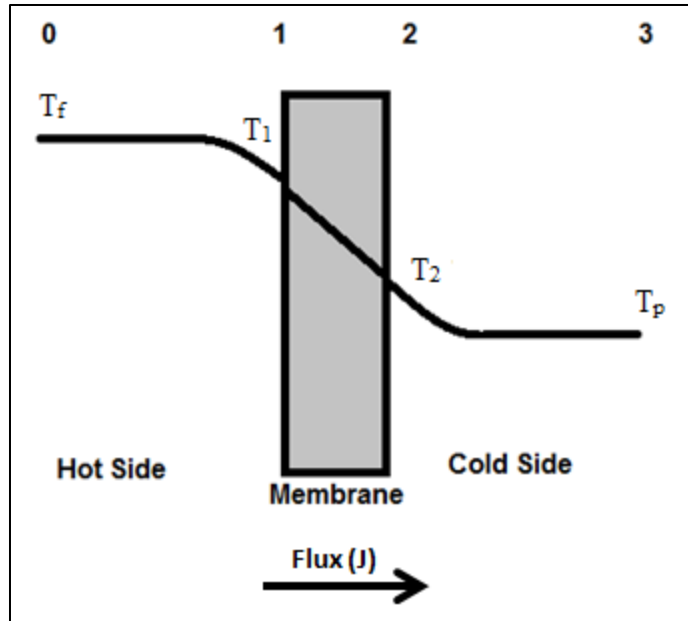
Figure 21: Heat Transfer across the MD Membrane

As a result of the boundary layer at the both sides of the membrane surface (location 1 and 2 in Figure 21), the temperature at 1, T_1, is lower than the temperature at 0, T_f, and the temperature at 2, T_2, is higher than the temperature at 3, T_p. This results in the temperature polarization phenomenon which is expressed as follows (Cath et al., 2004; El-Bourawi et al., 2006; Alkhudhiri et al., 2012; Hsu et al., 2002; Martinez-Diez et al., 1999):

$$\tau = \frac{T_1 - T_2}{T_f - T_p} \tag{23}$$

where

τ = the temperature polarization coefficient (TPC).

Therefore, TPC is the ratio between the useful energy for the vapor mass transfer to the total energy invested in the process (a fraction of the trans-membrane temperature to the bulk temperature difference).

The evaporation and condensation rates in MD depend on the interfacial temperatures (T_1 and T_2) which depend on the bulk temperatures. Therefore, keeping the difference between the temperature of the hot and cold streams as high as possible is favorable to get a higher TPC value (closer to unity). However, TPC in the range of 0.2 to 0.9 is reported in literatures (Cath et al., 2004).

Temperature polarization has a greater influence on the permeate flux compared to concentration polarization. Schofield et al. (1990) found that the temperature polarization coefficient can reach 0.6 at a feed temperature of 60 $^{\circ}$C, meaning that the flux is overestimated by 40% if the temperature polarization is ignored. Therefore, when modeling the MD process, temperature polarization should be considered.

The temperature polarization coefficient can be improved by enhancing the membrane module design and increasing the flow turbulence. As a result of increasing the flow mixing, the thermal boundary layer is reduced; hence, the difference between T_1 and T_2 is increased resulting in a higher vapor pressure difference and thus more flux.

3.6- Liquid Entry Pressure (LEP)

The membrane used in Membrane Distillation is hydrophobic; therefore, the feed solution must not penetrate through the membrane pores and cause membrane wetting. Liquid entry pressure (LEP) is the minimum value of the hydrostatic pressure difference. If LEP is exceeded, membrane pore wetting occurs; hence, affecting the distillate quality. Moreover, LEP is related to several parameters including the interfacial tension, the contact angle of the membrane, and size and shape of the membrane pores (Rácz et al., 2014). LEP can be determined by a model that has been suggested by Franken et al. (1987) based on Laplace-Young equation (Lawson & Lloyd, 1997; El-Bourawi et al., 2006; Cath et al., 2004):

$$\Delta P = P_f - P_p = LEP = \frac{-2B\gamma_l COS\theta}{r_{max}} \tag{24}$$

where P_f and P_p are the hydraulic pressure on the feed side and the permeate side, respectively, B is a dimensionless geometrical coefficient that accounts for the irregularities of the membrane pores (B = 1 for pores that are assumed to be cylindrical), γ_l is the liquid surface tension, θ is the contact angle, and r_{max} is the maximum pore radius.

García-Payo et al. (2000) have shown that for membranes with pore sizes of about 0.2 μm, the LEP would be in the range between 200–400 kPa, whereas for membranes with pore sizes of 0.45 μm the LEP might be as low as 100 kPa (Cath et al., 2004).

According to the Equation 24, a membrane with a high contact angle (high hydrophobicity), smaller pore size, lower surface energy, and high liquid surface tension will have a higher LEP. Table 9 shows the surface energy of the commonly used membranes. Moreover, although do not explicitly occur in Equation 24, this critical pressure difference is inversely proportional to the feed concentration and the presence of organic solutes (Weyl, 1967). In addition, the operating temperature and the feed solution composition can significantly influence the contact angle and the liquid surface tension (Rácz et al., 2014).

Table 9: The Surface Energy of the Commonly Used Membranes (Alkhudhiri et al., 2012)

Membrane Material	Surface Energy ($\times 10^3$ N/m)
Polytetrafluoroethylene (PTFE)	19.1
Polyvinylidene fluride (PVDF)	30.3
Polypropylene (PP)	30.0

The contact angle describes the hydrophobicity of a membrane. Therefore, wetting can be directly measured by the contact angle which is expressed as the interaction between the liquid phase (i.e. water) and the solid membrane surface (Rácz et al., 2014). Figure 22 illustrates the shape of a small droplet on a smooth hydrophobic solid surface.
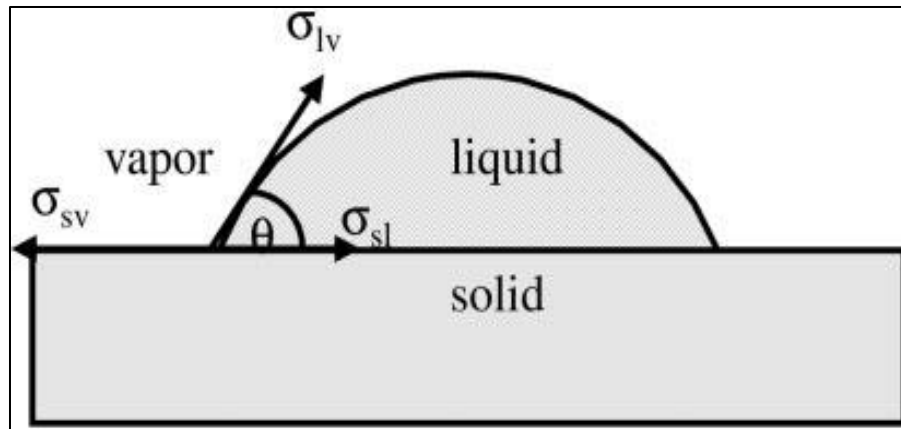
Figure 22: The Shape of a Small Droplet on a Smooth Hydrophobic Solid Surface

(Adapted from: Bachmann et al., 2000)

The theory behind the contact angle measurements is explained by a relation called the Young's equation which is expressed as follows (Bachmann et al., 2000):

$$\sigma_{lv} cos\theta = \sigma_{sv} - \sigma_{sl} \tag{25}$$

where

σ_{lv} = the liquid–vapor interfacial energy.

σ_{sv} = the solid–vapor interfacial energy.

σ_{sl} = the solid–liquid interfacial energy.

It is worth noting that the Young's equation is only applicable to uniform and smooth surfaces (Bachmann et al., 2000).

If a liquid drop is deposited on a hydrophobic or a semi-hydrophobic surface, it does not spread entirely. It undertakes a shape that depends on the relation between the free energies of the three involved phases. The angle that forms at the three-phase line

is called the contact angle as shown in Figure 22. For hydrophobic membranes, the contact angle has to be greater than 90° (the recommended value is around 130°). In extreme cases, contact angle of 180° has been reported (Khemakhem & Amar, 2011). On the other hand, in a very strong hydrophilic membrane, the liquid droplet is attracted to the solid surface of the membrane and it will completely spread out on the membrane surface forming a contact angle of a value close to 0°. A contact angle from 0° to 90° is formed for less strong hydrophilic membranes (Zeaman & Zydney, 1996).

According to Al-Obaidani et al. (2008), for a membrane of a pore size of about 0.2 μm, the LEP is around 2-4 atm and for a membrane of a pore size of about 0.45 μm, the LEP decreases and its value can be up to 1 atm.

According to Baek et al. (2012), there might be variations in the contact angle values when taking the measurements on a membrane sample. They observed that contact angles attained by the sessile drop method, which is the most commonly used method for measuring the contact angles in the literatures, showed inconsistent values with different measurement times and drop volumes. They also concluded that the membrane sample preparation is important when performing contact angle measurements. In addition, according to Xu, Huang, & Wan (2009), many factors affect the accuracy of the contact angle value including the surface roughness, the volume of the dropped liquid, the measurement time, the surface hetrogeneity, the measurement temperature, and the surface contamination among others. This was also

shared by Zhu et al. (2013) and Rajesh (2011). Nevertheless, in this study, it was made sure that the contact angles obtained (shown in Section 5.3) are as accurate as possible.

3.7- Flow Turbulence and Flow Distribution

The permeate flux can be increased by increasing the vapor pressure difference across the membrane or by reducing the temperature polarization (Phattaranawik & Jiraratananon,2001; Martínez-Díez et al., 1998). To achieve this, enhancing the convective heat transfer coefficient is essential to generate a higher flux according to the heat balance equation discussed in the heat transfer section (3.3.1). The convective heat transfer coefficient at the feed side can be written as follows (Martínez-Díez et al., 1998):

$$h_f = -\frac{\lambda_f}{T_f - T_1}\left(\frac{dT}{dy}\right)_{boundary} \tag{26}$$

where λ_f is the thermal conductivity of the feed and $\left(\frac{dT}{dy}\right)_{boundary}$ is the temperature gradient in the thermal boundary layer of the feed.

As suggested by Equation 26, h_f can be improved by reducing the thickness of the thermal boundary layer. In addition, the convective heat transfer coefficient can also be improved by improving the design of the flow passage and the arrangement of the membrane, and by enhancing the stream turbulence. As mentioned in Section 3.3.1, promoters such as mesh-like or zigzag spacers are designed to generate turbulence at

the surface of the membrane; consequently, reducing the thickness of the thermal boundary layer. As a result, the convective heat transfer coefficient is increased. Moreover, better mixing can be created by using high flow velocities which reduce the temperature polarization effect as well (Lawson & Lloyd, 1997; Cath et al., 2004; El-Bourawi et al., 2006). According to Cath et al. (2004), both flow mixing and turbulence improve the MD flux. In addition, they have stated that the temperature polarization coefficient of spacer-filled channels is in the range of 0.9–0.97. On the other hand, the temperature polarization coefficient is in the range of 0.57–0.76 for flowing channels without spacers. Furthermore, the higher the turbulence, the higher the Reynolds number, which is a measure of the mixing intensity expressed as the ratio of the inertial forces to the viscous forces (Cath et al., 2004). However, Camacho et al. (2013) have stated that the impact of turbulence on flux becomes less at higher turbulence levels. Therefore, turbulence should be controlled so that the energy cost associated with pumping is reduced.

3.8- Pressure Drop

Pressure drop is a natural phenomenon that occurs as a result of the flow of the fluid in the channel due to the imposed resistance to the flow by the walls and the fluid itself (Cath et al., 2004). To keep a fluid flowing in a channel, a minimum pressure must be maintained at the entrance to the flow channel. The pressure drop is expressed as follows (El-Bourawi et al., 2006; Cath et al., 2004):

$$\Delta P = f \frac{L}{d_h} \rho \frac{u^2}{2} \tag{27}$$

where f is the friction factor, d_h is the hydraulic diameter of the flow channel, and ρ and u are the fluid density and velocity, respectively.

An optimization process has to be carried out while designing and operating an MD unit and a lower pressure than the LEP has to be maintained to avoid membrane wetting.

3.9- Membrane Physical Properties

The physical properties of the membrane are important factors when designing MD processes. MD membrane should have the following requirements (Smolders & Franken, 1989; Drioli et al., 1986; Khayet et al., 2006; Criscuoli et al., 2008; Khayet & Matsuura, 2003):

- A suitable thickness, basing on a compromise between increased membrane permeability and decreased thermal resistance.

- Narrow pore size distribution and reasonably large pore size, limited by the LEP needed of the membrane. As mentioned earlier, the hydrostatic pressure must be lower than the LEP in order to avoid membrane wetting in MD processes.

- Low surface energy translating into high hydrophobicity.

- Low thermal conductivity.

- High porosity.

3.9.1- Membrane Porosity

Membrane porosity is referred to the membrane void volume. MD membrane porosity of 30% to 85% is mostly reported in literature (El-Bourawi et al., 2006). Usually, the porosity is in the range of 0.06 to 0.95 (Camacho et al., 2013). Higher porosity membranes allow for greater surface area for evaporation; hence, generating higher permeate flux. Another advantage of using membranes with higher porosity is their lower conductive heat loss because the conductive heat transfer coefficient of the gases entrapped within the membrane pores is an order of magnitude smaller than that of the hydrophobic polymer used for the membrane's preparation (El-Bourawi et al., 2006; Lawson & Lloyd, 1997). Despite the fact that high membrane porosity increases both the thermal resistance and the permeability of MD membranes, high porosity membranes have low mechanical strength. Therefore, under mild pressure, they will likely crack which leads to the loss of membrane performance (Camacho et al., 2013).

The heat transfer coefficient of the membrane is related to the membrane porosity according to the following equation (Lawson & Lloyd, 1997):

$$h_m = \varepsilon h_{mg} + (1 - \varepsilon) h_{ms} \qquad (28)$$

where ε is the membrane porosity, h_{mg} and h_{ms} are the heat transfer coefficient of the gas and the membrane solid, respectively. h_{mg} is always less than h_{ms}; therefore, the value of h_m can be reduced by increasing the membrane porosity.

3.9.2- Membrane Pore Size

The MD flux increases with increasing membrane pore size (El-Bourawi et al., 2006). Mainly, the pore size of the MD membrane is in the range of 0.2 to 1.0 µm (Camacho et al., 2013; El-Bourawi et al., 2006; Lawson & Lloyd, 1997). The pore size of a membrane is directly related to the type of mass transfer in the MD process. It is Knudsen diffusion for membranes having a small pore size and Knudsen-viscous for those having larger pore size (El-Bourawi et al., 2006). To enhance the flux by playing with membrane pore size it is better to have more likely Knudsen diffusion in case of small pore size and Knudsen-viscous transition where the membrane pore size are large (Cath et al., 2004; Schneider et al., 1988). Moreover, two factors have to be considered when deciding on a membrane pore size. The pores must be large enough to facilitate the desirable flux. In addition, the pores must be small enough to avoid membrane wettability under the MD operating conditions (Lawson & Lloyd, 1997).

3.9.3- Membrane Thickness

The permeate flux in MD is inversely proportional to the membrane thickness (El-Bourawi el al., 2006, Alkhudhiri et al., 2012). To obtain a reasonably high flux in MD, the hydrophobic membrane should be as thin as possible because the mass

transfer resistance increases with thicker membranes. In contrast, to have higher heat efficiency, the membrane should be as thick as possible due to the fact that the conductive heat loss takes place through the membrane matrix (Lawson & Lloyd, 1997; Hsu et al., 2002; Alkhudhiri et al., 2012). Therefore, the optimum membrane thickness is estimated to be in range of 30 to 60 µm (Hsu et al., 2002; Alkhudhiri et al., 2012). Nevertheless, the thickness of the membranes used in MD processes is between 0.04 and 0.25 mm (Alklaibi & Lior, 2005; Zhang et al., 2010).

3.9.4- Pore Size Distribution

The membranes used in MD process have different pore sizes rather than a uniform pore size. Therefore, more than one heat and mass transfer mechanisms can take place simultaneously. In general, pore size distribution has no significant effect on the performance of Membrane Distillation process (Laganà et al., 2000).

3.9.5- Pore Tortuosity

Membrane tortuosity is referred to the average length of the pores compared to the thickness of the membrane (El-Bourawi et al., 2006). Measuring the tortuosity of a membrane is very difficult; therefore, a constant value is usually assumed when calculating the flux. A tortuosity factor of 2 is usually assumed in literature (Lawson & Lloyd, 1997; Bandini et al., 1997; Phattaranawik et al., 2003; Khayet et al., 2004). In general, the permeate flux in MD processes is inversely proportional to the membrane thickness times its tortuosity.

3.9.6- Thermal Conductivity

As discussed in Section 3.3.1, the heat is transferred through the MD membrane material by conduction via sensible heat and the vapor is transported via latent heat. In general, when the used membrane has high thermal conductivity, the sensible heat transfer across the membrane is increased leading to a reduction in vapor flux due to the lowered interfacial temperature difference. Phattaranawik & Jiraratananon (2001) have stated that the best model for calculating the thermal conductivity of a membrane is the Isostrain or the parallel model which assumes a parallel heat flow through the air and the membrane material. The thermal conductivity of a membrane using the Isostrain model is expressed as follows:

$$k^M = \varepsilon k^G + (1 - \varepsilon)k^P \tag{29}$$

where k^G and k^P are the thermal conductivity of air and the polymeric material, respectively.

k^G and k^P are calculated using the following correlations (Ibrahim & Alsalhy, 2013; Lawson & Lloyd, 1997):

$$k^G_{water}(T) = 2.72 \times 10^{-3} + 5.71 \times 10^{-5}T \tag{30}$$

$$k^G_{air}(T) = 2.72 \times 10^{-3} + 7.77 \times 10^{-5}T \tag{31}$$

$$k^M_{PVDF}(T) = 9.2308 \times 10^{-3} + 5.77 \times 10^{-4}T \tag{32}$$

$$k^M_{PTFE}(T) = 0.087 + 6 \times 10^{-4}T \tag{33}$$

$$k_{PP}^{M}(T) = -0.248 \times 10^{-3} + 1.3 \times 10^{-3} \qquad (34)$$

where *T* is the temperature in Kelvin in range of 273–373 K.

Table 10 shows the thermal conductivities of water vapor, air, and the commonly used MD membranes.

Table 10: The Thermal Conductivities of Water Vapor, Air, and the commonly used MD Membranes (Ibrahim & Alsalhy, 2013)

Material	Thermal Conductivity Range (W/mK)
Water Vapor	0.026 at 298 K and 0.03 at 348 K
Air	0.020 at 298 K and 0.022 at 348 K
PTFE	0.25-0.27 at 296 K and 0.29 at 348 K
PP	0.11-0.16 at 296 K and 0.2 at 348 K
PVDF	0.17-0.19 at 296 K and 0.21 at 348 K

Among the commonly used MD membranes, PTFE membrane has the best hydrophobicity (the largest contact angle with water), good thermal and chemical stability and oxidation resistance. However, it has the highest thermal conductivity which results in greater heat losses. On the other hand, PVDF has good hydrophobicity, thermal resistance and mechanical strength. In addition, PP exhibits good thermal and chemical resistance (Curcio & Drioli, 2005). Moreover, recent research has shown that new membrane materials such as carbon nanotubes and

fluorinated copolymer materials have been developed to produce MD membranes with good mechanical strength and high porosity and hydrophobicity (Zhang et al., 2010; Camacho et al., 2013).

The MD membranes are prepared using several methods including sintering, phase inversion, and stretching (Mulder, 1996; Lloyd et al., 1990; Tomaszewska, 1996). PTFE membranes can be prepared using the sintering method. In the process of sintering, polymeric powder is pressed into a thin film and sintered below the melting point of the polymer. The membranes that are prepared using this method have a porosity of 10-40% and typical pore sizes of 0.2 to 20 μm (Huang et al., 2002; Zubir & Ismail, 2002). Moreover, the stretching technology can be utilized to produce PTFE and PP membranes. In this method, sheets of membranes are formed through extrusion from a polymeric powder at temperatures near the melting point of the polymer together with a rapid draw-down. The produced membranes have a porosity of approximately 90% and typical pore sizes of 0.2 to 20 μm (Huang et al., 2004; Curcio & Drioli, 2005; Zhang et al., 2010). Furthermore, the phase inversion method can be utilized to produce PVDF membranes. The polymer in this process is dissolved in an appropriate solvent and later spread as a film having a thickness of 20-200 μm on suitable supports such as non-woven polyester, PP backing or PP scrim backing (Khayet & Matsuura, 2001), and a suitable precipitant (typically water) is added in order to split the homogenous solution film into two phases which are a liquid rich phase and a solid polymer rich phase. The produced membranes using this

103

method have a porosity of approximately 80% and a typical pore size of 0.2 to 20 μm (Teoh & Chung, 2009).

3.10- Feed Temperature

In MD processes, the temperature of the feed solution is commonly in the range between 20 °C and 90 °C. The highest temperature used is below the boiling point of the feed's aqueous solution. Since the driving force in MD, which is the vapor pressure difference, varies exponentially with the stream temperature, the flux is greatly influenced by the temperature of the feed. Moreover, as the heat loss through thermal conduction is linear to the interface temperature difference (Equation 3), the fraction of energy used for evaporation will increase when the feed temperature is increased. However, as a result of an increase in the feed temperature, an increase of temperature polarization will be observed as well due to the high flux and greater heat and mass transfer. Nevertheless, as discussed in Section 3.7, turbulence promoters such as spacers can be used to reduce this effect (Zhang et al, 2010, Camacho et al., 2013).

3.11- Membrane Fouling

In membrane separation processes, the deposition and accumulation of undesirable materials that form a layer on the feed side of a membrane surface and/or be in the

membrane pores is referred to as fouling (El-Bourawi et al., 2006) which is less studied in MD systems.

Yan-jun et al. (2000) define fouling as the accumulation of unwanted material on solid faces to the detriment of function. The materials responsible for fouling can either be living organisms or non-living tissues. Fouling is usually differentiated from other surface growth phenomena since it occurs on a surface of a component or a system performing a defined and helpful role. Consequently, the fouling process impedes or deters this function.

Alklaibi & Lior (2004) define membrane fouling in MD processes as the deposition of unwanted materials on or in the membrane such as particles, colloids, and suspensions which will eventually result in damaging the membrane and terminating the efficiency of the MD process. Moreover, they emphasize that fouling in MD processes leads to foulant adsorption on the membrane surface, membrane pore blockage, and cake formation.

Gryta (2008) points out that the formation of deposit on the membrane faces is referred to as fouling and is one of the main operating problems of MD process.

3.11.1- Types of MD Membrane Fouling

The fouling layer on the membrane surface might be formed by particles that are suspended in the feed, corrosion products, biological growth, and several crystalline deposits that have formed as a result of scale formation fouling (El-Bourawi et al.,

2006). Therefore, the risk of membrane pore wetting is increased. El-Bourawi et al. (2006) state that despite the information available in literature, the role of membrane fouling in MD systems is not clearly understood yet.

There are several types of MD membrane fouling including crystallization fouling, biological fouling, and particulate or colloidal fouling (Lawson & Lloyd, 1997; El-Bourawi et al., 2006).

Crystallization fouling or scale formation fouling on MD membrane surface has been first reported in early 1980s (Cheng & Wiersma, 1983). Chernyshov et al. (2003) state that crystallization fouling is formed as a result of the deposition or the growth of crystals on the surface of the membrane during the treatment of salt concentrated feed solutions. As a consequence to the formation and deposition of scales, membranes might experience loss of hydrophobicity and water penetration through some membrane pores might occur (Sakai et al., 1988; Schofield, 1989; Lawson & Lloyd, 1997; Alkhudhiri et al., 2012). In fact, scaling is considered as one of the main problems encounters membranes in seawater desalination applications (Chernyshov et al., 2003).

During water demineralization from tap water, Karakulski et al. (2002) observed a rapid decrease in the permeate flux. Their study showed that the flux decrease was a result of calcium carbonate ($CaCO_3$) precipitation on the membrane surface.

During the concentration of NaCl solution that contained dissolved organic matter, Gryta et al. (2001) have reported a major decline in permeate flux as a result of sever

fouling deposits on the membrane. This was observed on the feed side of the MD membrane. Analysis of the membrane morphology showed that the membrane was completely covered with a fouling layer. Also, by examining the composition of the fouling layer, a significant amount of NaCl and proteins was observed.

Most of MD membrane scaling can be expected with salts having a lower solubility at lower temperatures (Chernyshov et al., 2003; El-Bourawi et al., 2006). Moreover, it is worth mentioning that crystal formation on the membrane surface was observed in DCMD configuration (Tun et al., 2005; Gryta et al., 2001; Drioli & Wu, 1985). In contrast, no fouling was detected during a 2 month run in AGMD (Banat & Simandl, 1994).

In addition to crystallization fouling, MD membranes might be fouled by biological fouling. Biological fouling is the attachment of biological microorganisms and/or macro-organisms to the surface of the MD membrane. The biological microorganisms include bacteria, algae, and fungi, whereas the macro-organisms include mussels, barnacles, hydroids, and seaweed. Since the biological fouling is caused by one or more of the abovementioned living matter, it is generally associated with aqueous systems in which the temperature is close to that of the natural environment (El-Bourawi et al., 2006). Therefore, Alklaibi & Lior (2004) state that biological fouling in MD is less of a problem compared to the other membrane processes such as RO.

Gryta (2000) observed a rapid flux decline during a DCMD process that was used to concentrate saline wastewater from the production of heparin. The decline in flux was attributed to scale formation and biological fouling.

In addition, Gryta (2002) observed a limited biological growth on the surfaces of the MD membrane of modules previously used in several MD applications. He stated that biological fouling was affected to a great extent by the operation conditions of the MD process.

In addition, particulate fouling is referred to the deposition of suspended solid particles onto the membrane surface (El-Bourawi et al., 2006). The deposition rate and the mechanism responsible for the transport of the particles in suspension to the membrane surface are highly dependent upon the size of the suspended particles (Bott & Walker, 1971).

Kimura et al. (1987) faced some problems during the concentration of milk using MD as a result of the adherence of the fat globules to the surface of the membrane.

It is worth mentioning that many MD authors agree that fouling is present in MD (Tun et al., 2005; Gryta et al., 2001; Gryta, 2000; Gryta, 2002; Srisurichan et al., 2005); however, others do not accept the presence of MD fouling (Ortiz de Zárate et al., 1998; Khayet et al., 2004; Khayet & Mengual, 2004). El-Bourawi et al. (2006) emphasized that fouling is a time dependent process; therefore, the fouling effect in MD systems can't be predicted. One should be careful when fouling effect on MD membrane is being studied as different degree of fouling may be exhibited by the

different types of MD membranes which may depend on the membrane's hydrophobicity, its surface structure, the feed solution characteristics, etc. (Khayet et al., 2004; Khayet & Mengual, 2004). The importance of understanding MD fouling has been emphasized (Lawson & Lloyd, 1997); still, there is lack of data and knowledge regarding fouling in MD process (Srisurichan et al., 2005).

3.11.2- Fouling Mechanism

According to Yan-jun et al. (2000), membrane fouling curtails severely the economical and practical implementation of the MD process. Fouling can possibly be chemical and/or physical phenomena. Generally, fouling may be a result of one or more of the following mechanisms (Razavi et al., 1996):

1- Formation of a fouling layer on the surface of the membrane.

2- Fouling within the membrane structure (within the pores).

3- Fouling at the entrance of the pore.

3.11.3- Factors Affecting MD Membrane Fouling

The factors that influence or contribute to membrane fouling include:

1- The effect of the feed properties: These include the feed concentration, pH and ionic strength, component interactions, pre-filtration, and the removal of aggregates. Aggregates have been shown to block the larger membrane pores, resulting in a disproportionate flux loss.

2- The effect of the membrane material: The membrane characteristics that influence fouling are (a) the porosity, the pore size, and the membrane surface morphology and (b) the membrane's physic-chemical properties. The loss of effective membrane porosity is reliant on the pore size of the membrane and the size of the depositing molecules (Yan-jun et al., 2000).

3- The effect of the processing variables: For instance, the transmembrane pressure, where an increase in the transmembrane pressure proportionately increases the permeate flux, and also increases the fouling rate; the cross-flow velocity and the turbulence promoters, membrane fouling decreases and the effective pore size increases with increasing velocity; the temperature, an increase in temperature increases the permeate flux, thereby assisting flow rate and increase diffusivity (Gryta, 2008; Gryta, 2002).

Moreover, Gryta (2008) asserts that permeate flux decline would be a result of an increase in the heat resistance of the fouling layer. Although in the case of the non-porous deposit, a certain level of the permeate flux was also established despite the resistance of water transport by means of the deposit layer. It was found that the deposits not only formed on the membrane surface, but also inside the pores. The crystallization of salt inside the membrane pores, in addition to wetting, also cause mechanical damage to the membrane structure.

According to Peinemann & Nunes (2010), fouling and wetting are not significant factors in membrane distillation when utilizing PTFE membranes, particularly for

tests conducted at low feed inlet temperature, for example 40 $^{\circ}$C, as the performance of the membrane will be fully recovered by rinsing the scale off the membrane surface with deionized water. Moreover, fouling is very ubiquitous and generates great operational losses. The losses originally are due to reduced heat transfer, rising pressure drop, and flow blockages.

3.11.4- Characterization of Scale

The morphology and composition of the fouling layer is studied using Fourier Transform Infrared (FTIR) Spectroscopy with Diffuse Reflectance Spectroscopy (DRS) and Scanning Electron Microscopy (SEM) together with Energy Dispersive Spectroscopy (EDS). In most of the studied cases, fouling would be seen (Razavi et al., 1996).

As noted by Lu (2007), one way of quantifying uniform fouling is by stating the average deposit surface loading, such as kg of deposit per m² of surface area. Thereafter, the fouling rate will then be conveyed in kg/m²s, and it is attained by dividing the deposit surface loading by the effective operating time. Furthermore, Peinemann & Nunes (2010) argue that the porosity and the deposit thickness are also used for the description of fouling quantity.

3.11.5- Cleaning of the Fouled Membrane

Yan-jun et al. (2000) state that membrane fouling can be reduced through cleaning. Cleaning can be done physically, chemically, physico-chemically, or biologically. Firstly, the physical cleaning methods rely on mechanical treatments to remove the foulants from membrane surfaces. Some of the mechanical treatments include the following (Yan-jun et al., 2000):

1- Periodical back-flushing: applying pressure on the permeate side of the membrane, thus pushing back part of the permeate. However, the efficiency of this method depends to a great extent on the suspension type to be treated, the fouling type it causes, and the frequency and amplitude of the pulses of the applied reverse pressure. Nevertheless, this type of membrane cleaning method is the most widely used in industry.

2- Vibration: mechanical energy is exerted on the permeate vessel by a pneumatic hammer device attached to a pressure vessel. This causes a feed-to-brine flush causing any shaken loose matter to be removed from the membrane.

3- Air sparge: periodic bursts of air are directed towards the permeate. This forward flush is suitable for hollow fiber configuration. The air disturbs the fibers, loosening foulants from the walls of the membrane.

4- Automatic sponge ball cleaning: a sponge ball made of polyurethane or any other material is placed in the permeator to scrub the foulants from the

membrane. This is done for a few seconds. However, this method is only applicable for tubular modules.

5- Ultra-sonication: applying sound energy to agitate the foulants. The cake layer deposited on the membrane surface is removed using this method. Also, it prevents membrane pore plugging (Yan-jun et al., 2000). Hsu et al., (2002) have used the ultrasonic cleaning technique to clean their fouled membrane. It was found that this method of cleaning is effective in restoring the flux rate and extending the life span of the MD membrane.

Secondly, the chemical cleaning methods rely solely on chemical reactions to eliminate foulants from membranes. Each kind of foulant needs a particular type of chemical agent to be removed. These include hydroxides, phosphates, nitric acid, and phosphoric acid among others. The cleaning process should get rid of the deposits and restore the membrane's normal capacity and separation characteristics (Gryta, 2008). Gryta (2015) has shown that rinsing the MD module used for tap water desalination with diluted HCl solutions resulted in removing the $CaCO_3$ deposits formed on the membrane and the flux was maintained. In addition, cyclic rinsing of the module using HCl solutions limited the size of the deposited crystals. Thirdly, the physico-chemical cleaning methods utilize physical cleaning techniques along with chemical agents to improve the cleaning effectiveness of the membranes. Lastly, the biological cleaning methods can be described as the utilization of cleaning mixtures which contain bioactive agents (micro-organisms or enzymes) to enhance the removal of foulants. The biological cleaning methods, unlike the physical and chemical cleaning

methods, don't cause damage to the membrane but demand further cleaning (Yan-jun et al., 2000).

3.11.6- Mitigation of Membrane Fouling

Membrane fouling will eventually reduce the permeate flux of the MD process and its efficiency. Therefore, several MD authors have suggested ways to mitigate MD fouling.

Alklaibi & Lior (2004) indicate that pretreatment of the feed solution is a way of reducing membrane fouling. In addition, they proposed that de-aeration of the feed water, which is a way of pretreatment, could have a positive influence on the performance of the MD process to a small extent. This conclusion was also shared by Schofield et al., (1990).

Lawson & Lloyd (1997) state that biological fouling can be avoided by UV treatment of the feed solution or by the addition of appropriate chemicals.

Moreover, as discussed in Section 2.2.6, to prevent scale formation, certain anti-scalant additives are added to the feed including polyphosphate, polyphosponates, polycarboxylic acid, H_2SO_4 and HCl (Hassan et al., 1988). Hou et al. (2013) have used the antiscalant polyacrylic acid to mitigate membrane fouling. They showed that it could delay the deposit formation. They advisable dosage they suggested was 10 mg/L.

To prevent damage of MD membrane as a result of crystal formation, Gryta (2008) suggested using crystallization to constantly remove salt from contaminated solutions with sparingly soluble compounds.

Gryta (2000) has encountered scale formation and biological fouling on the membrane using a DCMD process. To prevent their occurrence, he found that boiling the wastewater (the feed to the process) for about 30 minutes followed by suitable filtration was effective.

Gryta (2008) asserts that the strength of fouling can be limited by pretreating the feed and choosing suitable operating environment and conditions for membrane distillation.

3.12- Water Quality

Water quality refers to the characteristics of water. Usually, the quality of water is reported as total dissolved solid (TDS) or salinity. Water salinity is categorized by salt concentration and ranges from fresh, to brackish, to saline water. The salinity ranges for several water sources and the typical salinity and temperature for the Arabian Gulf Sea were previously mentioned in Table 1 and 2, respectively.

The salinity of water is due to the presence of salts including calcium (Ca), sulfate (SO_4), sodium (Na), and chloride (Cl). The salt content of seawater varies from sea to sea depending on their location among other factors. Table 11 shows the major salt content of seawater in general according to two sources.

Table 11: Major Ion Composition of Seawater

Constituent	Normal Seawater Concentration (mg/L) (Younos, 2005)	Normal Seawater Concentration (mg/L) (WHO, 2007)	Arabian Gulf at Kuwait (mg/L) (WHO, 2007)
Chloride (Cl^-)	19,400	18,980	23,000
Sulfate (SO_4^{2-})	904	10,556	15,850
Calcium (Ca^{2+})	411	2,649	3,200
Sodium (Na^+)	10,800	1,262	1,765
Magnesium (Mg^{2+})	1,290	400	500
Potassium (K^+)	392	380	460

The feed solution, after being processed in a desalination process, is separated into two streams: one having a low concentration of dissolved salts and inorganic materials (the freshwater stream) and another comprising the remaining dissolved salts (the concentrate stream or the brine). The amount of brine discharged from desalination plants differs. In general, it is from 15 to 85 % of the feed flow, depending on the salinity of the feed water and the technology used. Usually, the term "brine" is used in literature for seawater concentrate having a salinity of greater than 6,000 mg/L (Bindra & Abosh, 2001). The brine usually contains several chemicals that were added to treat the feed water (based on the technology used and the desired product water quality) including antiscalants, surfactants, and acids used for reducing

the pH. The salts returned to the sea as a result of the brine discharge are identical to those originally present in the feed water; however, at a higher concentration.

The World Health Organization (WHO) states that a permissible salinity limit for potable drinking water is 0.5 ppt and 1.0 ppt under limited consumption (Khayet et al., 2006). The US Environmental Protection Agency (EPA) states that drinking water with TDS greater than 500 mg/L (0.5 ppt) can be distasteful. In Qatar, the drinking water quality is based on the WHO and the European (EU) standards. Table 12 shows the quality of drinking water in Qatar.

Table 12: The Quality of Drinking Water in Qatar (KAHRAMAA, 2009)

Parameter	Guide Level	Maximum Permissible Limit	Unit
pH	6.5 – 8.5	9.5	-
TDS	200 - 600	1,000	mg/L
Alkalinity	30	-	mg/L HCO_3
Total Hardness	60	500	mg/L $CaCO_3$
Chloride	25	250	mg/L Cl
Chlorine Residual	0.2	0.5	mg/L Cl_2
Fluoride	0.7	1.5	mg/L F
Sulphate	25	250	mg/L SO_4
Calcium	100	-	mg/L Ca
Copper	1	2	mg/L Cu
Sodium	20	200	mg/L Na
Iron	0.3	2	mg/l Fe
Manganese	0.1	0.5	mg/L Mn
Magnesium	30	50	mg/L Mg
Aluminum	0.05	0.2	mg/L Al
Nitrate	25	50	mg/L NO_3

3.12.1- Quality of MD Distillate

Many studies have been done using the different MD configurations in order to analyze the quality of distillate produced in MD. Generally, this can be quantified by calculating the salt rejection value and/or measuring the electrical conductivity of the distillate. The salt rejection percentage of the process is expressed as follows (Khayet et al., 2010):

$$Y = \frac{C_f - C_p}{C_f} \times 100 \tag{35}$$

where C_f and C_p are the concentration of salt, or TDS, in the feed and the permeate, respectively.

Alkhudhiri et al. (2013) have utilized a bench scale AGMD process with a PTFE membrane to purify four types of salt solutions: NaCl, MgCl$_2$, Na$_2$CO$_3$ and Na$_2$SO$_4$. The results show that the salt rejection obtained in the study was found to lie between 99.9% and 100% for all of the salts.

Hsu et al. (2002) have worked on both DCMD and AGMD using NaCl solution and real seawater as feed to the processes and PTFE membrane with different pore sizes (0.2 μm and 0.5 μm). The results showed that using the two MD configurations, the conductivities of the distillates were in the range of 7-12 μS/cm. Although different salinity solutions were used, the quality of the water produced remained the same in all of the experiments.

Tang et al. (2009) have worked on vacuum membrane distillation (VMD) with 6 wt.% aqueous NaCl solution. They have used a hydrophobic micro-porous PVDF hollow fiber membrane to investigate the performance of the VMD. The lab scale and pilot scale experiments showed that the salt rejection reached 99.8% at 70 $^{\circ}$C, 3 kPa, and a flow rate of 0.461 m/s.

Hou et al. (2013) have studied desalination by DCMD utilizing a flat-sheet self-prepared PVDF membrane with a pore size of 0.22 μm. Using seawater as the feed to the DCMD process, the salt rejection was over 99.9%.

Cath et al. (2004) have studied the performances of three hydrophobic microporous membranes using a DCMD process with 40 °C as the feed water inlet temperature. Their results showed that the salt rejection was greater than 99.9% for all of the membranes used.

A study by Feng et al. (2008) showed that for using NaCl solutions of different concentrations, salt rejection ranging from 98.7 to 99.9% was obtained. Moreover, the distillate analysis showed that the concentration of salt in the distillate was around 110-280 ppm. The distillates were obtained using an AGMD process utilizing PVDF membranes.

Khayet et al. (2010) have studied the effect of using different membrane materials on the salt rejection. Their results showed that salt rejection of 99.95% can be achieved regardless of the type of membrane used.

He et al. (2011) and Adham et al. (2013) have worked on MD processes and found that the conductivity of the distillates produced were in range of 1-3 µS/cm.

Gryta (2015) have shown that when analyzing the distillate of a DCMD process that was used for tap water desalination, the salt rejection was almost 100% and the electrical conductivity was in range of 2-3 µS/cm.

Kullab & Martin (2011) have studied MD-based water treatment using a pilot plant operated with waste heat from a cogeneration facility in Sweden. The MD configuration was AGMD with feed having a conductivity of about 467 µS/cm. The distillate quality tests showed conductivities in the range of 1-3 µS/cm.

In this study, distillate quality tests among other tests will be presented for repeated runs on a bench-scale DCMD unit in Chapter 5.

Chapter 4: Approach and Methodology

The experimental study was undertaken at the Chemical Engineering Research Laboratory in Qatar University on a laboratory scale DCMD apparatus which was used in a previous project. This section presents the details of the experimental setup and the methodology adopted followed by details on the membranes used. Later, details on the DCMD module dimensions, the auxiliary equipment used, and the experimental procedures are given.

4.1- DCMD Bench Scale Module

Figure 23 shows the process flow diagram (PFD) of the flat sheet DCMD apparatus used. The apparatus is composed of several instruments and parts and they are as follows:

1- Feed and distillate reservoire tanks.

2- Electronic balances.

3- Peristaltic pumps and associated tubing.

4- Hot and cold water bath units (heater and cooler).

5- DCMD cell.

6- Temperature sensors and display.

7- Pressure sensors and display.

8- Flow rate meters and display.

9- Data acquisition system and desktop computer (not shown in Figure 23).
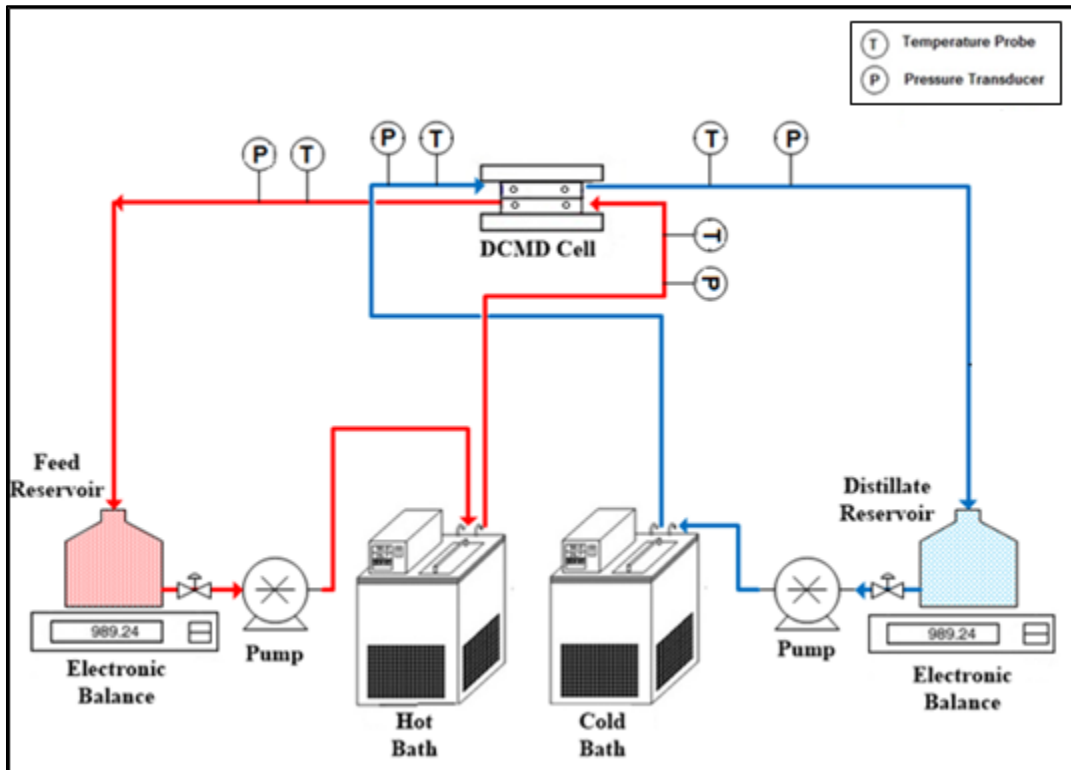
Figure 23: The Process Flow Diagram of the Bench Scale DCMD Unit

From the feed reservoir, the feed brine is pumped by a peristalic pump to the hot bath unit or the heater through a flexible tube. After being heated to a certain desired temperature, the hot water is fed to the DCMD cell. After entering the MD cell, it goes back to the feed reservoire as a recycled stream. Likewise, from the distillate reservoir, the distillate is pumped through another peristalic pump until it reaches the cold bath unit or the cooler. After being cooled to the desired temperature, the distillate reaches the DCMD cell then it goes back to the same distillate tank in a

closed loop. [Note: Initially, at the beginning of an experiment, the distillate tank contains about 2.5 L of de-ionized water to initiate the process].

The temperatures and pressures of the streams and their flow rate are continuously measured during the process. Four temperature probes are placed at the inlet and oulet of the hot and cold streams to and from the DCMD cell. This is done to monitor and record the temperature of the streams before and after entering the DCMD cell. Also, the pressure of the hot and cold streams into and from the DCMD cell is measured and recorded using four pressure probes that are placed next to the temperature probes. Moreover, the flow rate of the hot and cold streams is measured throughout the experiment and recorded. In addition, using a conductivity meter, the conductivity of the feed and distillate before and after performing the experiments is measured and kept on record.

The flux of the distillate was indirectly measured using the electronic balances beneath the feed and distillate tanks as shown in Figure 23. The initial and instantaneous weight of the water were continuously recorded. This was done using a data aquision (DAQ) system that besides automatically recording the temperature, pressure, and flow rate from the probes, recorded the weight of feed and distillate every 30 seconds of operation. The data saved were finally imported as CSV files into Microsoft Excel files for further processing. In addition to the DAQ system, the temperatures, pressures, flow rates, and weights readings of the water were manually recorded from the digital display (Omega Engineering, UK) to further monitor the

process during operation and serve as a back up means to collect data. Figure 24 illustrates the bench scale setup of the DCMD system in Qatar University's lab. It is worth mentioning that the feed tank initially contains 4-5 L of feed water at the beginning of an experiment.
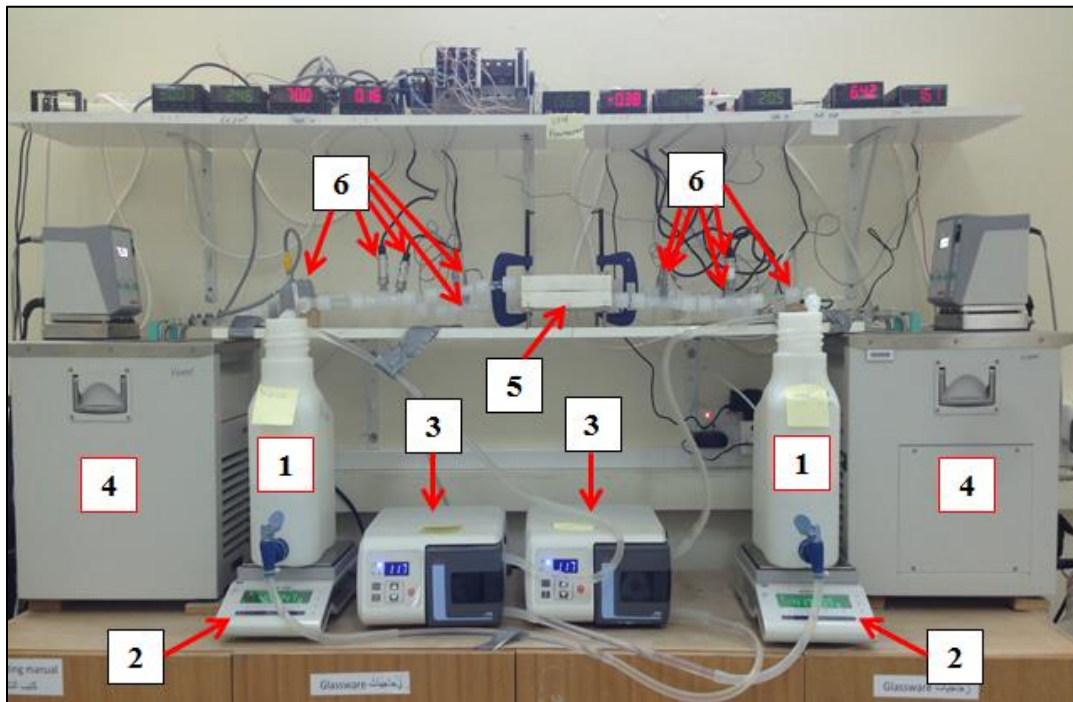
(1) Feed and distillate reservoire tanks. (2) Electronic balances. (3) Peristaltic pumps. (4) Hot and cold water bath units. (5) DCMD cell. (6) Temperature, pressure, and flow rate probes.

Figure 24: The Bench Scale Setup of the DCMD System in Qatar University's Lab

4.2- Feed Solution

In this study, two feed solutions were used to perform the experiments of the DCMD desalination. These solutions were seawater from the Arabian Gulf and synthetic NaCl solution. Table 13 shows the TDS and pH of the feed solutions used in the

study. The electrical conductivity of the seawater was measured with a probe and its TDS was obtained by a conversion factor of 0.69.

Table 13: The TDS and pH of the Feed Solutions Used in the Study

Feed Solution	Solution Source	TDS (mg/L)	pH
Seawater	Arabian Gulf Qatar East Coastline	64,380	8.00
Synthetic NaCl	De-ionized water + NaCl (100 g in 1 L)	100,000	6.98

4.3- Membrane Sheet

Three different polymeric and hydrophobic membranes were used to perform the experiments of this study. Table 14 shows the three membranes used and their properties.

Table 14: The Properties of the Membranes Used in the Study

Description	Membrane Type		
	PP	PP	PTFE
Membrane Trade Name	Polypropylene	Polypropylene	Teflon
Nominal Pore Size (µm)	0.22	0.45	0.22
Porosity (%)	70 - 80	70 - 80	70 - 80
Thickness (µm)	130 - 170	140 - 170	~ 175[*]
Vendor	Sterlitech	Sterlitech	Sterlitech
Reference	(Sterlitech, 2014)	(Sterlitech, 2014)	(Sterlitech, 2014)

* The thickness of the active membrane and the PP support.

Figure 25 illustrates an image of clean flat-sheet membranes.

Figure 25: The Appearance of Clean Flat-Sheet Membranes

Flat sheet membranes were selected over hollow fiber. This is due to several reasons. Flat sheets membranes are widely used for desalination purposes especially on laboratory scale (Alkhudhiri et al., 2012), they are claimed to have higher fluxes compared to those of the hollow fiber (Camacho et al., 2013), they are easier to clean and replaced when needed, and they are less prone to fouling compared to the hollow fiber membranes (Alkhudhiri et al., 2012). However, they have low packing density (area of the membrane over the packing volume). Hence, requiring a membrane support.

The support layer provides adequate mechanical strength that allows the active layer of the membrane to be extremly thin which will eventually reduce the mass transfer resistance. PTFE membrane was the only membrane used with a support. The backing support is a polypropylene non-woven layer that is laminated onto the PTFE membrane (as shown in Figure 80).

The length and width of the membrane coupons used in the bench scale DCMD cell is 19.2 cm and 14.1 cm, respectively. In additon, the active area of each membrane is 0.014 m^2.

4.4- DCMD Module Configuration (MD Block)

The MD block consists of two machined Teflon plates in which the membrane is sandwiched in between. Figure 26 depicts the top and bottom plates of the MD bock. The hot water that enters the block is carried out by the bottom plate, while the cold

stream and the permeate are carried by the top plate. The flow regime selected is counter-current.
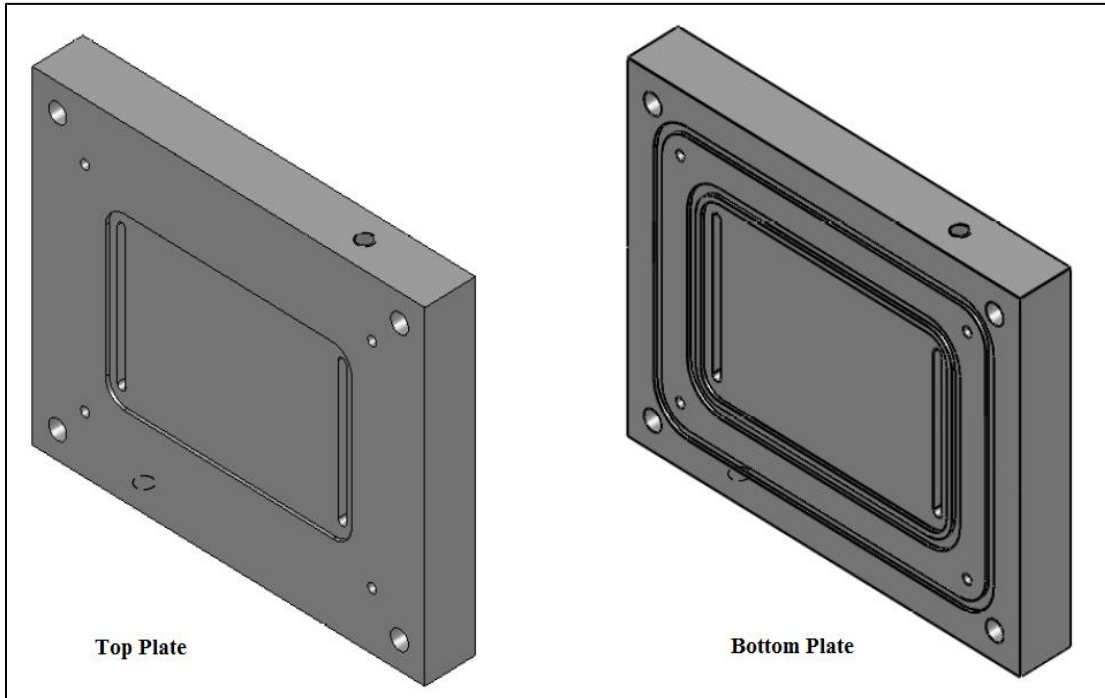
Figure 26: A Schematic Diagram of the Top and Bottom Plates of the MD Module

Moreover, Figure 27 shows the inner side of the plates. The 270.7 cm^2 membrane coupon is positioned on the bottom plate on a spacer over the inner O-ring cavity. The position of the membrane coupon is shown in Figure 28.
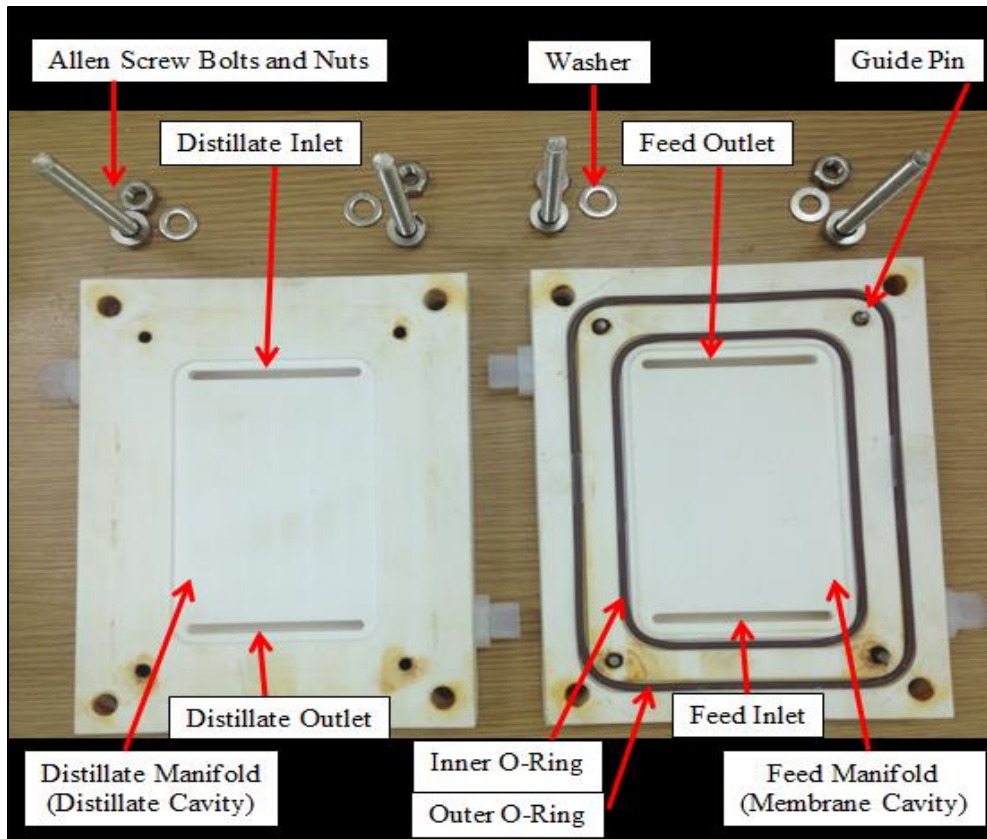
Figure 27: The Inner Side of the Top and Bottom Plates of the MD Block
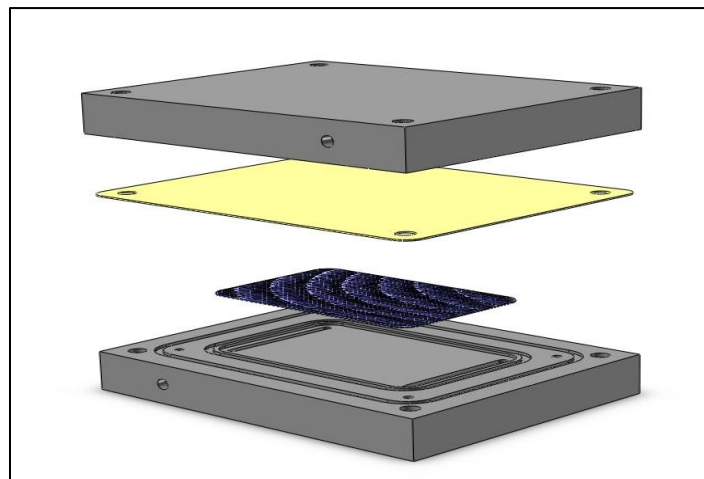
Figure 28: An Exploded View Diagram of the Position of the Membrane Coupon and

the Spacer in the MD Module

The spacer is used to provide turbulance for the flowing feed, while the inner O-ring prevents the hot water from mixing with the permeate flowing at the top plate. Moreover, the two Viton O-rings that are positioned in the inner and outer O-ring cavitities act as seals that prevent leakages. Furthermore, to insure proper alignment of the membrane and the plates when brought together, four stainless steel guide pins are placed in the bottom plate at the corners between the inner and outer O-rings cavities. Moreover, the two plates are secured together using four Allen screw bolts and nuts that are shown in Figure 27. Furthermore, to distribute the load of the screws when fitted in the flexible Teflon plates, four metal washers are used on each side of the plates. In addition, to futher prevent cell leakages, four clips are placed on the sides of the DCMD cell. Figure 29 shows the DCMD cell with the attached clips.

Figure 29: The DCMD Cell Used in the MD Unit with Clamping

The feed inlet and outlet and the cold water inlet and outlet ports were made in the bottom and top plates using National Pipe Thread (NPT) standards. Threaded channels offer effective seals to prevent liquid leakages. From the feed inlet, the hot water flows over the membrane cavity or the feed manifold that is carved in the middle of the bottom plate. Most of the water gets distilled by passing tangentially across the membrane surface and the rest gets recycled back into the feed tank in a closed loop fashion. The hot water is forced to move in this manner due to the location of the feed outlet that is in the opposite side of the plate. Likewise, the permeate flows through the top plate to the distillate manifold in the middle of plate and then flows out through the permeate outlet to the distillate tank.

4.5- Material of Construction

Several parts of the MD unit such as the MD block, the O-rings, and the fittings of the inlets and outlets of the streams are made of different materials. The MD module is made of solid PTFE (Teflon). Teflon has several advantages over the other polymeric materials such as polycarbonate, PVDF, and PP in that it is considered as a better insulating material due to its high thermal resistance in addition to its excellent chemical resistance. This is crucial in MD design as MD remains not an energy efficient technology. Therefore, Teflon prevents heat losses more efficiently. Other advantages of Teflon include:

- Good hydrophobicity.
- Having a low coefficient of friction.

- Resistance to various chemicals.

- Resistance to weather and UV.

- Exceptional performance at extreme temperatures (-240 ^{o}C – 260 ^{o}C).

- A non-stick material (Lenntech, 2014).

The O-rings that were used inside the MD cell to provide leak-proof seals are made of Viton of 2 mm diameter. Viton is a type of synthetic rubber and an elastomer with fluorocarbon based polymer. Viton has several advantages including:

- Exceptional performance at extreme temperatures (-23°C – 204 °C).

- Excellent resistance to degradation by a range of fluids and chemicals, offering the best proven fluid resistance of any commercial rubber.

- Extremely low permeability to a variety of substances.

- Highly resistant to atmospheric oxidation and weather.

- Low burning characteristics compared to other rubbers (Rainierrubber, 1998).

Furthermore, the fittings for the inlets and outlets of the streams (Parker, USA) are made of perfluoroalkoxy (PFA) Teflon nuts and ethylene tetra-fluoro-ethylene (ETFE) body. These high quality materials are corrosion resistant and exhibit excellent chemical and solvent resistant characteristics over a wide temperature range and can tolerate high pressures.

4.6- Dimensions

The length, width, and height of a single Teflon plate is 233 mm, 182.8 mm, and 30 mm, respectively. Therefore, the MD block dimensions are 233 mm × 182.8 mm × 60 mm. The exact sizes of the top and bottom plates are shown in Figure 30 and Figure 31, respectively.
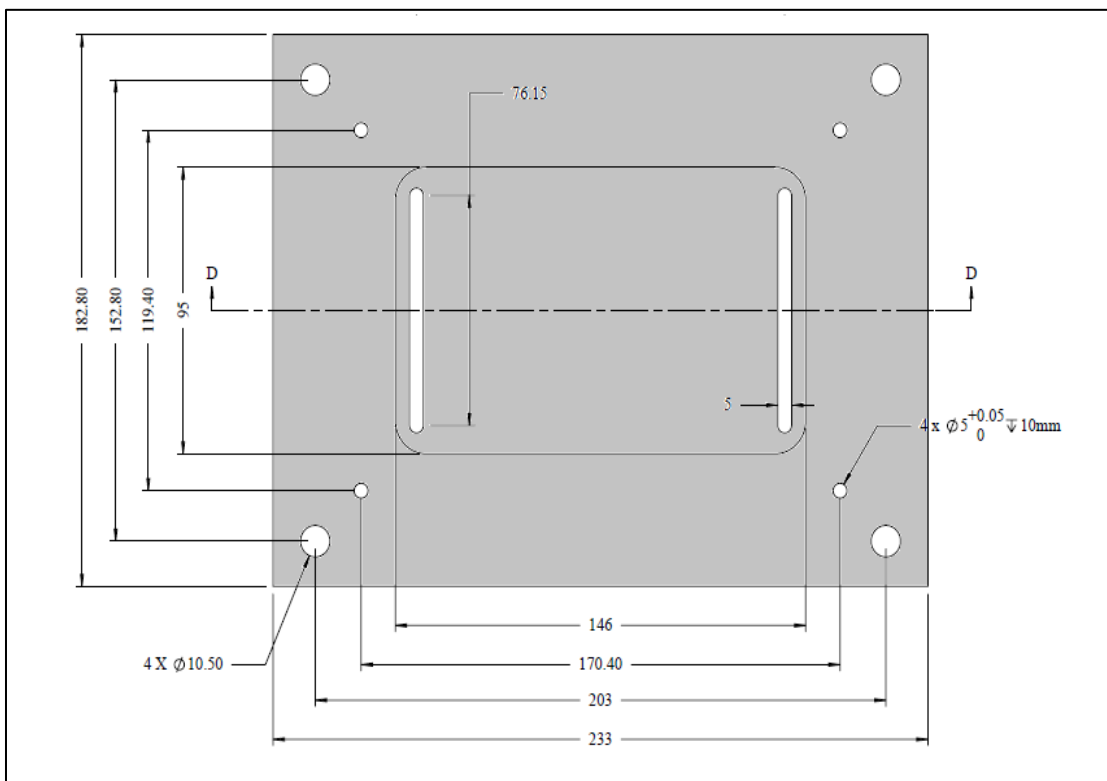
Figure 30: The Dimensions of the Outer Side of the Top Plate (in mm)
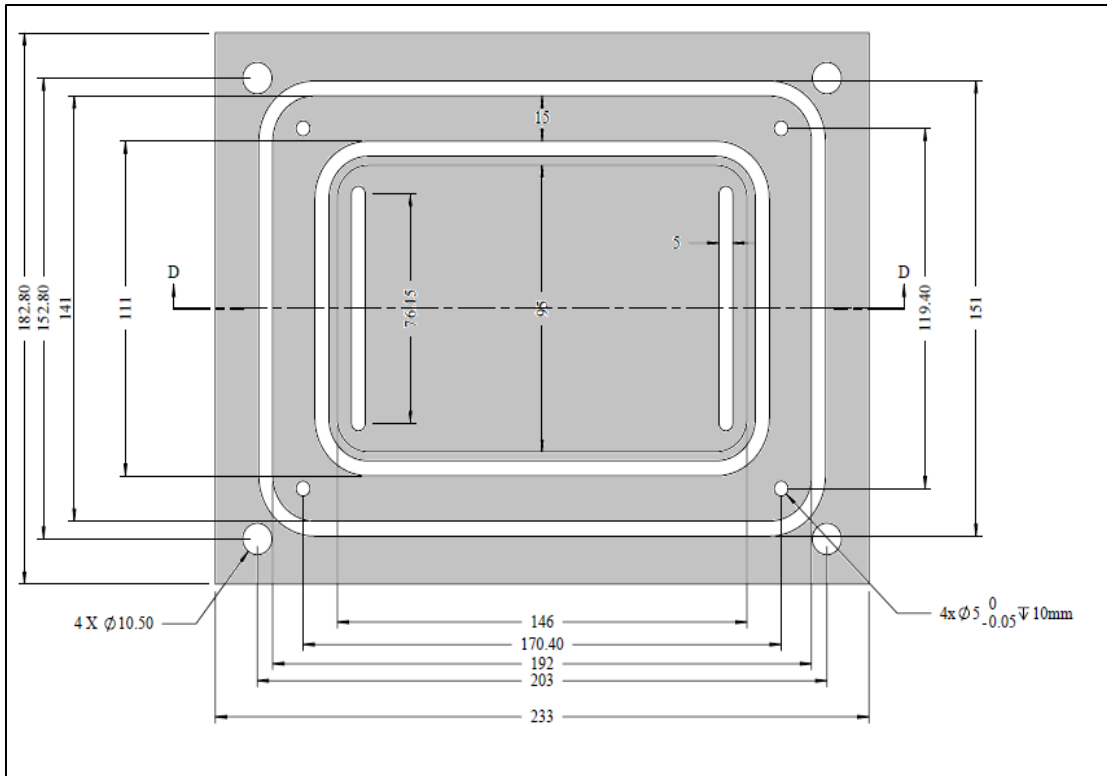
Figure 31: The Dimensions of the Inner Side of the Bottom Plate (in mm)

The depth of the membrane cavity is 2 mm. In addition, the depth of the grooves for the two 2 mm diameter O-rings is 2 mm to provide a water-tight seal. Figure 32 illustrates the dimensions of the sides of the bottom and top plates.
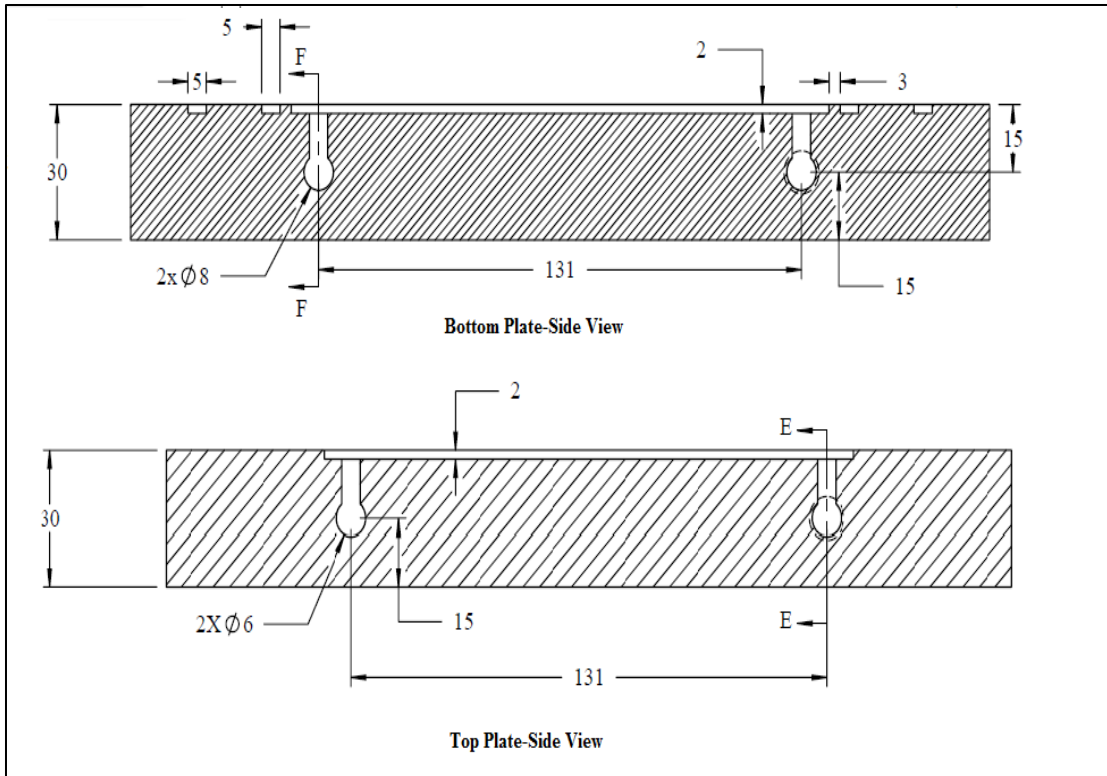
Figure 32: The Dimensions of the Sides of the Bottom and Top Plates (in mm)

The length of the membrane cavity and the inlets/outlets of the bottom and top plates is 132 mm. 3/8" FNPT fittings were used in the inlets and outlets. Figure 33 illustrates a front view of the bottom and top plates showing the length of the membrane cavity and the streams inlets and outlets.
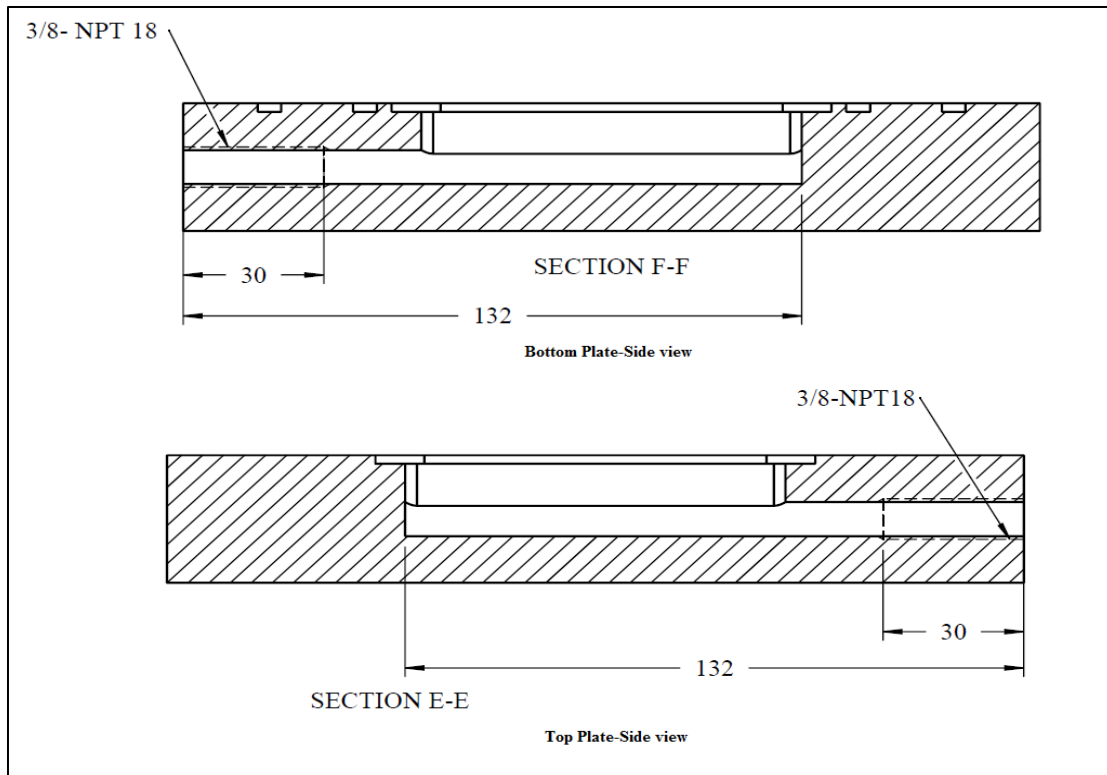
Figure 33: The Length of the Membrane Cavity and the Streams Inlets and Outlets in

mm (Front View)

4.7- Auxiliary Equipment

The operation of the DCMD unit was done using various auxiliary equipment. These include: pumps, a heater and a cooler, temperature and pressure sensors, flow rate meters, weighing balances, and a data acquisition system. This section presents the details of those equipment including their function in the DCMD unit.

4.7.1- Pump

Peristaltic pumps were used as parts of the DCMD unit. They deliver the feed water and distillate to the heater and cooler, respictively, before entering the MD block. The choice of using this type of pumps is due to their accuracy, low maintenance, and reliable control of flow. Also, the pumps are easily cleaned (Coleparmer, 2014).

The pump is a Thermo Scientific general purpose peristaltic pump (FH100X) that is digitally controlled. Table 15 shows the specifications of the peristaltic pumps used in the experiments.

Table 15: The Specifications of the Peristaltic Pumps Used in the Experiments
(Coleparmer, 2014)

Flow Rate	14 – 4000 mL/min
Maximum Pressure	4 bar
Temperature Range	0 to 40 ^{o}C
Dimensions (Length × Width × Height)	$31.7 \times 27.9 \times 15.2$ cm
Revolutions per Minute (RPM)	4 to 400
Accuracy	± 0.25 %

Vincon C-219-A flexible PVC tubing (ABH02028) with 3/8" ID x 9/16" OD x 3/32" Wall from Saint Gobain, USA was used with the peristaltic pumps. Table 16 shows the specifications of the tubing used.

Table 16: The Specifications of the Tubing Used for the Peristaltic Pumps (USplastic, 2014)

Type	PVC (Vincon)
Inner Tubing Diameter	9.5 mm
Outer Diameter	14.3 mm
Wall Thickness	2.4 mm
Color	Clear
Temperature Range	- 43 – 80 ^{o}C

4.7.2- Heaters and Coolers

For heating the feed and cooling the fresh water, two Julabo refrigerated/heating circulators were used. Table 17 shows the specifications of the refrigerated/heating circulators used.

Table 17: The Specifications of the Refrigerated/Heating Circulator Used in the MD Unit (Julabo, 2014)

Model	F32-MA, Julabo, Germany
Working Temperature Range	-35 – 200 $^{\circ}$C
Temperature Stability	± 0.02 $^{\circ}$C
Dimensions (W x L x H)	$31 \times 42 \times 64$ cm

The F32-MA refrigerated/heating circulator has several advantages as it has an LED display for the actual and set-point temperature values, an early warning system that gives an indication if the liquid level is low, and a venting grid that is easily removed to be cleaned from accumulated dust (Julabo, 2014).

As the feed solutions cause the metals they are in contact with to corrode, an anti-corrosive material needed to be used in the water bath. Therefore, a special coil of Hastelloy C-276 was used in the heater. Hastelloy C-276 is an alloy that is nickel-based. It has high concentrations of chromium (Cr) and molybdenum (Mo). Hastelloy C-276 has several applications due to its excellent corrosion resistance (Zhang et al., 2009).

4.7.3- Temperature and Pressure Measurement

The temperature of the streams into and from the MD cell was measured using resistance temperature detectors (RTDs) pipe plug probes with NPT fitting (RTD-NPT-72-E, Omega Engineering, UK). Table 18 shows the specifications of the RTDs used in the MD unit.

Table 18: The Specifications of the Temperature Transducers Used in the MD Unit

(Omega, 2014)

Maximum Temperature	230 °C
Maximum Pressure	2500 psi

On the other hand, the pressure of the streams was measured using general purpose pressure transducers (PX309-030GI, Omega Engineering, UK). Table 19 shows the specifications of the pressure transducers used in the MD unit.

Table 19: The Specifications of the Pressure Transducers used in the MD Unit

(Omega, 2014)

Operating Temperature	- 40 – 85 °C
Pressure Range	1 – 5 psi
Accuracy	± 0.25 %

Moreover, NPT was used to fit the temperature and the pressure sensors to prevent leakages.

4.7.4- Flow Meter

The hot feed flow rate was measured using a magmeter (magnetic flow meter) that is chemical and corrosion resistant, with no moving parts, and with NPT fittings (FMG82, Omega Engineering, UK). Table 20 shows the specifications of the flow meter used to measure the hot feed flow rate. This flow meter requires a minimum liquid conductivity to function.

Table 20: The Specifications of the Flow Meter Used to Measure the Hot Feed Flow Rate (Omega, 2014)

Fluid Temperature Range	$0 - 93\,^{\text{o}}\text{C}$
Pressure Rating	150 psi
Flow Range	$0.03 - 3$ GPM
Accuracy	$\pm\,1\,\%$

On the other hand, the distillate flow rate was measured using a PTFE liquid flow sensor (FPR1506, Omega Engineering, UK) that uses Pelton-type turbine wheel to measure the flow rate of the water. Table 21 shows the specifications of the flow meter used to measure the distillate flow rate.

Table 21: The Specifications of the Flow Meter Used to Measure the Distillate Flow

Rate (Omega, n. d.)

Fluid Temperature Range	$0 – 70\,^{o}C$
Pressure Rating	58 psi
Maximum ΔP	10 psi
Flow Rate Range	0.5 – 5 L/min
Accuracy	$\pm\ 3\ \%$

4.7.5- Conductivity Meter

One of the measures to assess the quality of the distillate is by measuring its conductivity. The conductivity of the feed and distillate was determined using a WTW Multi 3420 Multiparameter Meter with Tetracon 925 conductivity measuring cell. Table 22 shows the specifications of the conductivity meter used in the study.

Table 22: The Specifications of the Conductivity Meter Used in the Study (WTW,

2009)

Conductivity Measuring Range	$1\ \mu S/cm – 2\ S/cm$
Temperature Range	$-5 – 100\,^{o}C$

4.7.6- Digital Display

Digital display meters (DP25-E-230-A, Omega Engineering, UK) were used to check the readings of the temperatures, pressures, and flow rates of the streams during operation. These display meters convert analog data to digital data that is readable by a PC. Table 23 shows the specifications of the digital display meters used in the MD unit system.

Table 23: The Specifications of the Digital Display Meters Used in the MD Unit System (Tuner, n. d.)

Number of Digits	4
Display Technology	LED
Display Colors	Red, Amber, and Green
Dimensions	48 H × 96 W × 152 mm D

4.7.7- Weighing Balance

The weighing balances used during the experiments served two purposes: to monitor the changes in the feed and distillate weights and to determine the flux of the produced distillate. The balances used were NewClassic precision balances (MS4002SDR, Mettler Toledo, US) that provided high accuracy. Table 24 shows the specifications of the weighing balances used in the MD unit system.

144

Table 24: The Specifications of the Weighing Balances Used in the MD Unit System

(Mettler Toledo, n. d.)

Maximum Capacity	820/4200 g
Readability	0.01/0.1g
Weighing Pan Dimensions	170×200 mm
Balance Dimensions	347 L $\times$ 194 W $\times$ 96 mm H

The flux of the produced distillate was determined by dividing the weight of the distillate over the active membrane area and the given time.

4.7.8- Data Acquisition System

The control of the several equipment used in the MD unit system and the collection of data were accomplished by utilizing a PC and a National Instruments (NI) data acquisition hardware which included an 8-slot Ethernet chassis (NI cDAQ-1988, National Instruments, US) and an analog input module (NI 9219, National Instruments, US). The module has four analog-to-digital converters (ADCs) and it enables temperature, RTD, thermocouple, resistance, strain/bridge-based sensor, voltage, and current measurements (National Instruments, n. d.). In addition, LabVIEW software was used to manage the timing and control of the several instruments used.

Table 25 shows the specifications of the analog input module used in the MD unit system.

Table 25: The Specifications of the Analog Input Module Used in the MD Unit System (National Instruments, 2007)

Operating Temperature	-40 – 70 $^{\circ}$C
Resolution	24 bits
Voltage Range	-60 – 60 V
Maximum Current Range	-0.025 – 0.025 A
Length $\times$ Width	9 $\times$ 2.3 cm

The universal C-series chassis was connected to NI CompactDAQ 8-Slot USB Chassis (NI cDAQ-9178, National Instruments, US). It is capable of running analog input, analog output, digital input and output, and counter/timer input (National Instruments, 2015).

To obtain the weight of the feed and distillate from the balances, a serial server was used (NI ENET-232, National Instruments, US). A serial server connects any device with serial ports over Ethernet for access to network server applications (USB to RS232, RS422, and RS485) (Perle, n. d.).

4.7.9- Tubing

The feed brine and distillate were pumped through C-219-A flexible PVC tubing (ABH02028) with a brand name Vincon and with dimensions 3/8" ID x 9/16" OD x 3/32" Wall. It is manufactured by Saint Gobin in USA and marketed by Murdock Industrial, USA. It is essentially a special type of clear PVC with good wear resistance, suitable for peristaltic pump application. The specifications of the tubing are tabulated in Table 16 in Section 4.7.1.

4.8- Experimental Procedure

Different procedures were carried out to characterize fouling and to measure the quality of the distillate. The experimental procedures used to meet the objectives of the study are outlined in this section.

4.8.1- Membrane Material Characterization

Several experiments were conducted to meet the objectives of the study. The hot water and the cold water were set to identical flow rate of 1.5 L/min. This was done by adjusting the rotational speed of the pumps. The hot water temperature was set at 75 $^{\circ}$C and the cold water temperature was set at 20 $^{\circ}$C. The experiments were carried out using different feed solutions with different conductivity: Seawater from the Arabian Gulf and 100,000 ppm synthetic NaCl solution. In addition, deionized water was used as the cold water and it was mixed during the experiments with the

distillate. Table 26 shows the parameters of the conducted experiments on the lab scale DCMD unit. It was assumed that the structural integrity of the membranes at high temperatures remains as work done in the literature at high temperatures didn't report any problems (Manawi et al., 2014; Fard et al., 2015).

Table 26: The Operational Parameters of the Conducted Experiments on the Lab Scale DCMD Unit

Hot Water Inlet Temperature (^{o}C)	Cold Water Inlet Temperature (^{o}C)	Pressure (atm)	Feed/Permeate Flow Rate (L/min)
75	20	1	1.5

Moreover, several sets of experiments were conducted in this study using the different membranes. For each set of experiments, at least five runs were conducted.

4.8.2- Contact Angle Measurement

To indicate the membranes' hydrophobicity, contact angles of the membranes' active layer (and back layer in case of PTFE membrane) were measured before and after the operation of the MD unit. This was done using a state of the art drop shape analyzer (DSA25, KRÜSS, Germany) equipped with a video capturing system. The liquid

dosing using this analyzer can be done manually or it can be software-controlled. The instrument is controlled by the drop shape analysis proprietary software DSA4. Figure 34 shows the KRÜSS drop shape analyzer that was used to assess the contact angles of the membranes. The analysis was carried out at Qatar University's Chemical Engineering Research Laboratory.
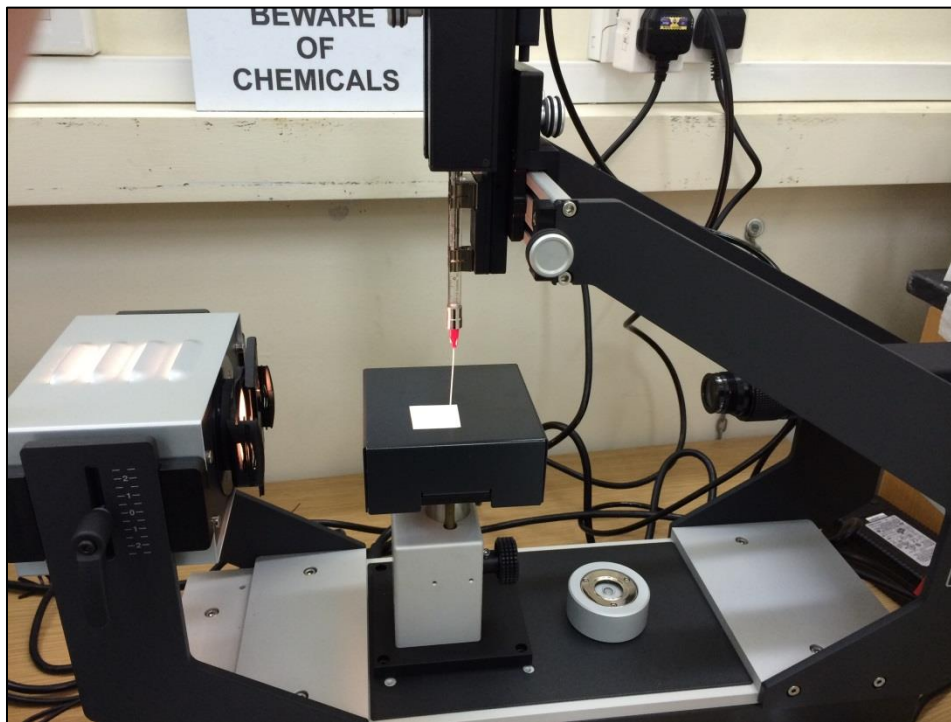
Figure 34: The KRÜSS Drop Shape Analyzer used for the Contact Angle Measurements

The contact angles were measured by the sessile drop method. A drop of about 6 μL was deposited manually on the flat and smooth surface of each membrane using a syringe that was placed perpendicular to the surface of the membranes. The contact angle was then calculated for each membrane with the aid of the computer software

using a digital image processor. The contact angle of each membrane was measured at least ten times using de-ionized water. Several measurements were taken to get reliable data. An average contact angle was later taken for each membrane used.

When performing the measurements, each membrane was brought into contact with a drop of the de-ionized water. A membrane sample was cut into thin strips or rectangles and the sides of the membrane were pasted using transparent tape onto the manual lift table of the drop shape analyzer for the measurement of contact angle. This is shown in Figure 35.
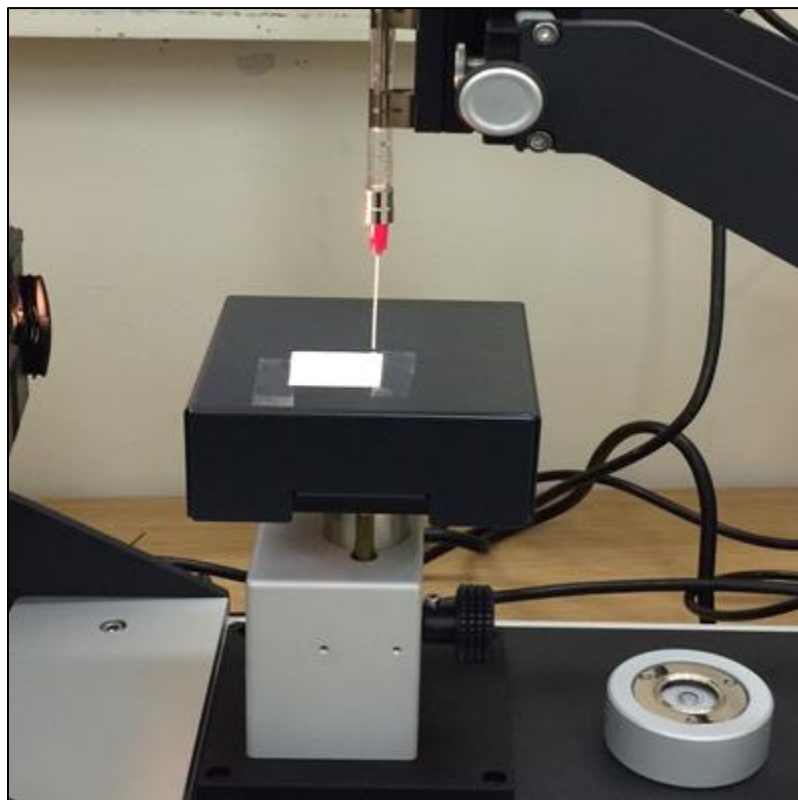
Figure 35: The Position of the Membrane Stripe in the Drop Shape Analyzer

As discussed in Section 3.6, theoretically, contact angles measured using the sessile drop method are described by the Young's equation (Equation 25) that is only applicable to completely uniform and smooth surfaces (Bachmann et al., 2000), which was assumed while performing the contact angle measurements.

4.8.3- SEM Imaging

Scanning Electron Microscope (SEM) is a type of electron microscopes. It is used to observe surface and cross sectional structures of a membrane along with other aspects of the membrane such as observing the membrane pores, bonding, and the membrane's support layer. Under each SEM image, the membrane name and scale of the image is able to be found. In addition, SEM produces detailed three-dimensional images. Moreover, with regard to SEM characterization, in order to observe a membrane's cross sections, the membrane needs to be frozen in liquid nitrogen to form an intact cross section and thereafter cut with a blade (Zhang et al., 2010). The membrane's thickness is then taken by SEM through imaging of the membrane cross section.

SEM imaging that was performed to study the fouling of the membranes used in this study was done using an FEI Quanta 200 Environmental Scanning Electron Microscope (ESEM) with a resolution of 5 nm. The SEM imaging was undertaken in Qatar University's Central Laboratory Unit (CLU). Moreover, the SEM was coupled with Energy Dispersive Spectroscopy (EDS) to determine the main chemical elements that cause MD fouling.

4.8.4- Water Quality Experiments

The quality of the distillate via desalination using the MD unit was tested after conducting all of the experiments using two different feed solutions with different conductivity values. The analysis was done for the feed samples and the distillates to compare the results.

To assess the quality of the distillate, four measures were used. For metals and trace elements analysis (cations), Inductively Coupled Plasma-Optical Emission Spectrometry (ICP-OES) was used. However, for non-metals (anions) analysis, Ion Chromatography (IC) was used. Moreover, the pH and conductivity of the samples were measured to judge the water quality.

4.8.4.1- Cations Analysis

An ICP-OES (iCAP 6500, Thermo Scientific, US) was used to measure the amount of cations present in the water samples. The objective of the experiment was accomplished by following several steps. Blanks were first prepared by pipetting 100 mL Nitric Acid into a volumetric flask that contained ultra-pure water (to the mark). After that, several standards were prepared. After placing the blanks, the standards, and the samples in the auto-sampler rack of the ICP-OES, the analysis was done using the ICP-OES compatible software.

4.8.4.2- Anions Analysis

An IC (850, Metrohm, Swaziland) was used to measure the amount of anions present in the water samples. The concentrations of the ionic species can be measured using ion chromatography by separating them based on their interaction with a resin or a gel matrix or the retention time of the different species which depends on the ionic species' type, charge and size. The analysis was done with the aid of a computer software (MagIC Net).

Chapter 5: Results and Discussion

The results and discussion of the carried out experiments that were designed to investigate membrane fouling using a bench-scale DCMD process used for water desalination are presented in this chapter.

The results of this study are divided into the following sections:

1- Flux Performance

2- Water Quality Analysis

3- Contact Angle Measurements

4- SEM Characterization and EDS Analysis

5.1- Flux Performance

Several experiments were conducted to first determine the flux profile generated from using different hydrophobic membranes and second to examine the flux performance of those membranes after long term MD operation to investigate membrane fouling. Moreover, the experiments were carried out using seawater as feed under the same conditions of hot water inlet temperature of 75 ^{o}C, cold water inlet temperature of 20 ^{o}C, and hot and cold water flow rate of 1.5 L/min and with counter-current mode to examine the fouling of the membranes used. It is worth noting that the hot and cold outlet temperatures were 69 °C and 24 °C, respectively. The experimental procedure was discussed in Section 4.8. Moreover, other sets of experiments were conducted

using a synthetic 100,000 ppm NaCl solution to examine the effect of a higher TDS solution on MD-membrane fouling and to explore what elements in the feed water will eventually cause membrane fouling. The experiments were performed using a bench-scale DCMD unit utilizing three different membranes: PP membrane of two pore sizes (0.22 μm and 0.45 μm), and PTFE membrane of pore size 0.22 μm. Each membrane used in this study had an active area of 0.014 m^2. The appearance of the flat-sheet membranes used is depicted in Figure 25 in Section 4.3.

In this chapter, the hot and cold inlet temperatures of the streams in the study are represented by two temperatures separated by a dash, i.e., 75-20 °C. Also, the flux unit that is used in the study is L/m^{2}h or simply LMH.

Figure 36 illustrates the permeate flux profile generated using PP membrane of pore size 0.22 microns at 75-20 ^{o}C and hot and cold water flow rate of 1.5 L/min.
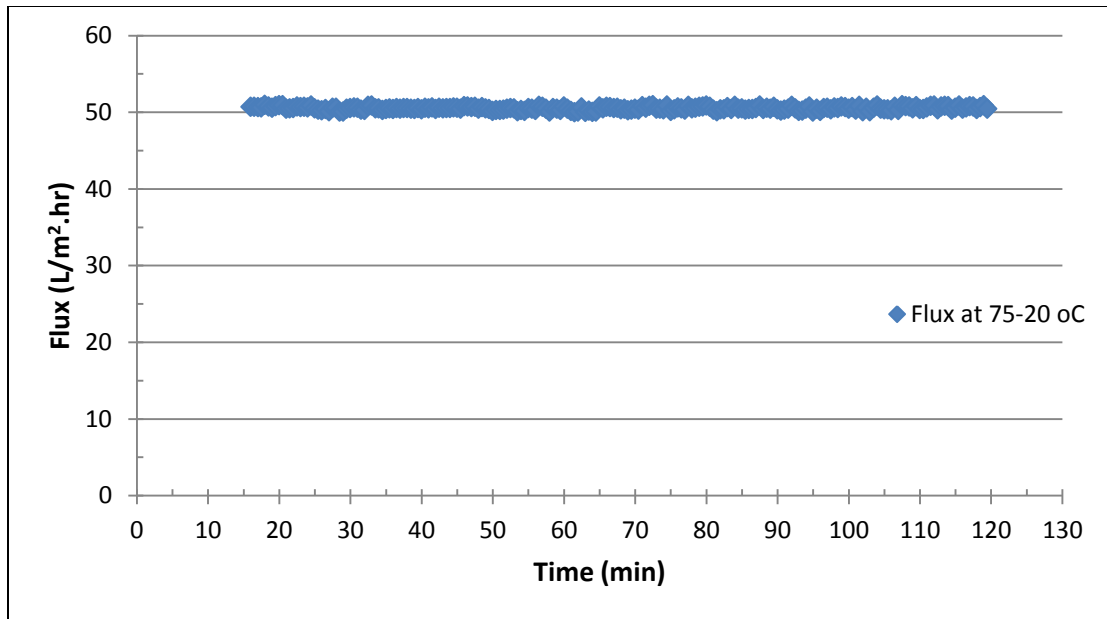
Figure 36: The Permeate Flux Profile Using PP (0.22 μm) Membrane and Seawater as

Feed at 75-20 °C and 1.5 L/min

Figure 36 shows that the average flux obtained was 50.5 LMH when PP membrane of 0.22 μm was used.

Moreover, Figure 36 illustrates the permeate flux profile generated using PP membrane of pore size 0.45 microns under the same conditions of hot water inlet temperature of 75 °C, cold water inlet temperature of 20 °C, and hot and cold water flow rate of 1.5 L/min.
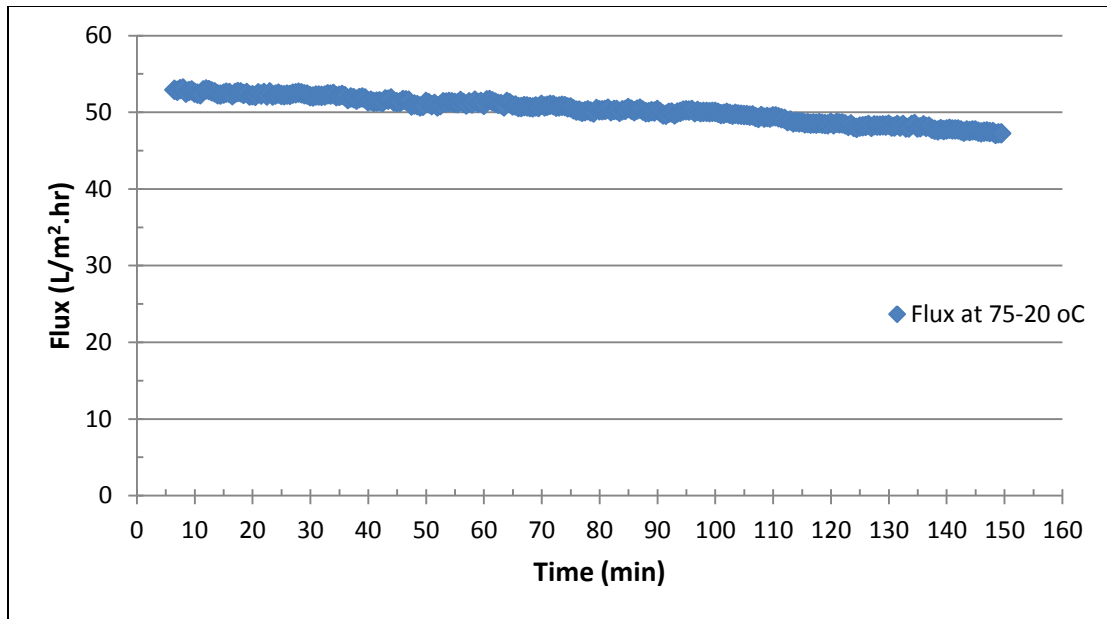
Figure 37: The Permeate Flux Profile Using PP (0.45 μm) Membrane and Seawater as

Feed at 75-20 ^{o}C and 1.5 L/min

Figure 37 shows that the average flux obtained was 50.3 LMH when PP membrane of 0.45 μm was used. The flux is almost the same as that generated when PP membrane of pore size 0.22 μm was used. However, as time passed, they behaved differently regarding flux decline. The flux profile of PP membrane of 0.22 microns was flat. On the other hand, the flux profile of PP membrane of 0.45 microns was higher initially but had a steeper slope indicating a decline in the flux with time. This means that the membrane is getting blocked in a way that reduces the flux to some extent. This might be due to the larger pore size of PP membrane of 0.45 microns which enables more vapor transfer. Schneider et al. (1988) state that the permeate flux increases with increasing membrane pore size, which is related to the improved mass transport. This was also shared by El-Bourawi et al. (2006) and Cath et al. (2004).

In addition, Figure 38 illustrates the permeate flux profile generated using PTFE membrane of 0.22 microns under the same conditions of 75-20 $^{\circ}$C and 1.5 L/min.
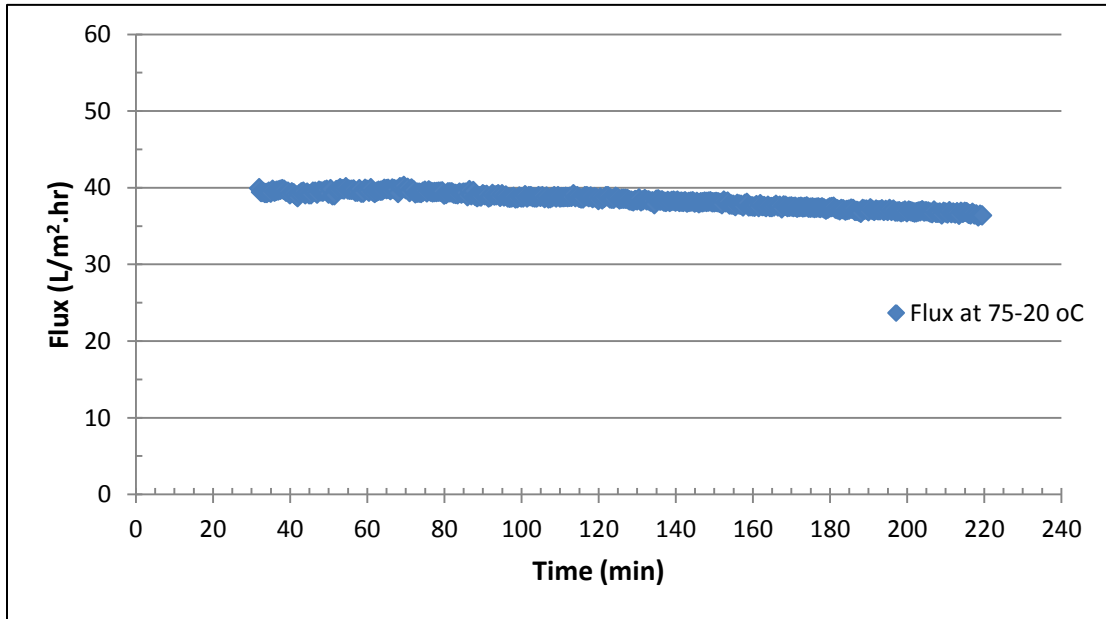
Figure 38: The Permeate Flux Profile Using PTFE Membrane at 75-20 $^{\circ}$C and 1.5 L/min

Figure 38 shows that the average flux obtained was 38.3 LMH when PTFE membrane was used, which is less than the one generated for PP membrane of the both sizes used. Nevertheless, the flux profile is smooth with a slight decrease after 3 hours of operation.

The larger pore size membrane had the highest flux which was expected as flux increases with increasing pore size. Cath et al. (2004) have conducted experiments on a DCMD unit. Their results showed that the membranes with larger pore sizes generated higher fluxes. This was the case as with increasing membrane pore size, the

mass transfer in the pores is controlled by Knudsen-viscous transition rather than Knudsen diffusion which results in increased permeability and hence a higher permeate flux (Lawson & Lloyd, 1997; Guijt et al., 2000; Cath et al., 2004; Schneider et al., 1988).

Figure 36, 37, and 38 show that the bench-scale DCMD unit used reproduces consistent results. Table 27 summarizes the average flux of the tests performed using the three membranes.

Table 27: The Average Flux Generated Using the Three Membranes Used in the Study

Membrane	PP (0.22 µm)	PP (0.45 µm)	PTFE (0.2 µm)
Flux (LMH)	50.5	50.3	38.3

Despite the type of membrane used, the high feed temperature of 75 °C led to generating a high permeate flux as the evaporation process increased. This is due to the exponential rise of the vapor pressure of the feed with temperature according to Antoine equation. On the same principle, decreasing the permeate temperature results in higher vapor pressure; hence, higher generation of permeate flux.

Therefore, since there is a linear relationship between the heat loss through thermal conduction and the temperature difference across the membrane, the proportion of energy used for evaporation will increase linearly with feed temperature (Zhang and

Dow et al., 2010). However, high feed temperature results in increased temperature polarization (Zhang & Dow et al., 2010; Zhang et al., 2012; Camacho et al., 2013) which let the membrane become more susceptible to fouling. Nevertheless, the effect of this phenomenon will be discussed in the next section.

Khayet & Matsuura (2011) emphasized that an exponential increase in the permeate flux is directly proportional to an increase in the feed temperature while maintaining a constant permeate temperature.

Mohammadi & Safavi (2009) have conducted an experimental study on a VMD process. The effect of temperature on the permeate flux was studied using a commercial PP membrane with a pore size of 0.2 μm and NaCl as the feed solution. The results showed that increasing the hot inlet temperature improves the permeate flux.

Cath et al. (2004) have worked on a DCMD unit using a feed temperature of 40 °C. The results showed that the permeate flux increases by more than 2 $L/(m^2.h)$ for every 1 °C increase in feed temperature.

Alklaibi & Lior (2004) state that increasing the hot feed temperature can significantly improve the permeate flux and that increasing the temperature from 50 °C to 70 °C increases the flux by more than three-fold.

Thus, the flux generated using PP membrane of 0.22 and 0.45 microns and PTFE membrane of 0.22 microns was reasonable.

In addition, Camacho et al. (2013) have stated that the reported flux from flat sheet membranes is between 20–30 L/(m^2.h) at inlet hot and cold streams temperatures of 60 °C and 20 °C, respectively. Therefore, the permeate flux values found in this study are consistent.

The effect of temperature on the permeate flux was also studied. Figure 39 and 40 demonstrate this effect using PP membrane of 0.22 microns and PTFE membrane of 0.22 microns, respectively, and seawater as feed to the bench-scale DCMD process. The effect of increasing the hot feed temperature can be seen before the flux is stabilized at 75 °C (the desired hot feed temperature of the study).
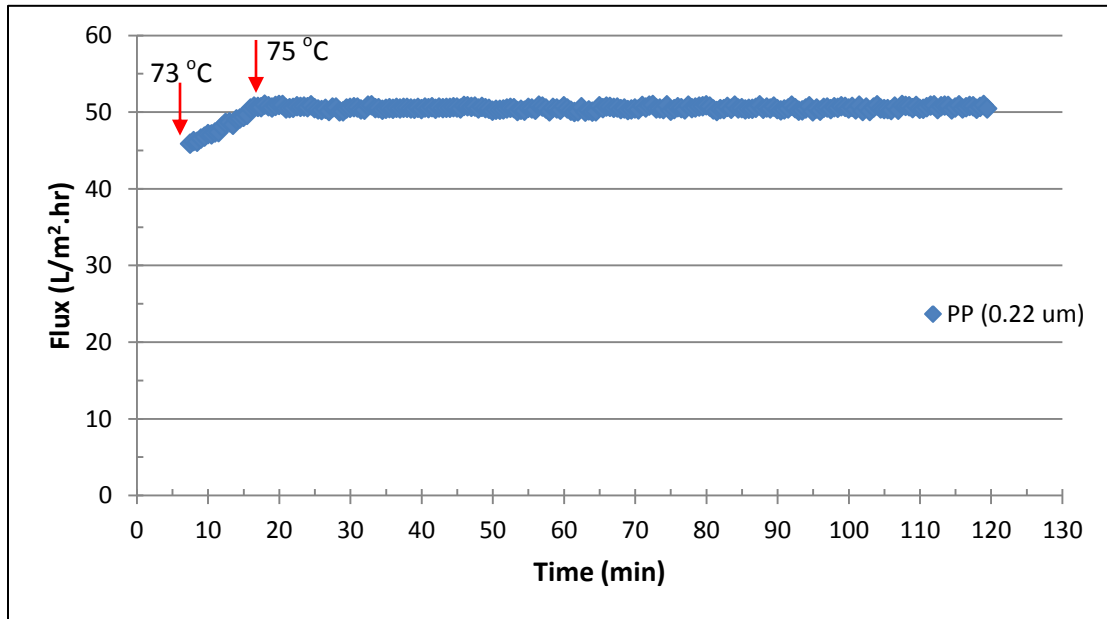
Figure 39: The Flux Performance with Increasing Temperature Prior to Being Stabilized at 75 °C Using PP (0.22 μm) Membrane
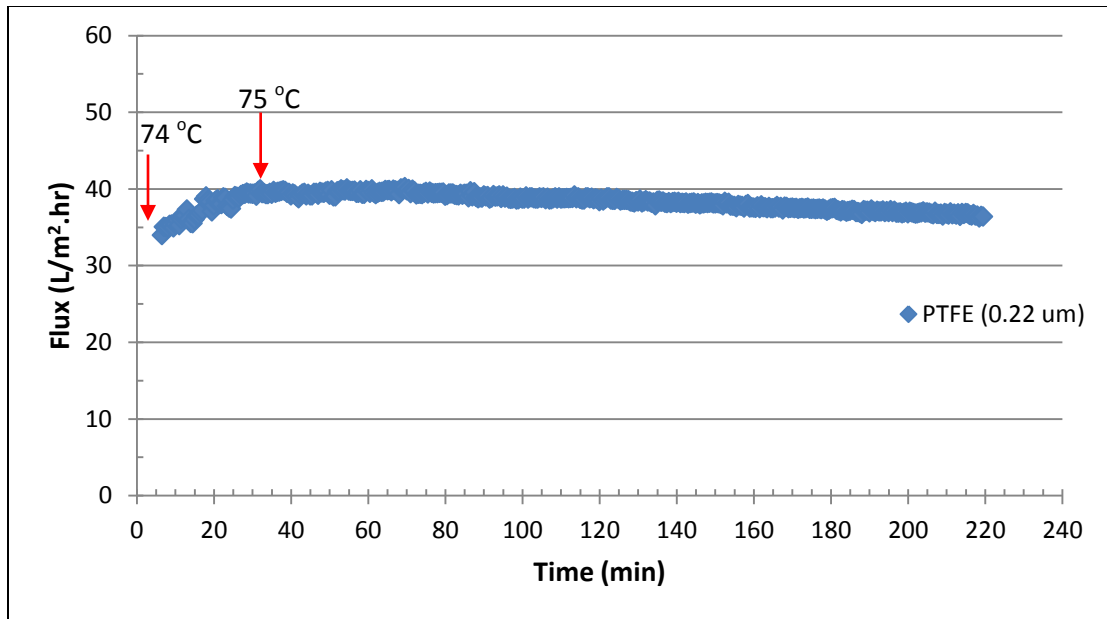
Figure 40: The Flux Performance with Increasing Temperature Prior to Being

Stabilized at 75 °C Using PTFE (0.22 μm) Membrane

Besides the effect of membrane pore size and feed temperature on the permeate flux, the effect of feed concentration was also studied. Figure 41 shows a comparison of the flux performance using seawater and 100,000 ppm NaCl solution at hot feed temperature of 75 °C, cold inlet temperature of 20 °C, and hot and cold flow rates of 1.5 L/min.
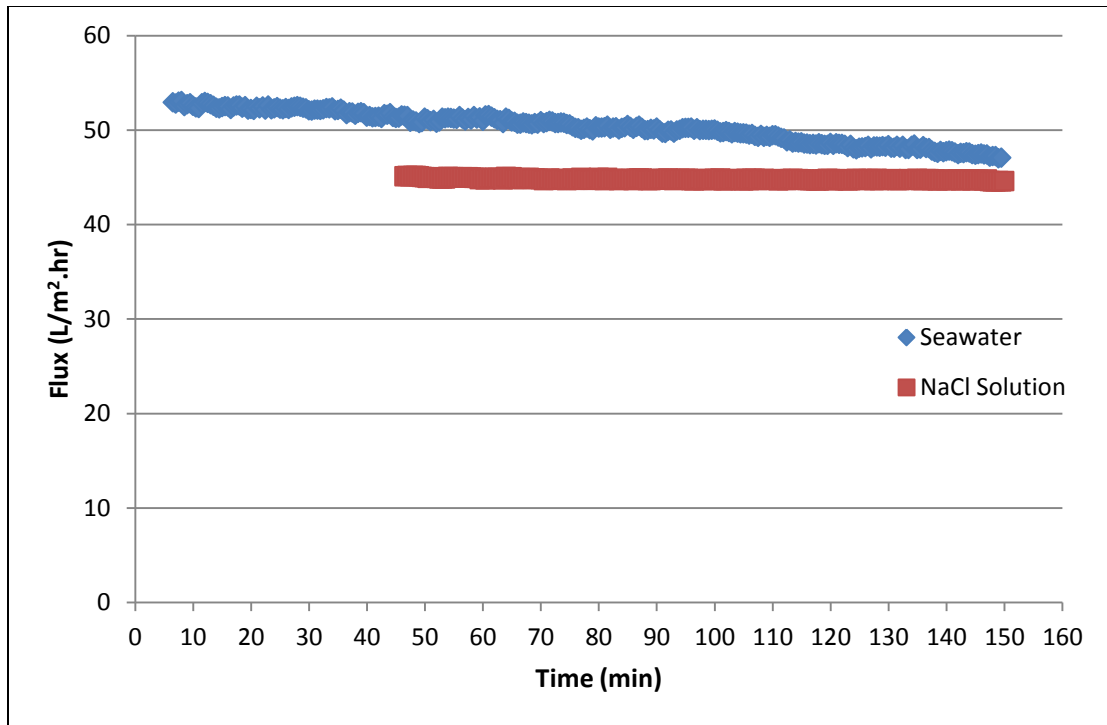
Figure 41: The Flux Performance at 75-20 °C Using Seawater and Synthetic Brine

Utilizing PP (0.45 μm) Membrane

Figure 41 shows that although the same membrane was used with the same operating conditions, the difference in the feed concentration affected the permeate flux slightly. The lower flux for the synthetic brine is probably due to vapor pressure depression due to its high salinity and is about 10% lower than the flux using the seawater. Also, the phenomenon called concentration polarization is enhanced, potentially adversely affecting the mass transport.

The results found are also consistent with literature (Adham et al., 2013; Winter et al., 2011).

In general, when the feed solution contains a high concentration of salts, concentration polarization is enhanced. Together with the temperature boundary layer, this layer reduces the driving force for water evaporation.

Moreover, the decrease in flux accompanied the increase in feed concentration was due to the fact that with this increase, the concentration polarization increases and the mass transfer coefficient decreases as well as the heat transfer coefficient (Lawson & Lloyd, 1997).

Nevertheless, to increase the transfer coefficients and to reduce the temperature and concentration polarization in order to enhance the permeate flux, the feed flow rate should be increased and the MD process should be operated under turbulent flow regime which can be done by employing a higher mixing intensity (El-Bourawi et al., 2006). This will result in increased transmembrane temperature difference, as the temperature at the membrane surface will be closer to the bulk feed temperature, which has a linear relationship with the permeate flux. Mohammadi & Safavi (2009) and Alklaibi & Lior (2004) also state that the thickness of the boundary layer decreases with increasing the flow velocity.

In addition, extended MD experiments were conducted to examine membrane fouling. Extreme conditions were chosen to enhance the rate of membrane fouling: high hot feed inlet temperature of 75 $^{\circ}$C, low cold stream inlet temperature of 20 $^{\circ}$C, and reasonably low hot and cold streams flow rate of 1.5 L/min.

Due to the limited available time and long nature of experiments, specific number of runs was carried out using the different membranes. Each run was of different duration. Table 28, 29, and 30 show the number of runs done for each experiment using a different membrane (with seawater as the feed solution to the process) and the duration of those runs. In addition, Table 31 shows the number and duration of the experiments done using the synthetic brine as feed to the bench-scale DCMD unit.

Table 28: The Duration of the Long Performed Runs Using PP (0.22 µm) Membrane and Seawater as Feed

Run #	Duration	
	h	min
1	1	43.5
2	3	17.5
3	4	24.5
4	3	49.5
5	5	20.0
Cumulative Time	18 hrs. and 35 min	

Table 29: The Duration of the Long Performed Runs Using PP (0.45 μm) Membrane

and Seawater as Feed

Run #	Duration	
	h	min
1	2	23.0
2	3	54.0
3	4	31.5
4	2	54.0
5	5	9.5
6	3	40.0
7	3	2.0
8	3	8.0
9		35.0
Cumulative Time	29 hrs. and 17 min	

Table 30: The Duration of the Long Performed Runs Using PTFE (0.22 μm)

Membrane and Seawater as Feed

Run #	Duration	
	h	min
1	3	7.5
2	4	27.0
3	3	33.5
4	2	59.0
5	4	6.0
6	3	44.0
7	2	47.0
Cumulative Time	24 hrs. and 44 min	

Table 31: The Duration of the Long Performed Runs Using PP (0.45 μm) Membrane

and Synthetic Brine as Feed

Run #	Duration	
	h	min
1	3	9.5
2	3	14.5
3	3	17.5
4	2	54.0
5	3	41.0
6		18.0
Cumulative Time	16 hrs. and 34.5 min	

It is worth mentioning that the overall durations of each experiment were longer than those specified in the tables. To start-up the experiment, the heater took a long time to heat the feed water to the desired high temperature of the study of 75 ^{o}C. In addition, for the first run using a new membrane, the membrane cell has to be opened to place the new membrane, washed and cleaned, and then closed, which is a time-consuming process. Besides, the tanks have to be cleaned prior to starting the experiments using a membrane. Also, in some of the experiments:

1- The data acquisition was done before reaching the desired hot water inlet temperature to observe the difference in flux. Therefore, it took time for the flux to be consistent due to flow rate fluctuations as well, so some data at the beginning of the experiments weren't considered.

2- The flux reached negative values, meaning that the membrane was blocked in a way and no distillate was produced. The negative flux is probably due to osmosis through the salt accumulation on the membrane. Therefore, some data at the end of an experiment weren't considered.

Therefore, the actual duration of an experiment was more than its "effective time" in which the flux readings were considered for this study.

Also, the distillate tank capacity was 5 L and there had to be some water initially in the tank for the experiments to be carried out successfully. Therefore, about 2-2.5 L of deionized water (with a conductivity of about 0.7 μS/cm) was already in the distillate tank. Hence, for the first experiments using each membrane, less time can be spent in operation as the membrane is new and more distillate is gained in the tank leading to the tank being full faster than the subsequent experiments using the same membrane. Therefore, in this case, the experiment was stopped.

5.1.1- Effect of Membrane Pore Size

To examine the effect of membrane pore size on membrane fouling, several experiment were conducted using PP membrane of 0.22 microns and 0.45 microns. Figure 42 shows the flux versus time graph for the combined runs using PP membrane with pore size of 0.22 μm.
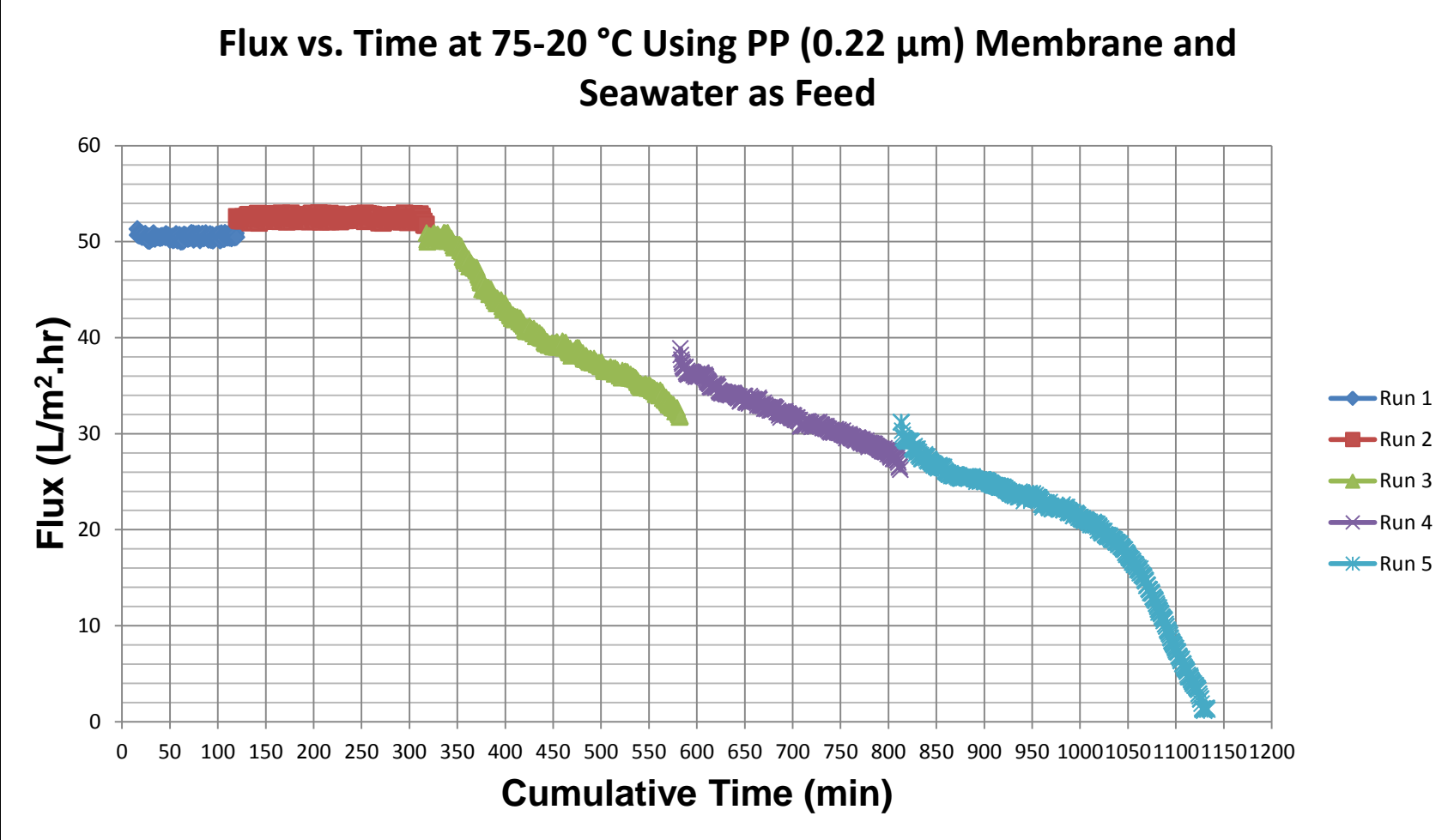
Figure 42: Flux versus Time for the Combined Runs Using PP (0.22 μm) Membrane

It is worth mentioning that the bench-scale DCMD system was carried out as batch, hence the appearance of the runs' flux profile in Figure 42. Five runs were carried out using PP membrane of 0.22 μm to examine MD-membrane fouling. Figure 42 shows that for Run 1, the flux profile was smooth and consistent. The initial flux obtained was 51.3 LMH which is high and considered very good. This was expected with the high temperature used as flux increases with feed temperature. The average flux for Run 1 was 50.5 LMH.

For Run 2, the flux profile was still smooth after about 6.3 hr of operation on the MD unit. The initial flux was 52.6 LMH and the average flux was 52.5 LMH. One explanation of this increase is that the pores might not be fully opened when the membrane was manufactured; therefore, with operation, the pores were fully opened and the flux was stable. Nevertheless, it is not a big increase and can't affect the fouling examination.

Moreover, for Run 3, the initial flux was 50.9 LMH which is lower than the first two runs but still not very low to assume that the membrane is fouled. The flux profile was smooth until about an hour, then it started to decrease. Therefore, fouling seems to appear after about 6 hours of operation under the specified conditions. The flux continued to decrease until it reached 31.9 LMH after about 10 hours. The average flux for this run was 40.7 LMH.

The generated flux profile for Run 4 and Run 5 was similar in that it started from a value followed by a sharp small decrease, then the flux was steady with a slight

decline that was almost the same in the two runs. Then, the flux started to decrease severely in the same way it decreased in the beginning of these two runs.

For Run 4, the initial flux was 38.9 LMH followed by a sharp small decrease until it reached 37.3 LMH. After a steady decline (about 3 hours and 40 minutes) to 27.4 LMH, the flux started decreasing sharply to 26.2 LMH after almost 4 hours of continuous operation for this run. The average flux for Run 4 was 32.0 LMH.

The flux in Run 5 started from 31.2 LMH. The steady decline started from 27.9 LMH and ended at 19.4 LMH. This phase took about 3 hours and 18 minutes. After that, there was a sudden decrease in flux until it reached 1.2 LMH which is an indication of severe membrane fouling. This was also confirmed by the water quality tests in Section 5.2, the contact angle measurements of the fouled membrane in Section 5.3, and the SEM-EDS analysis in Section 5.4.

Table 32 shows the results obtained using PP membrane of 0.22 microns and Figure 43 shows the flux drop with MD operation time.

Table 32: The Results Obtained Using PP Membrane (0.22 μm)

Run #	Cumulative Run Time (h)	Average Distillate Weight Gained Every 30 s (g)	Average Flux (LMH)	Flux Drop (%)
1	1.73	5.86	50.5	
2	5.02	6.13	52.5	-
3	9.43	4.71	40.7	19.4
4	13.25	3.67	32.0	36.6
5	18.58	2.28	20.1	60.2
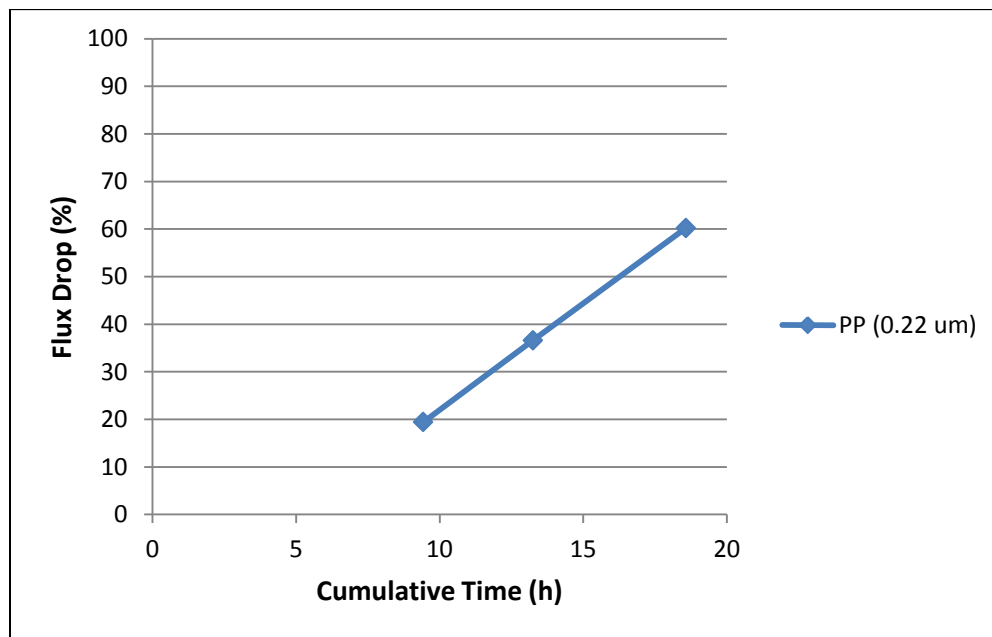
Figure 43: The Percentage of Flux Drop versus Time Using PP (0.22 μm) Membrane

Table 32 shows that after almost 19 hours of operating the MD unit using PP membrane of pore size 0.22 microns, the percentage of drop in the average flux was more than 60% (Figure 43). It is expected that it will be even less with continuous operation on the unit using this membrane. Moreover, Table 32 also shows that the average distillate weight gained is decreasing with each run on the MD unit which is also expected as less flux is generated due to membrane surface or pore blockage.

Figure 44 illustrates an image of the used membrane after it has been removed from the MD-membrane compartment, rinsed with deionized water, and left to dry naturally.

Figure 44: The Appearance of the Used PP (0.22 μm) Membrane

Figure 44 shows a visible salt layer formed on the membrane surface. However, it can be seen also that the layer formed is not uniform and that it is concentrated more in one part of the membrane, the hot inlet side, which can be caused by the concentration and temperature polarization effects at the surface of the membrane and more specifically at the hot water inlet rather than the outlet. Figure 45 shows the salt layer formed on the PP (0.22 μm) membrane.
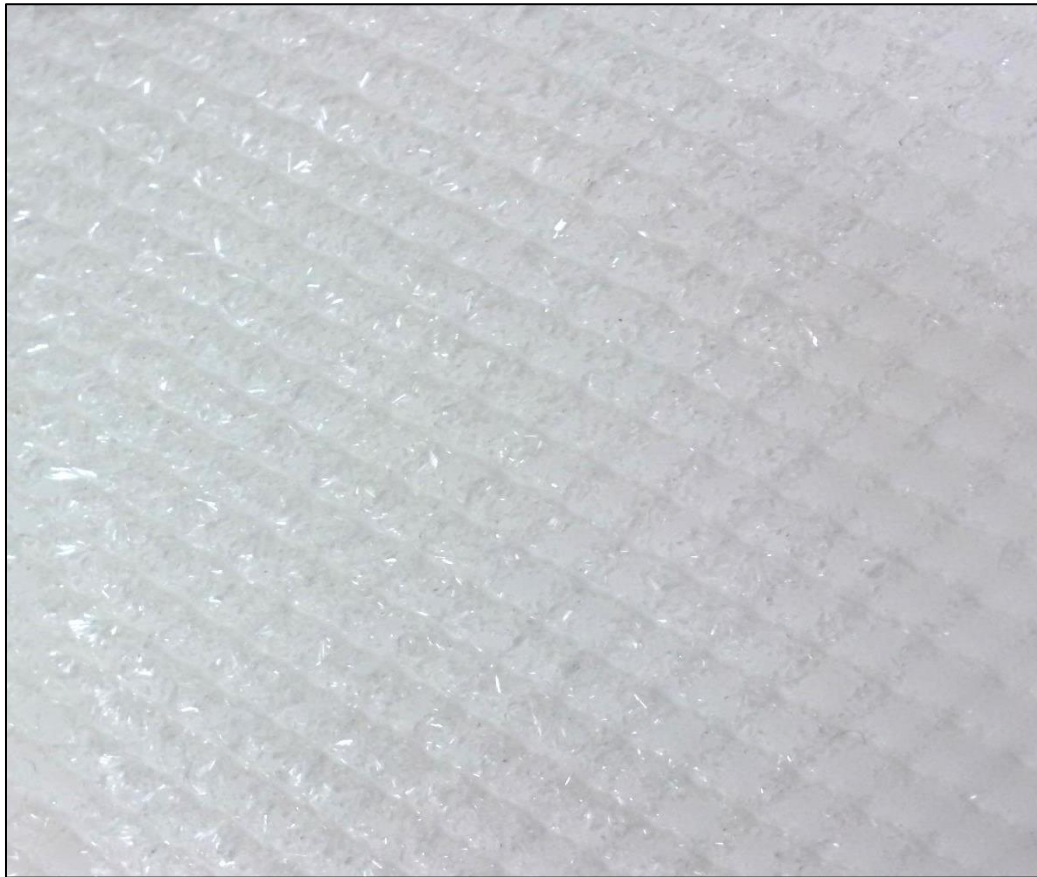
Figure 45: The Salt Layer Formed on the Surface of PP (0.22 μm) Membrane

For further membrane fouling analysis, thin stripes were later cut from the membrane to perform contact angle measurements. In addition, the membrane was analyzed by SEM-EDS. These analyses will be discussed in the later sections.

Additionally, experiments using PP membrane with pore size of 0.45 microns were carried out to examine membrane fouling. Figure 46 shows the flux versus time graph for the combined runs.

Figure 46: Flux versus Time for the Combined Runs Using PP (0.45 μm) Membrane

It is worth mentioning that the bench-scale DCMD system was run as batch, hence the appearance of the runs' flux profile in Figure 46. Nine runs were carried out using PP membrane of 0.45 µm to examine MD-membrane fouling. Figure 46 shows that for Run 1, the flux profile was smooth and consistent. The initial flux obtained was 52.9 LMH which is high and considered very good. This was expected with the high temperature used as flux increases with feed temperature. The average flux for Run 1 was 50.3 LMH.

For Run 2, the flux profile started smoothly in the same manner as Run 1 but with a lower initial flux of 50.9 LMH; however, when the flux decreased to 50.2 LMH, there was a sudden decrease in flux afterwards with another slope which is about the same as that of Run 1 till the flux reached 38.9 LMH. This segment took 2 hours and 45 minutes. After that, the flux continued to decrease until it reached 17.3 LMH. Therefore, fouling seems to start at this run.

Furthermore, for Run 3, the initial flux was 41.1 LMH. Again, there was a smooth decline in flux followed by a severe one at around 500 minutes in Figure 46 until the flux reached 7.4 LMH. Then, the decrease was smooth again until the flux reached 1.0 LMH which is very low.

For Run 1, 2, and 3, the flux profile was similar at the beginning. However, from Run 4, there was a steeper decline in flux. The initial flux was 34.1 LMH which is lower than the initial flux of Run 3 and the final flux was 1.7 LMH which is a gain very low. The average flux in Run 4 was 17.3 LMH.

The generated flux profile for Run 4 and Run 5 was similar in that it started from a value followed by a sharp small decrease, then the flux was steady with a slight decline that was almost the same in the two runs. Then, the flux started to decrease severely in the same way it decreased in the beginning of these two runs.

For Run 5, the average flux was 6.7 LMH which is even lower than that of Run 4. The initial and final fluxes were 21.8 LMH and 0.8 LMH, respectively. However, around 940 minutes in Figure 46, the decrease was not very sharp but there was a smooth decline in flux.

For Run 6, 7, and 8, the flux profile was very similar. The flux decline was smooth and the average fluxes were 5.4 LMH, 4.1 LMH, and 1.5 LMH, respectively. The flux decline was not very harsh and the values obtained were close to each other. The initial and final flux values were 14.1 LMH and 2.5 LMH for Run 6, 13.8 LMH and 0.5 LMH for Run 7, and 12.9 LMH and 0.1 LMH for Run 8.

From the low final fluxes reached in the later experiments using PP membrane of 0.45 microns, it is expected that if more runs were performed using the membrane, it will be severely damaged.

It is worth mentioning that towards the end of Run 8, for some of the data points generated from the data acquisition software, the change in distillate weight was negative, meaning that there was no distillate gained (not shown in Figure 46). This was a sign of membrane damage which was evident in Run 9. The initial flux for Run 9 was 5.8 LMH and the final flux that is seen in Figure 46 is 0, meaning that the

178

membrane is not producing any distillate. Beyond this point, the flux profile is not shown in Figure 46 as negative fluxes were obtained. Therefore, instead of producing fresh water, the water in the feed tank was increased. This could be due to membrane wetting due to a large deposit of salts that promoted Osmosis (reverse phenomenon of MD). Hence, fresh water has migrated to the salty side.

Table 33 shows the results obtained using PP membrane of 0.45 microns and Figure 47 shows the flux drop with MD operation time.

Table 33: The Results Obtained Using PP Membrane (0.45 μm)

Run #	Cumulative Time (h)	Average Distillate Weight Gained Every 30 s (g)	Average Flux (LMH)	Flux Drop (%)
1	2.38	5.82	50.3	-
2	6.28	4.73	41.5	17.5
3	10.81	2.71	24.0	52.3
4	13.71	1.93	17.3	65.6
5	18.86	0.75	6.7	86.7
6	22.53	0.61	5.4	89.3
7	25.56	0.44	4.1	91.8
8	28.70	0.15	1.5	97.0
9*	29.28	0.23	2.5	95.0

* Only the data points at the beginning of this run were considered
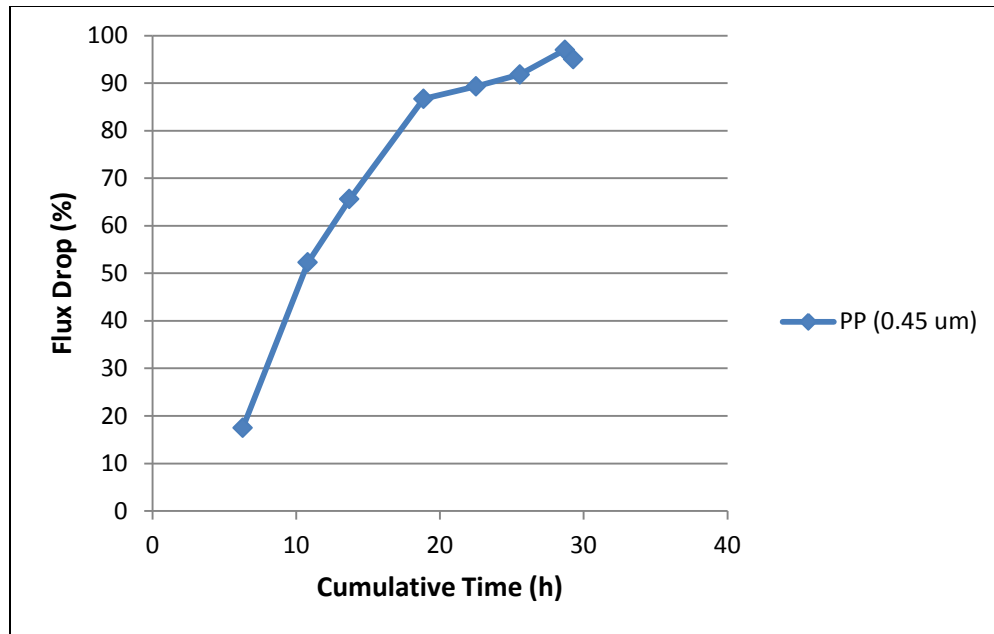
Figure 47: The Percentage of Flux Drop versus Time Using PP (0.45 μm) Membrane

Table 33 shows that after almost 30 hours of operating the MD unit using PP membrane of pore size 0.45 microns, the percentage of drop in the average flux was more than 97% (Figure 47). This means that the membrane is not functioning as it did before and is mostly blocked. Moreover, Table 33 also shows that the average distillate weight gained is decreasing with each run on the MD unit which is also expected as less flux is generated due to membrane surface or pore blockage.

Figure 48 illustrates an image of the used membrane after it has been removed from the MD-membrane compartment, rinsed with deionized water, and left to dry. It clearly shows a visible salt layer formed on the membrane surface.

Figure 48: The Appearance of the Used PP (0.45 μm) Membrane

After performing the experiments on the bench-scale DCMD unit using PP membranes of 0.22 microns and 0.45 microns, the following observations were made:

-   If there is a flux decline, the flux obtained using the hydrophobic membrane will eventually reach a very low value in a daily basis or every time there is a run on the MD unit under extreme operating conditions. However, the time the membrane takes to reach this point depends on the initial flux that was obtained in that day. For example, if the initial flux is 50 LMH, it will take the

membrane a longer time to have a very low flux than if the initial flux is 40 LMH.

- All of the fouling mechanisms (discussed in Section 3.11.2) seem to be present in the membranes used as the shape of the generated flux profile is not the same; however, a cake layer seems to be formed on the surface of the membrane and some of it is removed whenever a new run is undertaken.

- When starting a new run, the data acquisition doesn't start till the desired hot water temperature is reached. During this time, however, the circulated water washes off part of the cake layer that was formed on the surface of the membrane, hence, the lower initial flux for each subsequent run.

- The cake formation on the membrane could result from the elevated feed temperature that results in the formation of temperature polarization.

- Regarding the chemical analysis that is done on each obtained distillate from every run, the quality of distilled water deteriorates comparing a distillate to a distillate from a preceding run (as shown in Table 38, 41, 42, 44, and 49). This is also indicated by measuring the electrical conductivity of the attained distillate which indicates membrane wetting.

To compare the results of the experiments using PP membrane of the both sizes used, Figure 49 shows a combined graph of the generated flux profiles.
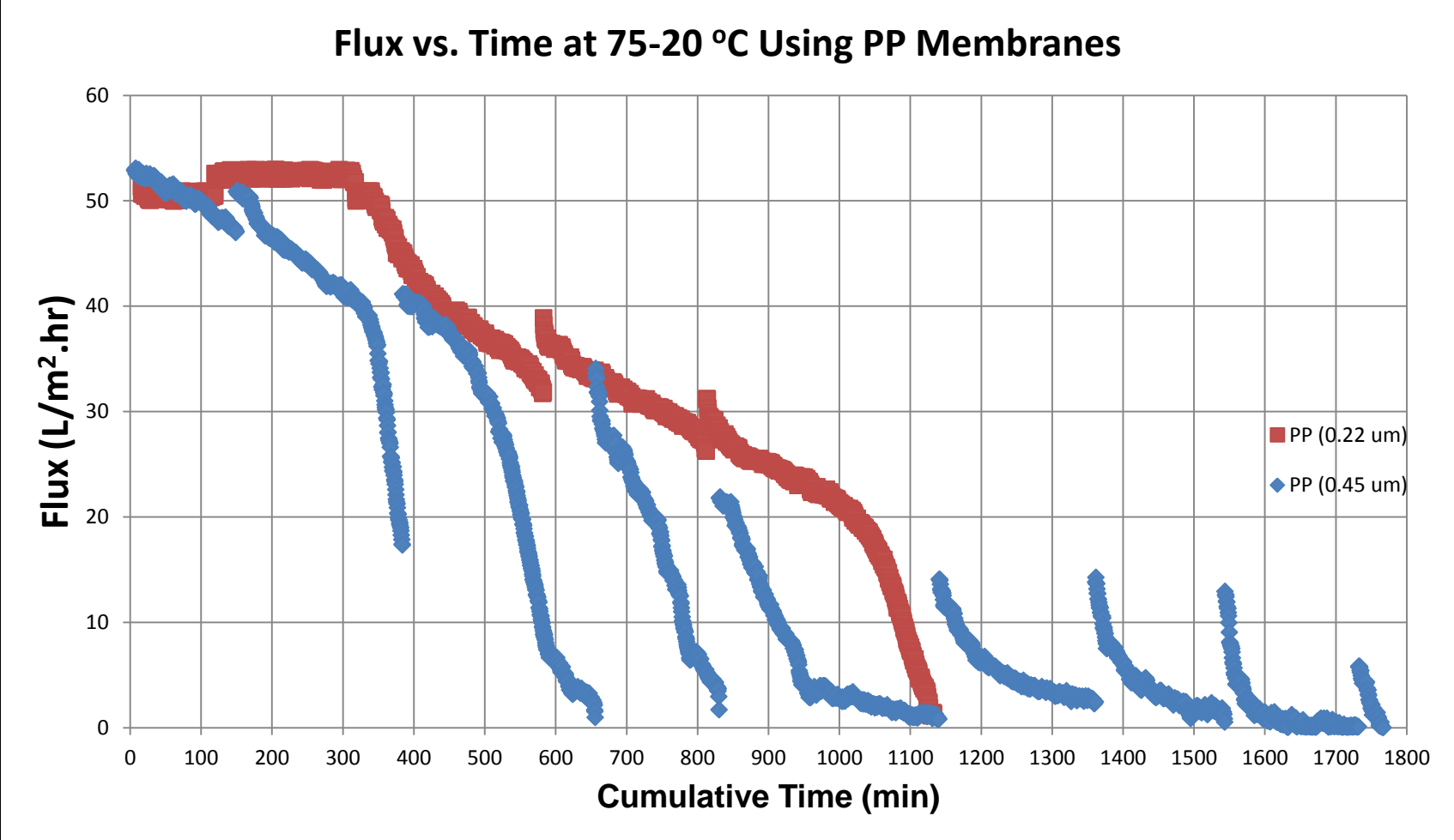
Figure 49: Flux versus Time for the Combined Runs Using PP Membrane of 0.22 μm and 0.45 μm

The bench-scale MD system was carried out as batch. Figure 49 shows that PP membrane of 0.45 microns generated a higher initial flux than PP membrane of 0.22 microns. However, it is more susceptible to fouling as from the first run, the flux profile was not horizontal as that of PP membrane of 0.22 microns but was declining. Also, for all of the subsequent runs, the initial flux was lower using PP membrane of 0.45 μm.

In addition, the initial flux in Run 2 when PP membrane of 0.45 microns was used (50.9 LMH) is the same as that of Run 3 when PP membrane of 0.22 microns was used (at 318 minutes in Figure 49). And for Run 3 using PP membrane of 0.45 microns, the initial flux was 41.1 LMH at about 385 minutes (where it was 40.7 at 318 min), meaning that PP membrane of 0.45 microns is getting blocked faster than PP membrane of 0.22 microns.

For PP membrane of 0.22 μm, fouling seemed to start after about 6 hours of operation under the specified operating conditions. On the other hand, for PP membrane of 0.45 μm, severe fouling started after 5 hours of operating the MD unit under the specified conditions.

Therefore, the effect of pore size can be clearly seen in that a larger pore size membrane is more prone to fouling and flux decay. This can be explained as bigger pores will allow more vapors to pass through the membrane as discussed earlier.

5.1.2- Effect of Membrane Material

The effect of membrane material on MD-membrane fouling was examined using PP and PTFE membranes of the same pore size (0.22 microns). Figure 50 shows the flux versus time graph for the combined runs using PTFE membrane.
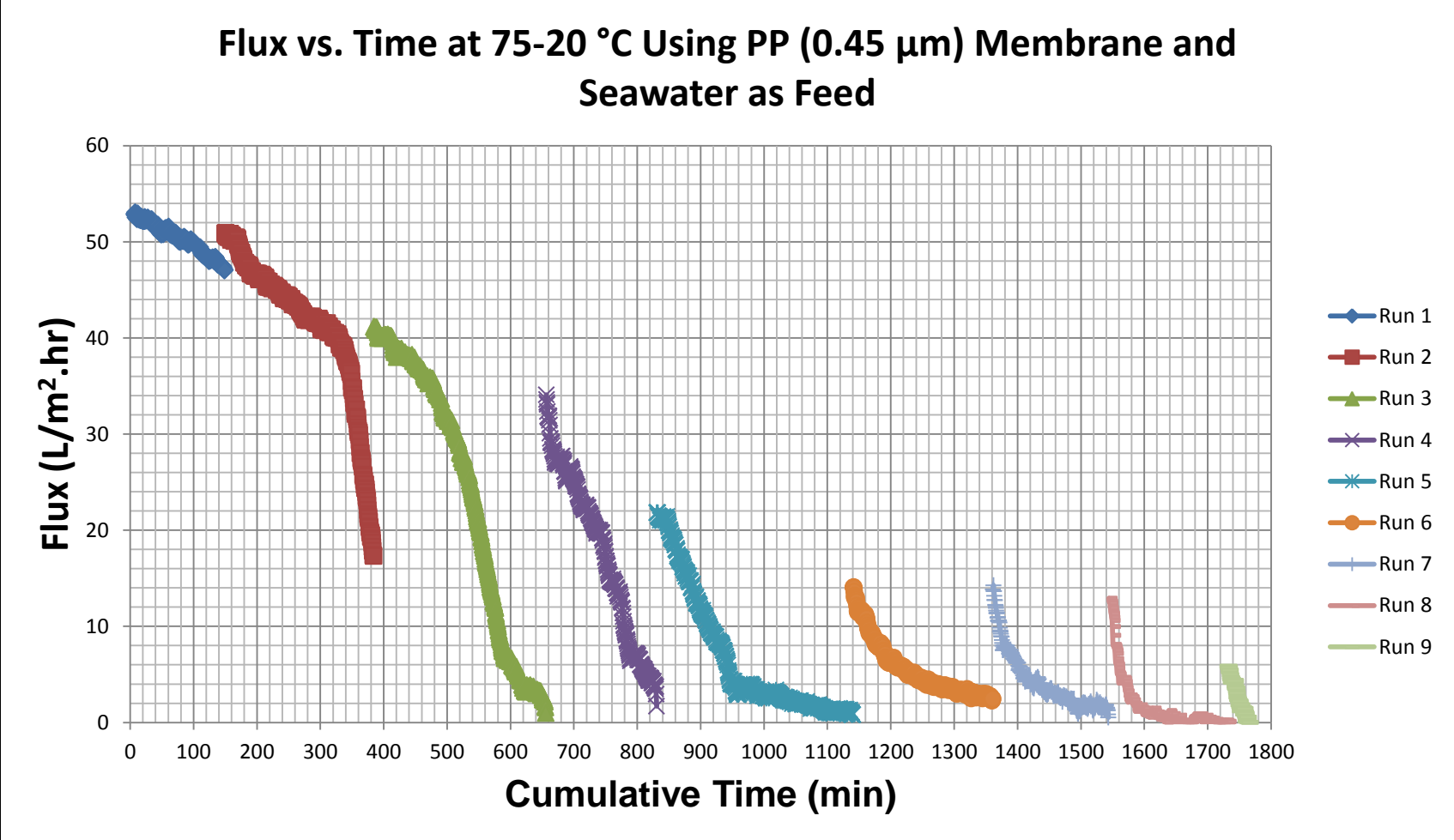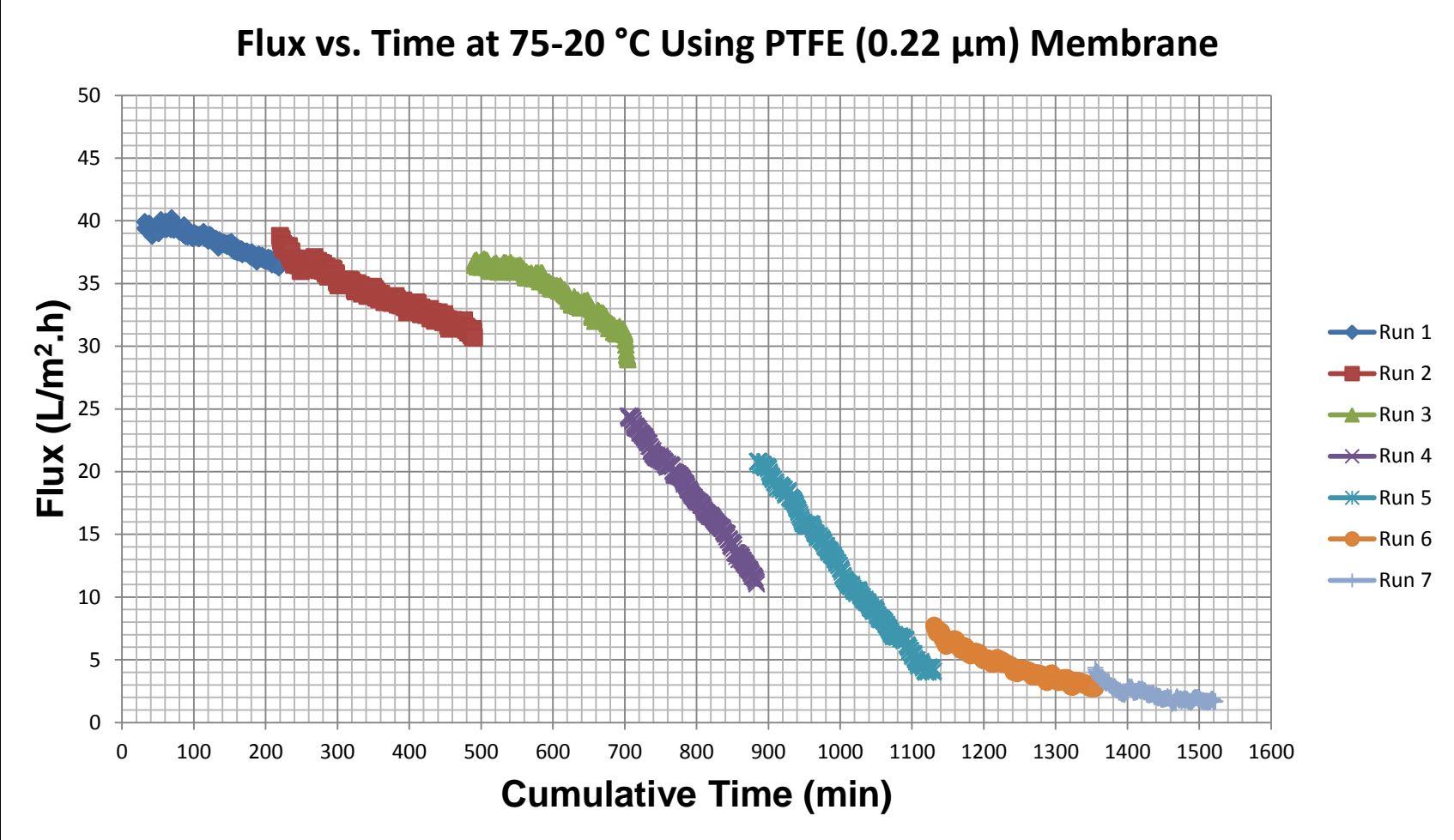
Figure 50: Flux versus Time for the Combined Runs Using PTFE (0.22 μm) Membrane

It is worth mentioning that the bench-scale DCMD system was run as batch, hence the appearance of the runs' flux profile in Figure 50. Seven runs were carried out using PTFE membrane of 0.22 µm to examine MD-membrane fouling. Figure 50 shows that for Run 1, the initial flux obtained was 39.9 LMH which is lower than those obtained by the PP membranes, yet, it is considered very good. However, after minute 71, at 39.4 LMH, the flux started to decrease which is a sign of surface or pore blockage. The final flux value for the run was 36.4 LMH and the average flux was 38.3 LMH.

In Run 2, the flux continued decreasing. The initial and final fluxes were 38.8 LMH and 30.7 LMH, respectively. The average flux was, as expected, lower than the first run with a value of 34.3 LMH.

The initial flux in Run 3 was 36.8 LMH which is lower than the previous run's initial flux. However, the average flux was 34.4 LMH which is similar to that of Run 2. This might be a result of some fluctuations in the hot and cold streams flow rate or, more precisely, a result of the duration of the experiment as less time was spent operating the MD unit in Run 3. Moreover, at minute 698 (11 hours and 38 minutes), it appears that there was a severe decline in flux indicating a severe membrane fouling. The final flux reached was 28.9 LMH. Nevertheless, it is expected that if the operation on the bench-scale MD unit continued, the final flux would be low.

Moreover, the flux profile for Run 4 and Run 5 looks similar. The flux decline is smooth and both appear to have the same slope. For Run 4, the initial and final fluxes

were 24.5 LMH and 11.0 LMH, respectively, and the average flux was 18.0 LMH. For Run 5, the initial and final fluxes were 20.8 LMH and 4.11 LMH, respectively, and the average flux was 12.0 LMH.

Likewise, the flux profile for Run 6 and Run 7 seems similar (with the same bend). For Run 6, the initial and final fluxes were 7.7 LMH and 2.7 LMH, respectively, and the average flux was 4.6 LMH. On the other hand, for Run 7, the initial and final fluxes were 4.4 LMH and 1.7 LMH, respectively, and the average flux was 2.3 LMH.

It is worth mentioning that the later part of Run 7 (not shown in Figure 50) or few minutes after the final flux obtained were not considered in the flux calculations as negative fluxes were obtained due to a decrease in the distillate weight instead of an increase. It is suspected that the membrane was completely blocked which promoted Osmosis (as observed with PP membrane of 0.45 microns). Contact angle measurements on the used membrane validate this hypothesis and will be discussed in the next section.

According to the previous observations regarding PP membrane, the results of the MD desalination using PTFE membrane were expected and were consistent with those specified earlier for PP membranes. Therefore, the same conclusions regarding membrane fouling apply in this case using PTFE membrane.

Table 34 shows the results obtained using PTFE membrane of 0.22 microns and Figure 51 shows the flux drop with MD operation time.

Table 34: The Results Obtained Using PTFE Membrane (0.22 µm)

Run #	Cumulative Run Time (h)	Average Distillate Weight Gained Every 30 s (g)	Average Flux (LMH)	Flux Drop (%)
1	3.13	4.40	38.8	-
2	7.58	3.96	34.3	11.6
3	11.13	3.94	34.4	11.3
4	14.12	0.53	18.0	53.6
5	18.22	1.37	12.0	69.1
6	21.95	0.52	4.6	88.1
7	24.73	0.10	2.3	94.1
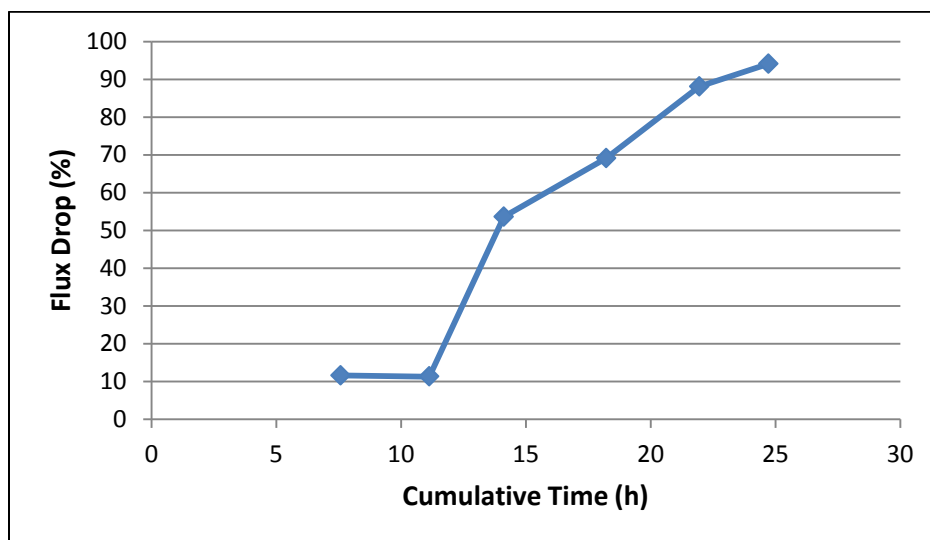
Figure 51: The Percentage of Flux Drop versus Time Using PTFE (0.22 µm)

Membrane

Table 34 shows that after almost 25 hours of operating the MD unit using PTFE membrane of pore size 0.22 microns, the percentage of drop in the average flux was more than 94% (Figure 51). This means that the membrane is severely fouled. Also, it can be seen from the table that the highest percentage drop from run to run was for Run 4 as fouling started from Run 3 as discussed earlier.

Furthermore, Figure 52 illustrates an image of the used membrane after it has been removed from the MD-membrane compartment, rinsed with deionized water, and left to dry naturally. It clearly shows a visible salt layer or crystal formation on the membrane surface.

Figure 52: The Appearance of the Used PTFE (0.22 μm) Membrane

It is worth mentioning that the crystals or the salts formed on the PTFE membrane surface were more visible than those formed on the PP membranes used in this study. Also, the salt layer formed on the PTFE membrane appeared denser than the one formed on PP membrane which might be attributed to the characteristics of the membrane material or the effect of the support layer on the PTFE membrane.

To examine the effect of membrane material on MD-membrane fouling, the results of the experiments using PP membrane of 0.22 microns and PTFE membrane of 0.22 microns were compared. Figure 53 shows a combined graph of the generated flux profiles.
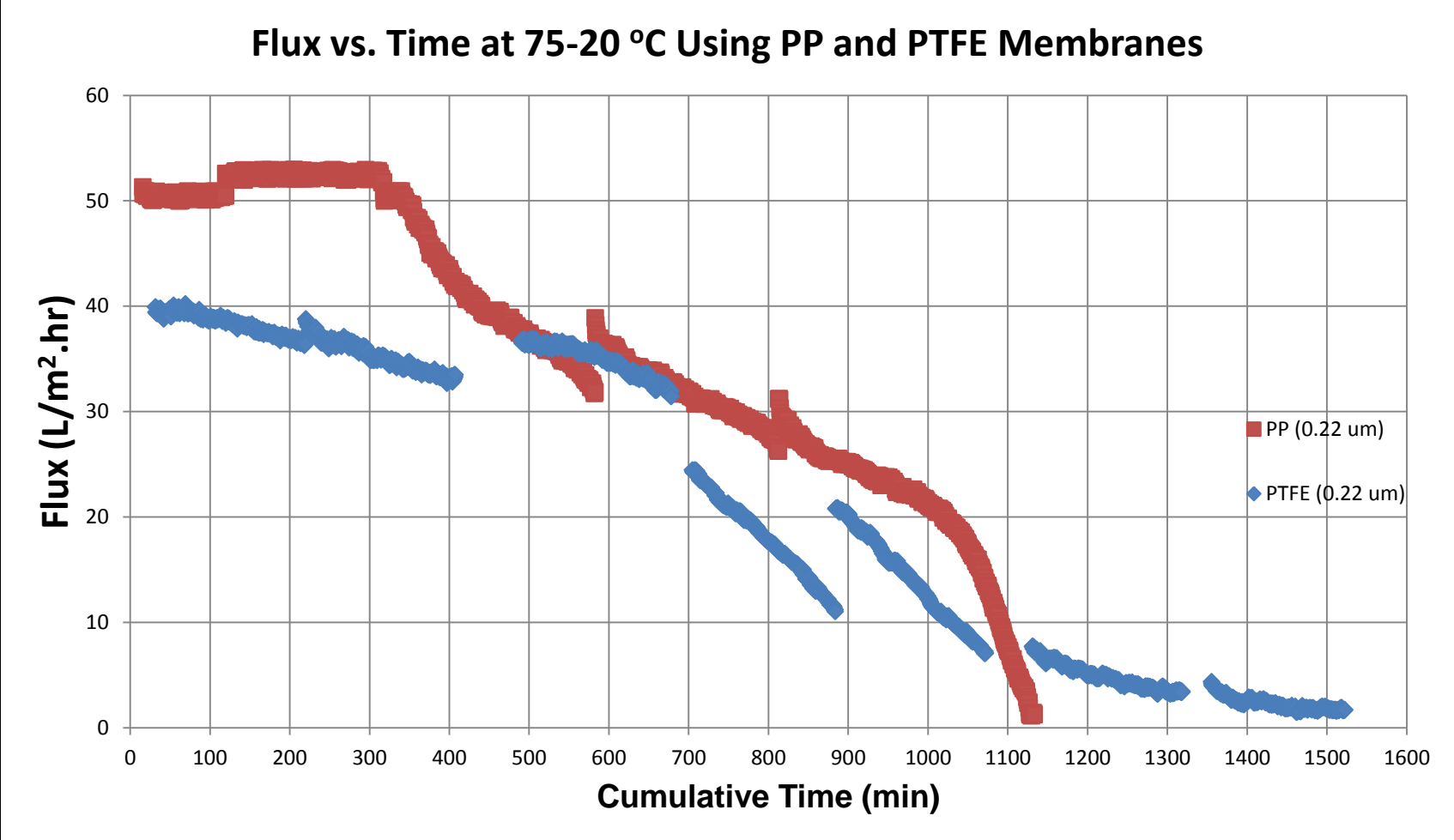
Figure 53: Flux versus Time for the Combined Runs Using PP Membrane of 0.22 μm and PTFE Membrane of 0.22 μm

Figure 53 shows that PP membrane of 0.22 microns generated a higher flux than PTFE membrane of 0.22 microns. Also, if the percentage drop using the two membranes were compared, after about 18 hours and 15 minutes, the percentage drop in flux when PP membrane was used was about 56.7% where it was 69.1% when PTFE membrane was used. This means that PTFE membrane is getting blocked faster than PP membrane. However, Figure 53 shows that the pattern of flux decline curve is more rapid when PP membrane was used and it is more "flat" towards the last runs when PTFE membrane was used. It is expected that if more runs were carried out, PP membrane would be more fouled and hence more damaged than PTFE membrane.

5.1.3- Effect of Feed Concentration

Besides examining the effect of membrane pore size and material on MD-membrane fouling, the effect of feed solution concentration was also studied. As the results of the study showed that PP membrane of 0.45 microns had the greatest fouling tendency, it was chosen to be used with 100,000 ppm synthetic NaCl solution as feed to the bench-scale DCMD unit. Figure 54 shows the flux versus time graph for the combined runs.
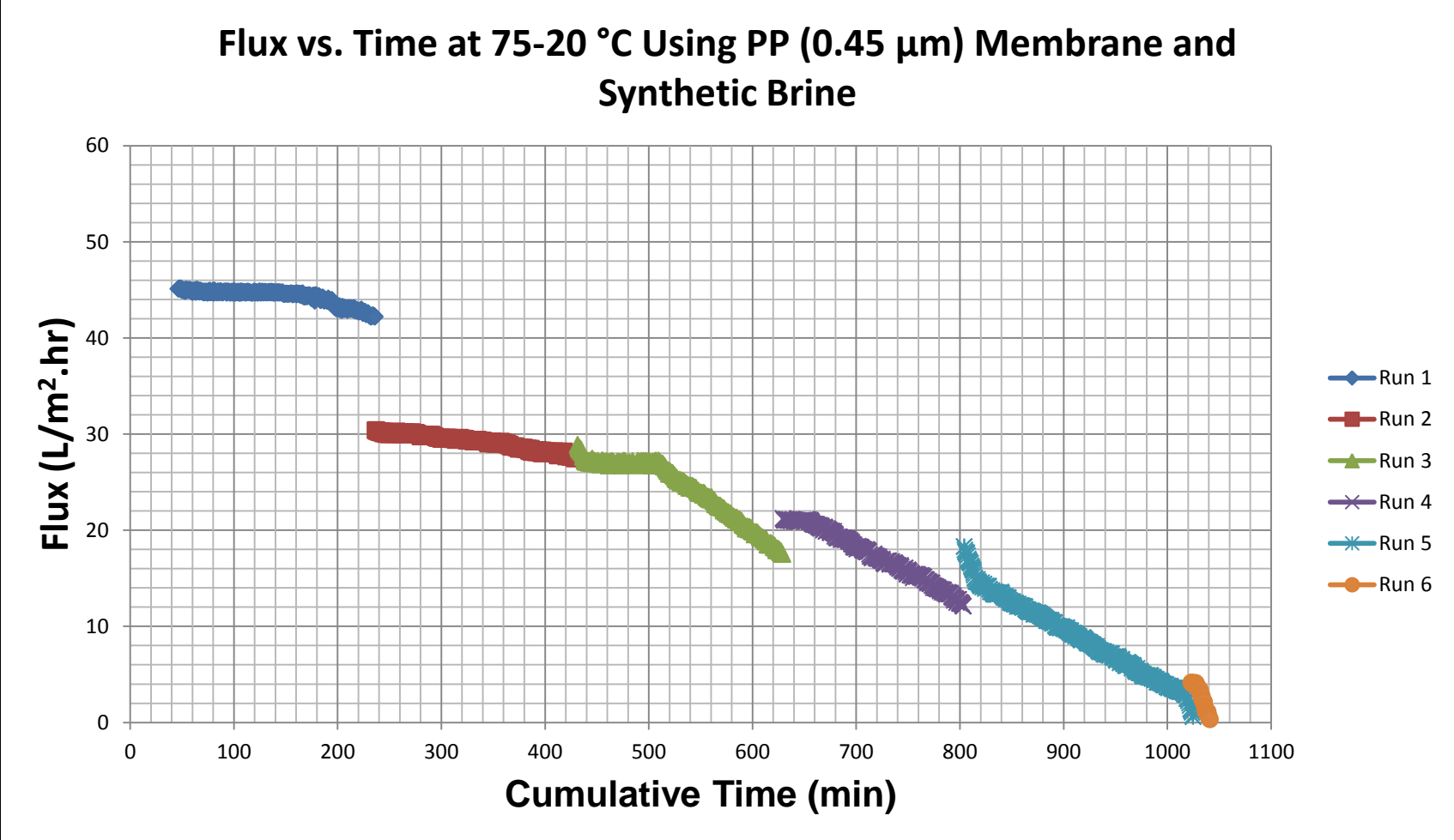
Figure 54: Flux versus Time for the Combined Runs Using PP (0.45 µm) Membrane and Synthetic Brine as Feed

It is worth mentioning that the bench-scale DCMD system was run as batch, hence the appearance of the runs' flux profile in Figure 54. Six runs were carried out using PP of 0.45 μm membrane and synthetic brine solution (100,000 ppm) to examine fouling of the membrane. Figure 54 shows that for Run 1, the flux profile is smooth and consistent. The initial flux obtained was 41.5 LMH which is high and considered very good. However, after about 2.4 hours (144 minutes), there was a decrease in flux which indicates membrane blockage. The average flux for Run 1 was 44.3 LMH.

A huge drop in flux appeared in Run 2. However, the flux profile is declining smoothly. This might be due to the blocking of the membrane that started in Run 1 and might be increased when the DCMD unit was in operation for Run 2 but before reaching the desired hot water inlet temperature. The initial and final fluxes were 30.4 LMH and 27.5 LMH, respectively, and the average flux was 29.1 LMH.

Moreover, for Run 3, the initial flux was 28.9 LMH. There was a slight decrease in flux for the first five minutes, and then the flux was consistent for about an hour and 15 minutes. After that, the flux decreased again with a steeper slope than that of Run 2 indicating a more severe membrane blocking. The final flux reached was 17.5 LMH and the average flux was 24.2 LMH.

For Run 4, the flux profile was somewhat flat and consistent (like that of Run 3) for the first 27 minutes. Then, it started to decrease having about the same slope as that of Run 3. The final flux reached was 12.1 LMH and the average flux was 17.4 LMH.

The initial flux for Run 5 was 18.3 LMH. After a 10 minute decrease in flux, the flux decline was the same as that of Run 3 and Run 4 with almost the same slope. This segment took 3 hours and 32 minutes. After that, the flux decline was steeper reaching a value of 0.6 LMH which is very low. The average flux for Run 5 was 8.9 LMH.

The flux in Run 6 started from 4.1 LMH. The flux generated was stable for 5 minutes before it decreased sharply to 0.3 LMH; again, with the same sharp decrease that took place at the end of Run 5. It is worth mentioning that this wasn't the final flux value reached. However, the flux continued to decrease (not shown in Figure 54) as a result of a decrease in the distillate weight that took place for 3 hours and 18 minutes before stopping the desalination process. This means that the membrane was not functioning properly and instead of adding water to the distillate tank, the reverse was happening. This was also the case when using PP membrane of 0.45 microns and PTFE membrane with seawater. Also, it is expected that this will also be the case if more runs were performed using PP membrane of 0.22 microns.

If membrane wetting occurs, the feed can flow directly across the membrane through the wetted pore. This will result in permeate contamination. However, Lawson & Lloyd (1997) state that in DCMD, this effect can be avoided by keeping the hydrostatic pressure of the permeate higher than the feed's hydrostatic pressure. As a result, if membrane wetting occurs, the permeate will flow to the feed side across the membrane. This will lead to a reduction in the overall flux; however, the permeate

quality is maintained. This seemed to happen when the distillate weight decreased instead of increasing probably after the occurrence of severe fouling and pore wetting.

Table 35 shows the results obtained using PP membrane of 0.45 microns and synthetic brine and Figure 55 shows the flux drop with MD operation time.

Table 35: The Results Obtained Using PP Membrane (0.45 μm) and NaCl Solution

Run #	Cumulative Run Time (h)	Average Distillate Weight Gained Every 30 s (g)	Average Flux (LMH)	Flux Drop (%)
1	3.16	5.11	44.3	
2	6.40	3.38	29.1	34.3
3	9.69	2.78	24.2	45.4
4	12.59	2.00	17.4	60.7
5	16.28	1.02	8.9	79.9
6	16.58	0.20	2.7	90.7
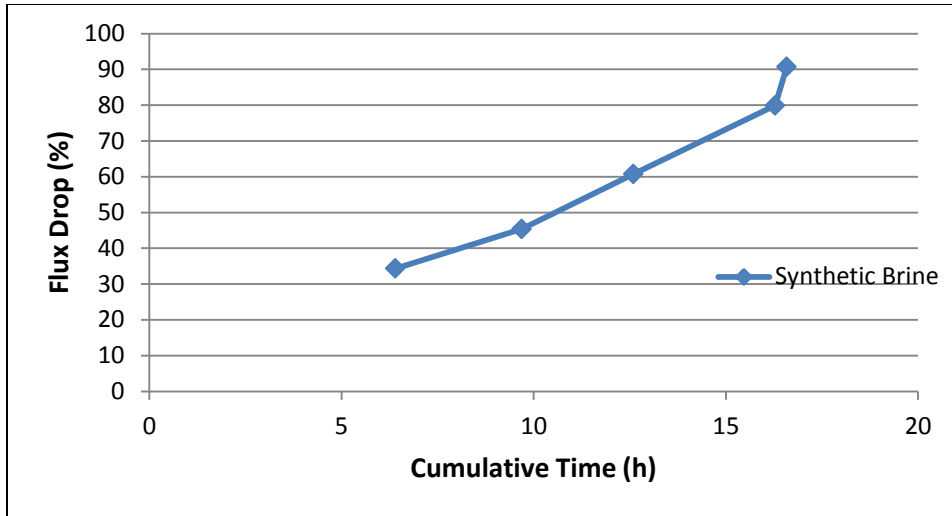
Figure 55: The Percentage of Flux Drop versus Time Using the NaCl Solution

Table 35 shows that after almost 17 hours of operating the MD unit under the previously specified operating conditions using PP membrane of pore size 0.45 microns and synthetic brine as feed, the percentage of drop in the average flux was about 91% (Figure 55). It is expected that it will be even less with continuous operation on the unit using this membrane. Moreover, Table 35 also shows that the average distillate weight gained is decreasing with each run on the MD unit which is also expected as less flux is generated due to membrane surface or pore blockage.

The previous observations regarding membrane fouling when seawater was used as feed apply in this case of using synthetic brine.

To examine the effect of feed solution on membrane fouling, the results of the experiments using PP membrane of 0.45 microns using seawater and 100,000 ppm NaCl solution were compared. Figure 56 shows a combined graph of the generated flux profiles.
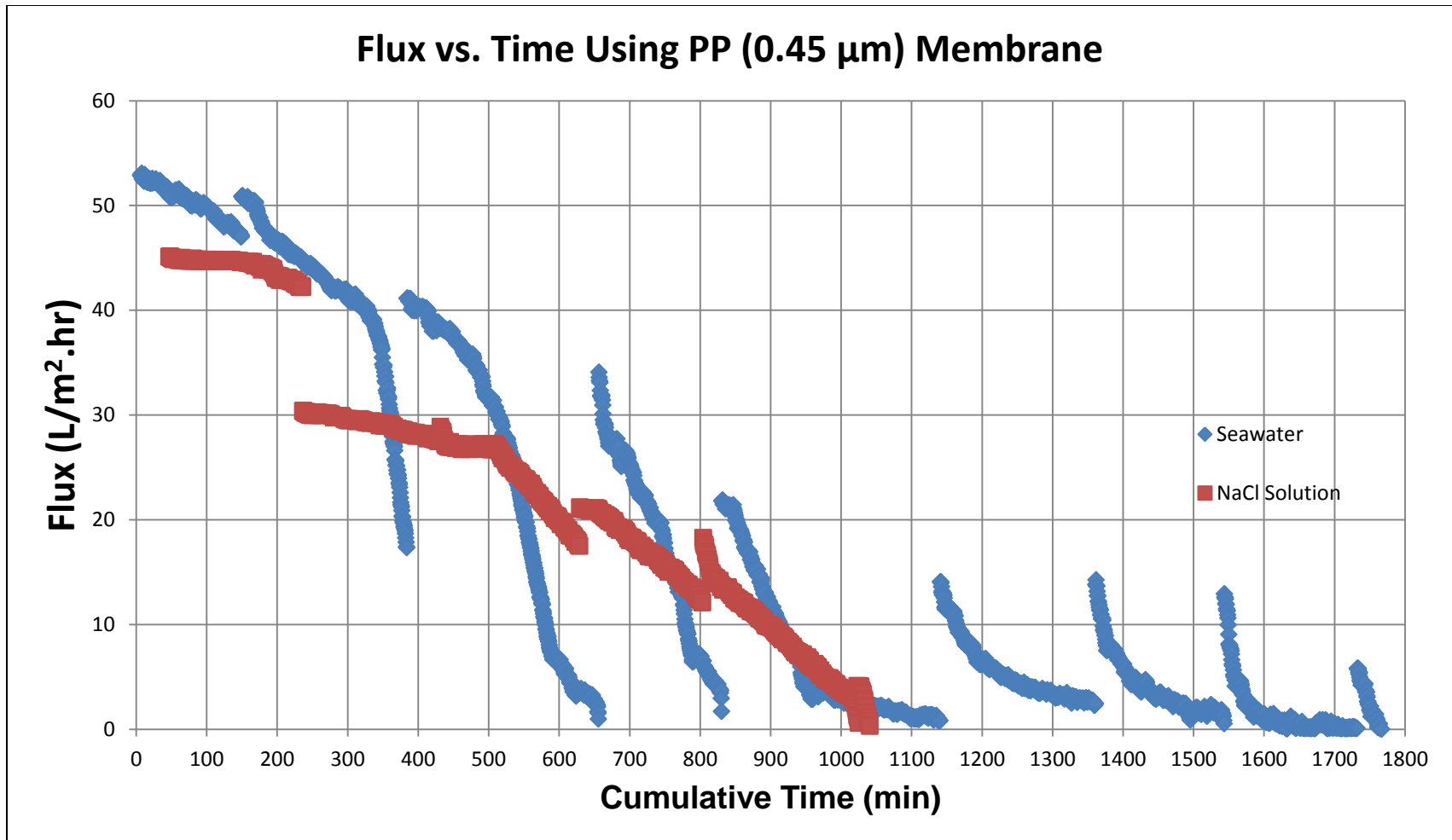
Figure 56: Flux Profile for the Combined Runs Using Seawater and Synthetic Brine as Feed Utilizing PP (0.45 μm) Membrane

Figure 56 shows that a higher flux was obtained when seawater was used as feed than when the synthetic brine was used. Also, it can be seen from the figure that membrane blockage started faster using the synthetic brine (at 2.4 h vs. 5 h). Figure 56 also shows that a very low flux was reached much faster when the membrane was used with the NaCl solution. In addition, as discussed earlier, Table 36 showed that after almost 17 hours of using PP membrane of 0.45 microns with the NaCl solution, the percentage of drop in the average flux was about 91% which is not only higher than that when using PP membrane of 0.45 microns with sweater at the same time, but in fact higher than those of all of the membranes used in the study. Therefore, the effect of feed concentration can be clearly seen in that a membrane is more susceptible to fouling if a high salinity solution is used.

The flux performance results in this study are consistent with those reported in literature. El-Bourawi et al. (2006) and Martínez-Díez & Vázquez-González (1999) state that flux decline is generally encountered in MD processes and that the main reason behind this decline is the effect of temperature polarization. In addition, Ge et al. (2014) have showed that membrane fouling in a long-term DCMD operation is more severe at high feed temperatures. Furthermore, Yun et al. (2006) have observed a sharp decrease in the permeate flux when synthetic NaCl solutions were used as feed to a DCMD process.

5.2- Water Quality Analysis

To assess the condition of the water produced using the bench-scale DCMD unit, water quality tests were performed. The analysis was done for the feed solutions and the distillates to compare the results. The analysis was carried out using Inductively Coupled Plasma-Optical Emission Spectrometry (ICP-OES) and Ion Chromatography (IC) at Qatar University's labs. Moreover, the salt rejection was measured based on the difference between the initial feed concentration and the final distillate concentration according to Equation 35 in Section 3.12.1.

Table 36 shows the feed solution characteristic (seawater).

Table 36: The Characteristic of the Feed Solution (Seawater)

Parameter	Parameter Formula	Unit	Value
Electrical Conductivity	EC	μS/cm	93,304.4
pH	pH	-	8.0
Total Dissolved Solids	TDS	mg/L	64,380.0
Cations			
Calcium	Ca^{2+}	mg/L	560.0
Potassium	K^+		510.0
Magnesium	Mg^{2+}		1,360.0
Sodium	Na^+		21,370.0
Anions			
Chloride	Cl^-	mg/L	32,810.0
Floride	F^-		UDL
Bromide	Br^-		UDL
Nitrate	NO_3^-		UDL
Sulfate	SO_4^{2-}		3,500.0
Heavy Metals			
Aluminum	Al	mg/L	UDL
Boron	B		UDL
Cadmium	Cd		UDL
Cobalt	Co		UDL
Chromium	Cr		UDL
Copper	Cu		UDL
Manganese	Mn		UDL
Molybdenum	Mo		UDL
Nickel	Ni		UDL
lead	Pb		UDL
Antimony	Sb		UDL
Selenium	Se		UDL
Strontium	Sr		UDL
Titanium	Ti		UDL
Zinc	Zn		UDL

Some of the parameters in Table 36 have values that are under the detection limit of the ICP-OES used for the analysis. Their values are denoted in the table as "UDL". Table 37 shows the detection limits of some elements for the ICP-OES used.

Table 37: The ICP-OES Detection Limits

Element	Detection Limit (mg/L)	Element	Detection Limit (mg/L)
Al	0.23	Mo	0.05
B	0.01	Na	0.04
Ca	0.15	Ni	0.01
Cd	0.35	Pb	0.14
Co	0.01	Sb	0.02
Cr	0.01	Se	0.08
Cu	0.01	Sr	0.37
K	0.08	Ti	0.04
Mg	0	Zn	0.28
Mn	0.01		

Water quality tests were done for the water produced from the bench-scale DCMD unit using several types of membranes which are PP membrane of pore size 0.22 microns and 0.45 microns, and PTFE of 0.22 microns (with and without using a spacer).

The analysis was carried out for the distillates produced under the following operating conditions: hot water inlet temperature of 75 $^{\circ}$C, cold water inlet temperature of 20 $^{\circ}$C, and hot and cold water flow rate of 1.5 L/min. In addition, counter-current mode was used. Table 38 shows the chemical analysis of the distillate produced using PP membrane of 0.22 μm.

Table 38: The Chemical Analysis of the Distillate Produced Using PP Membrane of

0.22 μm

Feed	Seawater						
Membrane	PP (0.22 μm)						
Parameter	**Parameter Formula**	**Unit**	**Run 1 Sample**	**Run 2 Sample**	**Run 3 Sample**	**Run 4 Sample**	**Run 5 Sample**
Electrical Conductivity	EC	μS/cm	8.78	4.84	2.33	12.82	96.20
pH	pH	-	7.37	8.08	7.95	7.41	7.55
Total Dissolved Solids	TDS	mg/L	6.06	3.34	1.61	8.85	66.38
Cations							
Calcium	Ca^{2+}	mg/L	0.06	0.04	0.02	0.09	0.70
Potassium	K^+		0.06	0.03	0.02	0.09	0.68
Magnesium	Mg^{2+}		0.19	0.11	0.05	0.28	2.13
Sodium	Na^+		1.81	1.00	0.48	2.64	19.8
Anions							
Chloride	Cl^-	mg/L	3.51	1.94	0.93	5.13	38.5
Sulfate	SO_4^{2-}		0.39	0.21	0.10	0.57	4.26

Table 38 shows that the quality of the distillate produced using PP membrane of pore

size 0.22 μm is excellent (initially) for more than 9 hours and 30 minutes under the

previously specified operating conditions as the distillate is considered as highly pure

water when comparing the electrical conductivity value of the distillate to the typical aqueous conductivities that are shown in Table 39.

Table 39: Typical Aqueous Conductivities (Heyda, 2008)

Solution	Electrical Conductivity (µS/cm)
Totally pure water	0.055
Typical Deionized water	0.1
Distilled water	0.5
RO water	50-100
Domestic "tap" water	500-800
Potable water (max)	1055
Sea water (Oceans)	56,000
Brackish water	100,000

In the first three runs in Table 38, the slight decrease in the electrical conductivity might be due to the fact that the MD system wasn't flushed prior to performing the first run; therefore, while operating the unit, the conductivity is slightly improved. However, by comparing the electrical conductivity of the first three runs in Table 38 to the flux performance of the PP membrane of 0.22 microns (Figure 41), it can be said that fouling has caused the flux to decline; however, the quality of the water was maintained. This means that the decline in flux was caused by fouling; yet, no wetting has occurred. Moreover, from Run 4, the electrical conductivity of the water produced started to increase which indicates membrane wetting.

Table 40 shows the salt rejection when the bench-scale DCMD unit was employed using PP membrane of 0.22 μm.

Table 40: The Calculated Salt Rejection When Using PP Membrane of 0.22 μm

	Run 1 Sample	Run 2 Sample	Run 3 Sample	Run 4 Sample	Run 5 Sample
Salt Rejection (%)	99.99	99.99	99.998	99.99	99.90

The salt rejection for the runs is more than 99.9% (about 100%). However, with time, the values of the EC, the TDS, the cations, and the anions in the distillate produced from the bench-scale DCMD unit using PP membrane of 0.22 microns were increased when performing the experiment over and over again. This means that for the first few runs, the membrane didn't allow the ions in the feed to pass through it, but later, with repeated runs, it appears that it started losing some of its hydrophobicity by allowing more ions to pass through and end up in the distillate. This is also confirmed by the contact angle measurements of the used membrane in Section 5.3. The EC, the TDS, the calcium ions, and the sulfate ions (which causes scaling) in the distillate produced using PP membrane of 0.22 μm are shown in Figure 57, 58, 59, and 60, respectively.

Figure 57: The Electrical Conductivity versus Time of the Distillate Produced Using
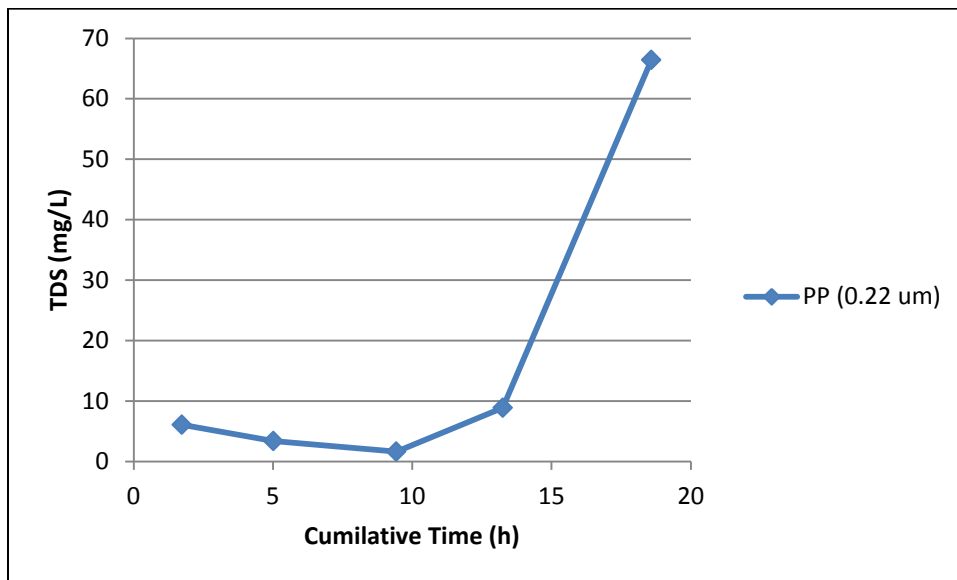
PP (0.22 μm) Membrane

Figure 58: The TDS versus Time of the Distillate Produced Using PP (0.22 μm)
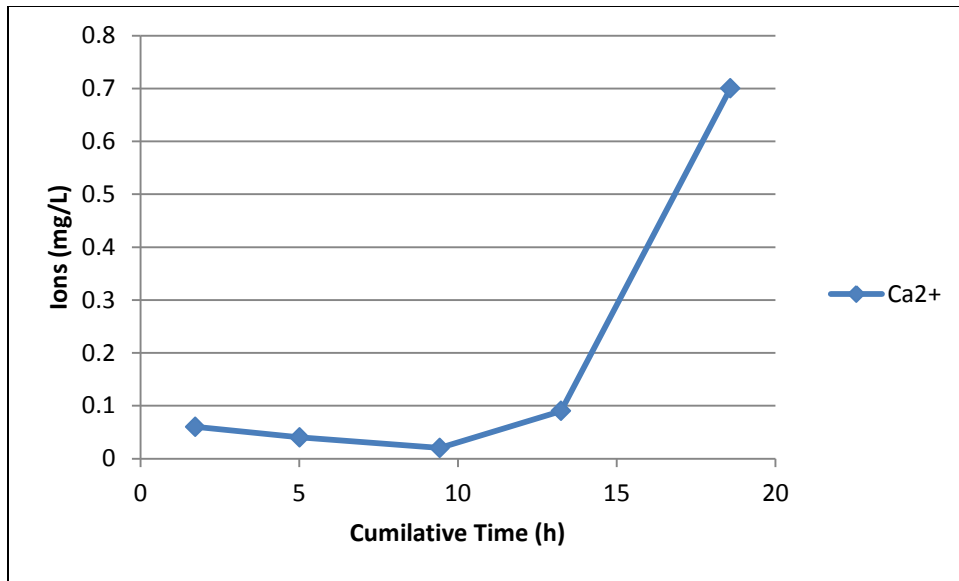
Membrane

Figure 59: The Calcium Ions versus Time of the Distillate Produced Using PP (0.22 μm) Membrane
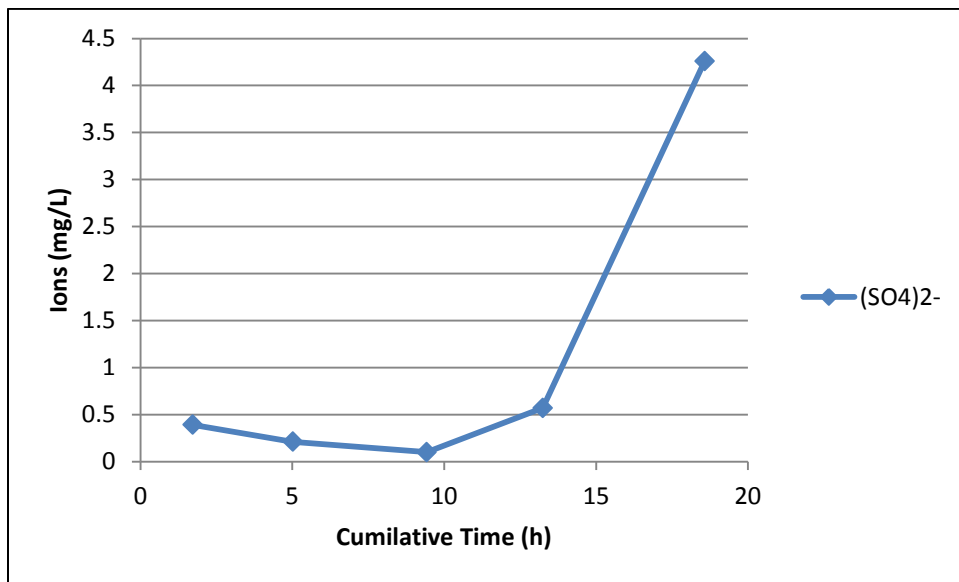
Figure 60: The Sulfate Ions versus Time of the Distillate Produced Using PP (0.22 μm) Membrane

Under the same operating conditions of 75 ^{o}C and 20 ^{o}C for the hot and cold water inlet temperature, respectively, and a flow rate of 1.5 L/min, the same chemical analysis was carried out for the distillates produced using PP membrane of pore size 0.45 μm. Table 41 and Table 42 show the quality of the distillate produced after performing several runs using PP membrane of pore size 0.45 μm.

Table 41: The Chemical Analysis of the Distillate Produced (Sample 1-5) Using PP

Membrane of 0.45 μm

Feed	Seawater						
Membrane	PP (0.45 μm)						
Parameter	**Parameter Formula**	**Unit**	**Run 1 Sample**	**Run 2 Sample**	**Run 3 Sample**	**Run 4 Sample**	**Run 5 Sample**
Electrical Conductivity	EC	μS/cm	5.81	4.88	323.00	929.00	2,910.00
pH	pH	-	8.14	8.02	7.46	8.12	8.04
Total Dissolved Solids	TDS	mg/L	4.01	3.37	222.87	641.01	2,007.90
Cations							
Calcium	Ca^{2+}	mg/L	0.04	0.04	2.57	7.40	21.02
Potassium	K^+		0.04	0.04	2.34	6.73	23.22
Magnesium	Mg^{2+}		0.13	0.11	7.02	20.19	87.06
Sodium	Na^+		1.20	1.00	66.30	190.70	606.07
Anions							
Chloride	Cl^-	mg/L	2.33	1.93	127.48	366.66	873.15
Sulfate	SO_4^{2-}		0.26	0.22	14.49	41.67	87.13

Table 42: The Chemical Analysis of the Distillate Produced (Sample 6-9) Using PP

Membrane of 0.45 μm

Feed	Seawater					
Membrane	PP (0.45 μm)					
Parameter	**Parameter Formula**	**Unit**	**Run 6 Sample**	**Run 7 Sample**	**Run 8 Sample**	**Run 9 Sample**
Electrical Conductivity	EC	μS/cm	5,870.00	8,960.00	11,510.00	15,390.00
pH	pH	-	7.92	7.92	8.04	8.12
Total Dissolved Solids	TDS	mg/L	4,050.30	6,182.40	7,941.90	10,619.10
Cations						
Calcium	Ca^{2+}		35.07	64.92	83.39	111.50
Potassium	K^+	mg/L	44.58	54.10	69.49	92.92
Magnesium	Mg^{2+}		113.80	194.75	250.17	334.50
Sodium	Na^+		812.20	1,839.26	2,362.72	3,159.18
Anions						
Chloride	Cl^-	mg/L	1,232.73	3,576.52	4,594.39	6,143.15
Sulfate	SO_4^{2-}		126.76	397.84	511.06	683.34

As PP membrane of pore size 0.22 microns, the distillate produced from the bench-scale DCMD unit using PP membrane of pore size 0.45 microns is highly pure (initially, for more than 6.3 hours); however, with less salt rejection than PP

membrane of 0.22 microns. The decrease in the electrical conductivity after the second run is probably due to the same reason mentioned before (the system wasn't flushed, so some impurities might be present in the tubes). When comparing the electrical conductivity of the first two runs in Table 41 to the flux performance of the first two runs using PP membrane of 0.45 microns (Figure 46), it can be said that despite the major decline in flux in Run 2, the quality of the water was maintained. This means that no wetting has occurred for more than 6 hours. However, from Run 3 to the last run (Run 9), the distillate quality was decreasing leading to an electrical conductivity value of 15,390 μS/cm. Membrane wetting is also confirmed by the contact angle measurements that were done on the used membrane (Section 5.3).

Table 43 shows the calculated salt rejection when using PP membrane of 0.45 μm.

Table 43: The Calculated Salt Rejection When Using PP of 0.45 μm

	Run 1 Sample	Run 2 Sample	Run 3 Sample	Run 4 Sample	
Salt Rejection (%)	99.99	99.99	99.65	99.00	
	Run 5 Sample	Run 6 Sample	Run 7 Sample	Run 8 Sample	Run 9 Sample
Salt Rejection (%)	96.88	93.71	90.40	87.66	83.51

Table 43 shows that for the first four runs (about 13.71 hours), the salt rejection was more than 99% when PP membrane of 0.45 microns was used. Later, with performing more runs, the value started to decrease until it reached 83.5% in Run 9. Therefore, after performing more runs using the same membrane, it is expected that the salt rejection will be even less.

The results showed that PP membrane of 0.45 μm has experienced pore wetting when performing the experiment over and over again. The EC, the TDS, the calcium ions, and the sulfate ions in the distillate produced using PP membrane of 0.45 μm are shown in Figure 61, 62, 63, and 64, respectively.
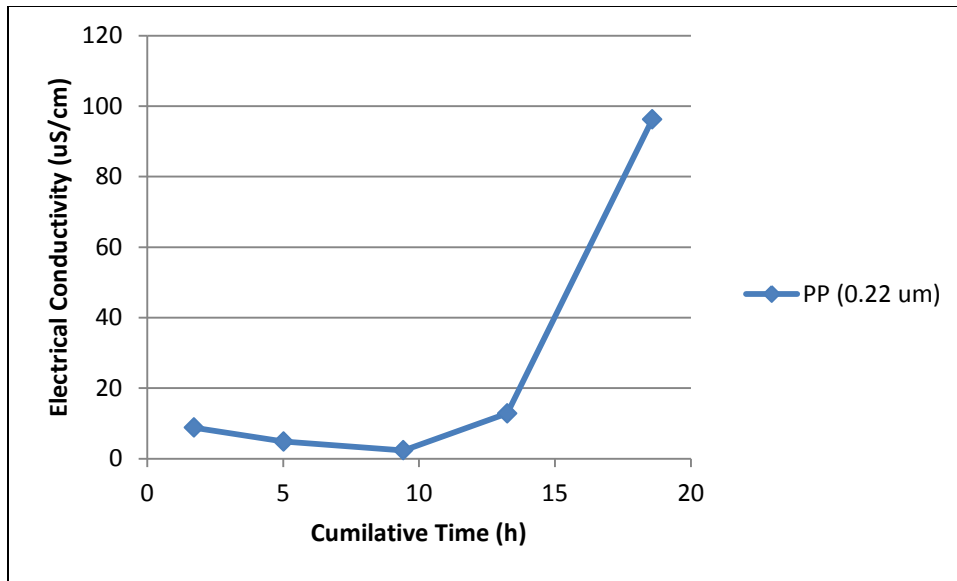
Figure 61: The Electrical Conductivity versus Time of the Distillate Produced Using

PP (0.45 μm) Membrane

Figure 62: The TDS versus Time of the Distillate Produced Using PP (0.45 μm)

Membrane

Figure 63: The Calcium Ions versus Time of the Distillate Produced Using PP (0.45
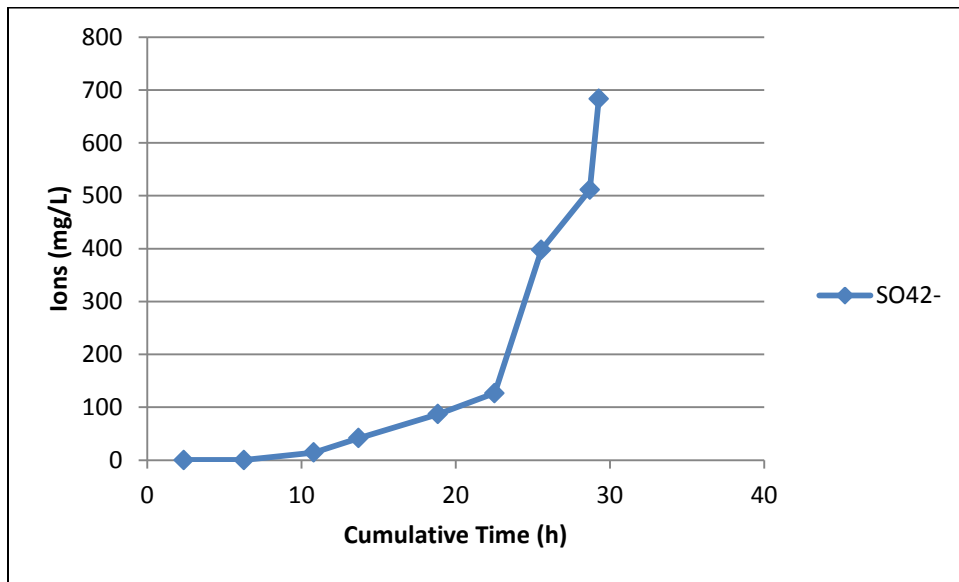
µm) Membrane

Figure 64: The Sulfate Ions versus Time of the Distillate Produced Using PP (0.45

µm) Membrane

In addition, under the same operating conditions of 75 $^{\circ}$C and 20 $^{\circ}$C for the hot and cold water inlet temperature, respectively, and a flow rate of 1.5 L/min, the same chemical analysis was carried out for the distillates produced from several sets of experiments using PTFE membrane of pore size 0.22 microns. Table 44 and Table 45 show the quality of the distillate produced with and without using a spacer (on the feed side), respectively, to examine the effects of using a spacer on the water quality.

Table 44: The Chemical Analysis of the Distillate Produced Using PTFE Membrane of 0.22 μm (With a Spacer in the Feed Side)

Membrane	PTFE (0.22 μm)								
Parameter	Parameter Formula	Unit	Run 1 Sample	Run 2 Sample	Run 3 Sample	Run 4 Sample	Run 5 Sample	Run 6 Sample	Run 7 Sample
Electrical Conductivity	EC	μS/cm	107.10	59.10	38.10	623.00	1,519.00	2,980.00	4,380.00
pH	pH	-	8.02	7.80	7.90	7.80	8.00	7.80	7.70
Total Dissolved Solids	TDS	mg/L	73.90	40.78	26.29	429.87	1048.11	2,056.20	3,022.20
Cations									
Calcium	Ca^{2+}	mg/L	0.78	0.43	0.28	2.85	8.69	17.22	21.93
Potassium	K^+		0.65	0.36	0.23	5.77	21.21	26.79	90.24
Magnesium	Mg^{2+}		2.33	1.28	0.83	7.02	18.28	37.18	65.82
Sodium	Na^+		21.98	12.13	7.82	150.90	400.80	685.40	1120.00
Anions									
Chloride	Cl^-	mg/L	42.75	23.59	15.21	225.80	605.78	1117.40	1709.89
Sulfate	SO_4^{2-}		4.76	2.62	1.69	9.02	13.41	79.77	82.43

Table 45: The Chemical Analysis of the Distillate Produced Using PTFE Membrane

(Without Using a Spacer)

Feed	Seawater					
Membrane	PTFE (0.22 μm)					
Parameter	**Parameter Formula**	**Unit**	**Run 1 Sample**	**Run 2 Sample**	**Run 3 Sample**	**Run 4 Sample**
Electrical Conductivity	EC	μS/cm	179.20	174.60	559.00	1,043.00
pH	pH	-	7.60	7.84	7.26	7.16
Total Dissolved Solids	TDS	mg/L	123.60	120.50	385.70	719.70
Cations						
Calcium	Ca^{2+}	mg/L	1.45 ± 0.05	1.02 ± 0.05	3.87 ± 0.5	7.00 ± 0.04
Potassium	K^+		0.88 ± 0.02	0.83 ± 0.01	4.26 ± 0.08	10.06 ± 0.14
Magnesium	Mg^{2+}		3.26 ± 0.23	3.13 ± 0.23	11.45 ± 0.27	21.76 ± 1.83
Sodium	Na^+		26.88 ± 1.54	26.24 ± 1.85	106.17 ± 6.58	238.48 ± 11.22
Anions						
Chloride	Cl^-	mg/L	59.32 ± 0.09	58.48 ± 0.08	226.57 ± 1.2	464.09 ± 1.5
Sulfate	SO_4^{2-}		7.20 ± 0.03	7.23 ± 0.09	26.05 ± 0.2	46.10 ± 0.45

The same explanation mentioned before regarding the electrical conductivity decline

in the first runs apply in this case using PTFE as the system wasn't flushed also prior

to performing the experiments. Like PP membrane of the both sizes used, Table 44 and Table 45 show that the DCMD unit produced good quality water initially.

Table 46 shows the calculated salt rejection when using PTFE membrane.

Table 46: The Calculated Salt Rejection When Using PTFE Membrane

Membrane	PTFE (With a Spacer)			
	Run 1 Sample	Run 2 Sample	Run 3 Sample	Run 4 Sample
Salt Rejection (%)	99.89	99.94	99.96	99.33
	Run 5 Sample	Run 6 Sample		Run 7 Sample
Salt Rejection (%)	98.37	96.81		95.31
Membrane	PTFE (Without Using a Spacer)			
	Run 1 Sample	Run 2 Sample	Run 3 Sample	Run 4 Sample
Salt Rejection (%)	99.81	99.81	99.40	98.88

Table 46 shows that for the first four runs when a spacer was used, the salt rejection was more than 99%. Later, with more performed runs, the value decreased to 95.3%. Therefore, after performing more runs on the same membrane, it is expected that the salt rejection will be even less. On the other hand, the salt rejection when the PTFE membrane was used without utilizing a spacer was more than 99.4% after performing four runs. The water produced is highly pure as that produced when PTFE membrane was used with spacer. The salt rejection in both cases for the first four runs is more than 99.4%. The difference in salt rejection is extremely low and it could be

considered as negligible. Therefore, using a spacer has no effect on the quality of distillate produced as it is used only to provide turbulance for the flowing feed.

The results in Table 44 show that PTFE membrane of 0.22 μm has experienced pore wetting when performing the experiment over and over again. The EC, the TDS, the calcium ions, and the sulfate ions in the distillate produced using PTFE membrane are shown in Figure 65, 66, 67, and 68, respectively.
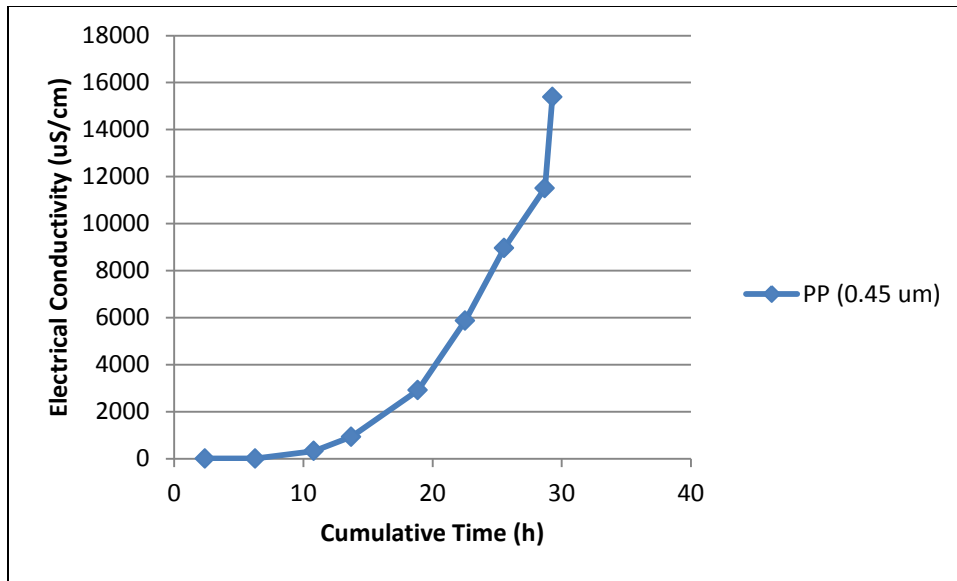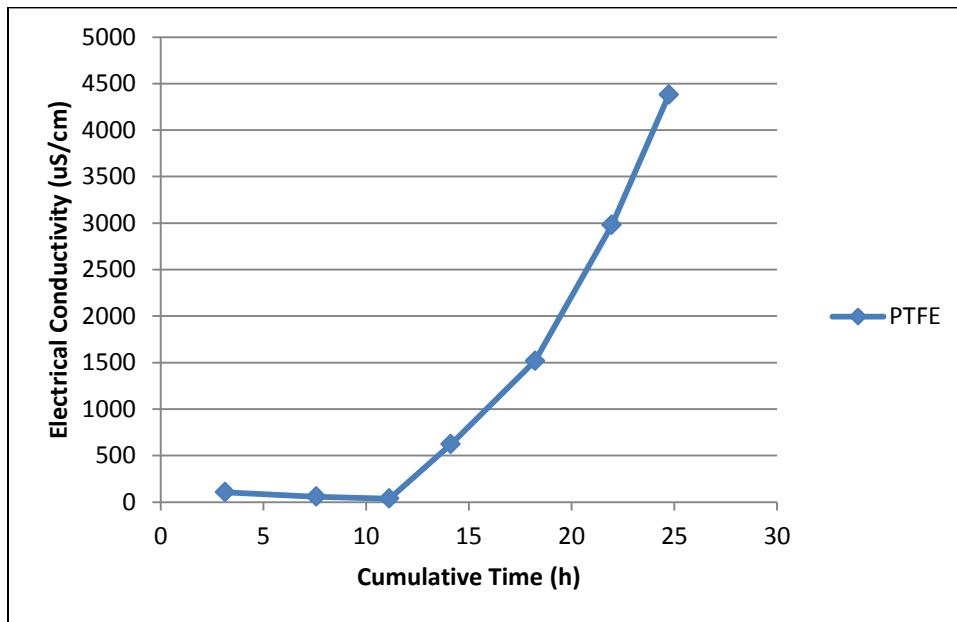

Figure 65: The Electrical Conductivity versus Time of the Distillate Produced Using

PTFE (0.22 μm) Membrane
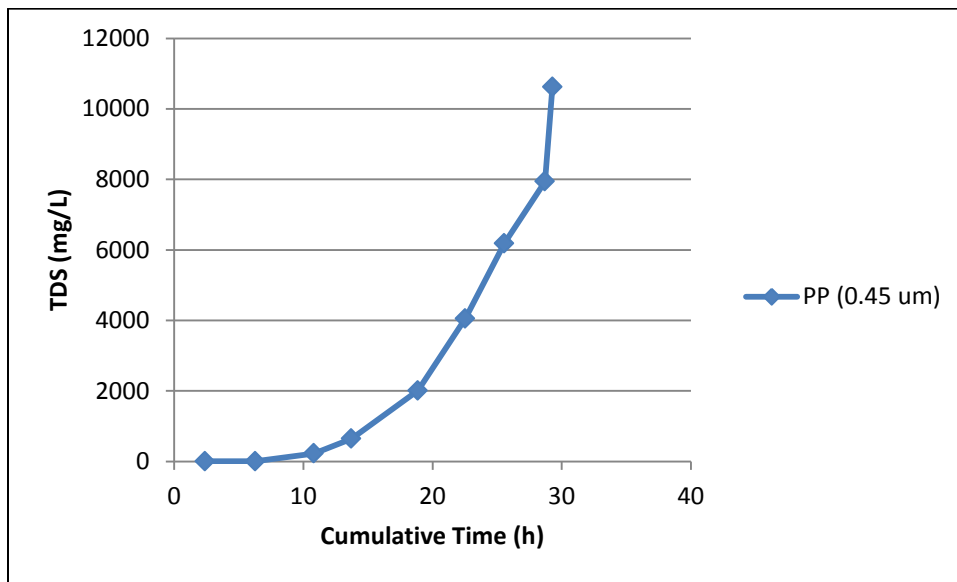
Figure 66: The TDS versus Time of the Distillate Produced Using PTFE (0.22 μm)
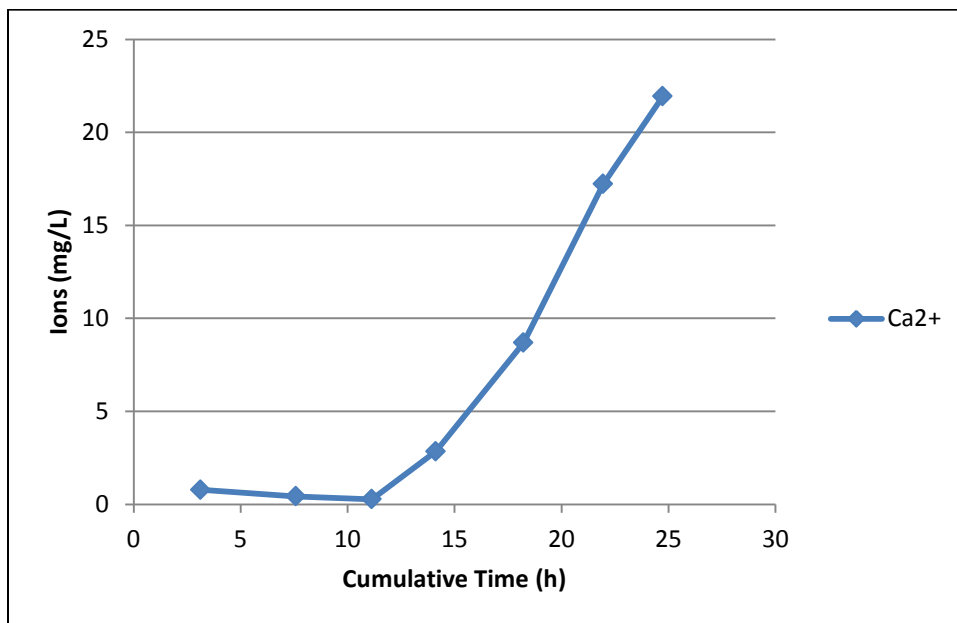
Membrane
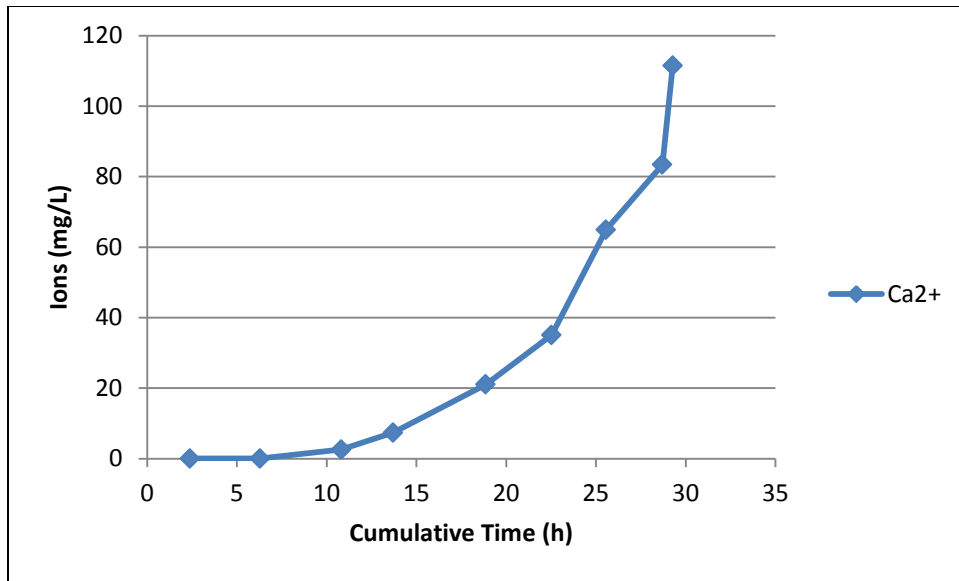

Figure 67: The Calcium Ions versus Time of the Distillate Produced Using PTFE

(0.22 μm) Membrane

221
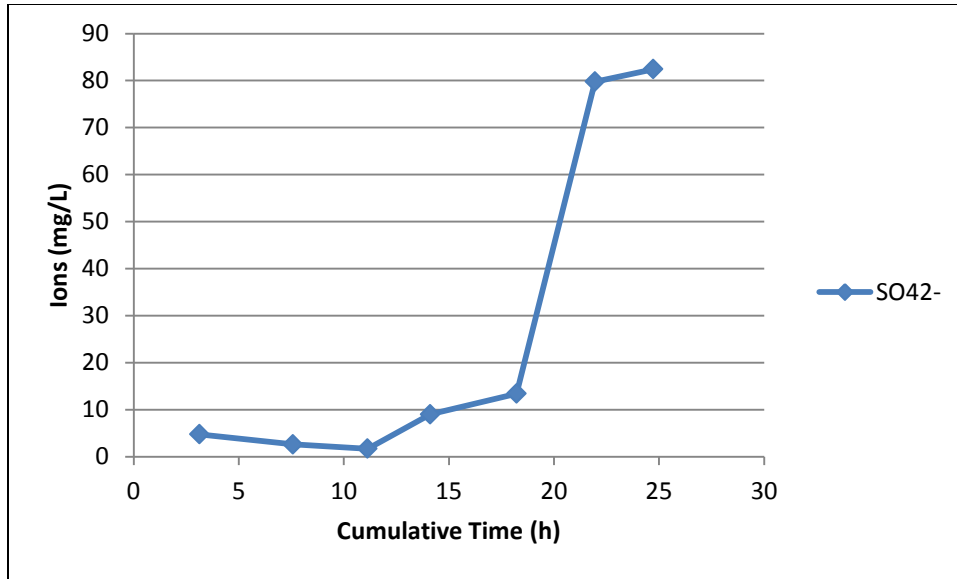
Figure 68: The Sulfate Ions versus Time of the Distillate Produced Using PTFE (0.22

μm) Membrane

Table 47 shows the calculated salt rejection of the first four runs (before the flux reduced significantly) using the DCMD unit utilizing PP and PTFE membranes.

Table 47: The Calculated Salt Rejection of the First Four Runs Using the DCMD Unit

Utilizing PP (0.22 μm and 0.45 μm) and PTFE (0.22 μm) Membranes

Membrane	PP (0.22 μm)		PP (0.45 μm)		PTFE (0.22 μm)	
Run #	Run Duration (h)	Salt Rejection (%)	Run Duration (h)	Salt Rejection (%)	Run Duration (h)	Salt Rejection (%)
1	1.725	99.99	2.383	99.99	3.125	99.89
2	3.292	99.99	3.900	99.99	4.450	99.94
3	4.408	99.998	4.525	99.65	3.558	99.96
4	3.825	99.98	2.900	99.00	2.983	99.33
Cumulative Run Duration (h)	13.25		13.71		14.12	

When comparing the salt rejection of the first four runs on the bench-scale DCMD unit (after about 13 hours of MD operation) using all of the membranes selected, it can be said that using PP membrane of pore size 0.22 microns gives a better salt rejection of more than 99.99% followed by PTFE membrane of almost the same size then by PP membrane of 0.45 μm.

The salinity of drinking water is determined usually by the amount of TDS in water. Drinking water standards in Qatar are adopted from EU and WHO. As demonstrated in Table 12, the permissible salinity level of drinking water in Qatar is in the range of 200-600 ppm and could reach 1000 ppm under limited consumptions. In this study, initially, all the distillates produced from the bench-scale DCMD unit have salinity levels less than those set by the state of Qatar (except for PP membrane of 0.22 μm which reached salinity levels of less than 100 ppm in all of the performed experiments). Hence, the distillates produced are of better quality. However, membrane fouling and pore wetting seems to occur when a membrane is reused for several times. This was indicated by the high electrical conductivity and TDS of the distillates.

Other sets of experiments were conducted using 100,000 ppm NaCl solution as the feed to the bench-scale DCMD unit under the same operating conditions of 75 ^{o}C and 20 ^{o}C for the hot and cold water inlet temperature, respectively, and a flow rate of 1.5 L/min. The same chemical analysis was carried out for the distillates produced using PP membrane of pore size 0.45 μm.

Table 48 shows the feed solution characteristic (synthetic brine) and Table 49 shows the chemical analysis of the distillates produced using PP membrane of 0.45 microns.

Table 48: The Feed Solution Characteristic (Synthetic Brine)

Parameter	Parameter Formula	Unit	Value
Electrical Conductivity	EC	μS/cm	144.927.5
pH	pH	-	6.98
Total Dissolved Solids	TDS	mg/L	100,000
Cations			
Calcium	Ca^{2+}		51.0
Potassium	K^+		< 5.0
Magnesium	Mg^{2+}		9.0
Sodium	Na^+	mg/L	41,228.0
Lithium	Li^+		< 5.0
Ammonium	NH_4^+		< 5.0
Anions			
Chloride	Cl^-		59,605.0
Floride	F^-		< 5.0
Bromide	Br^-		< 5.0
Nitrite	NO_2^-		< 5.0
Nitrate	NO_3^-	mg/L	< 5.0
Sulfate	SO_4^{2-}		87.0
Thiosulfate	$S_2O_3^{2-}$		< 5.0
Phosphate	PO_4^{3-}		< 5.0
Heavy Metals			
Aluminum	Al		UDL
Boron	B		UDL
Cadmium	Cd		UDL
Cobalt	Co		UDL
Chromium	Cr		UDL
Copper	Cu		UDL
Manganese	Mn		UDL
Molybdenum	Mo	mg/L	UDL
Nickel	Ni		UDL
lead	Pb		UDL
Antimony	Sb		UDL
Selenium	Se		UDL
Strontium	Sr		UDL
Titanium	Ti		UDL
Zinc	Zn		UDL

Table 49: The Chemical Analysis of the Distillates Produced Using PP (0.45 μm) and NaCl Solution as Feed

Feed	NaCl Solution (100,000 mg/L)								
Membrane	PP (0.45 μm)								
Parameter	**Parameter Formula**	**Unit**	**Run 1 Sample**	**Run 2 Sample**	**Run 3 Sample**	**Run 4 Sample**	**Run 5 Sample**	**Run 6 Sample**	
Electrical Conductivity	EC	μS/cm	27.30	31.60	197.10	1,380.00	6,280.00	28,100.00	
pH	pH	-	7.58	7.19	7.18	7.48	8.05	7.63	
Total Dissolved Solids	TDS	mg/L	18.84	21.80	136.00	952.20	4,333.20	19,389.00	
Cations									
Calcium	Ca^{2+}	mg/L	0.44	0.09	UDL	UDL	UDL	2.37	
Potassium	K^+		0.16	0.08	UDL	UDL	UDL	9.03	
Magnesium	Mg^{2+}		0.25	0.12	UDL	UDL	UDL	0.34	
Sodium	Na^+		5.57	6.96	47.06	396.30	1,748.00	7,840.00	
Anions									
Chloride	Cl^-	mg/L	6.18	7.87	72.34	575.24	2,688.20	12,052.60	
Sulfate	SO_4^{2-}		6.11	6.02	UDL	UDL	UDL	UDL	

The 100,000 ppm NaCl solution is of higher TDS than seawater. Still, Table 49 shows that the distillate produced is pure initially. However, for the later runs, the distillate quality deteriorated, indicating membrane wetting. Table 50 shows the calculated salt rejection using PP membrane of 0.45 µm and NaCl solution as feed.

Table 50: The Calculated Salt Rejection Using PP Membrane of 0.45 µm and NaCl Solution as Feed

	Run 1 Sample	Run 2 Sample	Run 3 Sample
Salt Rejection (%)	99.97	99.97	99.79

	Run 4 Sample	Run 5 Sample	Run 6 Sample	Run 7 Sample
Salt Rejection (%)	98.52	93.27	82.06	69.88

Table 50 shows that the salt rejection for the first three runs is more than 99.7% (about 100%). However, with repeated runs using the same membrane and under the same operating conditions, the TDS of the distillate increased and the salt rejection after performing all of the runs (till Run 7) dropped to about 69.9%. This means that for the first few runs, the membrane didn't allow the ions to pass through it. Later, it appears that pore wetting has occurred. Moreover, the EC, the TDS, the sodium ions, and the chloride ions in the distillate produced using PP membrane with pore size of 0.45 µm are shown in Figure 69, 70, 71, and 72, respectively.
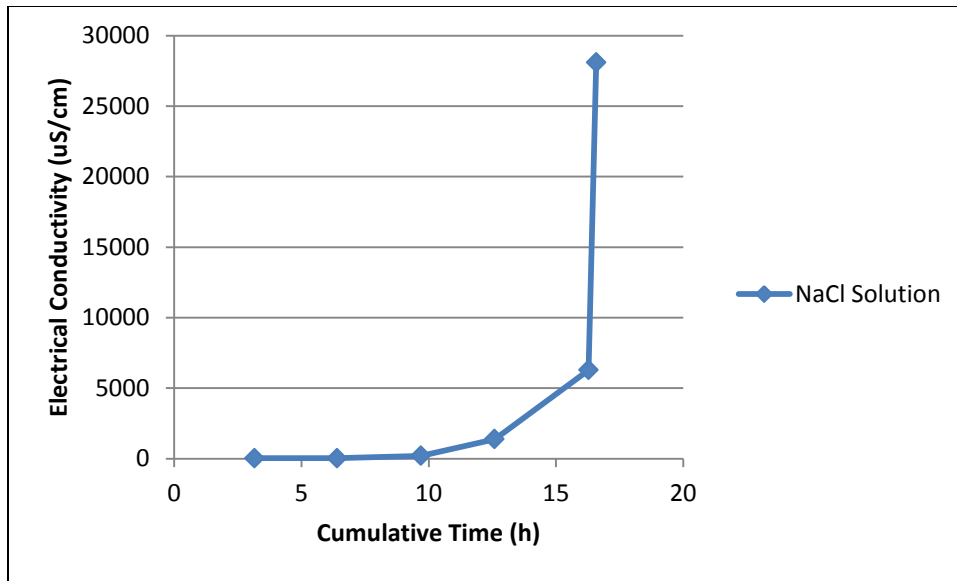
Figure 69: The Electrical Conductivity versus Time of the Distillate Produced Using

PP (0.45 μm) Membrane and Synthetic Brine Solution
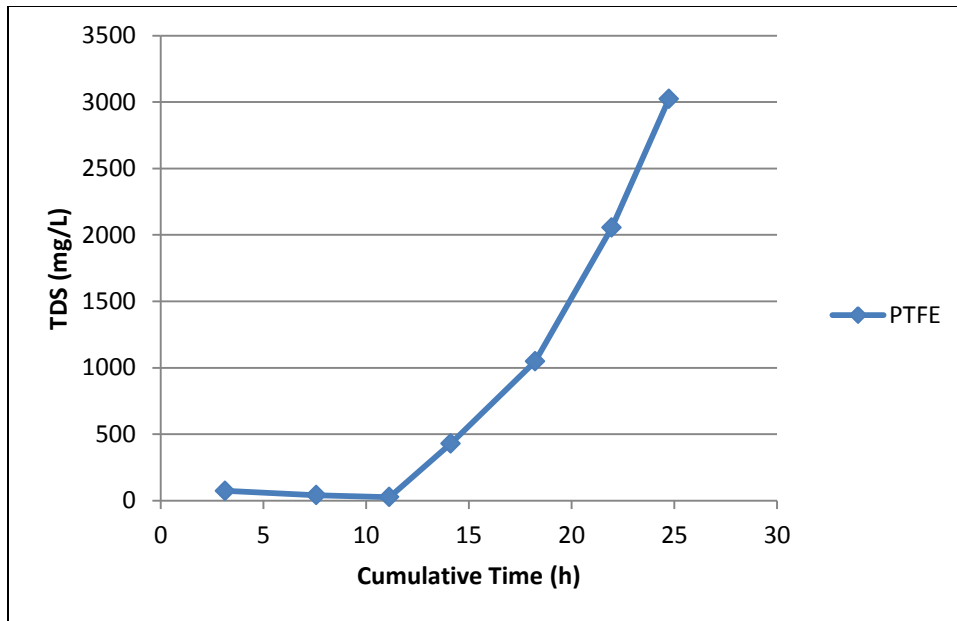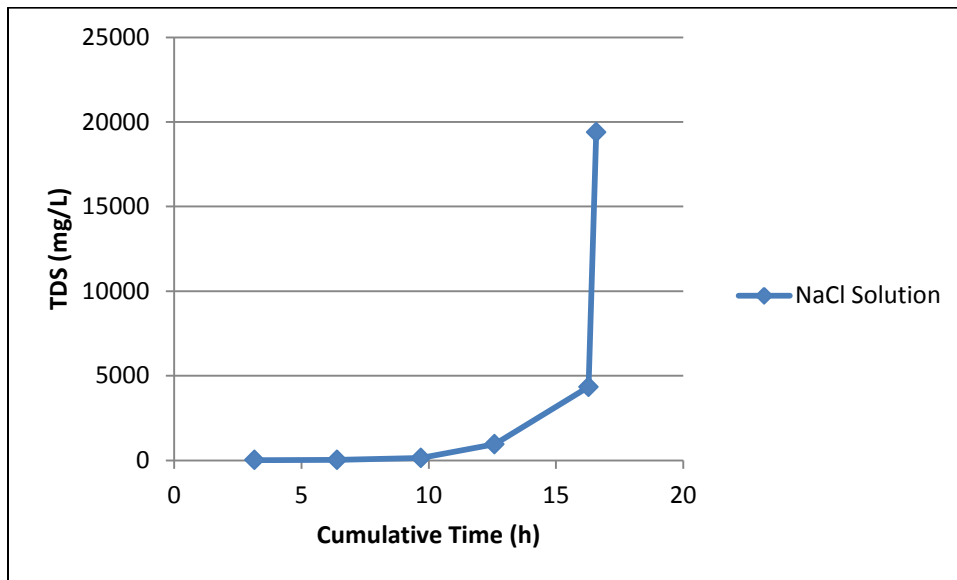

Figure 70: The TDS versus Time of the Distillate Produced Using PP (0.45 μm)

Membrane and Synthetic Brine Solution
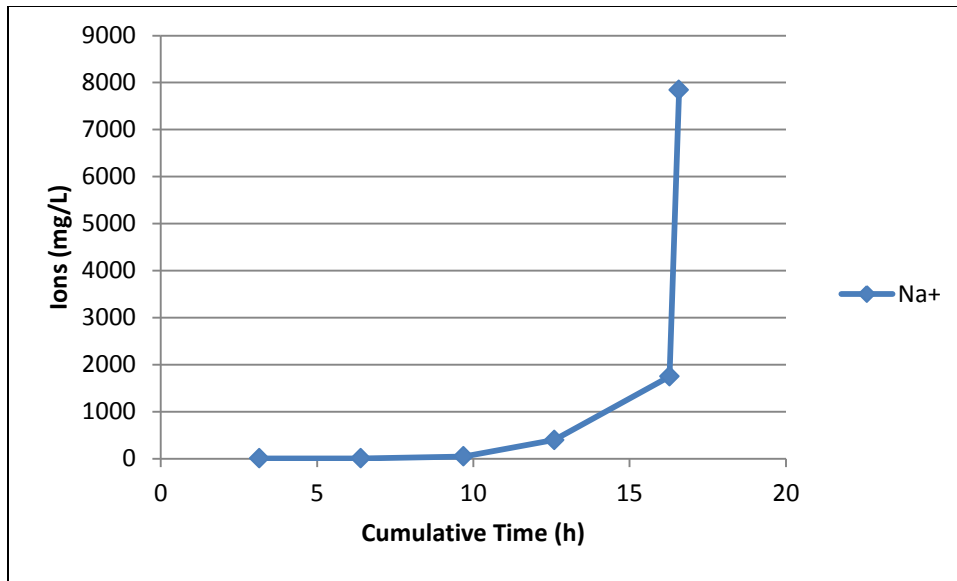
Figure 71: The Sodium Ions versus Time of the Distillate Produced Using PP (0.45 μm) Membrane and Synthetic Brine Solution
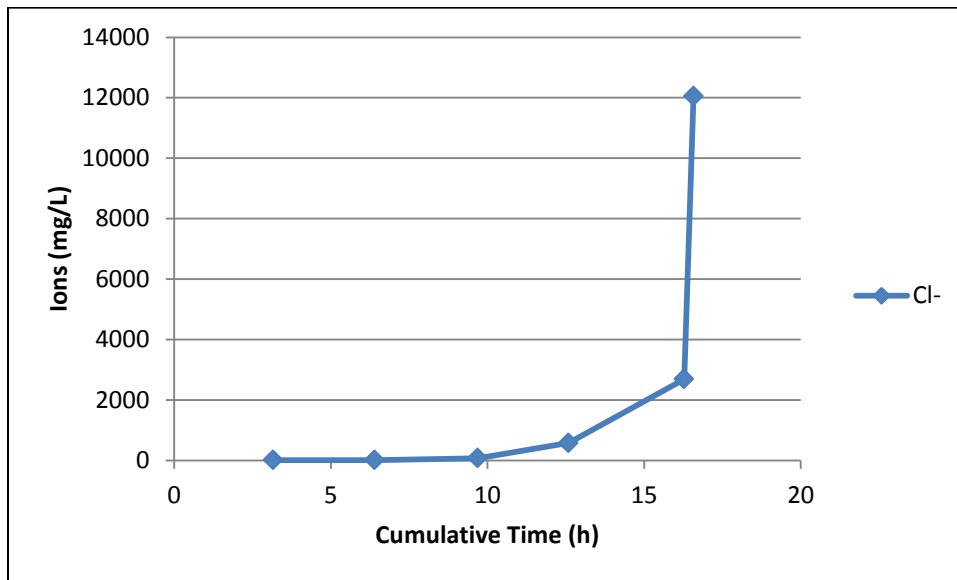
Figure 72: The Chloride Ions versus Time of the Distillate Produced Using PP (0.45 μm) Membrane and Synthetic Brine Solution

In addition, when comparing the electrical conductivity and the TDS of using PP membrane of 0.45 microns with seawater and the synthetic brine, it can be clearly seen that they are higher when the NaCl solution was used. Also, regarding the salt rejection, it is lower using the higher salinity solution. Therefore, the quality of water, probably due to pore wetting, is lower when a higher salinity solution is used as feed to the MD system.

It is clearly indicated that due to the hydrophobic nature of the membranes used in this study, the water produced is pure and the salts are rejected at the surface of the membranes; however, only initially or for few hours.

Table 51 shows the quality of the distillate produced from the main water production terminal in Qatar (an MSF thermal desalination plant) that is owned by QEWC and located in Ras Abu Fentas.

Table 51: Distillate Quality from Ras Abu Fentas MSF Thermal Desalination Plant

Parameter	Parameter Formula	Unit	Value
Electrical Conductivity	EC	µS/cm	0.02
pH	pH	-	7.08
Total Dissolved Solids	TDS	mg/L	10.35
Cations			
Calcium	Ca^{2+}		0.12
Potassium	K^+		1.40
Magnesium	Mg^{2+}	mg/L	0.15
Sodium	Na^+		2.03
Lithium	Li^+		<0.10
Ammonium	$NH4^+$		<0.10
Anions			
Chloride	Cl^-		3.57
Floride	F^-		0.39
Bromide	Br^-		<0.10
Phosphate	PO_4^{3-}		0.58
Nitrate	NO_3^-	mg/L	2.17
Nitrite	NO_2^-		1.20
Sulfate	SO_4^{2-}		0.14
Thiosulfate	$S_2O_3^{2-}$		0.11

Compared to the distillate produced from Ras Abu Fentas MSF thermal desalination plant, the MD distillate is of great quality and in some cases (Table 39 and Table 42), it is of better quality in terms of TDS, but again, only initially.

Using the bench-scale DCMD unit of this study, more than 99 % salt rejection was obtained at first which is comparable to the results found in literature.

Alkhudhiri et al. (2013) have utilized a bench scale AGMD process with a PTFE membrane to purify four types of salt solutions: NaCl, $MgCl_2$, Na_2CO_3 and Na_2SO_4. The results show that the salt rejection obtained in the study was found to lie between 99.9% and 100% for all of the salts.

Hsu et al. (2002) have worked on both DCMD and AGMD using NaCl solution and real seawater as feed to the processes and PTFE membrane with different pore sizes (0.2 µm and 0.5 µm). The results showed that using the two MD configurations, the conductivities of the distillates were in the range of 7-12 µS/cm.

Tang et al. (2009) have worked on vacuum membrane distillation (VMD) with 6 wt.% aqueous NaCl solution (at the same concentration of the brine of seawater desalination). They have used a hydrophobic micro-porous PVDF hollow fiber membrane to investigate the performance of the VMD. The lab scale and pilot scale experiments showed that the salt rejection reached 99.8% at 70 $^{\circ}$C, 3 kPa, and a flow rate of 0.461 m/s.

Hou et al. (2013) have studied desalination by DCMD utilizing a flat-sheet self-prepared PVDF membrane with a pore size of 0.22 µm. Using seawater as the feed to the DCMD process, the salt rejection was over 99.9%.

Cath et al. (2004) have studied the performances of three hydrophobic microporous membranes using a DCMD process with 40 °C as the feed water inlet temperature. Their results showed that the salt rejection was greater than 99.9% for all of the membranes used.

A study by Feng et al. (2008) showed that for using NaCl solutions of different concentrations, salt rejection ranging from 98.7 to 99.9% was obtained. The distillates were obtained using an AGMD process utilizing PVDF membranes.

The findings in this study are consistent with the aforementioned researchers' findings before membrane pore wetting that was encountered with all of the membranes used. This is confirmed by the contact angle measurements that will be discussed in the next section.

5.3- Contact Angle Measurements

To assess the membranes' hydrophobicity, contact angles of the membranes' active layer (and back layer for PTFE membrane) were measured before and after the operation of the bench-scale MD unit. As discussed earlier, the larger the contact angle, the more hydrophobic the membrane is. However, membranes with a contact angle of less than 90° are considered slightly hydrophobic or hydrophilic depending on how small the contact angle is.

Contact angle measurements were done using a drop shape analyzer (DSA25; KRÜSS, Germany) equipped with a video capturing system. Deionized water was used to measure the contact angles and the sessile drop method was employed. The experimental procedure was discussed in Section 4.8.2. Using a digital image processor, the contact angles were calculated for each membrane with the aid of a compatible computer software.

Figure 73, 74, 75, and 76 show the shape of a deionized water droplet on a flat-sheet PP membrane of 0.22 μm, PP membrane of 0.45 μm, PTFE membrane of 0.22 μm (active layer), and PTFE membrane of 0.22 μm (support layer), respectively.
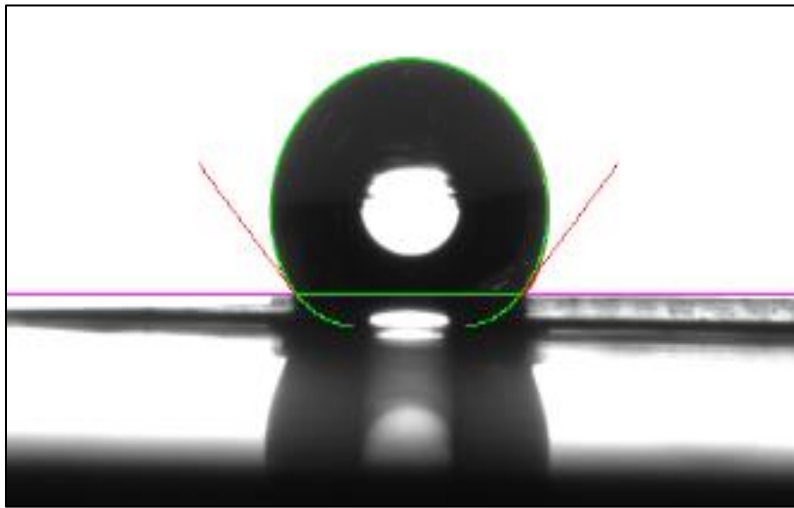
Figure 73: The Shape of a Deionized Water Droplet on a Flat-Sheet PP (0.22 μm) Membrane
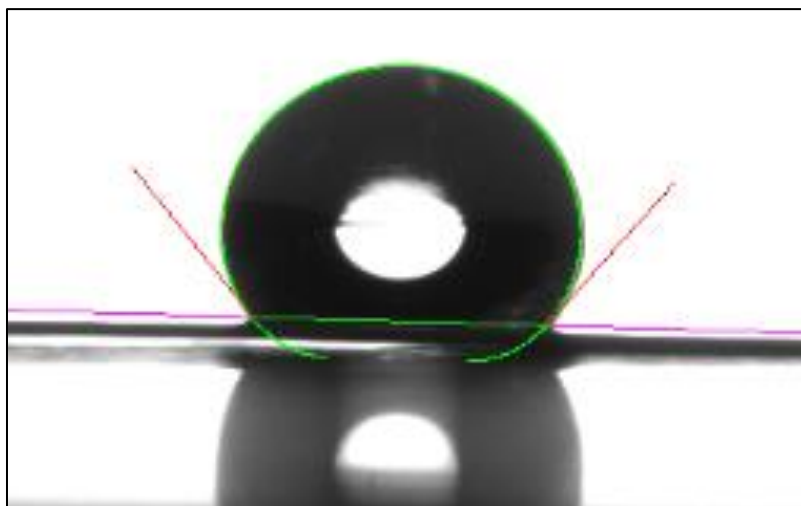
Figure 74: The Shape of a Deionized Water Droplet on a Flat-Sheet PP (0.45 μm) Membrane
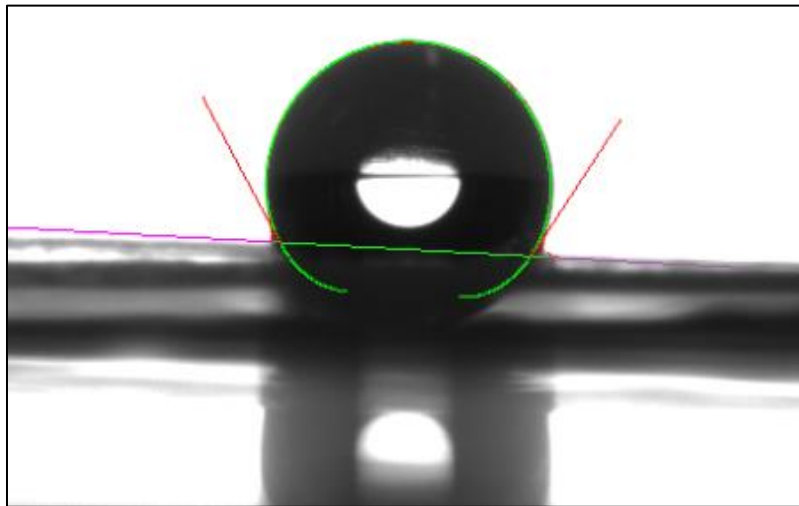
Figure 75: The Shape of a Deionized Water Droplet on the Active Layer of a Flat-

Sheet PTFE (0.22 μm) Membrane
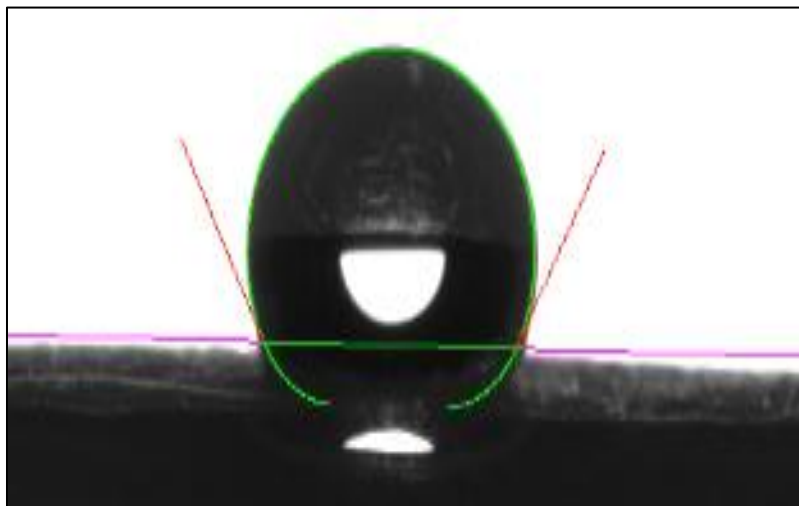
Figure 76: The Shape of a Deionized Water Droplet on the Support Layer of a Flat-

Sheet PTFE (0.22 μm) Membrane

Several contact angle (CA) measurements were taken to get reliable results and an average value of the contact angles was taken. Table 52 shows the contact angle measurements of a new flat-sheet PP membrane with a pore size of 0.22 μm.

Table 52: The Contact Angle Measurements of a New Flat-Sheet PP (0.22 μm) Membrane

Membrane	PP (0.22 μm)
Contact Angle (CA) (°)	135.5
	134.8
	131.8
	131.1
	135.0
	137.8
	134.6
	137.1
	136.7
	137.1
	134.0
	134.1
	132.3
Minimum CA (°)	131.1
Maximum CA (°)	137.8
Average CA (°)	**134.8**

The measured contact angle of PP membrane (0.22 μm) ranged from 131.1°-137.8°. The average contact angle was found to be 134.8°.

Using the same procedure, the contact angle of PP membrane of 0.45 microns was attained. Table 53 shows the measured contact angles.

Table 53: The Contact Angle Measurements of a New Flat-Sheet PP (0.45 μm)

Membrane

Membrane	PP (0.45 μm)
Contact Angle (CA) (°)	130.3
	134.6
	133.3
	136.1
	134.3
	131.2
	133.1
	135.6
	132.6
	130.5
Minimum CA (°)	130.3
Maximum CA (°)	136.1
Average CA (°)	**133.2**

The measured contact angle of PP (0.45 μm) membrane ranged from 130.3°-136.1°. The average contact angle was found to be 133.2°.

In addition, Table 54 and Table 55 show the contact angle measurements of the active layer of a new flat-sheet PTFE membrane and its support layer, respectively.

Table 54: The Contact Angle Measurements of the Active Side of a New Flat-Sheet

PTFE (0.22 μm) Membrane

Membrane	PTFE (0.2 μm)
Contact Angle (CA) (°)	142.6
	139.5
	135.0
	141.7
	145.4
	123.0
	125.1
	131.2
	134.6
	146.1
	144.3
	136.5
	139.8
	134.4
	146.6
Minimum CA (°)	123.0
Maximum CA (°)	146.6
Average CA (°)	**137.7**

Table 55: The Contact Angle Measurements of the Back Side of a New Flat-Sheet

PTFE (0.22 μm) Membrane

Membrane	PTFE (0.2 μm)
Contact Angle (CA) (°)	131.4
	123.6
	125.3
	135.3
	133.8
Minimum CA (°)	123.6
Maximum CA (°)	135.3
Average CA (°)	**129.9**

The measured contact angle of the active side of PTFE (0.22 μm) membrane ranged from 120.9°-146.6°. The average contact angle was found to be 136.7°. On the other hand, the measured contact angle for the back side of the PTFE membrane ranged from 123.6°-135.3° with an average of 129.9°.

The variation in the contact angle measurements of a membrane (specially for the active side of PTFE membrane in this study) were previously discussed in Section 3.6 which is mainly due to the fact that the measurements are very sensitive to the volume of the dropped liquid (it was manually dropped), the measurement time, and the smoothness of the membrane.

The results show that the membranes used in this study have contact angles of greater than 90°. The high contact angles obtained proves that the membranes used are highly hydrophobic. The hydrophobicity of the membranes allows only vapor to be passed through and rejects water; hence, ensuring high selectivity of the MD process.

In addition, PTFE membrane had the highest contact angle (average); although, the minimum contact angle for PTFE membrane was smaller than those measured for PP membranes. Nevertheless, the range of the measured contact angles was bigger. Therefore, the highest contact angle measured was for PTFE membrane of 0.22 microns followed by PP membrane of 0.22 microns and then PP membrane of 0.45 microns. Previous observations showed that PP membrane of 0.45 microns (the least hydrophobic membrane) was the first membrane to be fouled (the first membrane to experience severe flux declines) and the first to experience membrane pore wetting as was indicated by the water quality results.

Furthermore, the measured contact angles in this study were consistent with the values reported in literature.

Lawson & Lloyd (1997) state that the typical contact angle for a hydrophobic membrane is 130°.

Camacho et al. (2013) state that the contact angle of PTFE membrane is reported to be 140°, which is about the same as the average contact angle of PTFE membrane found in this study.

Nghiem et al. (2011) have conducted MD experiments using a flat sheet PTFE membrane with a pore size of 0.22 μm. A contact angle of 137.7° was reported in their study, which is exactly the same as the one found in this study.

Adnan et al. (2012) have tested six PTFE membranes from three different sources. The results of their study showed that the contact angle of PTFE membrane ranged from 126 ° to 165 °.

Zhang et al. (2010) showed that depending on the membrane pore size, its thickness, and the geometric structure of the support layer, PTFE membrane had contact angles ranged from 126-150°.

Zhang J. (2011) and Camacho et al. (2013) state that of the membrane materials used for MD applications, PTFE membrane has the largest contact angle with water (has the best hydrophobicity). This was also confirmed by the contact angle measurements of this study as PTFE membrane had a greater contact angle than PP membrane.

Zhang et al. (2010) state that the hydrophobicity of a membrane is essential for MD operation; however, they found that it is not linked to flux as strongly as other physical features of the membranes used in their study. This is also the case in this study as PTFE membrane had the highest contact angle (the best hydrophobicity) but didn't show the highest flux performance. This is possibly due to the effect of the overall thickness of the membrane, its pore size, its structure geometry, its porosity, and the effect of a support layer. Moreover, Zhu et al. (2013) state that not only the hydrophobicity of a membrane is crucial in MD but other membrane characteristics such as thickness, porosity, and pore size distribution can also influence membrane performance. This is also shared by Phattaranawik et al., (2003) and Gryta (2007).

According to Camacho et al. (2013), increased membrane hydrophobicity leads to decreased thermal conductivity which is favorable in DCMD as the heat losses by conduction across the membrane would be reduced. Also, this won't lead to the formation of strong heat polarization layers.

Membrane wetting occurs when the pressure difference between a membrane's liquid/vapor interface exceeds the liquid entry pressure (Rácz et al., 2014). Therefore, a high contact angle along with smaller membrane pore size, lower surface energy, and higher surface tension lead to higher liquid entry pressure that prevents pore wetting. Consequently, a low contact angle means a low membrane ability of non-volatile feed rejection. The penetration of liquid as a result of pore wetting affect the quality of the distillate produced (Camacho et al., 2013).

Further tests were carried out on the same contact angle apparatus to measure the contact angles of the membranes after being used in the bench-scale DCMD unit to examine membrane fouling. The used membranes were first rinsed with deionized water to remove soft fouling if it has formed on the membrane; thus, keeping only the hard/permanent fouling to be examined.

Table 56 shows the contact angle measurements for the used flat-sheet PP (0.22 μm) membrane after being left to dry naturally.

Table 56: The Contact Angle Measurements of the Used PP (0.22 μm) Membrane

(Feed: Seawater)

Membrane	PP (0.22 μm)	
	More Fouled Part	**Less Fouled Part**
Contact Angle (CA) (°)	38.0	83.9
	26.0	74.5
	56.0	68.1
	42.0	81.4
Minimum CA (°)	26.0	68.1
Maximum CA (°)	56.0	83.9
Average CA (°)	**40.5**	**77.0**

As mentioned earlier (Section 5.3.1), the salt layer formed on PP membrane of 0.22 microns was not uniform. However, one side had more salts than the other side which was previously shown in Figure 49. Therefore, contact angle measurements were done on the both sides of the active layer of the membrane. Table 56 shows that the more fouled part of the membrane had contact angles ranged from 26.0° to 56.0° with an average contact angle of 40.5°. On the other hand, the less fouled part of the membrane had contact angles ranged from 68.1° to 83.9° with an average contact angle of 77.0°.

The results clearly show that the membrane has lost its hydrophobicity as the contact angles after the membrane usage were found to be less than 90°. This was also indicated with the water quality tests performed and the flux performance of the membrane.

Moreover, Table 57 shows the contact angle measurements of the used flat-sheet PP (0.45 μm) membrane with seawater as feed. The measurements were done after the membrane was left to dry naturally.

Table 57: The Contact Angle Measurements of the Used PP (0.45 μm) Membrane (Feed: Seawater)

Membrane	PP (0.45 μm)	
	More Fouled Part	**Less Fouled Part**
	39.2	65.4
	37.6	74.7
Contact Angle (CA) (°)	33.3	63.6
	34.2	85.4
Minimum CA (°)	33.3	63.6
Maximum CA (°)	39.2	85.4
Average CA (°)	**36.1**	**72.3**

Similar to PP membrane of 0.22 microns, the salt layer formed on the PP membrane of 0.45 microns membrane was not uniform. Therefore, likewise, contact angle measurements were done on the both sides of the active layer of the membrane. Table 57 shows that the more fouled part of the membrane had contact angles ranged from 33.3° to 39.2° with an average contact angle of 36.1°. On the other hand, the less fouled part of the membrane had contact angles ranged from 63.6° to 85.4° with an average contact angle of 72.3°.

After being used for several extended experiments, PP membrane of 0.45 microns had lost its hydrophobicity. The results show that the contact angles obtained were less

than those obtained for PP membrane of 0.22 microns indicating a more severe membrane pore wetting. This was also the case in the flux performance and water quality analysis.

Furthermore, Table 58 shows the contact angle measurements of the used flat-sheet PTFE (0.22 μm) membrane with seawater as feed. The measurements were done after the membrane was left to dry naturally.

Table 58: The Contact Angle Measurements of the Used PTFE (0.22 μm) Membrane (Feed: Seawater)

Membrane	PTFE
Contact Angle (CA) (°)	0.0
	12.8
	31.6
	10.8
Minimum CA (°)	0.0
Maximum CA (°)	31.6
Average CA (°)	**13.8**

As discussed earlier, the salt layer on the PTFE membrane was not uniform. However, the difference in the salt layer wasn't as clear as that formed on PP membranes, meaning that the deposition of salts was random and not concentrated on one side of the membrane. In addition, a denser fouling layer was formed on the PTFE membrane. Therefore, the lowest contact angle found was 0°. This suggests that the membrane was completely covered by deposits and that pore wetting has

occurred. Moreover, the largest contact angle found on PTFE membrane was 31.6° and the average contact angle was 13.8°. Again, the results show that the membrane had lost its hydrophobicity and has experienced pore wetting which was indicated by the membrane's flux performance and water quality test.

In addition, contact angle measurements of the fouled PP (0.45 μm) membrane were done when the synthetic brine was the feed solution. Table 59 shows the contact angle measurements of the used flat-sheet PP (0.45 μm) membrane utilizing the 100,000 ppm NaCl solution as the feed to the process. The measurements were done after the membrane was left to dry naturally.

Table 59: The Contact Angle Measurements of the Used PP (0.45 μm) Membrane

(Feed: NaCl Solution)

Membrane	PP (0.45 μm)
	0.0
	40.6
Contact Angle (CA) (°)	33.1
	18.2
	10.1
Minimum CA (°)	0.0
Maximum CA (°)	40.6
Average CA (°)	**20.4**

Table 59 clearly shows the effect of the feed solution concentration on the membrane performance as lower contact angles were obtained when PP membrane of 0.45 microns was used with the higher salinity NaCl solution than with the seawater.

Similarly, the salt deposition on the membrane surface was not uniform; hence, the variation of contact angle values obtained. However, similar to the PTEF membrane, there wasn't a clear distinction between the sides of the membrane's active layer in which the salt deposition is higher, but the salt was randomly distributed. This might be attributed to the heavy salt deposition that resulted in lower contact angles. Similar observation was seen with the thick salt layer on the PTFE membrane.

It is worth mentioning that measuring the contact angle of the used membranes was harder than obtaining those of the fresh membranes due to the fact that the membrane surface was not smooth anymore as a result of the deposited salt layer. Bachmann et al. (2000) had the same observation. In addition, according to Zisman (1964), to accurately measure small contact angles, the surface used must be much smoother than when large contact angles are measured.

The largest contact angle found for the fouled PP membrane of 0.45 microns when the synthetic brine was feed to the bench-scale DCMD unit was 40.6° and the lowest was 0° which suggest that the membrane was fully covered by deposits and that pore wetting has occurred. Nevertheless, the average contact angle was found to be 20.4°.

The results of the contact angle measurements of the fouled membranes revealed a significant reduction in the membranes' hydrophobicity. This is shown in all of the membranes used. The largest contact angle (average) after using the membranes was for PP membrane of 0.22 microns and the lowest was for PTFE membrane of 0.22 microns.

The contact angles give more insight on the fouling mechanism in the membranes used. PP membrane had a higher contact angle after being fouled than PTFE membrane. However, water quality tests and flux performance showed that PP membrane of pore size 0.45 μm was the most fouled membrane. The lower contact angle of PTFE membrane (0°) might suggest that pore blocking was more sever using PTFE membrane. This is also indicated by the SEM imaging of the fouled PTFE membrane (Section 5.4).

Franken et al. (1987) state that as a consequence to fouling, the contact angle will decrease. In addition, if the contact angle becomes smaller than 90°, the liquid will wet the solid surface.

Nghiem et al. (2011) have reported contact angle values of a flat sheet PTFE membrane with pore size of 0.22 μm. After treating seawater, a contact angle of 8.9° was reported in their study which is in the range of the contact angle values found in this study for the used PTFE membrane.

Therefore, the results of this study are consistent with those reported in MD literature.

5.4- SEM Characterization and EDS Analysis

SEM imaging was undertaken in Qatar University's Central Laboratory Unit to observe the membranes' active layer, pores, and cross section. To get the images and study the morphology of the membranes, samples of the membranes were frozen in liquid nitrogen and were later fractured prior to being transferred to the microscope.

Figure 77, 78, 79, and 80 show SEM images of a clean (fresh) PP of 0.22 μm membrane, PP of 0.45 μm membrane, PTFE of 0.22 μm membrane, and a cross section image of the support layer of PTFE membrane, respectively.
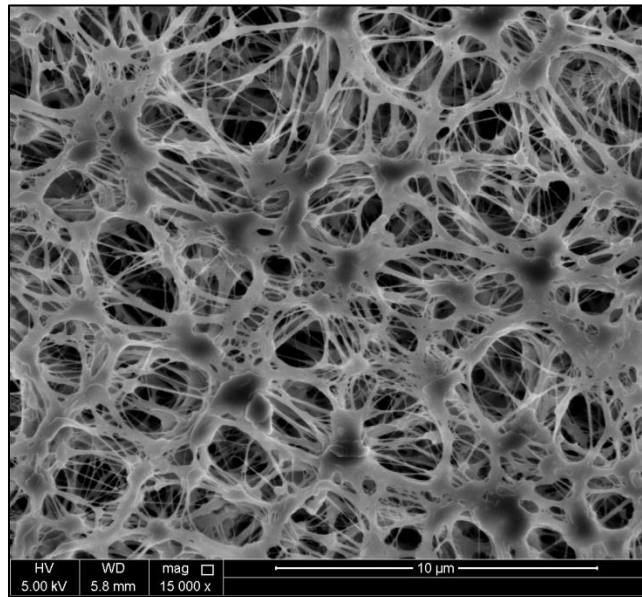
Figure 77: SEM Image of a Fresh PP (0.22 μm) Membrane at 15,000 x Magnification
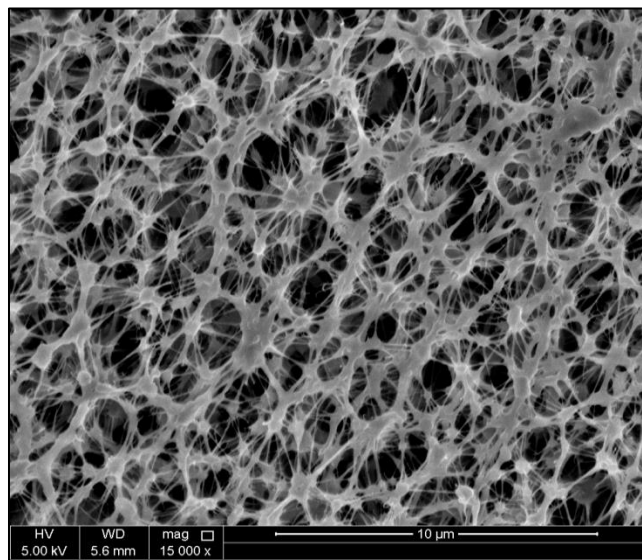
Figure 78: SEM Image of a Fresh PP (0.45 μm) Membrane at 15,000 x Magnification
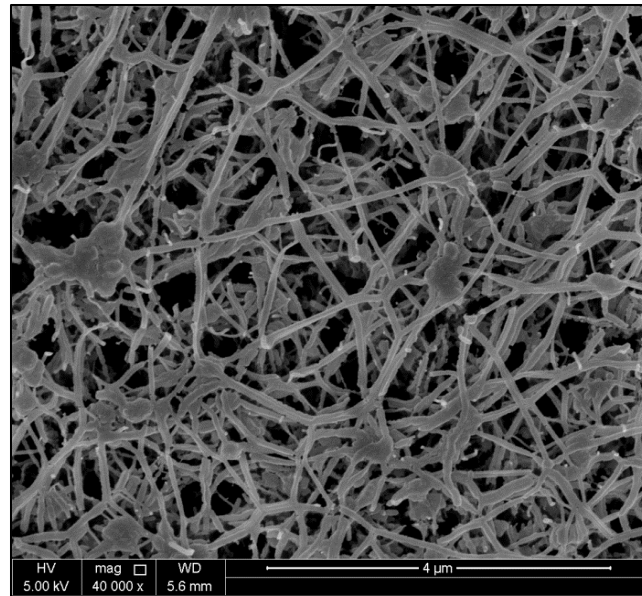
Figure 79: SEM Image of a Fresh PTFE (0.22 μm) Membrane at 40,000 x

Magnification
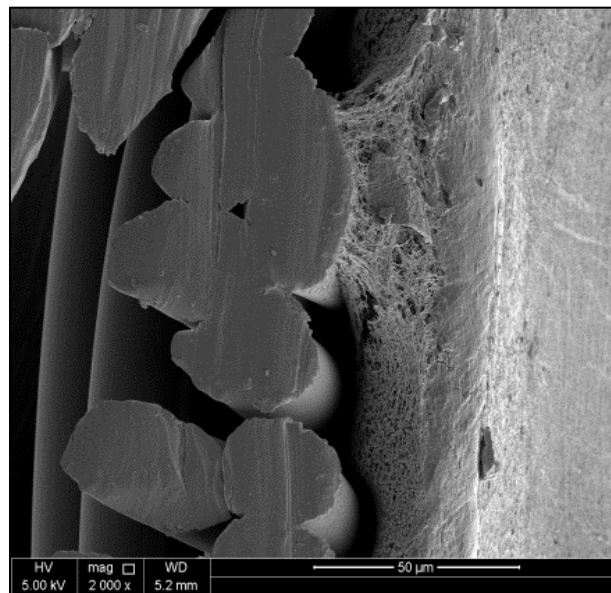
Figure 80: A Cross Section SEM Image of the Thermal Bonding of the Support Layer

to the Active Layer of PTFE (0.22 μm) Membrane at 2,000 x Magnification

Figure 77, 78, and 79 clearly show that the structure of PP membrane is different than that of PTFE membrane in that the pores of PP membrane are more like circles whereas they exhibit different shapes in PTFE membrane such as circles, rectangles, or cylinders.

For fouling investigations, several SEM images were taken for the fouled membranes after being utilized for several extended runs using the bench-scale DCMD unit under the previously specified conditions. Figure 81 shows SEM images of the fouled PP (0.22 μm) membrane at different locations of the membrane's surface.

Figure 81: SEM Images of the Fouled PP (0.22 µm) Membrane at Different Locations

of the Membrane's Surface

The SEM analysis revealed that PP membrane of 0.22 μm underwent severe fouling. Figure 81 shows that the formed deposits on the PP (0.22 μm) membrane surface were not uniform and that they were localized in some parts more than others (image (a) and (b)). On the other hand, image (c) and (d) show that the membrane was completely covered by deposits which formed local "flowers" on the membrane surface. This is indicated also by comparing Figure 77 of the clean membrane to image (d) of almost the same magnification. Furthermore, image (f) shows that not only thick "blade-like" deposits (image (e)) were found on the membrane surface, but also "sand-like" deposits were present. Figure 81 shows that the deposits on PP membrane of 0.22 μm exhibited different shapes indicating different types of foulants. Overall, according to their shape, the crystals in Figure 81 are clearly of calcium sulfate.

Elemental analysis of several parts of the membranes used in the study was done using SEM-EDS. For PP (0.22 μm) membrane, five arbitrary locations (positions) on the membrane surface were analyzed (position (a) to (e)). The EDS spectrum of two positions is shown in the Appendix. Figure 82 shows two of the SEM-EDS images of PP membrane of 0.22 microns at 300 x (position (a)) and 2500 x (position (e)) magnification.
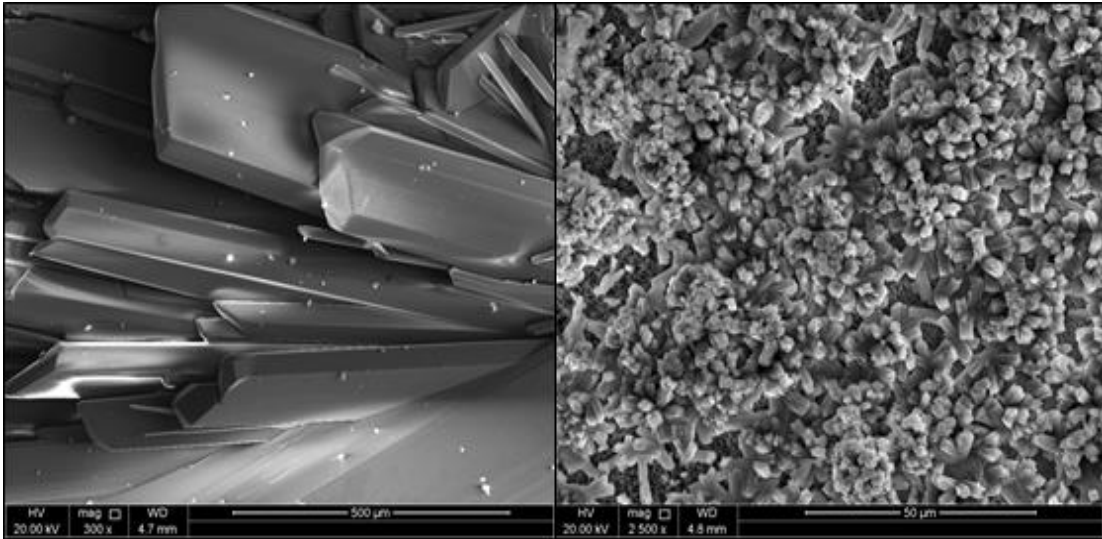
Figure 82: SEM-EDS Images of PP Membrane of 0.22 μm Membrane at 300 x (left)

and 2,500 x (right) Magnification

Table 60 illustrates the elements found on the membrane surface.

Table 60: The Foulants of PP (0.22 μm) Membrane Indicated by the EDS Spectra

Membrane	PP (0.22 μm)				
Feed	Seawater				
	Arbitrary Position on the Membrane				
Element	(a)	(b)	(c)	(d)	(e)
C	✓	✓	✓	✓	✓
O	✓	✓	✓	✓	✓
F	✓				
S	✓		✓		
Ca	✓	✓	✓	✓	✓
Na		✓		✓	✓
Cl				✓	✓

Table 60 shows that there were several foulants of PP (0.22 μm) membrane. These

were C, O, F, S, Ca, Na, and Cl. However, as stated earlier, the salt layer formed on

the membrane was not uniform; therefore, not only the amount of salts deposition on

the membrane was different, but also the elements deposited on the different positions of the membranes were different. Nevertheless, in all of the tested membrane positions, C, O, and Ca were found. This indicates that the major foulant/scalant found using PP of 0.22 microns under the conditions of the study was $CaCO_3$. Also, the EDS spectra of the membrane indicated the presence of $CaSO_4$.

The same procedure was followed for investigating fouling of PP membrane of 0.45 µm membrane. Figure 83 shows SEM images of the fouled PP (0.45 µm) membrane at different locations of the membrane's surface.
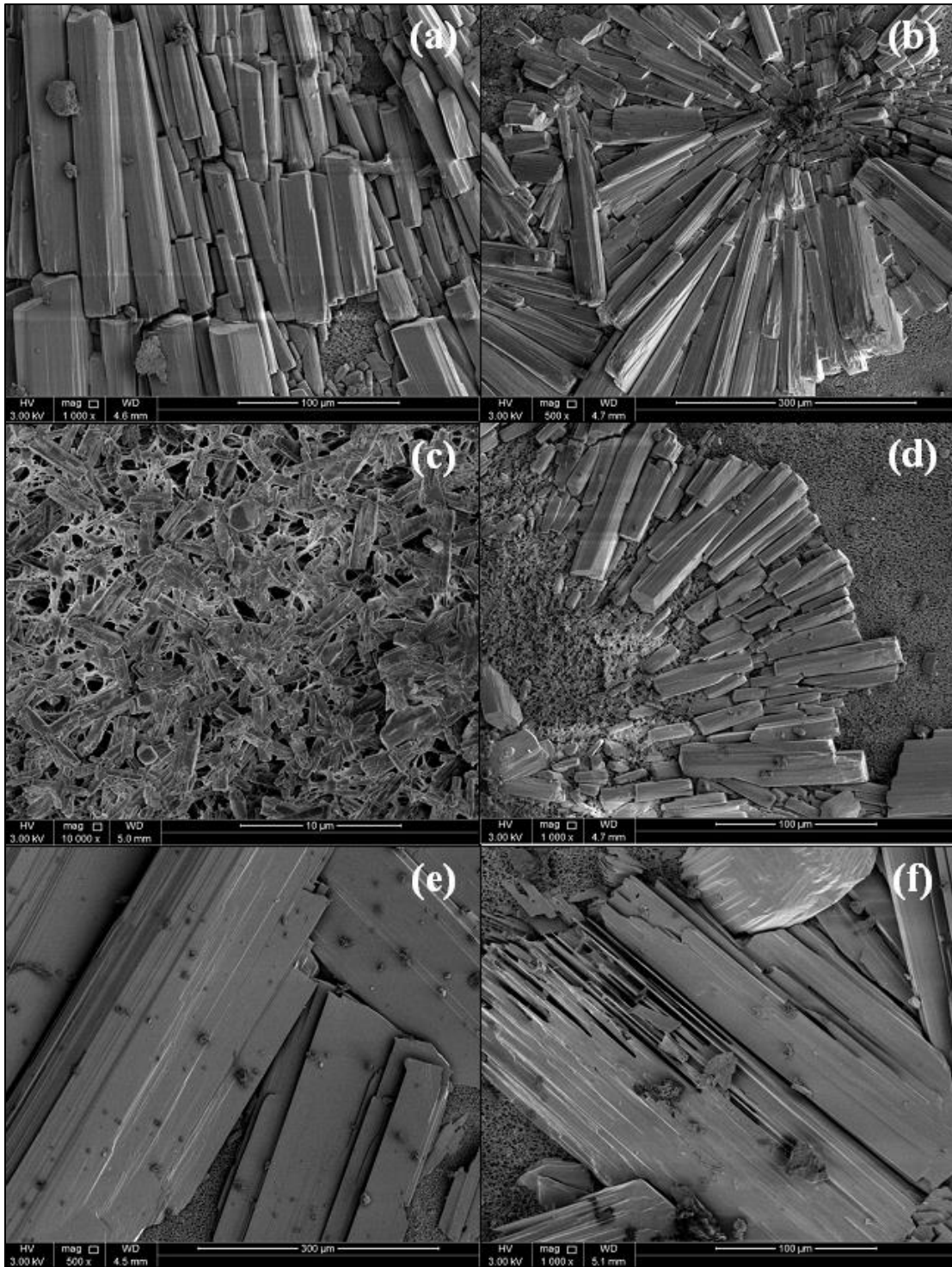
Figure 83: SEM Images of the Fouled PP (0.45 μm) Membrane at Different Locations

of the Membrane's Surface

The SEM analysis revealed that PP of 0.45 μm underwent severe fouling. Figure 83 shows that the formed deposits on the PP (0.45 μm) membrane surface were not uniform. The deposits formed were "rod-like" in shape (image (a)) and they formed local "flowers" on the membrane surface (image (b)) similar to the deposits on PP membrane of 0.22 microns. Moreover, image (c) shows that the scales even penetrated into the membrane pores. Furthermore, image (d) shows a different kind of deposits as well as some colloidal particles. In image (e) and (f), the suspended substances that are spread on the deposits of the membrane appear to be pieces of the membrane itself which indicate membrane damage. Like PP membrane of 0.22 microns, the crystals shown in Figure 83 are clearly of calcium sulfate.

For the elemental analysis using SEM-EDS, five arbitrary locations (positions) on the PP (0.45 μm) membrane surface were analyzed (position (a) to (e)). The EDS spectrum of three positions is shown in the Appendix. Figure 84 shows two of the SEM-EDS images of PP membrane of 0.45 microns at 1,000 x (position (d)) and 5,000 x (position (c)) magnification.
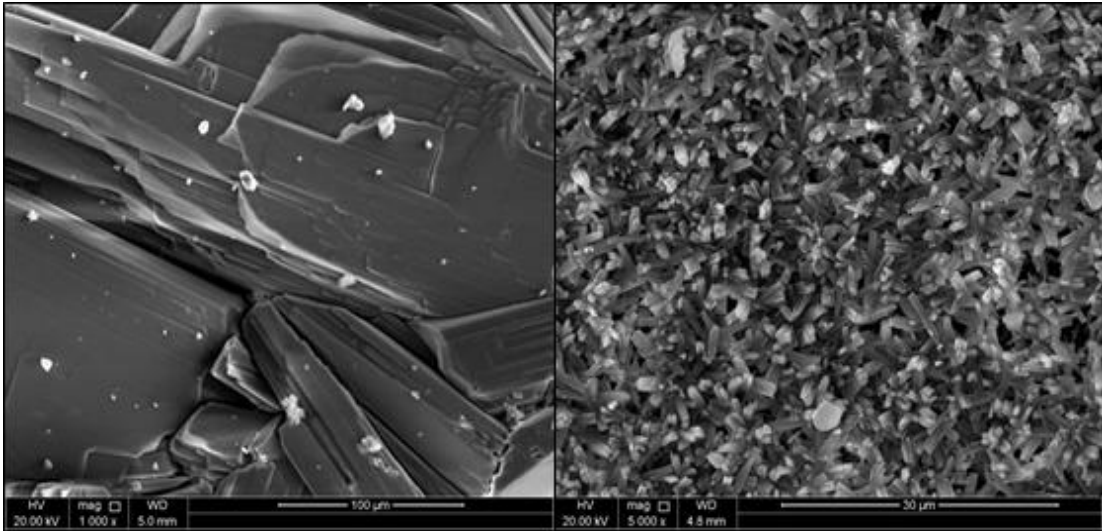
Figure 84: SEM-EDS Images of PP Membrane of 0.45 μm Membrane at 1,000 x

(left) and 5,000 x (right) Magnification

Table 61 illustrates the elements found on the membrane surface.

Table 61: The Foulants of PP (0.45 μm) Membrane Indicated by the EDS Spectra

Membrane	PP (0.45 μm)				
Feed	Seawater				
	Arbitrary Position on the Membrane				
Element	(a)	(b)	(c)	(d)	(e)
C	✓	✓	✓	✓	✓
O	✓	✓	✓	✓	✓
S	✓	✓		✓	
Ca	✓	✓	✓	✓	✓
Na	✓	✓	✓		✓
Cl		✓	✓		✓
Mg		✓	✓		✓

Table 61 shows that there were several foulants of PP (0.45 μm) membrane including

C, O, S, Ca, Na, Cl and Mg. In contrast to PP membrane of 0.22 microns, F was not

detected by the EDS spectra; however, Mg was found on the membrane.

Nevertheless, in all of the tested membrane positions, C, O, and Ca were found which indicate that the major foulant/scalant found using PP membrane of 0.45 microns under the conditions of the study was $CaCO_3$. Also, the EDS spectra of the membrane indicated the presence of $CaSO_4$.

Moreover, the SEM analysis confirmed that the salt layer formed on the membrane surface was not uniform and that the thickness of the deposits layer varied significantly. Figure 85 shows SEM images of the cross section of different locations of PP membrane of 0.45 μm membrane.
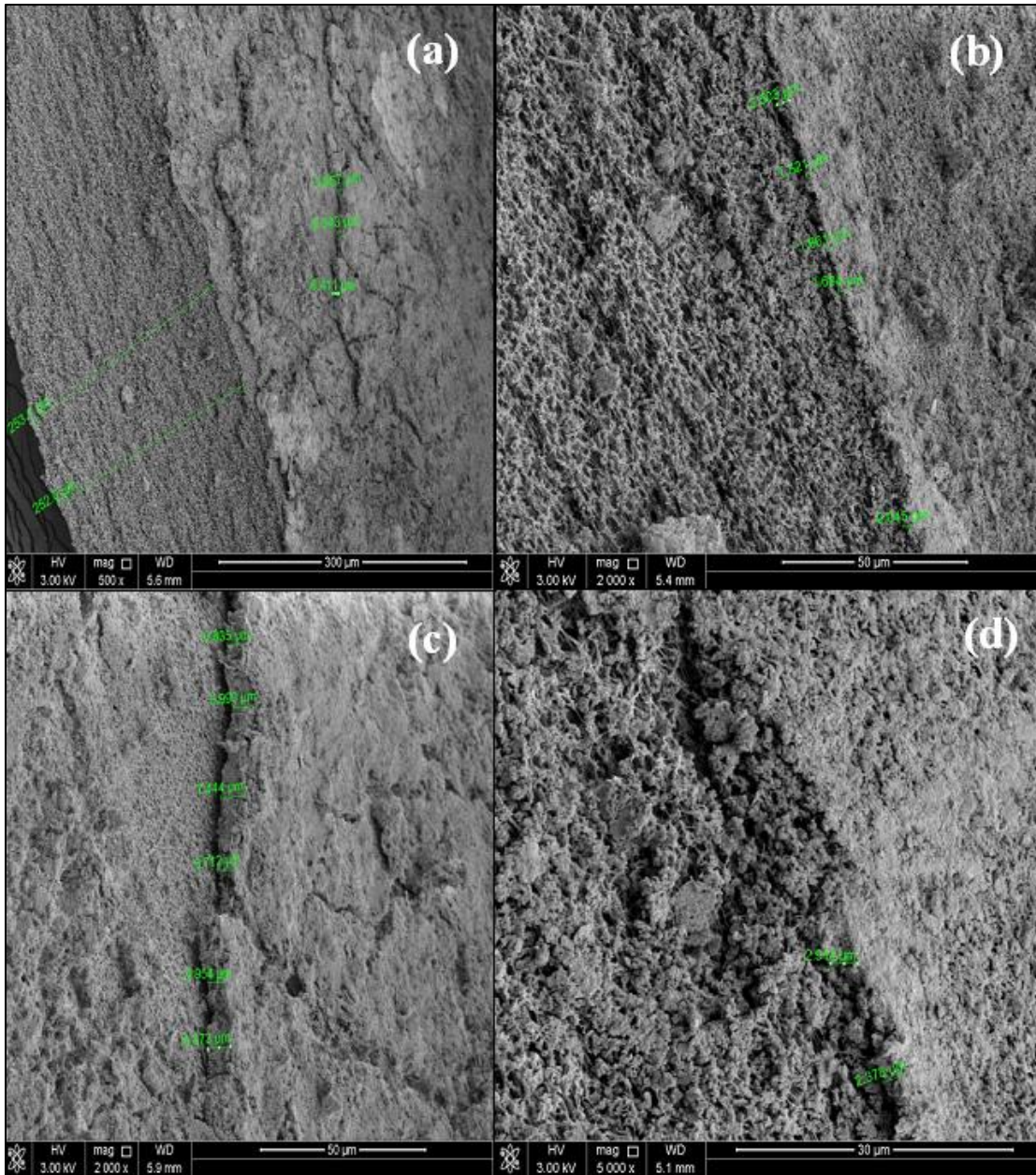
Figure 85: SEM Images of the Cross Section of Different Parts of PP Membrane

(0.45 μm) Membrane at (a) 500 x, (b) 2,000 x, (c) 2,000 x, and (d) 5,000 x

Magnification

Figure 85 shows that the measured thickness of the deposited salt layer on PP of 0.45 μm membrane ranged from 1.521 μm to 9.343 μm.

The same procedure was also followed for investigating fouling of PTFE (0.22 μm) membrane. Figure 86 shows SEM images of the fouled PTFE membrane at different locations of the membrane's surface.
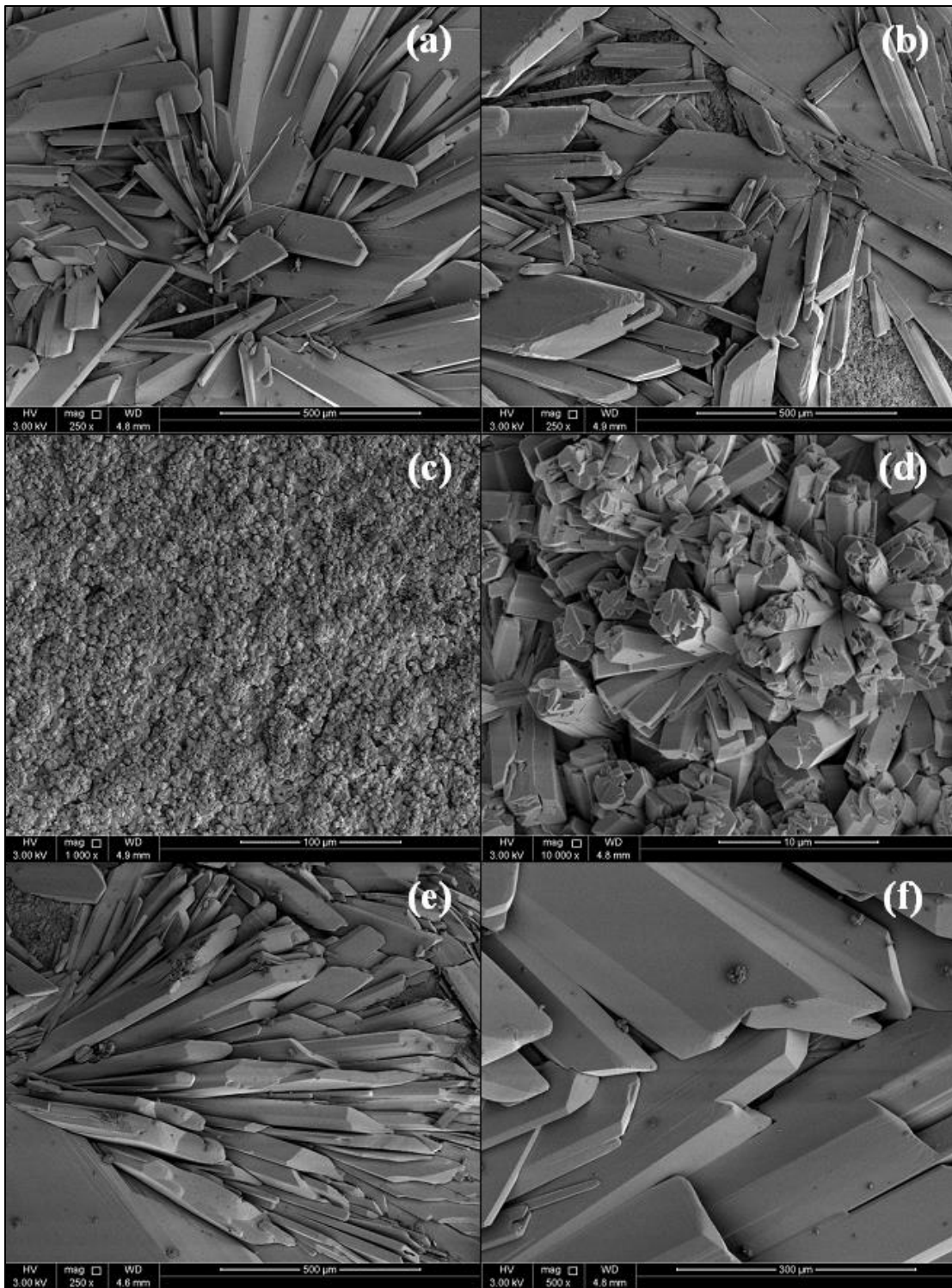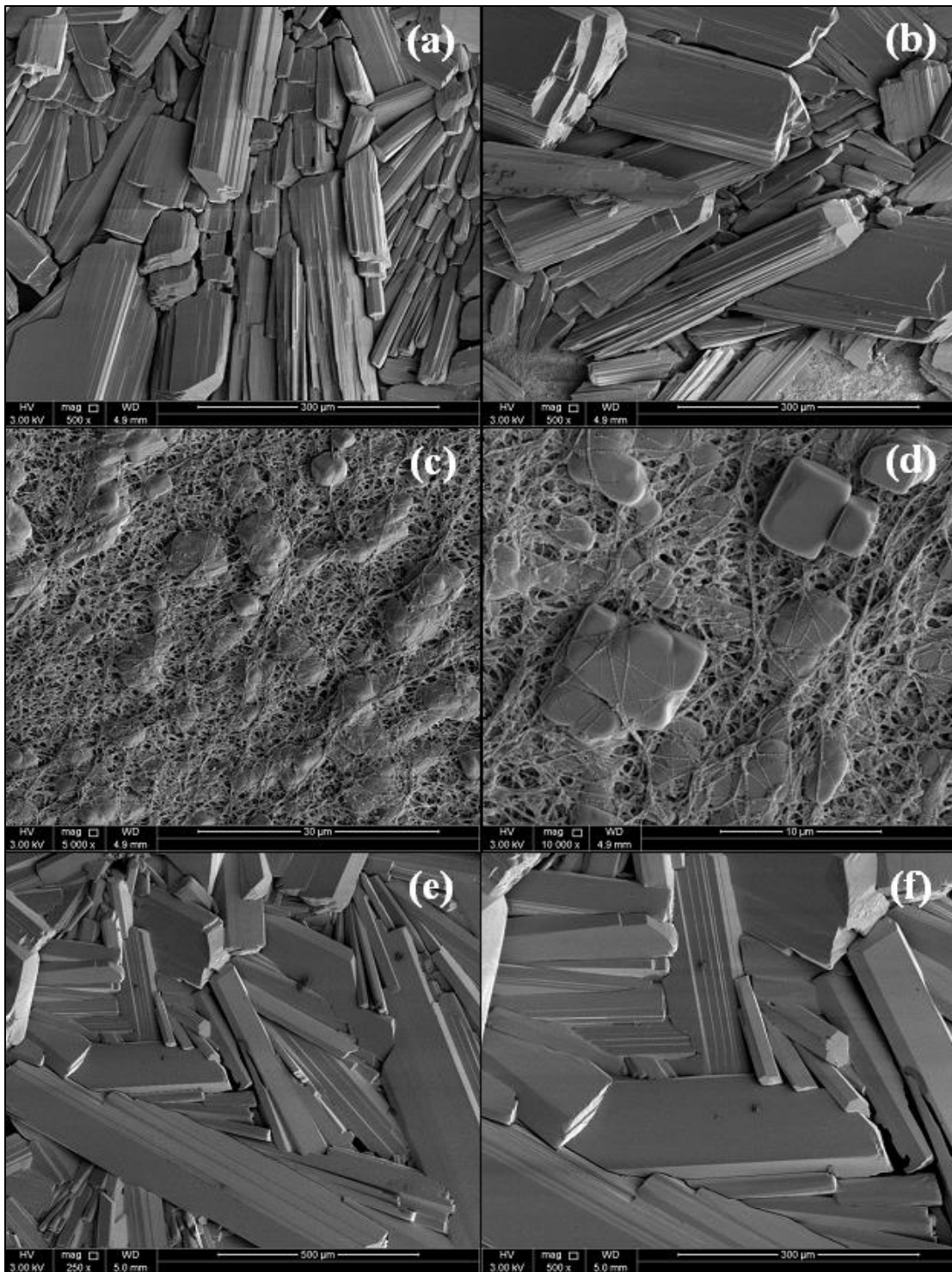
Figure 86: SEM Images of the Fouled PTFE (0.22 μm) Membrane at Different

Locations of the Membrane's Surface

The SEM analysis revealed that PTFE membrane of 0.45 μm underwent severe fouling after being utilized in the bench-scale DCMD unit for several days. Figure 86 shows that the fouling formed on the membrane surface was random (image (a) and (b)) and the deposits were "wreckage-like". Moreover, image (c) and (d) clearly show that the scales even penetrated into the membrane pores. Also, besides the crystal structure in Figure 86 that indicates the presence of calcium sulfate, image (d) clearly shows calcium carbonate crystals. Furthermore, image (e) and (f) show some colloidal particles that might be from the feed, or pieces from the deposits, or even pieces from the membrane itself.

For the elemental analysis using SEM-EDS, three arbitrary locations (positions) on the PTFE (0.22 μm) membrane surface were analyzed (position (a) to (c)). The EDS spectrum of two positions is shown in the Appendix. Figure 87 shows two of the SEM-EDS images of PTFE membrane of 0.22 microns at 100 x (position (c)) and 500 x (position (b)) magnification showing calcium sulfate and calcium carbonate crystals, respectively.
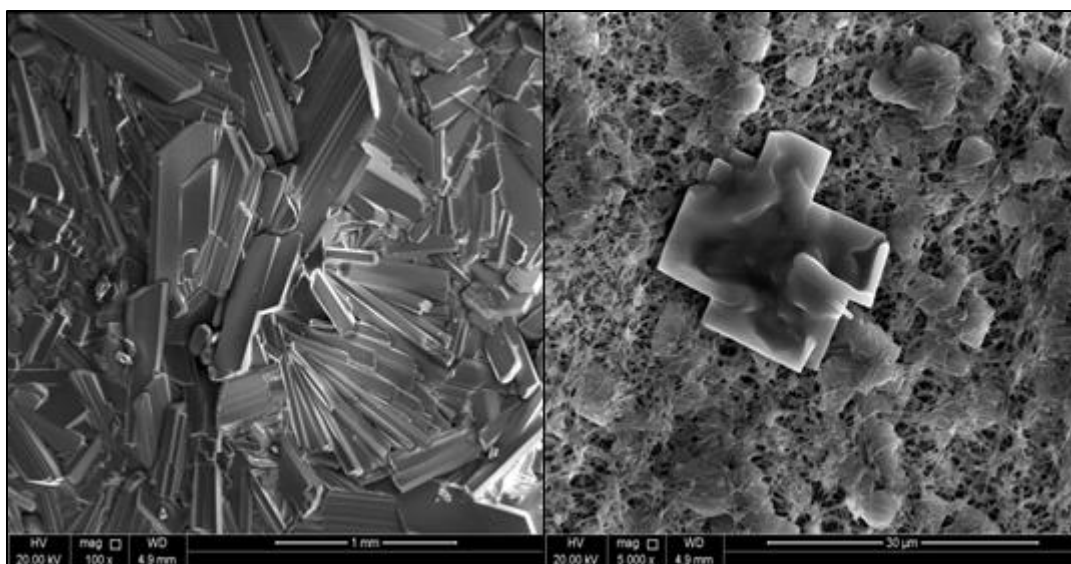
Figure 87: SEM-EDS Images of PTFE of 0.22 μm Membrane Showing Calcium

Sulfate Crystals (left) and Calcium Carbonate Crystals (right)

Table 62 illustrates the elements found on the membrane surface.

Table 62: The Foulants of PTFE (0.22 μm) Membrane Indicated by the EDS Spectra

Membrane	PTFE (0.22 μm)		
Feed	Seawater		
	Arbitrary Position on the Membrane		
Element	(a)	(b)	(c)
C	✓	✓	✓
O	✓	✓	✓
S	✓		✓
Ca	✓		✓
Na		✓	
Cl		✓	
Mg		✓	
K		✓	

Table 62 shows that there were several foulants of PTFE (0.22 μm) membrane including C, O, S, Ca, Na, Cl, Mg and K. In contrast to PP membrane, K was found on the membrane which might be attributed to the different structure of PTFE. As PP membrane, the EDS spectra of the PTFE membrane indicated the presence of $CaCO_3$ and $CaSO_4$.

The results of the study are consistent with those reported in literature. As the solubility of both $CaCO_3$ and $CaSO_4$ is inversely proportional to temperature (He et al., 2009), with the high feed inlet temperature of the study, deposits of these scalants on the surface of the membranes used were expected.

Karakulski et al., (2002) and Gryta (2006) have reported permeate flux decline due to MD membrane pore blocking and membrane wetting by $CaCO_3$.

He et al., (2009) stated that a high feed temperature increases the rate of $CaCO_3$ precipitation.

He et al. (2008) have showed that operating an MD process at a high feed temperature will result in the highest scaling potential.

Gryta (2009) has investigated the crystal formation of $CaSO_4$ on MD membrane surface. It was reported that MD permeate flux decline and membrane wetting are results of the deposited layer on the surface of the membrane. Scales have also penetrated into the membrane pores leading to membrane damage.

Gryta et al., (2006), Gryta (2008), and He et al. (2008) have encountered severe fouling as a result of protein and $CaCO_3$ deposition which increased with increasing feed temperature.

Gryta (2008) has shown that sclaes were not only found on the surface of the MD membrane, but have also penetrated inside the pores of the membrane which, according to the study, could lead to membrane damage.

Gryta (2007) has shown that the large pores on the surface of the membrane allowed $CaCO_3$ crystallites to be deposited into their interior and that the scaling potential was less with smaller membrane pore sizes; however, the flux perfrmance was also influenced.

Gryta (2015) has encountered a decline in the permeate flux which was attributed to crystalline deposits of several elements that formed on the surface of the membrane; however, the deposits were mainly of $CaCO_3$.

Tun et al. (2005) have encountered a severe deline in flux which was attributed to the deposition of crystallites on the membrane and the loss of membrane permeability. At first, the decline was gradual; however, when the feed solution became supersaturated, a sharp decline in the permeate flux was observed. Scales were found to fully cover the surface of the membrane.

In addition, for PP membrane of 0.45 μm and the NaCl solution, the same procedure was also followed to characterize membrane fouling. Figure 88 shows SEM images of the fouled PP (0.45 μm) membrane at different locations of the membrane's surface.
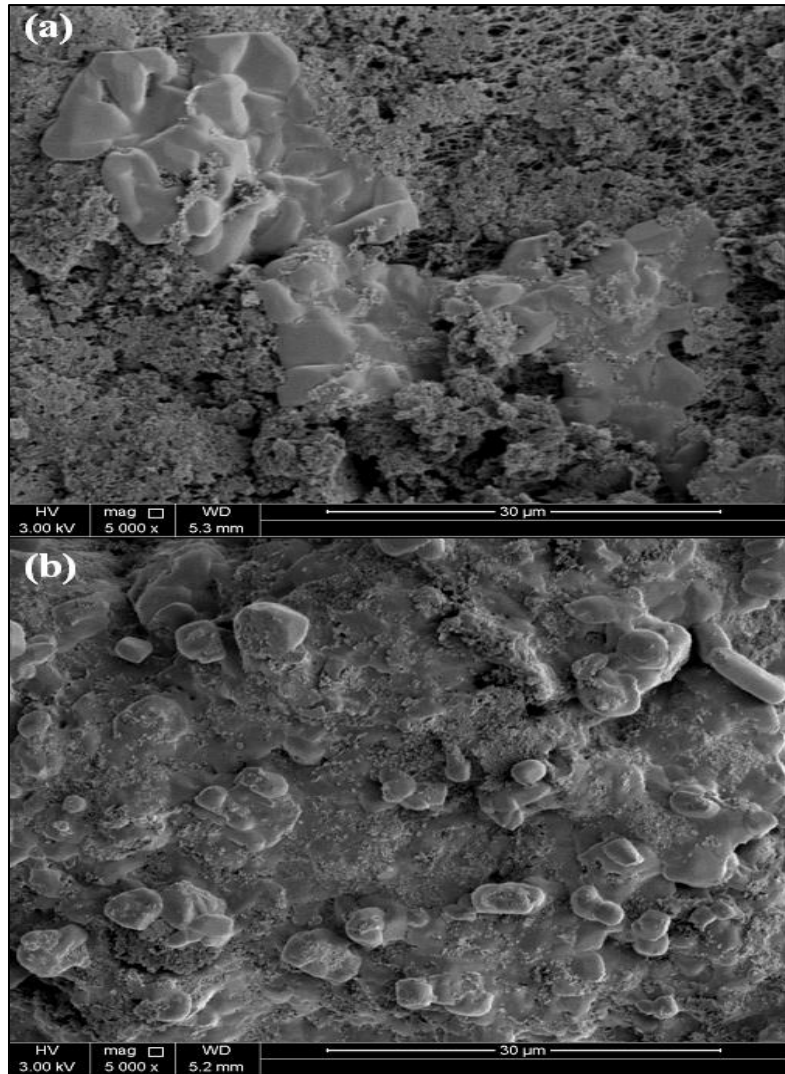
Figure 88: SEM Images of the Fouled PP (0.45 μm) Membrane (Using the NaCl Solution) at Different Locations of the Membrane's Surface

The SEM analysis revealed that PP membrane of 0.45 μm underwent severe fouling after being utilized in the bench-scale DCMD unit for several days using the synthetic brine solution. Figure 88 shows that the fouling formed on the PP (0.45 μm) membrane was like a viscous liquid (image (a)) and that the scales formed on the membrane have even penetrated into the membrane pores. In addition, it seems that the membrane was probably damaged and that pieces of it appear to be trapped or mixed with the deposits formed (image (b)). Also, image (b) shows "round-like" and "rod-like" deposits formed on the membrane besides the dispersed "thick fluid".

For the elemental analysis using SEM-EDS, several positions of PP (0.45 μm) membrane were analyzed (position (a) to (k)). The EDS spectrum of two positions is shown in the Appendix. Figure 89 shows two of the SEM-EDS images of PP membrane of 0.45 microns at 10,000 x and 5,000 x magnification.
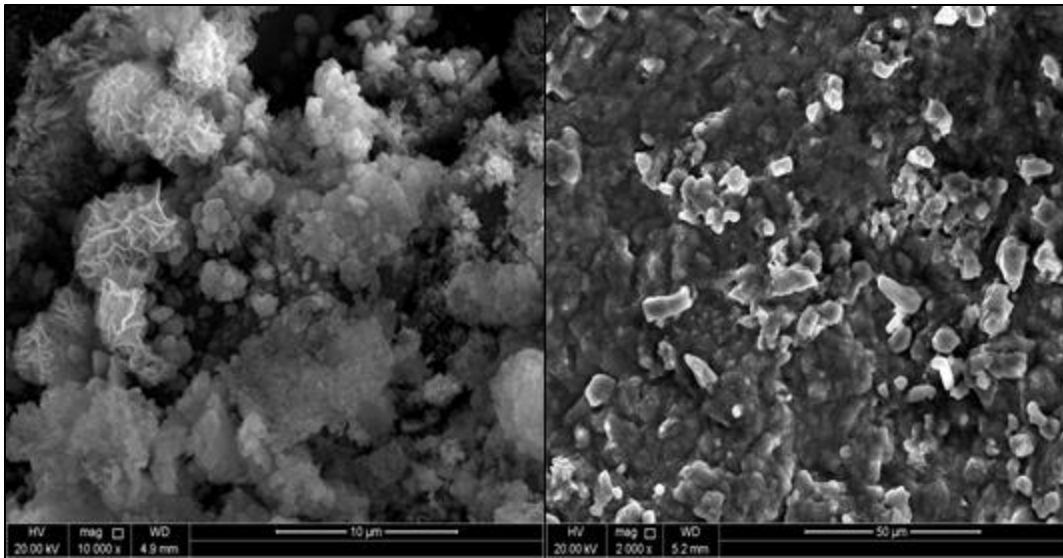
Figure 89: SEM-EDS Images of PP of 0.45 µm Membrane Using the Synthetic Brine

Solution at 10,000 x (left) and 5,000 x (right) Magnification

Table 63 illustrates the elements found on the membrane surface.

Table 63: The Foulants of PP (0.45 µm) Membrane Indicated by the EDS Spectra

(Using the Synthetic Brine Solution)

Membrane	PP (0.45 µm)										
Feed	NaCl Solution										
	Arbitrary Position on the Membrane										
Element	(a)	(b)	(c)	(d)	(e)	(f)	(g)	(h)	(i)	(j)	(k)
C	✓	✓	✓	✓	✓	✓	✓	✓	✓	✓	✓
O	✓	✓	✓	✓	✓	✓	✓	✓	✓	✓	✓
Na	✓	✓	✓	✓	✓	✓	✓	✓	✓	✓	✓
Mg			✓		✓	✓	✓	✓			
Si	✓	✓	✓	✓	✓	✓	✓	✓	✓	✓	✓
Cl	✓	✓	✓	✓	✓	✓	✓	✓	✓	✓	✓
Ca			✓		✓						
Fe								✓	✓		

Table 63 shows that there were several foulants of PP (0.45 μm) membrane when the synthetic brine was used as feed. The major foulants were Na and Cl as well as C and O that may have come from the previous seawater tests. In addition, Si and Fe were detected by the EDS which might be from the system piping and the flow meter's metal, respectively. Traces of Mg and Ca were also found which might be from the solution itself or from previous seawater tests as well. Therefore, flux decline in MD process is a result of not only the presence of $CaCO_3$ and $CaSO_4$ on the membrane but also NaCl as a foulant.

Several studies have reported permeate flux decline in MD processes due to the deposition of NaCl salt crystals (Drioli & Wu, 1985; Yun et al., 2006; Guillen-Burrieza et al., 2013). In addition, Gryta et al. (2001) have studied the concentration of NaCl solution containing natural organic matter (NOM) using an MD process. Their results showed that besides protein, NaCl was the main contributor to the fouling of the membrane used.

Chapter 6: Conclusion and Recommendations

This thesis presented desalination experiments of saline water (seawater from the Arabian Gulf and synthetic NaCl solution) using fully automated bench-scale Direct Contact Membrane Distillation (DCMD) unit. This was done using different hydrophobic flat-sheet membranes including PP membrane with pore size of 0.22 μm and 0.45 μm and PTFE membrane with pore size of 0.22 μm to investigate membrane fouling.

After analyzing the flux performance of the membranes used in this study using the two saline solutions, the following conclusions were made:

- The permeate flux increases with increasing membrane pore size, which is related to the improved mass transport. However, as time passes, the larger pore size membrane is more prone to flux decline due to membrane fouling.

- Since there is a linear relationship between the heat loss through thermal conduction and the temperature difference across the membrane, the proportion of energy used for evaporation will increase linearly with feed temperature. However, high feed temperature results in increased temperature polarization which let the membrane become more susceptible to fouling.

- The feed concentration has a minor effect on the permeate flux; however, only initially (for the first few hours of MD operation).

- In terms of membrane material, PTFE membrane generated a lower flux than PP membrane which might be attributed to the different structure of the membranes and the effect of membrane support layer of PTFE which acted as added resistance. However, PP and PTFE membranes were observed to behave somewhat differently regarding flux decline due to membrane fouling. PP membrane showed a more rapid flux decline than PTFE membrane.

- In terms of the effect of feed concentration, a membrane is more susceptible to fouling if a high salinity feed solution is used. In general, when the feed solution contains a high concentration of salts, an extra boundary layer forms on the surface of the membrane next to the temperature boundary layer. Together with the temperature boundary layer, this layer reduces the driving force for water evaporation.

- The percentage of drop in the average flux was more than 60%, 97%, and 94% for PP (0.22 μm) membrane, PP (0.45 μm) membrane, and PTFE (0.22 μm) membrane, respectively, after almost 19 h, 30 h, and 25 h of MD operation, respectively.

- The cake formation on the membrane is a result of the elevated feed temperature that results in the formation of temperature polarization.

- The initial permeate flux decreases when comparing a run to its subsequent run due to membrane fouling. When starting a new run, the data acquisition doesn't start till the desired hot water temperature is reached. During this time, however, the circulated water washes off part of the loose cake layer that was

formed on the surface of the membrane, hence, the lower initial flux for each subsequent run.

- The salt layer formed on the membrane surface due to crystallization fouling is not uniform. For PP membrane, it was concentrated in one part of the active layer of the membrane (the hot feed inlet) more than the other which might be due to the temperature polarization effect at the feed inlet. As the water vapor is lost by transport from the hot side, the feed temperature drops slightly towards the outlet and this may well contribute to the non-uniform scale deposition on the membrane surface.

After testing the quality of the distillates produced utilizing the membranes used in this study and using the two saline solutions, the following conclusions were made:

- Initially, the MD process is capable of producing highly pure water with almost 100% salt rejection; however, with MD operation time, the salt rejection capability of the membrane (and thus the quality of the distillate) decreases due to membrane fouling and wetting.

- Electrical conductivity as low as 2.33 µS/cm was obtained indicating the high purity of the distillate produced using MD. However, electrical conductivity as high as 15,390.00 µS/cm was later obtained indicating the vulnerability of the MD membrane to wetting.

- Permeate flux decline indicates scaling or pore clogging but does not necessarily mean pore wetting if the water quality is maintained or has not

changed much. Therefore, if there is fouling or flux decline, wetting doesn't necessary occur.

- A bigger pore membrane is more prone to membrane wetting compared to a smaller pore MD membrane of the same material.

- The quality of the distillate was lower when the higher salinity 100,000 ppm NaCl solution was used as feed to the MD system when compared to the results when seawater was used as feed and using the same membrane, which is probably due to pore wetting at a faster rate as a result of the increased feed salinity.

After performing the contact angle measurements of the new and the used membranes, the following conclusions were made:

- The results showed that the membranes used in this study have contact angles of greater than 90° which means that they were highly hydrophobic. The hydrophobicity of the membranes allows only vapor to be passed through and rejects water; hence, ensuring high selectivity of the MD process.

- The highest contact angle measured was for PTFE membrane of 0.22 microns (136.7°) followed by PP membrane of 0.22 microns (134.8°) and then PP membrane of 0.45 microns (133.2°).

- The hydrophobicity of a membrane is crucial in MD processes; however, the results of this study showed that it is not strongly linked to flux as PTFE had the highest contact angle, however, it didn't show the highest flux performance. This might be attributed to other physical features of the

membranes such as the overall thickness of the membrane, its structure geometry, and its porosity.

- The results of the contact angle measurements of the fouled membranes conclusively confirmed a transformation of the membranes' surface from being hydrophobic prior to performing the experiments to very hydrophilic utilizing any of the two feed solutions used.

- The results showed that PP membrane with pore size of 0.45 microns (the least hydrophobic membrane) was the first membrane to be fouled (the first membrane to experience severe flux declines) and the first to experience membrane pore wetting as was indicated by the water quality results, which might be attributed to its larger pore size.

After performing the SEM imaging and the EDS analysis of the membranes used in this study using the two saline solutions, the following conclusions were made:

- The deposited layer on the membranes' surface caused both permeate flux decline and membrane wetting as confirmed by the flux performance analysis and water quality tests.

- The SEM analysis revealed that all of the membranes used underwent severe fouling. The deposits on the membranes exhibited different shapes indicating different types of foulants.

- Scaling and colloidal fouling were observed after operating the bench-scale DCMD unit, which resulted in permeate flux decline.

- All fouling mechanisms were encountered including pore entrance blocking, formation of a salt layer on the membrane surface, and foulants that penetrated inside the pores of the membranes.

- Temperature polarization not only hindered the heat and mass transfer but also has intensified the rate of salt deposition on the membrane surface.

- Several elements were found to be present on the membranes using the SEM-EDS analysis including C, O, S, Ca, Na, Mg, and Cl. However, the results showed that the main scalants that were responsible for the membranes' wetting were $CaCO_3$, $CaSO_4$, and NaCl.

- Scaling is dependent on the feed water composition and concentration.

The results of this study showed that membrane fouling is a challenge facing the deployment of MD in large commercial scale desalination of seawater. Therefore, membrane fouling needs to be more investigated in MD process to be practically implemented and considered as competitive to the conventional desalination technologies. An optimum temperature and flow rate should be explored; however, the results of the study urge the need for developing new membranes and improved membrane modules and MD configurations as well as finding optimum procedures for membrane cleaning.

At the end of this study, several recommendations are proposed to improve the performance of MD and to reduce the fouling propensity:

1- To enhance the mass transfer, the operating conditions such as the temperature, the flow rate, and the concentration of the feed and the permeate streams should be optimized taking into account a reasonable permeate flux.

2- Pretreatment of the feed solution is essential especially if direct intake of seawater is considered. Seawater needs pH adjustments and addition of antiscalants to reduce or delay membrane fouling and prevent flux decline.

3- Although a higher feed temperature leads to generating a higher permeate flux, operating an MD process at high temperature will result in higher temperature polarization; thus, a compromise between a high flux and reduced membrane fouling should be made.

4- Due to the high scaling potential of the current commercial membranes available for MD processes, there is a need for improved membranes with increased lifetime in order to have a smoother operation of the process and to reduce the costs of replacing the damaged membrane such as investigating the use of superhydrophobic membranes in long term MD operations.

5- Considering concentration and temperature polarization effects and fouling inside the membrane pores in modeling MD processes will give a better insight into MD membrane fouling to optimize the process.

6- There is a need for a better understanding of MD membrane fouling under various operating conditions and membrane modules. This understanding may allow a better control of MD performance by means of better mitigation of fouling.

7- For laboratory investigations, using insulating materials on the process's tubing is recommended to reduce the heat losses along the path of the feed stream.

8- For industrial implementation, long term experiments using seawater as well as reject brines are recommended. A better understanding of the wetting phenomenon is required for MD to be commercially feasible.

9- Besides crystallization and colloidal fouling, biological fouling should be more studied especially if sweater is used as feed to the MD process.

10- To better investigate membrane fouling, different configurations of MD have to be studied to find the optimum design to be employed for real desalination processes.

11- Utilizing the available low grade or waste heat from industry or using solar energy to heat the feed solution to an MD process is recommended in order to reduce the reliance on expensive and ecologically destructive sources of energy.

12- Although MD might not be the perfect option for large scale desalination, it can be used to serve small communities with limited fresh water sources.

References

Abdel-Jawad, M. (2011). Energy Consumption and Performance for Various Desalination Processes. Lebanon: ESCWA.

Adham, S., Hussain, A., Matar, J. M., Dores, R., & Janson, A. (2013). Application of Membrane Distillation for desalting brines from thermal desalination plants. *Desalination*, *314*, 101–108.

Al-Obaidani, S., Curcio, E., Macedonio, F., Di Profio, G., Ai-Hinai, H., & Drioli, E. (2008). Potential of membrane distillation in seawater desalination: Thermal efficiency, sensitivity study and cost estimation. *Journal of Membrane Science*, *323*, 85–98.

Al-Subaie, K. Z. (2007). Precise way to select a desalination technology. *Desalination*, *206*, 29–35.

Albert, R. A., & Silbey, R. J. (1997). *Physical Chemistry*. 2nd ed. New York: Wiley.

Alkhudhiri, A., Darwish, N., & Hilal, N. (2012). Membrane distillation: A comprehensive review. *Desalination*, *287*, 2–18.

Alkhudhiri, A., Darwish, N., & Hilal, N. (2013). Treatment of Saline Solutions using Air Gap Membrane Distillation: Experimental study. *Desalination*, *323*, 2–7.

Alklaibi, A. M., & Lior, N. (2004). Membrane-distillation desalination: Status and potential. *Desalination*, *171*, 111–131.

Almalki, A. (2008). *Business Opportunities in Water Industry in Qatar*. Singapore International Water Week. KAHRAMAA.

Amtaorg. (2007). *Water Desalination Processes*. American Membrane Technology Association.

Andersson, S.-I., Kjellander, N., & Rodesjö, B. (1985). Design and field tests of a new membrane distillation desalination process. *Desalination*, *56*, 345-354.

Bachmann, J., Ellies, A., & Hartge, K. H. (2000). Development and application of a new sessile drop contact angle method to assess soil water repellency. *Journal of Hydrology*, *231–232*, 66–75.

Bahmanyar, A., Asghari, M., & Khoobi, N. (2012). Numerical simulation and theoretical study on simultaneously effects of operating parameters in direct contact membrane distillation. *Chemical Engineering and Processing: Process Intensification*, *61*, 42–50.

Baker, R. W. (2012). *Membrane Technology and Applications*. New York: John Wiley & Sons.

Banat, F. A. (1994). *Membrane distillation for desalination and removal of volatile organic compounds from water*. Ph.D. thesis. McGill University, Canada.

Banat, F. A., & Simandl, J. (1994). Theoretical and experimental study in membrane distillation. *Desalination*, *95*, 39–52.

Banat, F. A., Abu Al-Rub, F., Jumah, R., & Shannag, M. (1999). On the effect of inert gases in breaking the formic acid-water azeotrope by gas-gap membrane distillation. *Chemical Engineering Journal*, *73*, 37–42.

Bandini, S., Gostoli, C., & Sarti, G. C. (1991). Role of heat and mass transfer in membrane distillation process. *Desalination*, *81*, 91–106.

Bandini, S., Gostoli, C., & Sarti, G. C. (1992). Separation efficiency in vacuum membrane distillation. *Journal of Membrane Science*, *73*, 217–229.

Bandini, S., Saavedra, A., & Sarti, G. C. (1997). Vacuum membrane distillation: experiments and modeling, *AIChE Journal*, *43*, 398–408.

Barlow, M. & Clark, T. (2002). *Blue Gold: The Fight to Stop the Corporate Theft of the World's Water*. New York: New Press.

Basini, L., D'Angelo, G., Gobbi, M., Sarti, G. C., & Gostoli, C. (1987). A desalination process through sweeping gas membrane distillation. *Desalination*, *64*, 245–257.

Bindra, S. P., & Abosh, W. (2001). Recent developments in water desalination. *Desalination*, *136*, 49–56.

Bodell, B. R. (1963). *Silicone Rubber Vapor Diffusion in Saline Water Distillation*. US Pat. 285032, USA.

Bonyadi, S., & Chung, T. S. (2007). Flux enhancement in membrane distillation by fabrication of dual layer hydrophilic-hydrophobic hollow fiber membranes. *Journal of Membrane Science*, *306*, 134–146.

Bonyadi, S., & Chung, T.-S. (2009). Highly porous and macrovoid-free PVDF hollow fiber membranes for membrane distillation by a solvent-dope solution co-extrusion approach. *Journal of Membrane Science*, *331*(1-2), 66–74.

Bonyadi, S., Chung, T. S., Rajagopalan, R. (2009). A novel approach to fabricate macrovoid-free and highly permeable PVDF hollow fiber membranes for membrane distillation. *AIChE Journal*, *55*, 828–833.

Bott, T. R. & Walker, R. A. (1971). Fouling in heat transfer equipment. *Chemical Engineering*, *251*, 391–395.

Bourne, G. (2008). *California Desalination Planning Handbook*. Sacramento: Center for Collaborative Policy (CCP), California State University.

Bui, V. A., Nguyen, M. H., & Muller, J. (2007). *The Energy Challenge of Direct Contact Membrane Distillation in Low Temperature Concentration*. Asia-Pacific Journal of Chemical Engineering, 2.5, 400–406.

Busch, M., & Mickols, W. E. (2004). Reducing energy consumption in seawater desalination. *Desalination*, *165*, 299–312.

Bushnak, A. A. (1989). *Proceedings of the Fourth World Congress on Desalination and Water Reuse*: Kuwait, November 4-8, 1989. Amsterdam: Elsevier.

Calabro, V., Drioli, E., & Matera, F., (1991). Membrane distillation in the textile wastes water treatment. *Desalination*, *83*, 209–224.

Calabro, V., Jiao, B. L., & Drioli, E. (1994). Theoretical and Experimental Study on Membrane Distillation in the Concentration of Orange Juice. *Industrial & Engineering Chemistry Research*, *33*, 1803–1808.

Camacho, L. M., Dumée, L., Zhang, J., Li, J-d., Duke, M., Gomez, J. & Gray, S. (2013). Advances in Membrane Distillation for Water Desalination and Purification Applications. *Water*, *5*, 94–196.

Cath, T. Y., Adams, V. D., & Childress, A. E. (2004). Experimental study of desalination using direct contact membrane distillation: A new approach to flux enhancement. *Journal of Membrane Science*, *228*, 5–16.

Chaudhry, S. (2012). *New and Emerging Desalination Technologies*. Energy - Water Nexus: Status and Prospectus IAPWS/ASME Symposium 3 October 2012 Boulder, Colorado. Boulder: California Energy Commission.

Cheng, D. Y., (1981). Method and apparatus for distillation. US Pat. 4, 265,713, USA.

Cheng, D. Y., & Wiersma, S. J., (1982). Composite membranes for a membrane distillation system. US Pat. 4, 316,772, USA.

Cheng, D. Y., & Wiersma, S. J., (1983). Apparatus and method for thermal membrane distillation. US Pat. 4,419,187. USA.

Chen, G., Yang, X., Wang, R., & Fane, A. G. (2013). Performance enhancement and scaling control with gas bubbling in direct contact membrane distillation. *Desalination*, *308*, 47–55.

Chen, J. P., Mou, H., Wang, L. K., Matsuura, T., & Wei, Y. (2011). Membrane Separation: Basics and Applications. *Membrane and Desalination Technologies Handbook of Environmental Engineering Vol. 13*. Lawrence K. Wang, et al. (Eds). New York: Humana Press. 271–332.

Chernyshov, M. N., Meindersma, G. W., & de Haan, A. B. (2003). Modelling temperature and salt concentration distribution in membrane distillation feed channel. *Desalination*, *157*, 315–324.

Chernyshov, M. N., Meindersma, G. W., & de Haan, A. B. (2005). Comparison of spacers for temperature polarization reduction in air gap membrane distillation. *Desalination*, *183*, 363–374.

Chouikh, R., Bouguecha, S., & Dhahbi, M. (2005). Modelling of a modified air gap distillation membrane for the desalination of seawater. *Desalination*, *181*, 257–265.

Cipollina, A., Micale, G., & Rizzuti, L. (2009). Conventional Thermal Process. *Seawater desalination: conventional and renewable energy processes*. Heidelberg: Springer. 17–37.

Coleparmer. (2014). *FH100 and FH100X General-Purpose Peristaltic Pumps*. [online] Available at: <http://www.coleparmer.com/Category/Peristaltic_Pumps/17410?referred_id =21140 > [Accessed 17 May. 2014].

Cooley, H. & Heberger, M. (2013). *Key Issues for Seawater Desalination in California: Energy and Greenhouse Gas Emissions*. Oakland: Pacific Institute. 1–44.

Criscuoli, A., Bafaro, P., & Drioli, E. (2013). Vacuum membrane distillation for purifying waters containing arsenic. *Desalination*, *323*, 17–21.

Criscuoli, A., Carnevale, M. C., & Drioli, E. (2008). Evaluation of energy requirements in membrane distillation. *Chemical Engineering and Processing: Process Intensification*, *47*, 1098–1105.

Criscuoli, A., Zhong, J., Figoli, A., Carnevale, M. C., Huang, R., & Drioli, E. (2008). Treatment of dye solutions by vacuum membrane distillation. *Water Research*, *42*, 5031–5037.

Cuenca, C. J. (2012). *Report on Water Desalination Status in the Mediterranean Countries*. Murcia, Spain: Instintuto Murciano de Investigacion y Desarrollo Agrario y Alimentario.

Curcio, E., & Drioli, E. (2005). Membrane Distillation and Related Operations - A Review. *Separation & Purification Reviews*, *34*, 35–86.

Cussler, E. L. (1997). *Diffusion: Mass Transfer in Fluid System*. 2nd ed. New York: Cambridge University Press.

Davis, T. A. (2006). Zero Discharge Seawater Desalination: Integrating the Production of Freshwater, Salt, Magnesium, and Bromine. *USBR Desalination and Water Purification Research and Development Program Report No. 111*. Washington, D.C.: U.S. Bureau of Reclamation.

Dawoud, M. A., & Al Mulla, M. M. (2012). Environmental Impacts of Seawater Desalination: Arabian Gulf Case Study. *International Journal of Environment and Sustainability (IJES)*, *1*, 22–37.

De Zaarate, J. M. O., Velázquez, A., Peña, L, & Mengual, J. I. (1993). Influence of Temperature Polarization on Separation by Membrane Distillation. *Separation Science and Technology*, *28*, 1421–1436.

Delaney, R. A. M, & Donnelly, H. K. (1977). *Application of Reverse Osmosis in Dairy Industry*. Ottawa, Canada: NRC.

DesalData.com. (2012). *Global Water Intelligence,* Media Analytics Ltd., Oxford, UK.

Dickie, P. (2007). *Making Water - Desalination: Option or Distraction for a Thirsty World?*. WWF's Global Freshwater Programme.

Ding, Z., Ma, R., & Fane, A. (2003). A New Model for Mass Transfer In Direct Contact Membrane Distillation. *Desalination*, 151, 217-227.

Dolnicar, S., & Schafer, A. I. (2006). *Public perception of desalinated versus recycled water in Australia*. AWWA Desalination Symposium 7-9 May 2006 Honolulu, Hawaii.

Drioli, E., & Wu, Y. (1985). Membrane Distillation: An Experimental Study. *Desalination*, *53*, 339–346.

Drioli, E., Calabro, V. & Wu, Y. (1986). Microporous Membranes in Membrane Distillation. *Pure and Applied Chemistry*, *58*, 1657–1662.

Drioli, E., Wu, Y., & Calabro, V. (1987). Membrane distillataion in the treatment of aqueous solutions. *Journal of Membrane Science*, *33*, 277–284.

El-Bourawi, M. S., Ding, Z., Ma, R., & Khayet, M. (2006). A framework for better understanding membrane distillation separation process. *Journal of Membrane Science*, *285*, 4–29.

El-Dessouky, H. T., & Ettouney, H. M. (2002). *Fundamentals of Salt Water Desalination*. Amsterdam: Elsevier Science B.V.

El-Nashar, A. M. (2001). Cogeneration for power and desalination - state of the art review. *Desalination*, *134*, 7–28.

Elhakeem, A., & Elshorbagy, W. (2013). Evaluation of the long-term variability of seawater salinity and temperature in response to natural and anthropogenic stressors in the Arabian Gulf. *Marine Pollution Bulletin*, *76*, 355–359.

Elimelech, M., & Phillip, W. A. (2011). The Future of Seawater Desalination: Energy, Technology, and the Environment. *Science (New York)*, *333*, 712–717.

Escobar, I. C., & Van der Bruggen, B. (2011). *Modern Applications in Membrane Science and Technology*. Washington, DC: American Chemical Society.

Fane, A. G., Schofield, R. W., & Fell, C. J. D. (1987). The efficient use of energy in membrane distillation. *Desalination*, *64*, 231–243.

Fane, A. G., Wang, R. & Jia, Y. (2011). Membrane Technology: Past, Present and Future. *Membrane and Desalination Technologies Handbook of Environmental Engineering Vol. 13*. Lawrence K. Wang, et al. (Eds). New York: Humana Press. 1–46.

Fard, A., Manawi, Y., Rhadfi, T., Mahmoud, K., Khraisheh, M., & Benyahia, F. (2015). Synoptic analysis of direct contact membrane distillation performance in Qatar: A case study. *Desalination*, *360*, 97–107.

Feng, C., Khulbe, K. C., Matsuura, T., Gopal, R., Kaur, S., Ramakrishna, S., & Khayet, M. (2008). Production of drinking water from saline water by air-gap membrane distillation using polyvinylidene fluoride nanofiber membrane. *Journal of Membrane Science*, *311*, 1–6.

Fernández-Pineda, C., Izquierdo-Gil, M. A., & García-Payo, M. C. (2002). Gas permeation and direct contact membrane distillation experiments and their analysis using different models. *Journal of Membrane Science*, *198*, 33–49.

Fichtner and DLR. (2011). *MENA Regional Water Outlook, Part II, Desalination Using Renewable Energy*. The World Bank.

Findley, M. E. (1967). Vaporization through Porous Membranes. *Industrial & Engineering Chemistry Process Design and Development*, *6*, 226–230.

Findley, M. E., Tanna, V. V., Rao, Y. B., & Yeh, C. L. (1969). Mass and heat transfer relations in evaporation through porous membranes. *AIChE Journal*, *15*, 483–489.

Franken, A. C. M., Nolten, J. A. M., Mulder, M. H. V., Bargeman, D., & Smolders, C. A., (1987). Wetting criteria for the applicability of membrane distillation. *Journal of Membrane Science*, *33 (3)*, 315-328.

Fritzmann, C., Löwenberg, J., Wintgens, T., & Melin, T. (2007). State-of-the-art of reverse osmosis desalination. *Desalination*, *216*, 1–76.

Gagliardo, P., Adham, S., Trussell, R., & Olivieri, A. (1998). Water repurification via reverse osmosis. *Desalination*, *117*, 73–78.

García-Payo, M. C., Izquierdo-Gil, M. A., & Fernández-Pineda, C. (2000). Air gap membrane distillation of aqueous alcohol solutions. *Journal of Membrane Science*, *169*, 61–80.

García-Payo, M., Izquierdo-Gil, M., & Fernández-Pineda, C. (2000). Wetting Study of Hydrophobic Membranes via Liquid Entry Pressure Measurements with Aqueous Alcohol Solutions. *Journal of colloid and interface science*, *230*, 420–431.

García-Payo, M. C., Rivier, C. A., Marison, I. W., & Von Stockar, U. (2002). Separation of binary mixtures by thermostatic sweeping gas membrane distillation II. Experimental results with aqueous formic acid solutions. *Journal of Membrane Science*, *198*, 197–210.

Ge, J., Peng, Y., Li, Z., Chen, P., & Wang, S. (2014). Membrane fouling and wetting in a DCMD process for RO brine concentration. *Desalination*, *344*, 97–107.

Ghaffour, N., Missimer, T. M., & Amy, G. L. (2013). Technical review and evaluation of the economics of water desalination: Current and future challenges for better water supply sustainability. *Desalination*, *309*, 197–207.

Global Water Intelligence. (2011). *Global Water Market 2011 - Meeting The World's Water And Wastewater Needs Until 2016*. Media Analytics Ltd., Oxford, UK.

Gostoli, C., & Sarti, G. C., (1987). Thermally driven mass transport through porous membranes. In *Synthetic Polymeric Membranes*, Sedlacek, B., and Kahovec, J., (Eds.), Berlin, Walter de Gryter and Co., 515–529.

Gostoli, C., Sarti, G. C., & Matulli, S. (1987). Low Temperature Distillation through Hydrophobic Membranes. *Separation Science and Technology*, *22*, 855–872.

Gray, S., Semiat, R., Duke, M., Rahardianto, A., & Cohen, Y. (2011). Seawater Use and Desalination Technology. *Reference Module in Earth Systems and Environmental Sciences*, from *Treatise on Water Science*, *4*, 73–109.

Gryta, M. (2000). Concentration of saline wastewater from the production of heparine. *Desalination*, *129*, 35–44.

Gryta, M. (2002). The assessment of microorganism growth in the membrane distillation system. *Desalination*, *142*, 79–88.

Gryta, M. (2005). Long-term performance of membrane distillation process. *Journal of Membrane Science*, *265*, 153–159.

Gryta, M. (2007). Influence of polypropylene membrane surface porosity on the performance of membrane distillation process. *Journal of Membrane Science*, *287*, 67–78.

Gryta, M. (2008). Alkaline scaling in the membrane distillation process. *Desalination*, *228*, 128–134.

Gryta, M. (2008). Fouling in direct contact membrane distillation process. *Journal of Membrane Science*, *325*, 383–394.

Gryta, M. (2009). Calcium sulphate scaling in membrane distillation process. *Chemical Papers*, *63(2)*, 146–151.

Gryta, M. (2010). Desalination of thermally softened water by membrane distillation process. *Desalination*, *257*, 30–35.

Gryta, M. (2015). Water desalination using membrane distillation with acidic stabilization of scaling layer thickness. *Desalination*, *365*, 160–166.

Gryta, M., Grzechulska-Damszel, J., Markowska, A., & Karakulski, K. (2009). The influence of polypropylene degradation on the membrane wettability during membrane distillation. *Journal of Membrane Science*, *326*, 493–502.

Gryta, M., Tomaszewska, M., & Karakulski, K. (2006). Wastewater treatment by membrane distillation. *Desalination*, *198*, 67–73.

Gryta, M., Tomaszewska, M., & Morawski, A. W. (2000). A Capillary Module for Membrane Distillation Process. *Chemical Papers*, *54*, 370-374.

Gryta, M., Tomaszewska, M., Grzechulska, J., & Morawski, A. W. (2001). Membrane distillation of NaCl solution containing natural organic matter. *Journal of Membrane Science*, *181*, 279–287.

Guillen-Burrieza, E., Thomas, R., Mansoor, B., Johnson, D., Hilal, N., & Arafat, H. (2013). Effect of dry-out on the fouling of PVDF and PTFE membranes under conditions simulating intermittent seawater membrane distillation (SWMD). *Journal of Membrane Science*, *438*, 126–139.

Gullinkala, T., Digman, B., Gorey, C., Hausman, R., & Escobar, I. C. (2010). Chapter 4 Desalination: Reverse Osmosis and Membrane Distillation. *Sustainability Science and Engineering: Water Recycling versus Desalination*. Isabel C. Escobar and Andrea I. Scha¨fer. (eds). Amsterdam: Elsevier B.V. 65–93.

Hassan, A. M., Al-Sofi, M. A. K., Al-Amoudi, A. S., Jamaluddin, A. T. M., Farooque, A. M., Rowaili, A., Dalvi, A. G. I., Kither, N. M., Mustafa, G. M., & Al-Tisan, I. A. R. (1998). A new approach to membrane and thermal seawater desalination processes using nanofiltration membranes (Part 1). *Desalination*, *118*, 35–51.

He, F., Gilron, J., Lee, H., Song, L., & Sirkar, K. K. (2008). Potential for scaling by sparingly soluble salts in crossflow DCMD. *Journal of Membrane Science*, *311*, 68–80.

He, F., Sirkar, K. K., & Gilron, J. (2009). Studies on scaling of membranes in desalination by direct contact membrane distillation: $CaCO_3$ and mixed $CaCO_3/CaSO_4$ systems. *Chemical Engineering Science*, *64*, 1844–1859.

He, K., Hwang, H. J., Woo, M. W., & Moon, I. S. (2011). Production of drinking water from saline water by direct contact membrane distillation (DCMD). *Journal of Industrial and Engineering Chemistry*, *17*, 41–48.

Hilal, N., Al-Zoubi, H., Darwish, N. A., & Mohammad, A. W. (2005). Characterisation of nanofiltration membranes using atomic force microscopy. *Desalination*, *177*, 187–199.

Hosseini, S. M., Gholami, A., Madaeni, S. S., Moghadassi, A. R., & Hamidi, A. R. (2012). Fabrication of (polyvinyl chloride/cellulose acetate) Electrodialysis Heterogeneous Cation Exchange Membrane: Characterization and Performance in Desalination Process. *Desalination*, *306*, 51–59.

Hou, D., Dai, G., Wang, J., Fan, H., Luan, Z., & Fu, C. (2013). Boron removal and desalination from seawater by PVDF flat-sheet membrane through direct contact membrane distillation. *Desalination*, *326*, 115–124.

Hou, D., Wang, J., Zhao, C., Wang, B., Luan, Z., & Sun, X. (2010). Fluoride removal from brackish groundwater by direct contact membrane distillation. *Journal of Environmental Sciences*, *22*, 1860–1867.

Hsu, S. T., Cheng, K. T., & Chiou, J. S. (2002). Seawater Desalination by Direct Contact Membrane Distillation. *Desalination*, *143(3)*, 279–287.

Huang, J., Wang, Y. C., Li, C. L., Lee, K. R., Fan, S. C., Wu, T. T., & Lai, J. Y. (2002). Dehydration of water-alcohol mixtures by pervaporation and vapor permeation through surface resintering expanded poly(tetrafluoroethylene) membranes. *European Polymer Journal*, *38*, 179–186.

Huang, J., Zhang, J., Hao, X., & Guo, Y. (2004). Studu of a new novel process for preparing and co-stretching PTFE membrane and its propertie. *European Polymer Journal*, *40*, 667–671.

Hwang, H. J., He, K., Gray, S., Zhang, J., & Moon, I. S. (2011). Direct contact membrane distillation (DCMD): Experimental study on the commercial PTFE membrane and modeling. *Journal of Membrane Science*, *371*, 90–98.

Ibrahim, S. S., & Alsalhy, Q. F. (2013). Modeling and simulation for direct contact membrane distillation in hollow fiber modules. *AIChE Journal*, *59*, 589–603.

Julabo. (2014). *F32-MA*. [online] Available at: <http://www.julabo.com/en/products/refrigerated-circulators/refrigerated-heating-circulators/f32-ma-refrigerated-heating-circulator> [Accessed 17 May. 2014].

Jonsson, A.-S., Wimmerstedt, R., & Harrysson, A.-C. (1985). Membrane distillation - a theoretical study of evaporation through microporous membranes. *Desalination*, *56*, 237–249.

KAHRAMAA. (2009). *Regulations of Internal Water Installations and Connection Works*. Doha: Qatar General Electricity & Water Corporation "KAHRAMAA".

Kalogirou, S. A. (2005). Seawater desalination using renewable energy sources. *Progress in Energy and Combustion Science*, *31*, 242–281.

Karakulski, K., Gryta, M., & Morawski, A. (2002). Membrane processes used for potable water quality improvement. *Desalination*, *145*, 315–319.

Karavoltsos, S., Sakellari, A., Mihopoulos, N., Dassenakis, M., & Scoullos, M. J. (2008). Evaluation of the quality of drinking water in regions of Greece. *Desalination*, *224*, 317–329.

Kast, W., & Hohenthanner, C. R. (2000). Mass transfer within the gas-phase of porous media. *International Journal of Heat and Mass Transfer*, *43*, 807–823.

Kent, F. C., Citulski, J., & Farahbakhsh, K. (2011). Water reclamation using membranes: Permeate water quality comparison of MBR and tertiary membrane filtration. *Desalination*, *274*, 237–245.

Khayet, M., & Matsuura, T. (2001). Preparation and characterization of polyvinylidene fluoride membranes for membrane distillation. *Industrial & engineering chemistry Research*, *40* (24), 5710–5718.

Khayet, M., & Matsuura, T. (2003). Application of surface modifying macromolecules for the preparation of membranes for membrane distillation. *Desalination*, *158*, 51–56.

Khayet, M. & Matsuura, T. (2011). *Membrane Distillation: Principles and Applications.* New York: Elsevier.

Khayet, M., & Mengual, J. I. (2004). Effect of salt concentration during the treatment of humic acid solutions by membrane distillation. *Desalination*, *168*, 373–381.

Khayet, M., Cojocaru, C., & García-Payo, M. C. (2010). Experimental design and optimization of asymmetric flat-sheet membranes prepared for direct contact membrane distillation. *Journal of Membrane Science*, *351*, 234–245.

Khayet, M., Godino, P., & Mengual, J. I. (2000). Nature of flow on sweeping gas membrane distillation. *Journal of Membrane Science*, *170*, 243–255.

Khayet, M., Godino, P., & Mengual, J. I. (2000). Theory and experiments on sweeping gas membrane distillation. *Journal of Membrane Science*, *165*, 261–272.

Khayet, M., Khulbe, K. C., & Matsuura, T. (2004). Characterization of membrane distillation by atomic force microscopy and estimation of their water vapor transfer coefficients in vacuum membrane distillation process. *Journal of Membrane Science*, *238*, 199–211.

Khayet, M., Matsuura, T., Mengual, J. I., & Qtaishat, M. (2006). Design of novel direct contact membrane distillation membranes. *Desalination*, *192*, 105–111.

Khayet, M., Mengual, J. I., & Zakrzewska-Trznadel, G. (2006). Direct Contact Membrane Distillation For Nuclear Desalination, Part II: Experiments with Radioactive Solutions. *International Journal of Nuclear Desalination*, *2*, 56.

Khayet, M., Velázquez, A., & Mengual, J. I. (2004). Direct contact membrane distillation of humic acid solutions. *Journal of Membrane Science*, *240*, 123–128.

Khayet, M., Velazquez, A. & Mengual, J. I. (2004). Modelling Mass Transport through a Porous Partition: Effect of Pore Size Distribution. *Journal of Non-Equilibrium Thermodynamics*, 29, 279–299.

Khemakhem, S., & Amar, R. B. (2011). Modification of Tunisian clay membrane surface by silane grafting: Application for desalination with Air Gap Membrane Distillation process. *Colloids and Surfaces A: Physicochemical and Engineering Aspects*, *387*, 79–85.

Kim, K. J., Fane, A. G., Aim, R. Ben, Liu, M. G., Jonsson, G., Tessaro, I. C., Broek, A. P., Bargeman, D. (1994). A comparative study of techniques used for porous membrane characterization: Pore characterization. *Journal of Membrane Science*, *87*, 35–46.

Kim, S., Park, N., Lee, S., & Cho, J. (2009). Membrane characterizations for mitigation of organic fouling during desalination and wastewater reclamation. *Desalination*, *238*, 70–77.

Kimura, S., Nakao, S.-I., & Shimatani, S.-I. (1987). Transport phenomena in membrane distillation. *Journal of Membrane Science*, *33*, 285–298.

Kubota, S., Ohta, K., Hayano, I., Hirai, M., Kikuchi, K., & Murayama, Y. (1988). Experiments on Seawater Desalination by Membrane Distillation. *Desalination*, *69*, 19–26.

Kuhn, H., & Forstering, H.-D. (2000). *Principles of Physical Chemistry*. New York: Wiley.

Kullab, A., & Martin, A. (2011). Membrane distillation and applications for water purification in thermal cogeneration plants. *Separation and Purification Technology*, *76*, 231–237.

Kumar, M., Adham, S., DeCarolis, J., & Pearce, W. (2007). Comparative seawater RO pretreatment evaluation using bench- and pilot-scale testing. *Journal / American Water Works Association*, *99*, 168–178.

Laganà, F., Barbieri, G., & Drioli, E. (2000). Direct contact membrane distillation: modeling and concentration experiments. *Journal of Membrane Science*, *166*, 1–11.

LaPorte, R. J. (2000). *Hydrophilic Polymer Coatings for Medical Devices.* Boca Raton: CRC Press LLC.

Lattemann, S., & Höpner, T. (2008). Environmental Impact and Impact Assessment of Seawater Desalination. *Desalination*, *220*, 1–15.

Lattemann, S., Kennedy, M. D., Schippers, J. C., & Amy, G. (2010). Global Desalination Situation. *Sustainability Science and Engineering: Water Recycling versus Desalination*. Isabel C. Escobar and Andrea I. Scha¨fer. (Eds). Amsterdam: Elsevier B.V. 7–39.

Lawson, K. W., & Lloyd, D. R. (1996). Membrane distillation. I. Module design and performance evaluation using vacuum membrane distillation. *Journal of Membrane Science*, *120*, 111–121.

Lawson, K. W., & Lloyd, D. R. (1997). Membrane distillation. *Journal of Membrane Science*, *124*, 1–25.

Lei, Z., Chen, B., & Ding, Z. (2005). *Membrane distillation*, in: Z. Lei, B. Chen, Z. Ding (Z. Lei, B. Chen, Z. Dings), Special Distillation Processes. Amsterdam: Elsevier Science, 241–319.

Lenntech. (2014). *Teflon*. [online] Available at: <http://www.lenntech.com/teflon.htm> [Accessed 17 May. 2014].

Levin, T. (2004). Turning Oceans into Tap Water. *OnEarth*. Summer 2004.

Li, N., Fane, A. G., Ho, W. S., & Matsuura, T. (2011). *Advanced Membrane Technology and Applications.* New York: John Wiley & Sons.

Lior, N. (2005). Water Desalination. *CRC Mechanical Engineering Handbook 2nd Ed* Frank Kreith and D. Yogi Goswami. (Eds.) Boca Raton: CRC Press.

Liu, G. L., Zhu, C., Cheung, C. S., & Leung, C. W. (1998). Theoretical and experimental studies on air gap membrane distillation. *Heat and Mass Transfer*, *34*, 329-335.

Lloyd, D. R., Kinzer, K. E., & Tseng, H. S. (1990). Microporous membrane formation via thermally induced phase separation. I. Solid-Liquid phase separation. *Journal of Membrane Science*, *52*, 239–261.

Lu, H. (2007). *Composite Fouling of Heat Exchanger Surfaces.* New York: Nova Science Books.

National Academy of Sciences. (2004). *Review of the Desalination and Water Purification Technology Roadmap.* Washington, D. C.: National Academies Press.

Manawi, Y., Khraisheh, M., Fard, A., Benyahia, F., & Adham, S. (2014). Effect of operational parameters on distillate flux in Direct Contact Membrane Distillation (DCMD): comparison between experimental and model predicted performance. *Desalination*, *336*, 110–120.

Martínez-Díez, L., & Florido-Díaz, F. J. (2001). Theoretical and experimental studies on desalination using membrane distillation. *Desalination*, *139*, 373–379.

Martínez-Díez, L., Florido-Díaz, F. J., & Vázquez-González, M. I. (1999). Study of evaporation efficiency in membrane distillation. *Desalination*, *126*, 193–198.

Martínez-Díez, L., Vázquez-González, M. I., & Florido-Díaz, F. J. (1998). Study of membrane distillation using channel spacers. *Jounrnal of Membrane Science*, *144*, 45–56.

Martínez-Díez, L., & Vázquez-González, M. . (1999). Temperature and concentration polarization in membrane distillation of aqueous salt solutions. *Journal of Membrane Science*, *156*, 265–273.

Mason, E. A., & Malinauskas, A. P. (1983). Gas transport in porous media: the dusty-gas model. Amsterdam, the Netherlands: Elsevier.

Mason, E. A., Malinauskas, A. P., & Evans, R. B. (1967). Flow and Diffusion of Gases in Porous Media. The Journal of Chemical Physics, 46, 3199-3216.

Mathioulakis, E., Belessiotis, V., Delyannis, E. (2007). Desalination by using alternative energy: Review and state-of-the-art. *Desalination*, *203*, 346–365.

Matsuura, T. (2001). Progress in membrane scince and technology for seawater desalination - A review. *Desalination*, *134*, 47–54.

Meerganz von Medeazza, G. L. (2005). "Direct" and socially-induced environmental impacts of desalination. *Desalination*, *185*, 57–70.

Meindersma, G. W., Guijt, C. M., & de Haan, A. B. (2006). Desalination and water recycling by air gap membrane distillation. *Desalination*, *187*, 291–301.

Mettler Toledo. (n. d.). *MS Precision Balances*. [online] Available at: <http://us.mt.com/us/en/home/products/Laboratory_Weighing_Solutions/Precision_Balances/MS_Precision_Balances.html> [Accessed 17 May. 2014].

Miller, J. E. (2003). Review of water resources and desalination technologies. *Sandia National Laboratories Report, SAND2003-0800*, 1–54.

Misdan, N., Lau, W. J., & Ismail, A. F. (2012). Seawater Reverse Osmosis (SWRO) desalination by thin-film composite membrane-Current development, challenges and future prospects. *Desalination*, *287*, 228–237.

Mohammadi, T., & Safavi, M. A. (2009). Application of Taguchi method in optimization of desalination by vacuum membrane distillation. *Desalination*, *249*, 83–89.

Mulder, M. (1996). *Basic Principles of Membrane Technology*, 2nd ed. Kluwer: Dordrecht, the Netherlands.

Nadim, F., Bagtzoglou, A., & Iranmahboob, J. (2008). Coastal Management in the Persian Gulf Region within the Framework of the ROPME Programme of Action. *Ocean & Coastal Management*, *51*, 556–65.

Namboodiri, V., & Rajagopalan, N. (2014). Desalination. *Reference Module in Earth Systems and Environmental Sciences*, from *Comprehensive Water Quality and Purification*, *2*, 98–119.

National Instruments. (2007). *NI 9219 Specifications*. [online] Available at: <http://web.mst.edu/~cottrell/ME240/Homework/transducers/DAQ/NI-9219ds.pdf> [Accessed 17 May. 2014].

National Instruments. (2015). NI cDAQ-9178. [online] Available at: <http://sine.ni.com/nips/cds/view/p/lang/en/nid/207534> [Accessed 3 May. 2015].

National Instruments. (n. d.). *NI 9219*. [online] Available at: <http://sine.ni.com/nips/cds/view/p/lang/en/nid/208789> [Accessed 17 May. 2014].

NDS. (2011). *Qatar National Development Strategy 2011-2016*. Qatar General Secretariat for Development Planning. Doha, Qatar.

Omega. (2014). *High Performance Pressure Transducer Rugged All Stainless Steel Construction*. [online] Available at: < http://www.omega.com/pptst/Px309.html> [Accessed 17 May. 2014].

Omega. (2014). *Low Flow Magmeter*. [online] Available at: <http://www.omega.com/pptst/FMG80.html> [Accessed 17 May. 2014].

Omega. (2014). *RTD Pipe Plug Probe with NPT Fitting*. [online] Available at: <http://www.omega.com/pptst/RTD-NPT.html> [Accessed 17 May. 2014].

Omega. (n. d.). *PTFE Liquid Flow Sensors*. Available at: < http://www.omega.com/Green/pdf/FPR1500.pdf> [Accessed 17 May. 2014].

Ortiz de Zárate, J. M., Rinc´on, C., & Mengual, J. I. (1998). Concentration of bovine serum albumin aqueous solutions by membrane distillation, Separation Science and Technology, 33(3), 283–296.

Osada, Y., & Nakagawa, T. (2010). *Membrane Science and Technology*. New York: Marcel Dekker, Inc.

Pal, P., & Manna, A. K. (2010). Removal of arsenic from contaminated groundwater by solar-driven membrane distillation using three different commercial membranes. *Water Research*, *44*, 5750–5760.

Pangarkar, B. L., Sane, M. G., & Guddad, M. (2011). Reverse Osmosis and Membrane Distillation for Desalination of Groundwater: A Review. *ISRN Materials Science*, *2011*, 1 – 9.

Pankratz, T. (2012). *IDA Desalination Yearbook 2012–2013*. Media Analytics Ltd., Oxford, UK.

Peinemann, K. V., & Nunes, S. P. (2010). *Membrane Technology: Volume 4: Membranes for Water Treatment.* New York: John Wiley & Sons.

Perle. (n. d.). *Serial Terminal Server.* [online] Available at: <http://www.perle.com/products/terminal-server.shtml> [Accessed 17 May. 2014].

Phattaranawik, J., & Jiraratananon, R. (2001). Direct contact membrane distillation: Effect of mass transfer on heat transfer. *Journal of Membrane Science*, *188*, 137–143.

Phattaranawik, J., Jiraratananon, R., & Fane, A. G. (2003). Effect of pore size distribution and air flux on mass transport in direct contact membrane distillation. *Journal of Membrane Science*, *215*, 75–85.

Phattaranawik, J., Jiraratananon, R., & Fane, A. G. (2003). Heat transport and membrane distillation coefficients in direct contact membrane distillation. *Journal of Membrane Science*, *212*(1-2), 177–193.

Pulat, M., & Akdoan, A. (2002). The diffusion and bulk properties of polyurethane (PU)-based hydrophilic and hydrophobic membranes. *Journal of Applied Polymer Science*, *85*, 193–198.

Purnama, A., Albarwani, H. H., & Smith, R. (2005). Calculating the Environmental Cost of Seawater Desalination in the Arabian Marginal Seas. *Desalination*, *185*, 79–86.

Purser, B. H., & Seibold, E. (1973). The principal environmental factors influencing Holocene sedimentation and diagenesis in the Persian Gulf. In: Purser, B.H. (Ed.), The Persian Gulf: Holocene Carbonate Sedimentation and Diagenesis in a Shallow Epicontinental Sea. *Springer-Verlag*, 1–9.

Qtaishat, M., Matsuura, T., Kruczek, B., & Khayet, M. (2008). Heat and mass transfer analysis in direct contact membrane distillation. *Desalination*, *219*, 272–292.

Rainierrubber. (1998). *Viton fluoroelastomer*. [online] Available at: <http://rainierrubber.com/wp-content/uploads/2014/01/Viton-Selection-Guide.pdf> [Accessed 17 May. 2014].

Raluy, G., Serra, L., & Uche, J. (2006). Life cycle assessment of MSF, MED and RO desalination technologies. *Energy*, *31*, 2025–2036.

Raluy, R. G., Serra, L., Uche, J., & Valero, A. (2004). Life-cycle assessment of desalination technologies integrated with energy production systems. *Desalination*, *167*, 445–458.

Rácz, G., Kerker, S., Kovács, Z., Vatai, G., Ebrahimi, M., & Czermak, P. (2014). Theoretical and Experimental Approaches of Liquid Entry Pressure Determination in Membrane Distillation Processes. *Chemical Engineering*, *58(2)*, 81-91.

Ramaswamy, S., Huang, H., & Ramarao, B. (2013). *Separation and Purification Technologies in Biorefineries.* New Jersey: John Wiley & Sons.

Razavi, S. S., Harris, J., & Sherkat, F. (1996). Fouling and cleaning of membranes in the ultrafiltration of the aqueous extract of soy flour. *Journal of Membrane Science*, *114*, 93–104.

Reid, R. N. (1996). *Water Quality & Systems: A Guide for Facility Managers Facilities Management*. New York: The Fairmont Press.

Rivier, C., García-Payo, M., Marison, I., & Stockar, U. von. (2002). Separation of binary mixtures by thermostatic sweeping gas membrane distillation: I. Theory and simulations. *Journal of Membrane Science*, *201*, 1–16.

Saidur, R., Elcevvadi, E. T., Mekhilef, S., Safari, A., & Mohammed, H. A. (2011). An overview of different distillation methods for small scale applications. *Renewable and Sustainable Energy Reviews*, *15*, 4756–4764.

Saif, O. (2012). *The Future Outlook of Desalination in the Gulf: Challenges & opportunities faced by Qatar & the UAE*. United Nations University Institute for Water, Environment and Health (UNU-INWEH), 1–63.

Sakai, K., Ano, T. K., Muroi, T. & Tamura, M. (1988). Effects of temperature concentration polarization on water vapor permeability for blood in membrane distillation. *The Chemical Engineering Journal*, *38*, B33-B39.

Sarti, G. C., Gostoli, C., & Bardini, S. (1993). Extraction of organic components from aqueous streams by vacuum membrane distillation. In *Journal of Membrane Science*, 80, 21–33.

Sarti, G. C., Gostoli, C., & Matulli, S. (1985). Low Energy Cost Desalination Processes Using Hydrophobic Membranes. *Desalination*, *56*, 277–286.

Sarti, G. C., & Gostoli, C., (1986). Use of hydrophobic membranes in thermal separation of liquid mixtures: theory and experiments. In *Membrane and Membrane Processes*, Drioli, E., and Nakagaki, M., (Eds.), Plenum Press, 349–360.

Schneider, K., Hölz, W., Wollbeck, R., & Ripperger, S. (1988). Membranes and modules for transmembrane distillation. *Journal of Membrane Science*, *39*, 25-42.

Schofield, R. W. (1989). *Membrane distillation*. Doctor of Philosophy Thesis, The University of New South Wales.

Schofield, R. W., Fane, A. G., & Fell, C. J. D. (1987). Heat and mass transfer in membrane distillation. *Journal of Membrane Science*, *33*, 299–313.

Schofield, R. W., Fane, A. G., & Fell, C. J. D. (1990). Gas and vapour transport through microporous membranes. I. Knudsen-Poiseuille transition. In *Journal of Membrane Scienc*, *53*, 159–171.

Schofield, R. W., Fane, A. G., & Fell, C. J. D. (1990). Gas and vapour transport through microporous membranes. II. Membrane distillation. *Journal Of Membrane Science*, *53*, 173–185.

Schofield, R. W., Fane, A. G., Fell, C. J. D., & Macoun, R. (1990). Factors affecting flux in membrane distillation. *Desalination*, *77*, 279–294.

Shannon, M. A., Bohn, P. W., Elimelech, M., Georgiadis, J. G., Mariñas, B. J., & Mayes, A. M. (2008). Science and technology for water purification in the coming decades. *Nature*, *452*, 301–310.

Shirazi, M. M. A., Kargari, A., Bazgir, S., Tabatabaei, M., Shirazi, M. J. A., Abdullah, M. S., Matsuura, T., Ismail, A. F. (2013). Characterization of electrospun polystyrene membrane for treatment of biodiesel's water-washing effluent using atomic force microscopy. *Desalination*, *329*, 1–8.

Smolders, K., & Franken, A. C. M. (1989). Terminology for Membrane Distillation, *Desalination*, *72*, 249–262.

Song, L., Li, B., Sirkar, K. K., & Gilron, J. L. (2007). Direct contact membrane distillation-based desalination: Novel membranes, devices, larger-scale studies, and a model. *Industrial and Engineering Chemistry Research*, *46*, 2307-2323.

Sperati, C. A., & DuPont de Nemours, E. I. (1999). *Polymer handbook*. 4th ed. Hoboken, NJ: Wiley.

Srisurichan, S., Jiraratananon, R., & Fane, A. G. (2005). Humic acid fouling in the membrane distillation process. *Desalination*, *174*, 63–72.

Sterlitech. (2014). *Polypropylene Filters*. [online] Available at: <http://www.sterlitech.com/filters/membrane-disc-filters/polypropylene-membrane-filters/polypropylene-membrane-filters.html> [Accessed 17 May. 2014].

Sterlitech. (2014). *PTFE Laminated Membrane Filters*. [online] Available at: <http://www.sterlitech.com/filters/membrane-disc-filters/ptfe/ptfe-laminated-membrane-filters.html> [Accessed 17 May. 2014].

Strathmann, H. (2009). *Ion-Exchange Membrane Separation Processes*. Amsterdam: Elsevier.

Suzuki, T., Watanabe, Y., Ozawa, G., & Ikeda, S. (1998). Removal of soluble organics and manganese by a hybrid MF hollow fiber membrane system. *Desalination*, *117*, 119–130.

Tam, C. M., & Tremblay, A. Y. (1991). Membrane pore characterization - Comparison between single and multicomponent solute probe techniques. *Journal of Membrane Science*, *57*, 271–287.

Tang, N., Cheng, P., Wang, X., & Zhang, H. (2009). Study on the vacuum membrane distillation performances of PVDF Hollow Fiber membranes for aqueous NaCl solution. In *Chemical Engineering Transactions*, *17*, 1537–1542.

Teoh, M. M., & Chung, T. S. (2009). Membrane distillation with hydrophobic macrovoid-free PVDF-PTFE hollow fiber membranes. *Separation and Purification Technology*, *66*, 229–236.

The World Bank. (2012). *Renewable Energy Desalination: An Emerging Solution to Close the Water Gap in the Middle East and North Africa*. Washington DC: World Bank.

Tomaszewska, M. (1994). An experimental study of isothermal and non-isothermal phenomena in a hydrophobic-hydrophilic membrane system. *Journal of Membrane Science*, *88*, 223–229.

Tomaszewska, M. (1996). Preparation and properties of flat-sheet membranes from poly(vinylidene fluoride) for membrane distillation. *Desalination*, *104*, 1–11.

Tun, C. M., Fane, A. G., Matheickal, J. T., & Sheikholeslami, R. (2005). Membrane distillation crystallization of concentrated salts - Flux and crystal formation. *Journal of Membrane Science*, *257*, 144–155.

Tuner. (n. d.). *STRAIN, PROCESS & TEMPERATURE METERS WITH OPTIONAL RELAYS AND ANALOG OUTPUT*. [online] Available at: < http://www.tuner.tw/omega%20cd/Pressure/pdf/DP25B_E.pdf> [Accessed 17 May. 2014].

USplastic. (2014). *Vincon™ C-219-A Flexible PVC Tubing*. [online] Available at: <http://www.usplastic.com/catalog/item.aspx?itemid=102161> [Accessed 17 May. 2014].

Van der Bruggen, B., Schaep, J., Maes, W., Wilms, D., & Vandecasteele, C. (1998). Nanofiltration as a treatment method for the removal of pesticides from ground waters. *Desalination*, *117*, 139–147.

Veza, J. M. (2001). Desalination in the Canary Islands: an update. *Desalination*, *133*, 259–279.

Voutchkov, N. S. (2008). Planning for Carbon-neutral Desalination in Carlsbad, California. *Environmental Engineer: Applied Research and Practice*, 6, 1–11.

Wang, X., Zhang, L., Yang, H., & Chen, H. (2009). Feasibility research of potable water production via solar-heated hollow fiber membrane distillation system. *Desalination*, *247*, 403–411.

Weyl, P. K. (1967). *Recovery of Demineralized Water from Saline Waters*. US Pat. 3,340,186. Research Corporation, New York, USA.

WHO. (2007). *Desalination for Safe Water Supply: Guidance for the Health and Environmental Aspects Applicable to Desalination*. The World Health Organization. Geneva.

Wilf, M., & Bartels, C. (2005). Optimization of seawater RO systems design. *Desalination*, *173*, 1–12.

Winckler, O. (1997). The Immigration Policy of the Gulf Cooperation Council (GCC) States. *Middle Eastern Studies*, *33*, 480–493.

Winter, D., Koschikowski, J., & Wieghaus, M. (2011). Desalination using membrane distillation: Experimental studies on full scale spiral wound modules. *Journal of Membrane Science*, *375*, 104–112.

WTW. (2009). *TetraCon 925: Standard Conductivity Measuring Cell*. [online] Available at: <http://www.globalw.com/downloads/WQ/TetraCon925.pdf> [Accessed 17 May. 2014].

Wu, Y., Kong, Y., Liu, J., Zhang, J., & Xu, J. (1991). An experimental study on membrane distillation-crystallization for treating waste water in taurine production. *Desalination*, 80, 235–242.

Yan-jun, Z., Kai-fen, W., Zheng-jun, W., Liang, Z., & Shu-shen, L., (2000). Fouling and Cleaning of Mmebrane – A Literature Review. *Journal of Environmental Science*, *12(2)*, 241-251.

Younos, T. (2005). Environmental Issues of Desalination. *Journal of Contemporary Water Research & Education*, *132*, 11–18.

Yun, Y., Ma, R., Zhang, W., Fane, A. G., & Li, J. (2006). Direct contact membrane distillation mechanism for high concentration NaCl solutions. *Desalination*, *188*, 251–262.

Zeaman, L. J., & Zydney, A. L., (1996). Microfiltration and Ultrafiltration: Principles and Applications. New York: Marcel Dekker, Inc.

Zhang, J., Dow, N., Duke, M., Ostarcevic, E., Li, J. D., & Gray, S. (2010). Identification of material and physical features of membrane distillation membranes for high performance desalination. *Journal of Membrane Science*, *349*, 295–303.

Zhang, J., Li, J. D., & Gray, S. (2011). Effect of applied pressure on performance of PTFE membrane in DCMD. *Journal of Membrane Science*, *369*, 514–525.

Zhang, J., Li, J. D., Duke, M., Hoang, M., Xie, Z., Groth, A., Tun, C., & Gray, S. (2013). Modeling of Vacuum Membrane Distillation. *Journal of Membrane Science*, *434*, 1–9.

Zhang, Q., Tang, R., Yin, K., Luo, X., & Zhang, L. (2009). Corrosion behavior of Hastelloy C-276 in supercritical water. *Corrosion Science*, 51(9), 2092–2097.

Zhang, W., & Hallstrom, B. (1990). Membrane Characterization Using the Contact Angle Technique. I. Methodology of the Captive Bubble Technique. *Desalination*, *79*, 1–12.

Zhang, W., Wahlgren, M., & Sivik, B. (1989). Membrane Characterization by the Contact Angle Technique. II. Characterization of UF-Membranes and Comparison between the Captive Bubble and Sessile Drop as Methods to obtain Water Contact Angles. *Desalination*, *72*, 263–273.

Zubir, N. A., & Ismail, A. F. (2002). Effect of sintering temperature on the morphology and mechanical properties of PTFE membranes as a base substrate for proton exchange membrane. *Journal of Science and Technology*, *24*, 823–831.

Appendix

Appendix (A): SEM-EDS Spectra of the Different Membranes Used in the Study

PP (0.22 µm) EDS Spectra (Feed: Seawater)
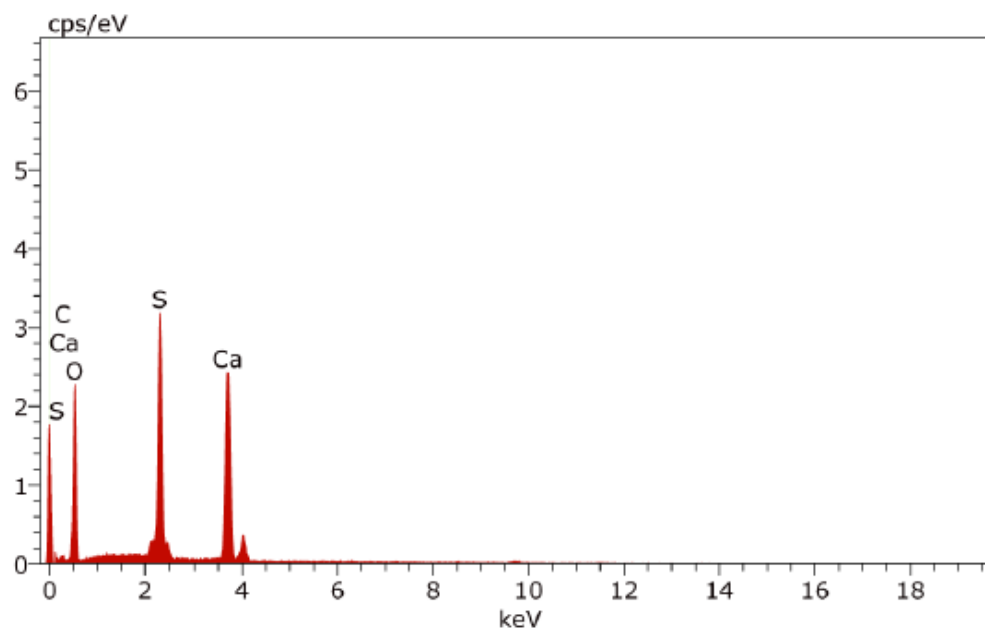

```
Spectrum: PP-0-22um-EDX3.spx

El AN  Series   unn. C norm. C Atom. C Error (1 Sigma)
                [wt.%]   [wt.%]  [at.%]       [wt.%]
-----------------------------------------------------
C   6  K-series   2.36     2.90    4.77        0.75
O   8  K-series  50.06    61.48   75.92        6.71
S  16  K-series  11.55    14.19    8.74        0.45
Ca 20  K-series  17.46    21.44   10.57        0.55
-----------------------------------------------------
       Total:    81.42   100.00  100.00
```
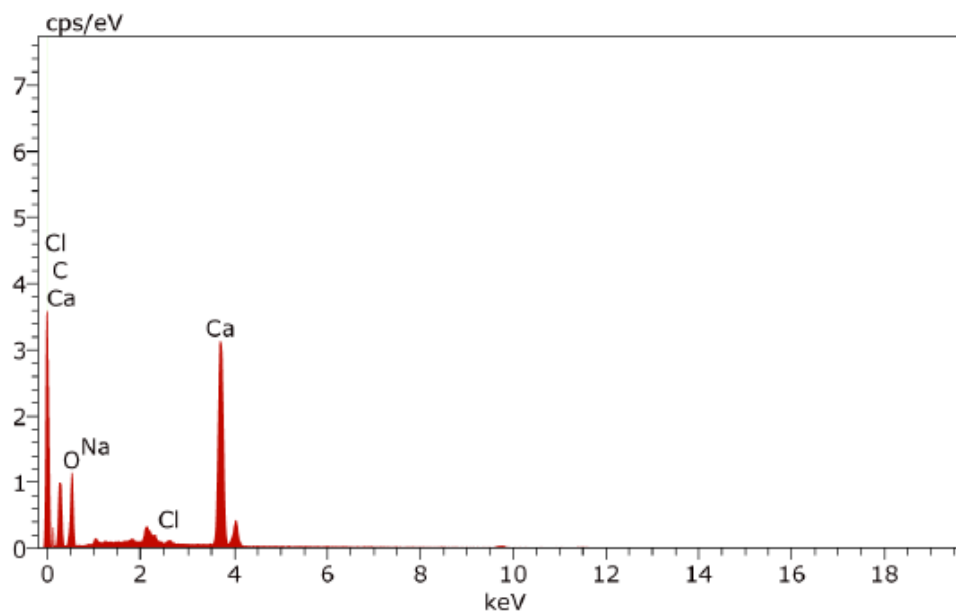
Spectrum: PP-0-22um-EDX4.spx

```
El AN  Series   unn. C norm. C Atom. C Error (1 Sigma)
                 [wt.%]  [wt.%]  [at.%]        [wt.%]
-------------------------------------------------------
C   6  K-series  18.57   21.62   32.22         2.57
O   8  K-series  41.49   48.30   54.04         5.53
Na 11  K-series   0.77    0.90    0.70         0.09
Cl 17  K-series   0.10    0.12    0.06         0.03
Ca 20  K-series  24.97   29.07   12.98         0.76
-------------------------------------------------------
       Total:    85.91  100.00  100.00
```

PP (0.45 µm) EDS Spectra (Feed: Seawater)
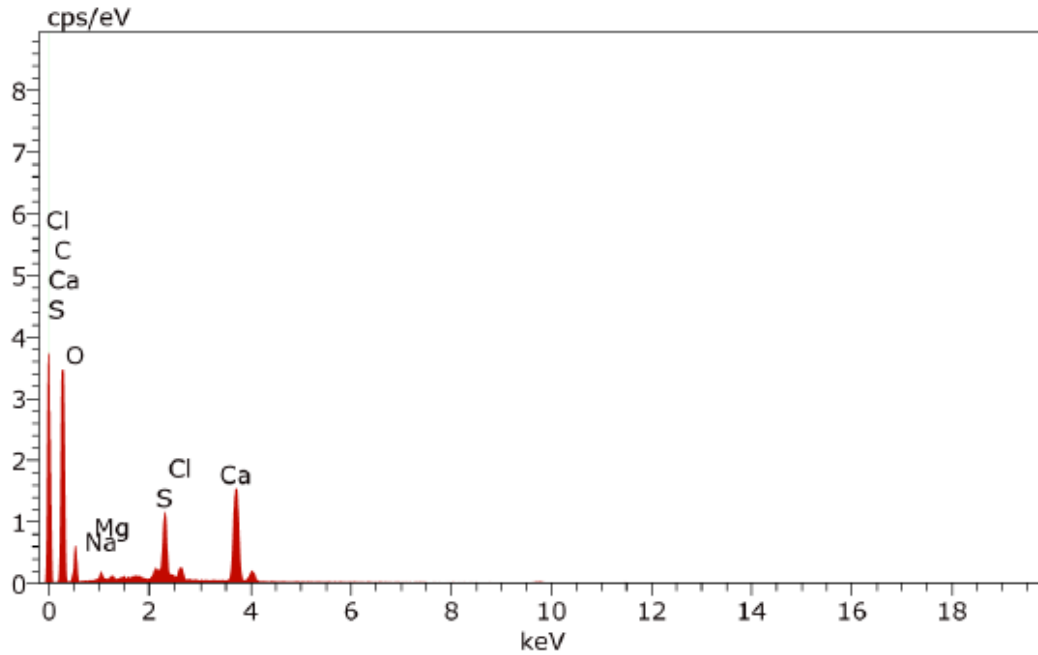
Spectrum: PP-0-45um-EDX2.spx

El	AN	Series	unn. C [wt.%]	norm. C [wt.%]	Atom. C [at.%]	Error (1 Sigma) [wt.%]
C	6	K-series	67.62	63.07	75.04	8.34
O	8	K-series	22.44	20.93	18.69	3.47
Na	11	K-series	0.62	0.58	0.36	0.08
Mg	12	K-series	0.11	0.10	0.06	0.04
S	16	K-series	4.16	3.88	1.73	0.18
Cl	17	K-series	0.85	0.79	0.32	0.06
Ca	20	K-series	11.41	10.65	3.80	0.37

| | | Total: | 107.21 | 100.00 | 100.00 | |
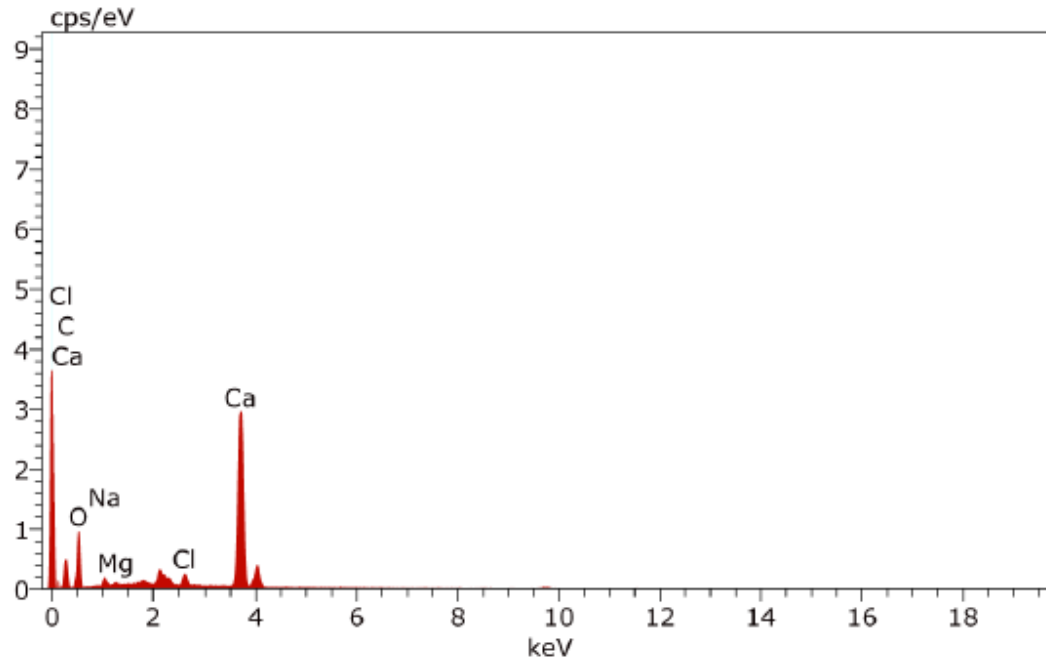
Spectrum: PP-0-45um-EDX3.spx

El	AN	Series	unn. C [wt.%]	norm. C [wt.%]	Atom. C [at.%]	Error (1 Sigma) [wt.%]
C	6	K-series	10.55	13.52	21.67	1.66
O	8	K-series	38.93	49.86	60.02	5.28
Na	11	K-series	1.25	1.60	1.34	0.12
Mg	12	K-series	0.17	0.22	0.17	0.04
Cl	17	K-series	0.82	1.05	0.57	0.06
Ca	20	K-series	26.35	33.75	16.22	0.80
		Total:	78.07	100.00	100.00	
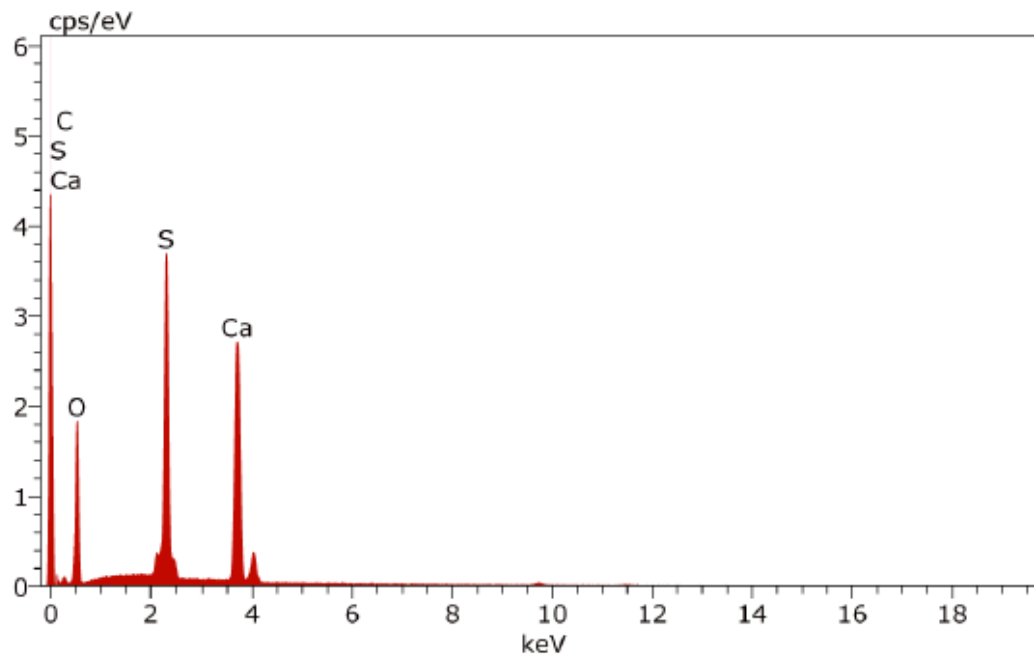
Spectrum: PP-0-45um-EDX4.spx

El	AN	Series	unn. C [wt.%]	norm. C [wt.%]	Atom. C [at.%]	Error (1 Sigma) [wt.%]
C	6	K-series	2.60	3.20	5.46	0.65
O	8	K-series	45.50	55.98	71.58	5.72
S	16	K-series	13.57	16.69	10.65	0.51
Ca	20	K-series	19.61	24.12	12.31	0.60
		Total:	81.28	100.00	100.00	

PTFE (0.22 µm) EDS Spectra (Feed: Seawater)
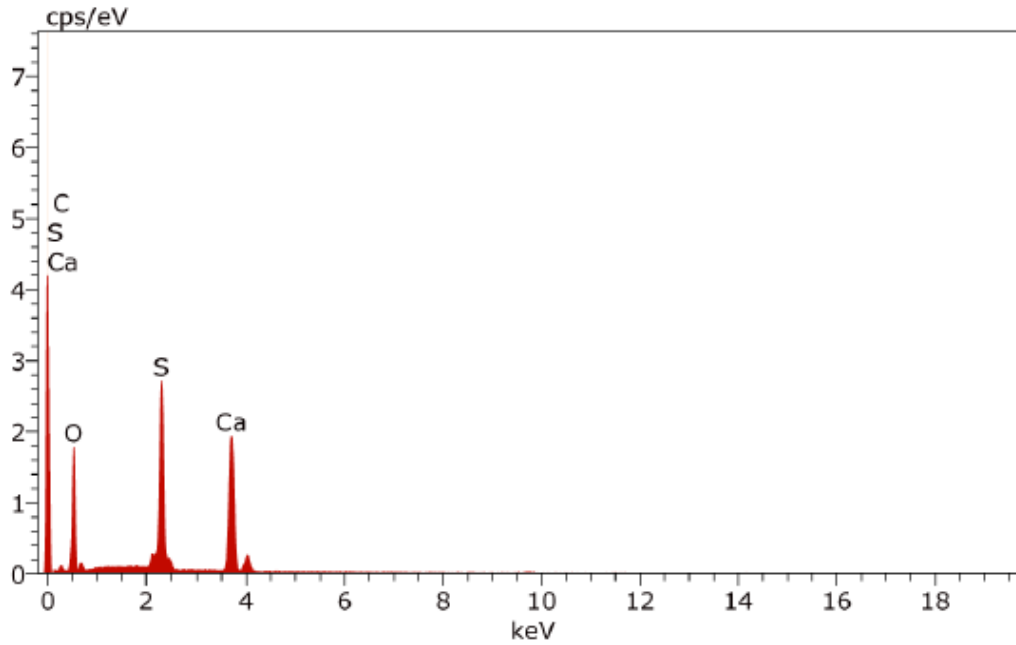
Spectrum: PTFE-EDX1.spx

```
El AN  Series  unn. C norm. C Atom. C Error (1 Sigma)
                [wt.%]  [wt.%]  [at.%]        [wt.%]
----------------------------------------------------
C  6  K-series   3.54    4.29    7.05          1.03
O  8  K-series  49.01   59.34   73.17          6.72
S  16 K-series  12.59   15.25    9.38          0.49
Ca 20 K-series  17.44   21.12   10.40          0.55
----------------------------------------------------
        Total:  82.59  100.00  100.00
```
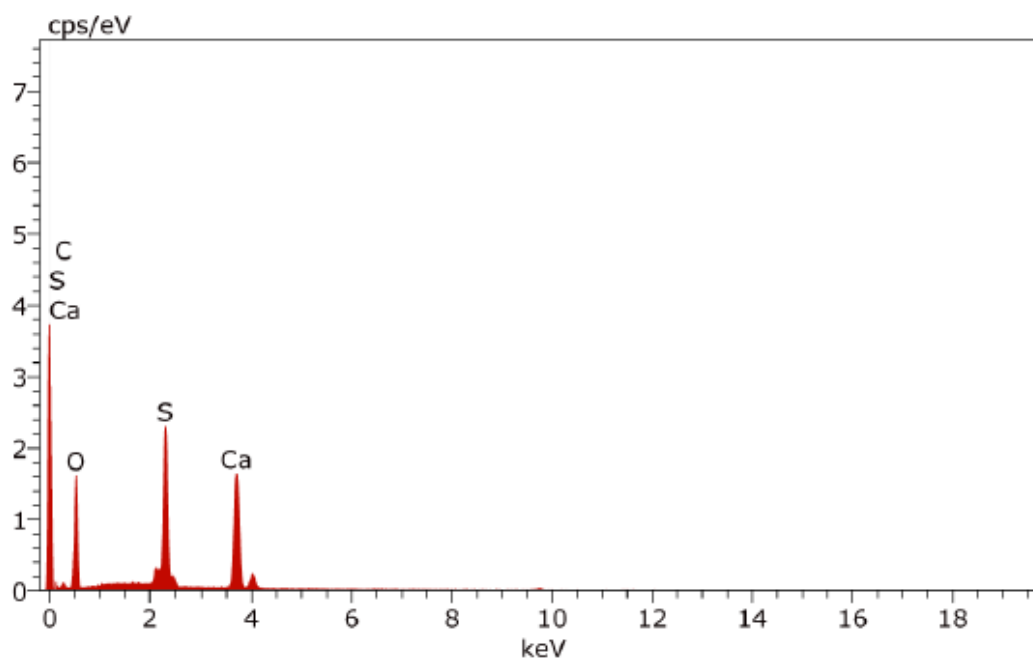
Spectrum: PTFE-EDX3.spx

El	AN	Series	unn. C [wt.%]	norm. C [wt.%]	Atom. C [at.%]	Error (1 Sigma) [wt.%]
C	6	K-series	3.41	4.44	7.21	0.98
O	8	K-series	46.62	60.68	74.00	6.33
S	16	K-series	11.42	14.86	9.04	0.44
Ca	20	K-series	15.38	20.02	9.75	0.49
		Total:	76.83	100.00	100.00	

PP (0.45 μm) EDS Spectra (Feed: NaCl Solution)
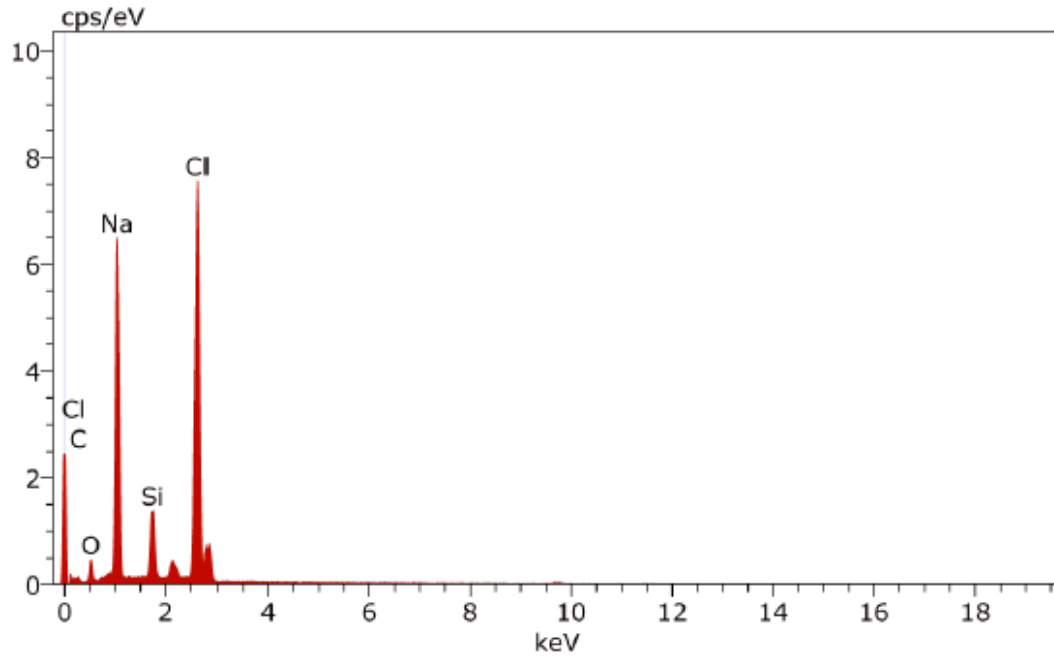

```
Spectrum: PP-0-45-d.spx

El AN  Series   unn. C norm. C Atom. C Error (1 Sigma)
                [wt.%]  [wt.%]  [at.%]         [wt.%]
--------------------------------------------------------
C   6  K-series  10.25   12.15   22.75          2.47
O   8  K-series  10.64   12.61   17.73          1.85
Na 11  K-series  26.97   31.98   31.29          1.77
Si 14  K-series   4.03    4.78    3.83          0.20
Cl 17  K-series  32.44   38.47   24.40          1.12
--------------------------------------------------------
        Total:   84.33  100.00  100.00
```
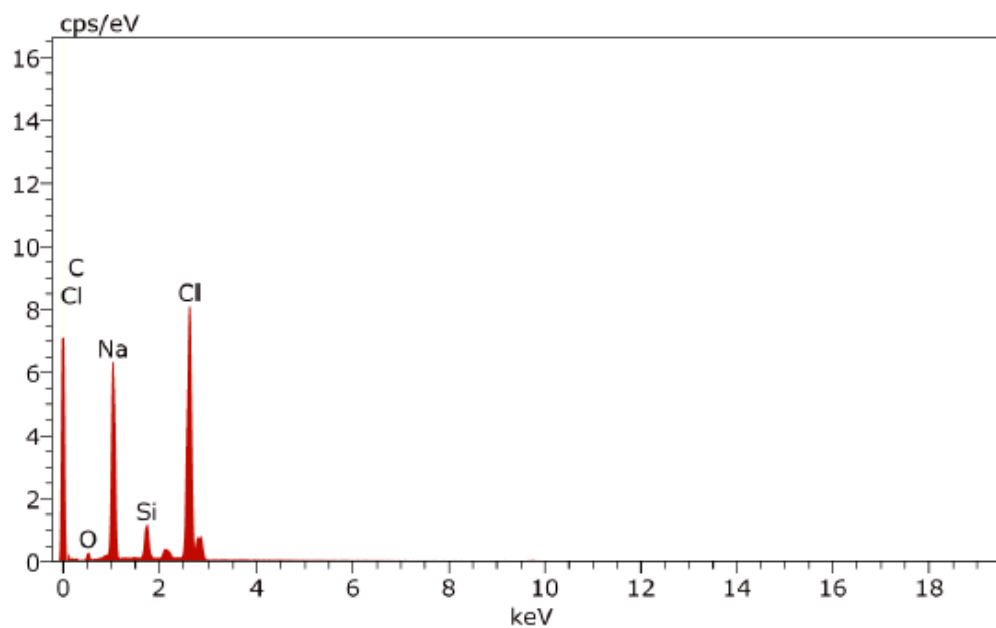
Spectrum: PP-0-45-f.spx

```
El AN  Series  unn. C norm. C Atom. C Error (1 Sigma)
                [wt.%]  [wt.%]  [at.%]        [wt.%]
--------------------------------------------------------
C   6  K-series   8.73   10.96   21.48         1.85
O   8  K-series   6.70    8.41   12.37         1.14
Na 11  K-series  26.35   33.07   33.87         1.73
Si 14  K-series   3.20    4.02    3.37         0.17
Cl 17  K-series  34.69   43.54   28.91         1.19
--------------------------------------------------------
       Total:    79.66  100.00  100.00
```

Nomenclature

a	Exponent factor of d
B	Geometrical pore coefficient
b or δ	Membrane thickness
C_C	Mass transfer coefficient when the transition region is dominant
C_D	Mass transfer coefficient when Molecular diffusion is dominant
C_f	Salt concentration of the feed
C_{kn}	Mass transfer coefficient when Knudsen diffusion is dominant
C_m	Membrane mass transfer coefficient
C_p	Salt concentration of the permeate
D	Diffusion coefficient
d	Mean pore size of the membrane
d_h	Hydraulic diameter of the flow channel
f	Frication factor
h_f	Feed boundary layer heat transfer coefficient
h_m	Membrane heat transfer coefficient
h_{mg}	Heat transfer coefficient of the gas
h_{ms}	Heat transfer coefficient of the membrane solid
h_p	Permeate boundary layer heat transfer coefficient
H_v	Enthalpy of the vapor
J	Permeate flux
k_B	Boltzmann constant
k^G	Thermal conductivity of air
k_m	Thermal conductivity of membrane
Kn	Knudsen number
k^P	Thermal conductivity of the polymeric material
l or λ	Mean free path of the molecules

M_a	Molecular weight of air
M_w	Molecular weight of water
P	Total pressure inside the pores
P_1	Vapor pressure at the feed side membrane surface
P_2	Vapor pressure at the permeate side membrane surface
P_{air}	Pressure within the membrane pore
PD	Diffusivity of water vapor in the pores
P_f	Hydraulic pressure on the feed side
P_p	Hydraulic pressure on the permeate side
P_{pore}	Mean pressure in the pores
Q_C	Conductive heat transfer through the membrane
Q_f	Convectional heat transfer in the feed boundary layer
Q_m	Total heat transferred through the membrane
Q_p	Convectional heat transfer in the permeate thermal boundary layer
Q_V	Heat transferred due to water vapor transport through the pores
r	Membrane pore radius
r_{max}	Maximum pore radius
T	Mean temperature in the pores
t	Membrane pore tortuosity
T_f	Feed temperature
T_1	Feed side membrane surface temperature
T_2	Permeate side membrane surface temperature
T_p	Permeate temperature
u	Velocity
$\bar{v}$	Gas' mean molecular speed
Y	Salt rejection percentage
γ_l	Liquid surface tension
ε	Membrane porosity
θ	Contact angle

λ_f	Thermal conductivity of the feed
μ	Viscosity
ρ	Density
σ_a	Collision diameters for air
σ_{lv}	Liquid–vapor interfacial energy
σ_{sl}	Solid–liquid interfacial energy
σ_{sv}	Solid–vapor interfacial energy
σ_w	Collision diameters for water vapor
τ	Temperature polarization coefficient